JOURNAL OF BIOLOGICAL REGULATORS & HOMEOSTATIC AGENTS
Volume 36, No. 1, January-February, 2022

CONTENTS

Editorials

G. Ronconi, C.E. Gallenga, Al. Caraffa, S.K. Kritas, I. Frydas, P. Conti, V. Calvisi and M. Trimarchi. Contribution of mast cells in SARS-CoV-2-induced inflammation 1

Original Articles

N. Ayubi, E. Yuniarti, NW. Kusnanik, L. Herawati, PM. Indika, RY. Putra and A. Komaini. Acute effects of n-3 polyunsaturated fatty acids (PUFAs) reducing tumor necrosis factor-alpha (TNF-a) levels and not lowering malondialdehyde (MDA) levels after anaerobic exercise 7

S. Bokhari, S. Ahmad, U. Rafi, MA. Iqbal, MA Khan and N. Roohi. Deranged growth factors as a prognosticator of cardiovascular risks in patients with uterine fibroids 13

H. Chai, Y. Geng, C. Hu, J. Wang, Y. Quan, T. Yu and X. Zhou. Circ_0000419 acts as a miR-580 sponge to accelerate colorectal cancer progression via regulating DNMT3B 21

G. Damiani, K. Kridin, S. Garbarino, V. Chattu, H. Amital, M. Adawi, A. Watad, A. Pacifico, P. D.M. Pigatto, M. Del Fabbro, P. Malagoli, Young Dermatologists Italian Network and N. L. Bragazzi. Sleep quality in partners with spouses and children affected by psoriasis and psoriatic arthritis: insights and implications from a pilot study 35

C. Guo, H. Duan, W. Fu, H. He, F. Xie, Z. Yang, M. Zheng and L. Zhang. A DNA damage response mutation-related prognostic gene signature associated with survival outcomes and the immune microenvironment in patients with hepatocellular carcinoma 45

E. Guo, Y. Wu and L. Zhang. TTN-AS1 is altered during inhalation therapy in COPD patients and aggravates cigarette smoke extracts-induced lung epithelial cell injury via sponging miR-15b-5p 57

H.L. Jia, R. Zhang, Q.Q. Liang, X.F. Jiang. Effects of 5-azacytidine on Th cell Differentiation and IFN-γ, IL-4, GATA3, ROR-γ, and Foxp3 Cytokine Expression in Allergic Rhinitis 71

C. Shi, H. Xu, and H. Ding. Investigation of key ubiquitination-related genes associated with cervical cancer 81

X-P. Xu, M. Shi and H. Huang. Wilms' tumor 1-associated protein facilitates the progression of CC by silencing BRCA1 95

Y. Xu, C. Li, G. Liu, H. Zhang, S. Tian, H. Hao and Y. Hao. Ang 1-7 increases nitric oxide synthesis by modulating endothelial nitric oxide synthase -caveolin-1 interaction in rat vascular smooth muscle cells 105

L. Wang, F. Wang, G. Su and G-H. Su. A rare case of ST-elevation myocardial infarction caused by thrombotic occlusion of a coronary artery aneurysm in the left anterior descending artery 115

Case Reports

G. Zirilli, G. Salzano, F. Galletta, P. Basile, F. Caime, U. Cucinotta, M. Licciardello, S. Passanisi, G. Russo and F. Lombardo. Vitamin B12 deficiency in type 1 diabetes patient with thalassemia trait: the challenge of early diagnosis 123

Letters to the Editor

G. Barassi, E. Di Simone, M. Supplizi, L. Prosperi, C. Marinucci, R. Pellegrino, P. Galasso, S. Guerri, M. Della Rovere, A. Younes, and A. Di Iorio. Bio-Physico-Metric approach: integrated postural assessment in musculoskeletal dysfunctions 129

Y.Q. Du, L.C. Lei, S.C. Wang, X.Y. Bian, M. Li, H. Liu and W. Chen. Magnetic resonance high-resolution black blood imaging for the diagnosis of intracranial arterial stenosis 137

G. Galbiati, L. Giannini, E. Del Rosso, P. Cressoni, FMR Parisi and L. Esposito. Correlation between dyslalia and skeletal and dental malocclusions 143

H. Li, H. Huang, Y.S. Li, Q. Zhang, X.T. Pan, H. Yang, Y. Zhang, F. Huo and J.H. Jiang. DLX6-AS1 increases the malignancy of oral squamous cell carcinoma cells via regulating miR-199a-5p/SOX4 axis 147

B. Liu, Y-J. Zhao, M. Zhang, X-Y Gao and P. Hu. The therapeutic effect of polygonum multiflorum on neurological tissue after spinal cord injury in rats 155

JW. Liu, Q. Yan, JJ. He, DT. Lin, SL. Zhang, F. Gao, ZH. Chen and H. Lin. Overexpression of CCR7 in tolerogenic dendritic cells on T lymphocyte immune function in ankylosing spondylitis 161

XZ. Liu, ZH. Shang, YP. Li, J. Liang, X. Lu, Z. Lu and N. Ru. Circ_0020378 promotes the osteosarcoma malignant progression through miR-1200 / CDH6 axis 169

Y. Lu, W. Chen, Y. Chang and YQ. Chen. Identification of immune-related genes associated with spared nerve injury neuropathic pain 177

E. Maffezzoni, K. Luciano, F. Maffezzoni, S. Agostini and M. Notargiacomo. Efficacy of oral intake of a compound medical device in the treatment of laryngopharyngeal reflux disease: a clinical investigation and nasal cytological correlations 185

X. Miao, LH. Wang, JH. Li, F. Xue and AP. Dong. High lncRNA DLEU1 predicts poor prognosis and promotes tumor progression by upregulating NUCKS1 through sponging miR-1286 in lung adenocarcinoma 193

Y-B. Shang, B. Qi, J. Wang, W-X. Hou and D. Zhou. A review on dry eyes in polycystic ovary syndrome patients 203

Y. Sun, C. Zhang, X-Q. Chen, X. Wang, C. Yuan and X-J. Chen. A case of combination of multiple interventional therapies: a potential indication of hepatocellular carcinoma treatment 207

M. Wei, L-X. Lu, B. Li, C-Y Li, Y. Zheng, J-K. Wang, P. Wang, L-W. Ren, X-H. Yu and J-C. Zhang. The promotion of the secretion of angiogenesis-related factors in hepatocellular carcinoma cells by macrophage migration inhibitory factor 213

G-Q. Yan, M-N. Dong, C-H. Zhang and M-W. Liu. Protective effect and mechanism of Baicalin on H9c2 cardiomyocyte inflammation induced by lipopolysaccharide by regulating the miR-181a-5p/HMGB1 axis 219

EDITORIAL

Contribution of mast cells in SARS-CoV-2-induced inflammation

G. Ronconi[1], C.E. Gallenga[2], Al. Caraffa[3], S.K. Kritas[4], I. Frydas[5], P. Conti[6], V. Calvisi[7] and M. Trimarchi[8]

[1]Clinica dei Pazienti del Territorio, Fondazione Policlinico Gemelli, Rome, Italy; [2]Department of Biomedical Sciences and Specialist Surgery, Section of Ophthalmology, University of Ferrara, Ferrara, Italy; [3]School of Pharmacy, University of Camerino, Camerino, Italy; [4]Department of Microbiology and Infectious Diseases, School of Veterinary Medicine, Aristotle University of Thessaloniki, Macedonia, Greece; [5]Aristotelian University, Thessaloniki, Greece; [6]Immunology Division, Postgraduate Medical School, University of Chieti, Pescara 65100, Italy [7]Department of Orthopedics, School of Medicine, L'Aquila, Italy; [8]Department of Medicine and Surgery, Centre of Neuroscience of Milan, University of Milan, Italy

COVID-19, which first appeared in China, has so far caused an unexpected number of deaths, as our immune system has not been able to annihilate the SARS-CoV-2 virus. SARS-CoV-2 reacts to both innate and acquired immunity. In the first instance, when the virus enters our organism, it is attacked by innate immune cells, including macrophages and mast cells (MCs), which produce defensive cytokines such as IL-1, IL-6, IL-33 and TNF; but the overproduction of these cytokines is very harmful to the patient. Here, in this editorial, we report that the inflammatory cytokine network established in COVID-19, in the most serious cases, can lead to the death of the patient. Therefore, it is pertinent to think that by blocking the pro-inflammatory cytokines that cause the "cytokine storm", a great therapeutical benefit can be achieved for COVID-19 disease.

In December 2019, a severe lung disease with respiratory syndrome induced by SARS-CoV-2 (coronavirus-2) appeared in Wuhan, China (1). A few months later, after so many people were infected, it was learned that it was a widespread pandemic that until today has not yet been eradicated.

COVID-19 pandemic, caused by severe acute respiratory syndrome coronavirus 2 (SARS-CoV-2), is potentially life-threatening and has affected almost all countries globally, but it is hoped that through vaccination, the situation will improve considerably (2). The serious pandemic that is taking place due to the SARS-CoV-2 infection that causes COVID-19 mainly affects the upper and lower respiratory tracts, causing pneumonia and death. COVID-19 has caused unexpected mortality among the elderly, adults and now also children, causing significant psychological stress and economic repercussions.

At the onset of SARS-CoV-2 infection, the virus is attacked by innate immune cells, including mast cells (MCs) and macrophages (3). SARS-CoV-2 infection induces an innate and adaptive immune response to protect the host. However, innate immune cells such as macrophages and mast cells (MCs), which are supposed to fight the virus, release an overproduction of pro-inflammatory cytokines with serious problems locally and systemically. Therefore, innate immunity is important for the clearance of the SARS-CoV-2 virus, but cells that generate it, such as macrophages and MCs, can contribute to the aggravation of

Keywords: *mast cell, inflammation, immunity, cytokine, cytokine storm, lung, SARS-CoV-2, COVID-19*

Corresponding author:
Professor Pio Conti,
Immunology Division,
Postgraduate Medical School,
University of Chieti-Pescara,
66013 Chieti, (CH), Italy
e-mail: pioconti@unich.it

0393-974X (2022)
Copyright © by BIOLIFE, s.a.s.
This publication and/or article is for individual use only and may not be further reproduced without written permission from the copyright holder.
Unauthorized reproduction may result in financial and other penalties
DISCLOSURE: ALL AUTHORS REPORT NO CONFLICTS OF INTEREST RELEVANT TO THIS ARTICLE.

COVID-19. The SARS-CoV-2 virus uses the ACE2 receptor, an angiotensin II peptidase, by activating pattern recognition receptor (PRR) signaling and DAMP-mediated signaling pathways.

The intervention of macrophages in the inflammatory processes induced by many chemical and biological compounds, including SARS-CoV-2, mainly causes the secretion of powerful pro-inflammatory cytokines of the IL-1 family in macrophages and MCs. IL-1, IL-6, TNF and IL-33 released by those cells produce an autocrine action on the inflammatory network. The overproduction of inflammatory cytokines can cause the so-called "cytokine storm", an excessive immune response that can end in fatal respiratory distress due to organ failure. Along with other immune cells, MCs are involved in the defence against viruses, including SARS-CoV-2 (4). In severe COVID-19, an accumulation of MCs in the lung tissue has been seen to cause edema, clotting and thrombosis.

The cytokine storm is considered the culmination of severe inflammation, such as that caused by SARS-CoV-2, which occurs with high concentrations of cytokines both systemically and in the tissues, together with high fever and many disrupted biological parameters. Removing the cause of this severe inflammatory phenomenon is certainly helpful in treating the disease and can be lifesaving. The main cytokines that intervene in the cytokine storm are IL-1, IL-6, TNF and IL-33, all produced after viral infection by macrophages and MCs. The immune and inflammatory response is manifested more severely when there is a high viral load, triggering the "cytokine storm". Furthermore, it should be noted that the host's unregulated innate and adaptive immune responses against SARS-CoV-2 depend on virulence, viral replication, and the number of cytokines produced by immune cells, including MCs.

Mast cells (MCs)

MCs arise from hematopoietic bone marrow cells that migrate and mature in vascularized tissues. They reside near blood vessels, epithelial, nerves, in the tissue of the airways, in the tissue of the gastrointestinal tract, and other strategic places in the body, where they can encounter and attack the external agents. MCs also reside in the central nervous system (CNS) and possess a series of receptors to recognise microbes that can induce neuroinflammation. Two populations of MCs are currently known in mice.

The first are CTMCs, of the connective tissue, which reside in the skin, peritoneum and gastrointestinal tract. The second are MMCs, belonging to the gastric mucosa, which contain low levels of histamine and heparin. MMCs are more active and increase in infectious processes. MCs contain numerous granules, a reservoir of chemical mediators, that can be released into the cellular environment seconds after an allergic stimulus. In adaptive immunity, Th2 cells and other immune cells produce IL-4, IL-5 and IL-13, which induce MC activation and IgE production, protecting the body from microbial invasion. Cytokines IL-17 and IL-22 activate phagocytes by triggering an innate immune response to microorganisms producing cytokines, including IL-1, TNF, and IL-33, that activate the MCs, inducing inflammatory processes without degranulation.

Therefore, MCs are involved in allergy and anaphylactic reactions when the IgE binds to its FceRI receptor, quickly causing aggregation and degranulation. They can also be activated by antigens of microorganisms, including viral ones, inducing the *de novo* synthesis (late release) of cytokines such as IL-1, IL-6, IL-33, and TNF. The immediate allergic activation system of MCs and the delayed one with the production of cytokines seem to be distinct and remain unclear. Shedding light on this topic could help in the therapy of the inflammatory process (5). Microorganisms such as SARS-CoV-2 activate TLR2 and TR4 of MCs, which selectively release pro-inflammatory cytokines, in turn activating PAR-2 on endothelial cells and causing increased vascular permeability, leukocyte recruitment and inflammation. MCs also have chemokine receptors that promote virus binding and are a source of cytokines and chemokines that can be induced by various inflammatory stimuli (6); therefore, it is pertinent to think that MCs intervene in SARS-CoV-2 infection where the innate and adaptive immune system is activated.

TNF

Inflammatory cytokines play an important role in

the pathogenesis of infections where they are produced nonspecifically. IL-1 and TNF act on different receptors, but in inflammation, they have a similar effect. In fact, IL-1 induces TNF and vice versa. TNF is released by LPS-stimulated macrophages and can lyse some types of tumor cells. During infection with SARS-CoV-2, there can be a high production of TNF in the tissues and circulation, causing hypotension and shock that can lead to death in the patient. Within activated MCs, TNF can be produced and secreted through two different pathways; one with the induction of the mRNA and protein synthesis (late release), and the other associated with degranulation (immediate release), as TNF is the only cytokine pre-formed and stored in the secretory granules of MCs.

TNF also plays a role in fighting against microorganisms, including SARS-CoV-2. In fact, in inflammatory infections, there is an increase in macrophages, which produce high levels of TNF, stimulating the recruitment of leukocytes into the inflammatory sites. In COVID-19, TNF is one of the factors that participate in the phenomenon of the "cytokine storm", which can be lethal for the patient (7).

IL-1

The IL-1 family cytokine influences both immunological and inflammatory processes. IL-1 has a receptor similar to TLR, which binds microorganisms, including viruses. IL-1, which is formed through the activation of caspase-1, is a dominant cytokine in innate immunity and induces inflammation by binding to its IL-1R receptor (8). Viruses and other microorganisms, including SARS-CoV-2, bind to TLR, inducing inflammation. SARS-CoV-2 induces IL-1 secretion via TLR, causing an inflammatory response.

The inflammatory effect of IL-1 and that induced through the TLR are very similar. Several pro-inflammatory cytokines are involved in the initial phase of severe COVID-19, including IL-1, which participates in the "cytokine storm". COVID-19, which can be fatal, can occur after SARS-CoV-2 infection, with an overproduction of cytokines, including IL-1. This effect can be systemic, but above all, it can affect the lung with serious consequences. Hence, IL-1 is a key cytokine in the inflammatory response induced by SARS-CoV-2, and its production is mainly due to virus-activated macrophages and MCs. Therefore, activated macrophages secrete IL-1, which stimulates MCs to produce IL-6 and TNF, which participate in the inflammatory pathogenic processes.

In severe COVID-19, the serum levels of IL-1 are significantly increased, as well as the pathological effects. The use of IL-1 blockers can prevent multiple organ failure, septic shock, and acute respiratory deficiency syndrome.

IL-33

IL-33 is produced by various cells, including macrophages and MCs, and is a ligand of the ST2 receptor (9). The pro-IL-33 matures into IL-33 and binds to the transmembrane receptor ST2, recruiting MyD88, which activates the factor 6 associated with the TNF receptor (TRAF6), and subsequently the NFkB, resulting in the production of cytokines and chemokines, as can be seen from Fig. 1. IL-33 is an important cytokine in inflammatory diseases, including COVID-19. IL-33, also called "alarmin", is a key cytokine in acute and chronic inflammation in COVID-19, where MCs play a crucial role. Moreover, this cytokine plays an important role in the pathology of various hypersensitivity diseases where MCs are the protagonists (10).

MCs release IL-33 into the virus-damaged and

TIR domain

PRO-IL-33→IL-33→ST2→----------→MyD88→IRAK4, TRAF6→IKbeta, p50, p65→NFkB→CYTOKINES/CHEMOKINES

Fig. 1. *IL-33 binds to its receptor, ST2, and regulates the transcription genes of cytokines and chemokines.*

inflamed lung, dysregulating immune Treg cells and causing dysfunction of the entire immune system. In COVID-19, IL-33 not only mediates the inflammatory process but can also be involved in pulmonary fibrosis by acting on epithelial cells and fibroblasts.

Upon exposure to the SARS-CoV-2 virus or other pathogens, MCs become activated and produce IL-33, triggering the immune response. SARS-CoV-2 induces MCs to produce IL-33, which promotes the maturation, activation and survival of the cells, and secretes various cytokines, including IL-6. Therefore, inhibition of IL-33 can help treat inflammatory diseases, including that generated by SARS-CoV-2.

IL-6

IL-6, which is part of the IL-6 family, is made up of 10 members with has various functions both in health and in inflammatory pathological states (11). The cellular IL-6 receptor (IL-6R) is composed of IL-6Rα and the signal transducer gp130. Because IL-6 is expressed in many cells, it can interact with various cell types (12). IL-6 correlates with the clinical severity of inflammatory diseases where plasma levels of this cytokine increase, and the patient is more likely to die from septic shock. Unlike IL-1 and TNF, IL-6 does not cause activation of arachidonic acid metabolites, such as prostaglandins and leukotrienes, nor does it induce hypotension. IL-6 is a pleiotropic cytokine, which like other cytokines released by macrophages, mediates the immune response and collaborates with IL-1 and TNF in inducing the "cytokine storm" in COVID-19 disease.

The transcription of IL-6 genes is induced by various factors, including TLR ligands, IL-1 and TNF. The synergy of NF-κB and STAT3 can result in the hyperactivation of NF-κB, causing the release of pro-inflammatory cytokines. IL-1, an activator of NFkB, induces the production of IL-6 and virus infection, causing a systemic increase of IL-6 secreted by MCs and macrophages. In the immune system, IL-6 favours the formation of plasma cell antibodies and the activation of IL-6Ra or gp130, leading to the formation of JAK, together with gp130 (13).

Macrophages, MCs, and other cell types produce IL-6, which participates in the COVID-19 disease and increases the CRP (C reactive protein) levels, contributing to inflammation. Lowering the levels of IL-6 in COVID-19 can be of great therapeutic benefit.

REFERENCES

1. Ackermann M, Verleden SE, Kuehnel M, et al. Pulmonary Vascular Endothelialitis, Thrombosis, and Angiogenesis in Covid-19. N Engl J Med 2020; 383(2):120-128.
2. Abrams EM, Szefler SJ. COVID-19 and the impact of social determinants of health. Lancet Respir Med. 2020; 8(7):659-661.
3. Theoharides TC, Conti P. COVID-19 and Multisystem Inflammatory Syndrome, or is it Mast Cell Activation Syndrome? J Biol Regul Homeost Agents. 2020; 34(5):1633-1636.
4. Conti P, Ronconi G, Caraffa A, et al. Induction of pro-inflammatory cytokines (IL-1 and IL-6) and lung inflammation by Coronavirus-19 (COVI-19 or SARS-CoV-2): anti-inflammatory strategies. J Biol Regul Homeost Agents. 2020; 34(2):327-331.
5. Contini C, Enrica Gallenga C, Neri G, et al A new pharmacological approach based on remdesivir aerosolized administration on SARS-CoV-2 pulmonary inflammation: A possible and rational therapeutic application. Med Hypotheses. 2020; 144:109876.
6. Kempuraj D, Selvakumar GP, Ahmed ME, COVID-19, Mast Cells, Cytokine Storm, Psychological Stress, and Neuroinflammation. Neuroscientist. 2020; 26(5-6):402-414.
7. Ribeiro Dos Santos Miggiolaro AF, da Silva Motta Junior J, Busatta Vaz de Paula C, et al. Covid-19 cytokine storm in pulmonary tissue: Anatomopathological and immunohistochemical findings. Respir Med Case Rep. 2020; 31:101292.
8. Cavalli G, Colafrancesco S, Emmi G, et al. Interleukin 1alpha: a comprehensive review on the role of IL-1alpha in the pathogenesis and treatment of autoimmune and inflammatory diseases. Autoimmun Rev. 2021; 20(3):102763.
9. Taracanova A, Tsilioni I, Conti P, et al. Substance P and IL-33 administered together stimulate a marked secretion of IL-1beta from human mast cells, inhibited by methoxyluteolin. Proc Natl Acad Sci U S A. 2018; 115(40):E9381-E9390.

10. Theoharides TC, Petra AI, Taracanova A, et al. Targeting IL-33 in autoimmunity and inflammation. J Pharmacol Exp Ther. 2015; 354(1):24-31.
11. Conti P, Kempuraj D, Di Gioacchino M, et al. Interleukin-6 and mast cells. Allergy Asthma Proc. 2002;23(5):331-5.
12. Conti P, Bartle L, Barbacane RC, Synergistic activation of serum amyloid A (SAA) by IL-6 and IL-1 in combination on human Hep 3B hepatoma cell line. Role of PGE2 and IL-1 receptor antagonist. Immunol Invest. 1995; 24(3):523-35.
13. Coomes EA, Haghbayan H.Interleukin-6 in Covid-19: A systematic review and meta-analysis. Rev Med Virol. 2020; 30(6):1-9.

Acute effects of n-3 polyunsaturated fatty acids (PUFAs) reducing tumor necrosis factor-alpha (TNF-α) levels and not lowering malondialdehyde (MDA) levels after anaerobic exercise

N. Ayubi[1], E. Yuniarti[2*], NW. Kusnanik[3], L. Herawati[4], PM. Indika[5], RY. Putra[6] and A. Komaini[5],

[1]Doctoral Program of Sport Science, Universitas Negeri Surabaya, Indonesia; [2]Faculty of Mathematics and Natural Science, Universitas Negeri Padang, Indonesia; [3]Faculty of Sport Science, Universitas Negeri Surabaya, Indonesia; [4]Departement of Physiology, Faculty of Medicine, Universitas Airlangga, Indonesia; [5]Faculty of Sport Science, Universitas Negeri Padang, Indonesia; [6]Faculty Islamic Economic and Business Studies, Universitas Islam Negeri Imam Bonjol, Padang, Indonesia

Received November 3, 2021 – Accepted February 11, 2022

This study aimed to analyze the acute effect of n-3 PUFA on TNF-α and MDA levels after anaerobic exercise. This experimental study involved 16 healthy adult men randomly selected with a BMI range of 19.00-24.00, and age ranged from 20-30 years. Subjects were selected randomly and then divided into 2 groups: group K1 using placebo and group K2 using n-3 PUFAs at a dose of 540 mg EPA and 360 DHA. The intervention was carried out 24 hours after the research subjects completed the anaerobic exercise. The data in this study were TNF-α levels measured using a human ELISA kit, and MDA was measured using a spectrophotometer taken before and after the intervention. The test of different levels of TNF-α in K2 ($p<0.05$) p=0.027, K1 ($p>0.05$) p=0.327, so that n-3 PUFAs significantly reduced TNF-α levels and the test of different levels of MDA in the group K2 ($p> 0.05$) p = 0.511, K2 ($p> 0.05$) p = 0.541 so that n-3 PUFAs did not significantly reduce MDA levels. Thus, it can be concluded that the administration of n-3 PUFAs has been shown to reduce TNF-α levels without a decrease in Malondialdehyde (MDA) levels after anaerobic exercise.

Anaerobic exercise with high intensity causes metabolic stress in the form of energy deficiency and muscle damage called Exercise Injured Muscle Damage (EIMD) (1). Uncontrolled muscle damage in the recovery phase causes Delayed Onset Muscle Soreness (DOMS) (2). DOMS will trigger the inflammatory process so that tumor necrosis factor-alpha TNF-α in the blood will increase because the response has occurred muscle damage (3). In addition, physical exercise triggers an increase in oxygen consumption by up to 10 times compared to at rest (4). As a result of metabolic processes, cells will produce free radicals or reactive oxygen species (ROS). Free radicals are characterized by increased malondialdehyde (MDA) (5). In addition to aerobic exercise, which generally triggers free radicals, anaerobic exercise that involves less oxygen circulation can also cause oxidative stress that triggers the increased production of free radicals through the xanthine oxidase and NADPH oxidase pathways, ischemia-reperfusion, increased purine oxidation, damage to iron-containing proteins, impaired Ca2+

Keywords: n-3 PUFAs, TNF-α, MDA, anaerobic exercise

*Corresponding author:
Dr. Elsa Yuniarti,
Jl. Prof. Dr. Hamka,
Air Tawar Barat, Padang City,
West Sumatra, Indonesia
e-mail: dr_elsa@fmipa.unp.ac.id

0393-974X (2022)
Copyright © by BIOLIFE, s.a.s.
This publication and/or article is for individual use only and may not be further reproduced without written permission from the copyright holder.
Unauthorized reproduction may result in financial and other penalties
DISCLOSURE: ALL AUTHORS REPORT NO CONFLICTS OF INTEREST RELEVANT TO THIS ARTICLE.

homeostasis and catecholamine autooxidation (5). Increased production of free radicals will also cause muscle damage (4).

The management of post-exercise DOMS uses pharmacological modalities; an estimated 30 million people worldwide who take non-steroidal anti-inflammatory drugs are very common in athletes and people who do high physical activity (6); this will certainly have a major impact on health and muscle growth (7). In addition, the increase in free radicals can lead to degenerative diseases such as cancer, diabetes mellitus and atherosclerosis, which are the causes of heart disease. It is estimated that as many as 17 million people worldwide die each year due to degenerative diseases. Several countries in the world, such as Brazil, Canada, China, India, Nigeria, Pakistan, Russia, England and Tanzania, have an incidence of death from degenerative diseases reaching 80% (5).

Solutions need to be found to overcome these problems; one way to reduce TNF-α production and excessive free radical production is by consuming one of the natural products derived from fish oil, namely n-3 Polyunsaturated Fatty Acids (PUFAs). The ingredients contained in n-3 PUFAs are α-linolenic acid (ALA), eicosapentaenoic acid (EPA), and docosahexaenoic acid (DHA) (7). n-3 PUFAs are also known for their anti-inflammatory properties (7).

Role of n-3 PUFAs in inhibiting inflammation through blockade of TNF-α signaling by activating protein responses in muscle (3). on the other hand, n-3 PUFAs play a role in suppressing pro-oxidant activity by increasing heme oxygenase 1 (HO-1) and glutathione peroxidase (GPx) genes (8).

Based on this, the study was designed to investigate the acute effect of n-3 PUFA on TNF-α and MDA after anaerobic exercise. It is hoped that this study can be a guideline to overcome the production of uncontrolled levels of TNF-α and MDA levels after anaerobic exercise.

MATERIAL AND METHODS

Participants and procedure

This research uses experimental research with pre and post control group design. This study involved 16 healthy adult men who were randomly selected with a BMI range of 19.00-24.00, age ranged from 20-30 years, and not currently taking non-steroidal anti-inflammatory drugs. The following procedure was used in the study:

Informed consent was filled out by the research subjects.

A randomized sample was created by dividing the participants into two groups: group 1 (K1) as a placebo group and group 2 (K2) as a group of n-3 PUFAs.

Subjects did anaerobic exercise (weight training) with high intensity ranging from 80-90% of maximum ability, performed 4 sets, 10 repetitions and recovery between sets of approximately 60 seconds.

Twenty-four hours after anaerobic exercise, pre-test blood samples were taken for analysis in the laboratory; then intervention was given to the subject. The intervention was given according to the group at the same time. K1 was given a placebo, and K2 was given n-3 PUFA with a dose of 540 mg EPA and 360 DHA.

Twenty-four hours after the intervention, a post-test blood sample was taken again, which would later be analyzed in the laboratory.

Instruments

Measurement of serum TNF-α levels were obtained using the Human TNF-α ELISA kit and the measurement of serum MDA levels using a spectrophotometer.

Statistical Analysis

Statistical analysis was carried out using SPSS application with Paired t-test and Independent t-test method.

RESULTS

In the Mann Whitney U difference test, there were no significant differences in the characteristics of the research subjects between the two research groups, so if there were differences at the end of the intervention, it could be ascertained that they were not due to the characteristics of the study.

Based on the normality test (Table II and III), data on the levels of TNF-α (Pre-test) and TNF-α (Post-test) in K1 and K2 showed data ($p<0.05$), meaning that the data was not normal. The delta data of TNF-α levels in K1 and K2 showed ($p>0.05$) so that the data were normally distributed. Then, based on the normality test of the data on the MDA (pre-test), (post-test), the deltas on K1 and K2 show ($p>0.05$)

so that the distribution is normal.

The test of different levels of TNF-α in K2 ($p<0.05$) $p=0.027$, K1 ($p>0.05$) $p=0.327$, so that n-3 PUFAs significantly reduced TNF-α levels and the test of different levels of MDA in the group K2 ($p> 0.05$) $p = 0.511$, K2 ($p> 0.05$) $p = 0.541$ so that n-3 PUFAs did not significantly reduce MDA levels. Thus, it can be concluded that the administration of n-3 PUFAs

Table I. *Characteristics of research subjects*

Characteristics	Group	n	x̄±SD	Shapiro-Wilk	p *(Mann Whitney u-test)*
Age	K1	8	21.63±4.20	0.000	0.251
	K2	8	24.63±6.67	0.009	
Height	K1	8	166.50±3.81	0.003	0.164
	K2	8	168.13±3.72	0.497	
Weight	K1	8	61.63±5.50	0.242	0.864
	K2	8	61.06±7.61	0.878	
BMI	K1	8	22.18±1.92	0.382	0.640
	K2	8	21.58±2.98	0.347	
Systolic	K1	8	107.50±8.86	0.054	0.242
	K2	8	112.50±7.07	0.056	
Diastolic	K1	8	71.52±6.40	0.037	0.424
	K1	8	73.75±5.17	0.000	

Table II. *Mean and standard deviation of TNF-α and MDA level in both groups*

Data	Group	n	Levels (ng/mL) *(pre-test)* x̄±SD	*(post-test)* x̄±SD	(Delta) x̄±SD
TNF-α	K1	8	5.24±2.98	4.67±2.84	0.56±0.44
	K2	8	4.45±1.16	4.81±1.71	0.64±0.54
MDA	K1	8	292.43±12.58	296.33±12.37	13.32±10.45
	K2	8	255.77±27.22	249.66±19.00	18.33±16.80

Table III. *Results of the normality test for TNF-α and MDA levels*

Data	Group	n	Shapiro-Wilk P
TNF-α (*Pre-test*)	K1	8	0.001
	K2	8	0.004
TNF-α (*Post-test*)	K1	8	0.000
	K2	8	0.011
Delta TNF-α	K1	8	0.375
	K2	8	0.287
MDA (*Pre-test*)	K1	8	0.196
	K2	8	0.315
MDA (*Post-test*)	K1	8	0.874
	K2	8	0.392
Delta MDA	K1	8	0.634
	K2	8	0.077

Table IV. *Results of Different Tests for TNF-α and MDA Levels*

Data	Different Test Method	Group	P
TNF-α	Wilcoxon Signed Ranks Test	K1 (pre-test and post-test)	0.327*
		K2 (pre-test and post-test)	0.027
	Independent t-test	Delta K1 and K2	0.768*
MDA	Pairet t-test	K1 (pre-test and post-test)	0.541*
		K2 (pre-test and post-test)	0.511*
	Independent t-test	Delta K1 and K2	0.468*

*$p>0.05$

has been shown to reduce TNF-α levels without a decrease in Malondialdehyde (MDA) levels after anaerobic exercise (Table IV).

DISCUSSION

The results of this study proved that K1 with placebo administration did not significantly reduce TNF-α levels after anaerobic exercise, while K2 with n-3 PUFAs administration could significantly reduce TNF-α levels after anaerobic exercise; this is confirmed by research carried out by Hedayatpour, Izanloo Falla, Kawamura and Muraoka, 2018 (1) that the administration of omega 3 (n-3 PUFAs) in 54 hemodialysis patients for 6 consecutive months can reduce TNF-α levels.

Anaerobic exercise with high intensity causes metabolic stress in the form of energy deficiency and muscle damage (1). Uncontrolled muscle breakdown in the recovery phase causes DOMS (2). DOMS can occur with many complex factors combined after exercise-induced muscle damage. The inflammatory response will occur after the morphological damage caused by the eccentric contraction. Cytokines are released in the damaged muscle, when inflammatory cells such as neutrophils and macrophages are more active. Inflammatory mediators are released, namely proinflammatory cytokines such as TNF-α and IL-6 and anti-inflammatory cytokines such as IL-10. Increased TNF-α in the blood will trigger an inflammatory process that will cause muscle pain in response to muscle damage. One of the efforts to reduce TNF-α overproduction) is giving n-3 PUFAs. n-3 PUFAs are known for their anti-inflammatory properties (9). n-3 PUFAs can inhibit inflammation by blocking TNF-α signaling by activating protein responses in muscle (10).

The results of this study proved that K1 with placebo administration and K2 with n-3 PUFAs did not significantly reduce malondialdehyde (MDA) levels after anaerobic exercise. Free radicals are characterized by increased MDA production; uncontrolled free radicals will cause muscle damage (2).

There are pros and cons to several studies of the effects of n-3 PUFAs on MDA levels. On research, Ateya et al., 2017 (8) reported that administration of n-3 PUFAs in 49 pediatric patients with kidney disease for 6 months at a dose of 1 gram for 6 months reduced markers of oxidative stress such as MDA. In addition, research Pooya et al., 2010 (11) reported that administration of n-3 PUFAs in 81 type-2 diabetic patients for 2 months only reduced hemocysteine levels without a decrease in MDA and C-Reactive protein (CRP). Research Vaagenes et al., 1998 (12) reported that administration of n-3 PUFAs at low doses (250 mg/day) in rats had no effect on decreasing MDA levels. The findings in this study reported that acute administration of n-3 PUFAs at high doses (1000 mg) did not decrease MDA levels after anaerobic exercise.

Acute effect of n-3 PUFAs was shown to reduce the level of TNF-α without a decrease in the level of MDA after anaerobic exercise.

Ethics statement:

This research was approved by the ethics committee of Universitas Airlangga with registration number No. 179/EC/KEPK/FKUA/2020.

REFERENCES

1. Hedayatpour N, Izanloo Z, Falla D. The effect of

eccentric exercise and delayed onset muscle soreness on the homologous muscle of the contralateral limb. J Electromyogr Kinesiol 2018; 41:154-159.
2. Ko GWY, Clarkson C. The effectiveness of acupuncture for pain reduction in delayed-onset muscle soreness: a systematic review. Acupunct Med 2020; 38(2):63-74
3. Calder PC, Albers R, Antoine JM, et al. Inflammatory disease processes and interactions with nutrition. Br J Nutr 2009, 101(S1):S1-45.
4. Morales M, Munné-Bosch S. Malondialdehyde: Facts and artifacts. Plant Physiol 2019; 180(3):1246-50.
5. Powers SK, Radak Z, Ji LL. Exercise-induced oxidative stress: past, present and future. J Physiol 2016; 594(18):5081-92.
6. Schoenfeld BJ. The use of non-steroidal anti-inflammatory drugs for exercise-induced muscle damage: Implications for skeletal muscle development. Sport Med 2012; 42(12):1017-28.
7. Ayubi N, Sastika Putri DR. Aerobic Exercise and Omega 3 Supplementation to Reduce Primary Dysmenorrhea (Literature Review). Indian J Forensic Med Toxicol 2021; 15(3 SE-):1413-17.
8. Ateya AM, Sabri NA, El Hakim I, Shaheen SM. Effect of Omega-3 Fatty Acids on Serum Lipid Profile and Oxidative Stress in Pediatric Patients on Regular Hemodialysis: A Randomized Placebo-Controlled Study. J Ren Nutr 2017; 27(3):169-174
9. Fritsche KL. The Science of Fatty Acids and Inflammation. Adv Nutr 2015; 6(3):S293-301.
10. Babcock TA, Novak T, Ong E, Jho DH, Helton WS, Espat NJ. Modulation of lipopolysaccharide-stimulated macrophage tumor necrosis factor-α production by ω-3 fatty acid is associated with differential cyclooxygenase-2 protein expression and is independent of interleukin-10. J Surg Res 2002; 107(1):135-9.
11. Pooya S, Jalali MD, Jazayery AD, Saedisomeolia A, Eshraghian MR, Toorang F. The efficacy of omega-3 fatty acid supplementation on plasma homocysteine and malondialdehyde levels of type 2 diabetic patients. Nutr Metab Cardiovasc Dis 2010; 20(5):326-31.
12. Vaagenes H, Muna ZA, Madsen L, Berge RK. Low doses of eicosapentaenoic acid, docosahexaenoic acid, and hypolipidemic eicosapentaenoic acid derivatives have no effect on lipid peroxidation in plasma. Lipids 1998; 33(11):1131-7.

Deranged growth factors as a prognosticator of cardiovascular risks in patients with uterine fibroids

S. Bokhari[1,3], S. Ahmad[2], U. Rafi[1,3], MA. Iqbal[1], MA Khan[3] and N. Roohi[1*]

[1]Institute of Zoology, Physiology/Endocrinology Laboratory, University of the Punjab, Lahore, Pakistan; [2]King Edward Medical University, Lahore, Pakistan; [3]Department of Biology, Lahore Garrison University, Lahore, Pakistan

Background: **Angiogenesis is a crucial factor for the pathogenesis and growth of fibroids. Among various growth factors, transforming growth factor (TGFβ1) and vascular endothelial growth factor (VEGF) are up-regulated in leiomyomas and have angiogenic as well as pro-atherogenic properties. Subsequently, their elevated values may be involved in developing cardiovascular disorders.**

Objective: **The current study was planned to evaluate the role of growth factors in females with uterine fibroids and investigate the future risks of developing cardiovascular disorders (CVD) in these patients.**

Method: **Eighty-two subjects of uterine fibroids and eighty-two healthy controls were selected from tertiary care hospitals. Enzyme-linked immunosorbent assay (ELISA) was utilized to assess growth factors. Results: The levels of TGFβ1 and VEGF were significantly higher ($P < 0.001$) in patients with uterine fibroids compared to healthy females without uterine fibroids.**

Conclusion: **High levels of circulating growth factors in patients with uterine fibroids prognosticate (CVD) events in these patients.**

Uterine fibroids (UF), or leiomyomas, are commonly described as benign tumors afflicting women reproductive system, and they usually disturb the working of the uterine area by causing profuse bleeding, anemia, infertility, faulty embryo's implantation, repeated abortion, early labour, difficulty in parturition process, pelvic distress and inability to control urine (1).

Uterine fibroids show themselves as vascularized capsules. More in detail, they consist of structures containing fibroblasts connective tissue and smooth muscle cells with a hypoxic and avascular core (2). Although UF may differ greatly in appearance, location, and size even in the same uterus. The fibroids' expressions of angiogenic factors, such as vascular endothelial growth factor (VEGF) and transforming growth factor (TGFβ1), are up-regulated. VEGF has higher levels in uterine fibroids (3, 4), and TGF-β1 levels are found to be doubled in UF patients in comparison to the control group (5).

VEGF is a vital growth factor; it binds to the associated receptors; after that, it triggers the proliferation of vascular endothelial cells and then migration (6), thus causing angiogenesis (7). The decrease in angiogenic balance within the fibroids is believed to play a role in vascular growth (2). Vascularization and angiogenesis are well-known processes responsible for fibroid growth and maintenance (2). Angiogenesis consists of developing new blood vessels that take place in both normal and diseases situations. New vessels are generated from endothelial progenitor cells (EPC) or existing vasculature in normal conditions. There are

Keywords: VEGF, TGFβ1, Uterine Fibroids, CVD

Corresponding author:
Dr Nabila Roohi
Institute of Zoology, Physiology/Endocrinology Laboratory,
University of the Punjab,
Lahore, Pakistan
e-mail: nabila.physiol@gmail.com

0393-974X (2022)
Copyright © by BIOLIFE, s.a.s.
This publication and/or article is for individual use only and may not be further reproduced without written permission from the copyright holder.
Unauthorized reproduction may result in financial and other penalties
DISCLOSURE: ALL AUTHORS REPORT NO CONFLICTS OF INTEREST RELEVANT TO THIS ARTICLE.

switches like "on" and "off" for the stimulation and inhibition of the angiogenic process present in the healthy body to regulate angiogenesis (8). However, due to deregulated angiogenic process, functionally abnormal structures are produced. Angiogenesis is multifactorial, involving growth factors, intracellular signaling molecules, extracellular matrix components, and membrane-bound receptors (9).

Angiogenesis starts with the enhancement of vascular permeability followed by the proteolytic breakdown of the nearby ECM. After that, endothelial cells chemotactically migrate and proliferate, the lumen is formed, and the newly developed capillary becomes functionally mature as inter endothelial cell junctions are tightened. Moreover, the thickening of intima would result from the up-regulation of VEGF (proangiogenic growth factors) in the wall of the vessel (10). Furthermore, abundant expression of VEGF and TGF-β1, in addition to other angiogenic factors, in human atherosclerotic lesions showed their angiogenic and pro atherosclerotic properties (11). Similarly, positive associations between cardiovascular disease (CVD) and VEGF (12) and TGFβ1 and CVD (13) were observed.

TGF-β1 plays pleiotropic roles in angiogenesis and vasculogenesis, and thus, it maintains homeostasis of the vascular system through its binding to a TGF-β1 receptors complex exhibited by endothelial cells. The signaling by these receptors depends on the situation where TGF-β1 can either suppress or promote endothelial permeability, proliferation, migration, and sprouting. TGF-β1 being the essential mediator of angiogenesis, performs conflicting roles conditional to the progression phase in cardiovascular syndromes (10).

TGF-β1 is also an important growth factor and is a potent chemoattractant for macrophages and fibroblasts (14). It inhibits the division of some cells, induces apoptosis, and affects the development of ECM (15). TGFβ1 is found in endothelial cells, macrophages, myofibroblasts, vascular smooth muscle cells (VSMCs), and other hematopoietic cells (13). Former researchers have mentioned a close relationship between the TGF-β1 instigation and prognosis of CVD (16), cardiac fibrosis (17), atherosclerosis (18), cardiac hypertrophy (19) resulting in restenosis, and cardiac failure (20). In addition, VEGF, along with TGFβ1, mediates angiogenesis through the increasing permeability of endothelial cells (21).

Since both the growth factors, i.e. vascular endothelial growth factors and transforming growth factors, are involved in the angiogenesis, which is critical for developing UFs and CVD. Therefore, the following study has been designed to evaluate the role of these growth factors as possible indicators of CVD in patients with uterine fibroids.

MATERIALS AND METHODS

The survey was conducted in a local tertiary care hospital to locate subjects with uterine fibroids with the assistance of gynecologists. Eighty-two reproductive-aged women (18–50 years) with fibroids (1–5 years) were randomly selected from the hospital's outpatient gynecological department. In addition, control subjects with and without a family history of uterine fibroid were identified in the same survey. A total of eighty-two women who appeared to be in good health were also enrolled as age-matched controls. The subjects were divided into groups based on the severity of the disease. The study was approved by the hospital's Ethics and Protocol Review Committee. All of the subjects willingly participated in the investigation.

Because UF may shrink or disappear due to menopause, postmenopausal subjects who had not had a menstrual cycle in the previous 12 months, as reported in their medical records, were excluded.

Women under 18-years-of-age, patients with hypertension, diabetes mellitus, thyroid disease, using hormonal therapy, and those with a family history of hyperlipidemia were also excluded from the study. Both groups were considered eligible when the following conditions were met: 1) Women with no acute, hormonal, or neoplastic conditions, 2) between the ages of 18 and 50, and 3) who were not pregnant or breastfeeding at the time of the study. After getting the informed consent from the participants, all of the subjects were interviewed to fill out the designed proforma. In addition, several physical parameters, such as blood pressure, body weight, and height, were measured at the time of venipuncture.

Later, blood samples from the same subjects were drawn with the assistance of registered technicians, processed for plasma and serum collection, and stored

at -80°C until used for further biochemical analysis. A quantity of blood equal to 5cc blood was drawn from all subjects via venipuncture; 5cc blood was drawn from each subject using a sterilized disposable syringe and placed in a serum vacutainer. On the person's identification badge, the patient's date and the time of his phlebotomy were noted in the logbook (the blood tubes were marked). Blood samples were centrifuged at 3000 rpm for 10 min. Separated serum was placed in autoclaved cryovials and stored at -80°C until further processing.

The growth factors VEGF and TGF ß1 were analyzed with ELISA kits (cat#PRS-01603hu, cat #PRS 01541hu, respectively) of Glory science Co, Ltd USA. Mindray Mr-96a ELISA microplate reader was used for Growth factors assessment in Physiology laboratory, Institute of Zoology, University of the Punjab, Lahore, Pakistan. All the data collected about different parameters, as mentioned in (Table I) were statistically analyzed and interpreted utilizing Graph Pad Prism version 6 software. Unpaired Student *t*-test was applied to compare the groups.

RESULTS

The serum level of TGF ß1 average in patients with uterine fibroids is equal to 330 ± 10 pg/mL, which is significantly higher ($P < 0.001$) if compared to the healthy control group in which the serum level of TGF ß1 average is equal to 140 ± 3.5 pg/mL (Fig. 1).

In subjects with uterine fibroids, the serum level of VEGF average was found to be equal to 0.40 ± 0.01 ng/mL, which was significantly higher ($P < 0.001$) in comparison to the value found in the control group in which it was equal to 0.25 ± 0.01 ng/mL (Fig. 2).

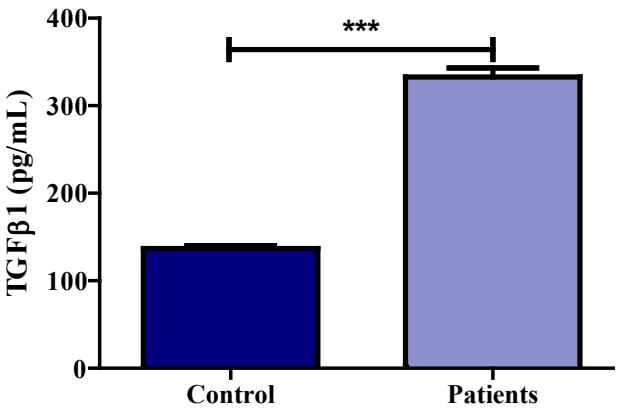


Fig. 1. *Comparison of TGFβ1 (pg/mL) in controls and patients. Value is Mean± SEM, ***significant at P ≤ 0.001.*

Table I. *Descriptive characteristics, VEGF and TGF β1 in the control group and Uterine Fibroid patients*

Parameters	Control N=82	Patients N=82	*P*-value	% age difference
Age (years)	35 ± 0.75	36 ± 0.71	0.06	↑2.8%
Weight (Kg)	64 ± 1.4	65 ± 1.4	0.5	↑1.56%
Height (m)	1.6 ± 0.006	1.6 ± 0.009	0.2	NS
BMI (Kg/m^2)	23 ± 0.40	24 ± 0.45	0.1	NS
SBP (mmHg)	120 ± 1.5	120 ± 1.6	< 0.001	NS
DBP (mmHg)	76.02 ± 1.38	76.93 ± 1.19	< 0.002	NS
TGF ß1(pg/mL)	140 ± 3.5	330 ± 10	< 0.001	↑135%
VEGF (ng/mL)	0.25 ± 0.01	0.40 ± 0.01	< 0.001	↑60%

****indicate significance at P < 0.0001, TGF 1= Transforming growth factor 1, VEGF= Vascular endothelial growth factor, BMI = Body mass index, SBP= Systolic Blood Pressure, DBP= Diastolic Blood Pressure, ↑ increase*

DISCUSSION

TGF-β1 and VEGF are growth factors that, along with their receptors, are involved in the development and progression of leiomyoma (22). In particular, VEGF has also been shown to promote angiogenesis in leiomyoma (23), and TGF-β1 too, being involved in angiogenesis is differentially expressed in leiomyoma compared with myometrium (2).

Elevated levels of TGF-β1 have been observed in the patients' group compared to the control one. The growth factor TGF-β1 is responsible for the pathophysiology of UF (24, 25) and is a vital element that promotes cellular movement within the tumor and is also involved in the increase in metabolism and size of the tumor. TGF-β1 regulates the expression and growth of uterine smooth muscle and UFs. TGF-β expression in the smooth muscle of the uterus, which is in direct contact with the fibroid, is significantly increased, as demonstrated in laboratory studies (26, 27).

TGF-β1 triggers the ECM production and enhances the formation of early fatty streak lesions (28). It also lowers the formation of collagenase and promotes the MMPs expression, which leads to the reduction of the degradation process of ECM and, finally, to a disproportionate accumulation of ECM (17, 29). Moreover, TGF-β1 can also enhance collagen production by Vascular smooth muscle cells (VSMCs). (30). Though TGF-β1 has further been suggested to affect plaque maintenance in both ways, positively or negatively (31). TGF-β1 also mediates vascular fibrosis induced by various stress factors of cardiovascular disease (32).

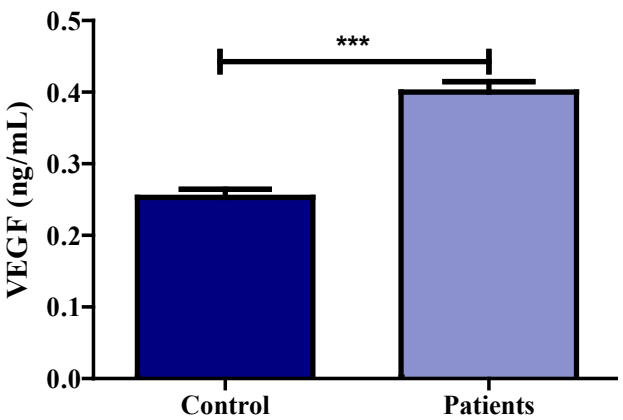


Fig. 2. *Comparison of VEGF (ng/mL) in controls and patients. Value is Mean± SEM, ***significant at P ≤ 0.001.*

Moreover, it has been reported that TGF-β1 expression changes cardiac myocyte's differentiation and gene expression, stimulating fetal contractile proteins (33). Overexpression of TGFβ1 shows cardiac hypertrophy due to interstitial fibrosis and hypertrophic growth of cardiomyocytes in transgenic mice (34).

It has been revealed that TGF-β1 maturation and, in turn, reduction in arterial diameter is controlled by ECM protein emilin1 related to elastic matrix myofibrils in the aortic media. Emilin1 binds only immature pro-TGFβ and prevents its maturation by the protein convertase furin. Therefore, a lack of Emilin1 would result in augmentation in TGF-β1 signaling because more pro-TGF-β1 are converted to mature TGF-β1 (35). Consequently, the acceleration in the TGF-β1 signaling pathway would lead to a reduced arterial lumen diameter and, resultantly, to increased vascular resistance (36). Furthermore, premature cytostasis of VSMCs is the outcome of abundant levels of TGF-β1, and all this leads to the suppression in the expansion of the arterial wall (37). Various studies have also documented that several components of the TGF-β family act as prognostic markers for CVD (13). After angioplasty, the chance of restenosis in patients with elevated levels of TGF-β1 in their blood is enhanced (38, 13).

TGF-β1 is produced and released into the ECM in an inactive form, and it is activated by thrombospondin-1, plasmin, acidic microenvironments, matrix metalloproteinases (MMPs) (17). In addition, TGF-β1 mRNA expression in VSMCs is enhanced by angiotensin II (Ang II), promoting its conversion to the biologically active form (39).

Raised levels of VEGF have been seen in subjects with uterine fibroid compared to control ones, indicating the possible risk of CVD in the future since VEGF is suggested to have pro-atherosclerotic and angiogenic characteristics (11). In addition, VEGF was positively related to cardiovascular disease (12) and is one of the best-known cytokines causing angiogenesis and neovascularization, both in inflammatory diseases and cancer (40).

In addition, VEGF causes the proliferation of endothelial cells in both conditions, either normal or diseased (41), increasing vascular permeability (42). Normally VEGF mediates angiogenesis in the development of an embryo and in the healing of wounds in the adults and in the case of cancer, where its secretion is up-regulated by several growth factors, oncogene expression and hypoxia. A tumor to grow in size needs a supply of nutrients and oxygen. New vasculature is required. More VEGF and other growth factors are produced by the tumor, causing the exponential growth of the tumor. New blood vessels will be formed, but the vessels formed by this process under the influence of VEGF are abnormal both structurally and functionally, hemorrhagic and leaky too, increasing interstitial pressure, resulting in the suboptimal flow of blood to the tumor leading to hypoxia and further VEGF formation. Due to the angiogenic and pro-atherosclerotic properties of VEGF, it is the main rational target in antitumor and anti-atherogenic therapies (43).

The etiopathology of uterine fibroids remains unclear, multifactorial, and enigmatic; in any case, it is characterized by excessive ECM production, high concentrations of chemokines, cytokines, and growth factors that play a key role in the development and progression of the disease. Growth factors such as VEGF and TGF-β1 cause the growth of fibroids, and, in addition, they are involved in the progression of atheromatous lesions and plaque formation through the process of angiogenesis and vascularization. So, the raised levels of these two growth factors may be the possible indicators of CVD in future in patients with uterine fibroids.

Conflict of interest:

There is no conflict of interest among the authors of the present investigation.

REFERENCES

1. Bar-Joseph H, Hikri E, Chuderland D, et al. Pigment epithelium derived factor as a novel multi-target treatment for uterine fibroids. Reprod Biomed Online 2020; 41(2):335-342.
2. Tal R, Segars JH. The role of angiogenic factors in fibroid pathogenesis: potential implications for future therapy. Human Reprod Update 2014; 20(2):194-216.
3. Hague S, Zhang L, Oehler MK, et al. Expression of the hypoxically regulated angiogenic factor adrenomedullin correlates with uterine leiomyoma vascular density. Clin Cancer Res 2000; 6(7):2808-2814.
4. Gentry CC, Okolo SO, Fong LF, et al. Quantification of vascular endothelial growth factor-A in leiomyomas and adjacent myometrium. Clin Sci 2001; 101(6):691-695.
5. Zeyneloglu HB, Esinler I, Ozdemir BH, et al. Immunohistochemical characteristics of intramural leiomyomata that enlarge during controlled ovarian hyperstimulation for in vitro fertilization. Gynecol Obstet Invest 2008; 65(4):252-257.
6. Mu Y, He J, Yan R, et al. IGF-1 and VEGF can be used as prognostic indicators for patients with uterine fibroids treated with uterine artery embolization. Exp Ther Med 2016; 11(2):645-649.
7. Pourgholami MH, Morris DL. Inhibitors of vascular endothelial growth factor in cancer. Cardiovasc Hematol Agents Med Chem 2008; 6(4):343-347.
8. Hanahan D, Folkman J. Patterns and emerging mechanisms of the angiogenic switch during tumorigenesis. Cell 1996; 86(3):353-364.
9. Modi H, Shrimanker M, Patel K, et al. Angiogenesis in cardiovascular disease: a review. IJPSR 2012; 3(9):3045-3057.
10. Doyle B, Caplice N. Plaque neovascularization and antiangiogenic therapy for atherosclerosis. J Am Coll Cardiol 2007; 49(21):2073-2080.
11. Taimeh Z, Loughran J, Birks EJ, Bolli R. Vascular endothelial growth factor in heart failure. Nat Rev Cardiol 2013. 10(9):519-30.
12. Kaess BM, Preis SR, Beiser A, et al. Circulating vascular endothelial growth factor and the risk of cardiovascular events. Heart 2016. 102(23):1898-1901.
13. Aihara KI, Ikeda Y, Yagi S, et al. Transforming growth factor-β1 as a common target molecule for development of cardiovascular diseases, renal insufficiency and metabolic syndrome. Cardiol Res Pract, 2011:175381.
14. Chegini N. Proinflammatory and profibrotic mediators: principal effectors of leiomyoma development as a fibrotic disorder. Semin Reprod Med 2010; 28(3):180-203.

15. Massagué J. TGFβ signalling in context. Nat Rev Mol Cell Biol 2012; 13(10):616-630.
16. Qiu H, Liu W, Lan T, et al. Salvianolate reduces atrial fibrillation through suppressing atrial interstitial fibrosis by inhibiting TGF-β1/Smad2/3 and TXNIP/NLRP3 inflammasome signaling pathways in post-MI rats. Phytomedicine 2018. 51: 255-265.
17. Leask A, Abraham DJ. TGF-β signaling and the fibrotic response. FASEB J 2004; 18(7):816-827.
18. Harradine KA, Akhurst RJ. Mutations of TGFß signaling molecules in human disease. Ann Med 2006; 38(6):403-414.
19. Rizzi E, Ceron CS, Guimaraes DA, et al. Temporal changes in cardiac matrix metalloproteinase activity, oxidative stress, and TGF-β in renovascular hypertension-induced cardiac hypertrophy. Exp Mol Pathol 2013; 94(1):1-9.
20. Osadnik T, Strzelczyk JK, Regula R, et al. The relationships between polymorphisms in genes encoding the growth factors TGF-β1, PDGFB, EGF, bFGF and VEGF-A and the restenosis process in patients with stable coronary artery disease treated with bare metal stent. PLoS One 2016; 11(3):e0150500.
21. Hicklin DJ, Ellis LM. Role of the vascular endothelial growth factor pathway in tumor growth and angiogenesis. J Clin Oncol 2005; 23(5):1011-1027.
22. Ciarmela P, Islam S, Reis FM, et al. Growth factors and myometrium: biological effects in uterine fibroid and possible clinical implications. Hum Reprod Update 2011; 17(6):772-790.
23. Arita S, Kikkawa F, Kajiyama H, et al. Prognostic importance of vascular endothelial growth factor and its receptors in the uterine sarcoma. Int J Gynecol Cancer 2005; 15(2):329-36.
24. Balun SE. Uterine fibroids. N Engl J Med 2013; 369(14):1344-55.
25. Lee BS, and Nowak RA. Human leiomyoma smooth muscle cells show increased expression of transforming growth factor-β3 (TGFβ3) and altered responses to the antiproliferative effects of TGFβ. J Clin Endocrinol Metab 2001; 86(2):913-920.
26. Arici A, Sozen I. Expression, menstrual cycle-dependent activation, and bimodal mitogenic effect of transforming growth factor-β1 in human myometrium and leiomyoma. Am J Obstet Gynecol 2003:188(1):76-83.
27. Halder SK, Osteen KG, Al-Hendy A. 1, 25-dihydroxyvitamin d3 reduces extracellular matrix-associated protein expression in human uterine fibroid cells. Biol Reprod 2013; 89(6):150.
28. Gourdy P, Schambourg A, Filipe C, et al. Transforming growth factor activity is a key determinant for the effect of estradiol on fatty streak deposit in hypercholesterolemic mice. Arterioscler Thromb Vasc Biol 2007; 27(10):2214-21.
29. Verrecchia F, Mauviel A. Transforming growth factor-β signaling through the Smad pathway: role in extracellular matrix gene expression and regulation. J Invest Dermatol 2002; 118(2):211-215.
30. Kubota K, Okazaki J, Louie O, et al. TGF-β stimulates collagen (I) in vascular smooth muscle cells via a short element in the proximal collagen promoter. J Surg Res 2003; 109(1):43-50.
31. Cipollone F, Fazia M, Mincione G, et al. Increased expression of transforming growth factor-β1 as a stabilizing factor in human atherosclerotic plaques. Stroke 2004; 35(10):2253-2257.
32. Li JH, Huang XR, Zhu HJ, et al. Advanced glycation end products activate Smad signaling via TGF-β-dependent and-independent mechanisms: implications for diabetic renal and vascular disease. FASEB J 2004; 18(1):176-178.
33. Parker TG, Packer SE, Schneider MD. Peptide growth factors can provoke 'fetal' contractile protein gene expression in rat cardiac myocytes. J Clin Invest 1990; 85(2):507-514.
34. Rosenkranz S, Flesch M, Amann K, et al. Alterations of β-adrenergic signaling and cardiac hypertrophy in transgenic mice overexpressing TGF-β1. Am J Physiol Heart Circ Physiol 2002; 283(3):H1253-62.
35. Matsuki K, Hathaway CK, Lawrence MG, et al. The role of transforming growth factor β1 in the regulation of blood pressure. Curr Hypertens Rev 2014; 10(4):223-238.
36. Zacchigna L, Vecchione C, Notte A, et al. Emilin1 links TGF-β maturation to blood pressure homeostasis. Cell 2006. 124(5):929-42.
37. August P, Suthanthiran M. Transforming growth factor β signaling, vascular remodeling, and hypertension. N Engl J Med 2006; 354(25):2721-23.
38. Wildgruber M, Weiss W, Berger H, et al. Association of circulating transforming growth factor beta, tumor

necrosis factor alpha and basic fibroblast growth factor with restenosis after transluminal angioplasty. Eur J Vasc Endovasc Surg 2007; 34(1):35-43.

39. Weigert C, Brodbeck K, Klopfer K, et al. Angiotensin II induces human TGF-β1 promoter activation: similarity to hyperglycaemia. Diabetologia 2002; 45(6):890-898.
40. Kieran, M.W., R. Kalluri, and Y.-J. Cho, The VEGF pathway in cancer and disease: responses, resistance, and the path forward. Cold Spring Harbor perspectives in medicine, 2012. 2(12): p. a006593.
41. Wang S, Li X, Parra M, et al. Control of endothelial cell proliferation and migration by VEGF signaling to histone deacetylase 7. Proc Natl Acad Sci U S A 2008; 105(22):7738-43.
42. Ferrara N. VEGF: an update on biological and therapeutic aspects. Curr Opin Biotechnol 2000; 11(6):617-624.
43. Carmeliet P. VEGF as a key mediator of angiogenesis in cancer. Oncology 2005; 69(Suppl. 3):4-10.

Circ_0000419 acts as a miR-580 sponge to accelerate colorectal cancer progression via regulating DNMT3B

H. Chai[1], Y. Geng[2], C. Hu[2], J. Wang[2], Y. Quan[2], T. Yu[3] and X. Zhou[1]

[1]Department of Gastroenterology, Renmin Hospital of Wuhan University, Wuhan, Hubei, China; [2]Department of Traditional Chinese Medicine, the Central Hospital of Wuhan, Tongji Medical College, Huazhong University of Science and Technology, Wuhan, Hubei, China; [3]Department of Oncology, Integrated Traditional Chinese and Western Medicine, Central Hospital of Wuhan, Tongji Medical College, Huazhong University of Science and Technology, Wuhan, Hubei, China

Received September 9, 2021 – Accepted February 24, 2022

BACKGROUND: Circular RNAs (circRNAs) have been demonstrated to function in tumorigenesis and cancer progression. Nonetheless, the molecular mechanisms of circRNAs in colorectal cancer (CRC) have not been fully clarified.

METHODS: The circRNA expression profile dataset GSE138589 was analyzed to find the differentially expressed circRNA in CRC. Circ_0000419, microRNA (miR)-580, and DNA methyltransferase 3 beta (DNMT3B) expressions in CRC were detected by qRT-PCR. The biological function of circ_0000419 on the growth, migration and invasion of CRC cells were analyzed by the CCK-8 method and Transwell experiment. Dual-luciferase reporter assay, RNA immunoprecipitation (RIP) assay, and RNA pull-down experiment were performed to validate the interrelationship among circ_0000419, miR-580, and DNMT3B. Then the regulatory function of circ_0000419 and miR-580 on DNMT3B expression was then measured by Western blot.

RESULTS: Circ_0000419 expression was up-regulated, and miR-580 expression was down-regulated in CRC tissues and cell lines. Circ_0000419 was positively linked to CRC patients' T stage and lymph node metastasis. Circ_0000419 knockdown or miR-580 overexpression impeded CRC cells' growth, migration, and invasion. Circ_0000419 expression was negatively correlated with miR-580 expression in CRC tissues. Circ_0000419 was identified as a molecular sponge for miR-580, and DNMT3B was identified as a target gene of miR-580. Furthermore, miR-580 inhibition or DNMT3B overexpression reversed the biological effects of circ_0000419 knockdown on CRC cells' proliferation, migration, and invasion.

CONCLUSION: Circ_0000419 exerts a pro-cancer effect in modulating CRC cell proliferation, migration, and invasion by regulating the miR-580/DNMT3B axis.

Colorectal cancer (CRC) is one of the main causes of cancer-related deaths worldwide (1). In 2020, about 147,950 people were diagnosed with CRC, and 53,200 people died from the disease (2). Although CRC morbidity and mortality decreased in recent decades; between 2000 and 2013 the morbidity of

Keywords: circ_0000419, CRC, miR-580, DNMT3B

**Corresponding Author:*
Dr Xuan Zhou
Department of Gastroenterology,
Renmin Hospital of Wuhan University,
Zhangzhidong Road, Wuchang District,
Wuhan 430061, Hubei, China.
e-mail: drzhouxuan2022@163.com

0393-974X (2022)
Copyright © by BIOLIFE, s.a.s.
This publication and/or article is for individual use only and may not be further reproduced without written permission from the copyright holder.
Unauthorized reproduction may result in financial and other penalties
DISCLOSURE: ALL AUTHORS REPORT NO CONFLICTS OF INTEREST RELEVANT TO THIS ARTICLE.

CRC increased by 22% among people under 50 (3, 4). In-depth research of the molecular mechanism of CRC is crucial to improve the diagnosis, prognosis, and treatment of the disease.

Recent research has identified circular RNAs (circRNAs) as important regulatory non-coding RNAs (ncRNA). CircRNA is a closed structure consisting of a ring-like loop (5). Additionally, circRNAs are strongly resistant to RNA endonucleases and are more stable with a longer half-life than linear RNAs (6). Accumulating research has unveiled that circRNAs are associated with diverse cancers such as gastric cancer, lung cancer, ovarian cancer, and CRC (7, 8). Our bioinformatics analysis implies that circ_0000419 is markedly up-regulated in CRC. Nonetheless, the exact role and mechanism of circ_0000419 in CRC progression is undefined.

CircRNAs have diverse miRNA binding sites called microRNA (miRNA) response elements (MREs), and circRNAs can modulate gene expression by competitively decoying miRNAs (6, 9). Aberrant miRNA expression is closely linked to tumorigenesis and cancer progression (10); for instance, miR-21 targets multiple tumor suppressors to enhance cancer cells' growth, migration, and invasion (11), while overexpression of miR-1587 inhibits CRC cell proliferation and promotes apoptosis (12). Several recently published studies report that miR-580 is a cancer-related miRNA in melanoma and oesophagal squamous cell carcinoma (13, 14). Nevertheless, the role of miR-580 in CRC is not fully clarified.

The present study investigated the biological function and underlying mechanism of circ_0000419 and miR-580 in CRC. Here we report that circ_0000419 can promote the malignant biological behaviours of CRC cells via repressing miR-580 and up-regulating DNA methyltransferase 3 beta (DNMT3B).

MATERIAL AND METHODS

CircRNA expression profile analysis

Gene Expression Omnibus (GEO) is a publicly accessible database that contains genomic information derived from high-throughput data (15). A CRC-related dataset, GSE138589 (data from 6 primary CRC tissues and 6 matched normal tissues) based on the GPL19978 platform of the Agilent-069978 Arraystar Human CircRNA microarray V1 was downloaded from the GEO database and analyzed in this study through GEO2R online. "$P < 0.05$ and Log2 (Fold Change) >1 or Log2 (Fold Change) < −1" were defined as the thresholds for the screening of differentially expressed circRNAs. Volcano plots and hierarchical clustering analysis were constructed using SangerBox and Heml 1.0.3.7-Heatmap Illustrator software, respectively.

Clinical sample collection

Ninety-three pairs of CRC and non-tumour tissues (3 cm away from the tumor) were collected from recruited CRC patients (48 male patients and 45 female patients, aged 35-73 years old with a mean age of 58 years old) undergone surgery at The Central Hospital of Wuhan (Wuhan, China) from March 2014 to February 2019. All the patients were diagnosed by histology and had received neither chemotherapy nor radiotherapy prior to section. Every subject enrolled in this work provided written informed consent, and this study was endorsed by the Ethics Committee of the Central Hospital of Wuhan (Approval no. 2018-03-105).

Cell culture

Normal colon epithelial cell line (NCECL) (NCM460) and CRC cell lines (HCT116, HT29, SW480, SW620, and LoVo) were procured from the American Type Culture Collection (ATCC, Manassas, VA, USA). Cells were maintained in RPMI 1640 medium (Gibco; Thermo Fisher Scientific, Inc., Waltham, MA, USA) containing 100 U/mL penicillin, 0.1 mg/mL streptomycin, 2.5 mM L-glutamine, and 10% fetal bovine serum (FBS) at 37°C with 5% CO_2.

Cell transfection

Human DNMT3B sequence was synthesized and cloned into pcDNA3.1 vector (Geenseed Biotech, Guangzhou, China) to construct a vector of overexpression (pc-DNMT3B), and pcDNA3.1 empty vector was used as negative control (pc-NC). As a result, three small interfering RNA (siRNA) against circ_0000419 (si-circ_0000419#1: 5′-GACCAAAGCTGACTTATCCTT-3′, si-circ_0000419#2: 5′-GGAGGACCAAAGCTGACTTAT-3′, and si-circ_0000419#3: 5′-GGACCAAAGCTGACTTATCCT-3′), negative control siRNA (si-NC, 5′-AACAGTCGCGTTTGCGACTGG-3′), miR-580 mimic

(miR-580, 5′-UUGAGAAUGAUGAAUCAUUAGG-3′), miR-580 inhibitor (anti-miR-580, 5′-CCUAAUGAUU CAUCAUUCUCAA-3′) and negative controls (miR-con, 5′-UUCUCCGAACGUGUCACGUTT-3′ and anti-miR-con, 5′-CAGUACUUUUGUGUAGUACAA-3′) were available from GenePharma (Shanghai, China). CRC cells were transferred in 6-well plates at 3×10^5 cells/well. When cell fusion reached 90%, the cells were transfected with 20 ng of the plasmid (pc-DNMT3B), 50 nM siRNA, mimics or inhibitor using Lipofectamine® 2000 (Invitrogen, Carlsbad, CA, USA) according to the manufacturer's instruction. After 48 h, cells were collected for follow-up experiments.

Real-time quantitative reverse transcription PCR (qRT-PCR)

TRIzol reagent (Invitrogen, Carlsbad, CA, USA) and NanoDrop 2000 were utilized to isolate and quantify the total RNA (Thermo Fisher Scientific Inc., Carlsbad, CA, USA). The RNA was transcribed into cDNA using ReverTra Ace qPCR RT Kit (Toyobo, Osaka, Japan). qRT-PCR was executed with THUNDERBIRD SYBR® qPCR Mix (Toyobo, Osaka, Japan). Gene expression levels were normalized by GAPDH/U6 expression. The data were calculated by the $2^{-\Delta\Delta Ct}$ method. Table I displays the primers designed for this research.

Cellular RNA fractionation experiment

NE-PER Nuclear and Cytoplasmic Extraction kit (Thermo Scientific, Waltham, MA, USA) was used to isolate cytoplasmic and nuclear extracts from CRC cells. RNAs extracted from the nucleus or cytoplasm were analyzed with qRT-PCR. The levels of nucleus control (U6), cytoplasm control (GAPDH), and circ_0000419 were respectively measured.

CCK-8 experiment

The HT29 and SW480 cells (5 × 103 cells / well, in 96-well plate) were cultured in the RPMI 1640 medium for 1 d, 2 d, 3 d, and 4 d, respectively. Subsequently, the CCK-8 reagent (10 μL / well, Dojindo, Tokyo, Japan) was supplemented into each well and incubated for 2 h. The absorbance of each well was determined by a microplate reader (Bio-Rad, Hercules, CA, USA) at 450 nm. 4 d later, the growth curve of CRC cells was plotted.

Migration and invasion experiments

Transwell assays were utilized to investigate CRC cell migration and invasion with 24-well Transwell chambers (Corning, Corning, NY, USA). The migration and invasion assay method is similar, but the filter was covered with a layer of Matrigel (BD Bioscience, San Jose, CA, USA) for the invasion experiment. HT29 and SW480 cells cultured in RPMI 1640 medium without FBS were inoculated into the top chamber (1×10^4 cells/well), while RPMI 1640 medium containing 10% FBS was added into the lower compartment. After 24 h of incubation, cells on the upper surface of the membrane were removed with a cotton swab, and cells on the lower surface of the membrane were fixed in methanol (100%) and stained with crystal violet (0.25%, Sigma, St. Louis, MO, USA). Under a microscope, the number of migrating or invading cells was counted in three different fields of view, and the average was calculated to indicate the migration and invasion of CRC cells.

Dual-luciferase reporter gene experiment

HEK-293T cells were plated into 96-well plates (1×10^4 cells / well) and cultured overnight. The binding site of miR-580 in hsa_circ_0000419 was predicted using the Circular RNA Interactome database (https://circinteractome.nia.nih.gov/index.html).

Wild-type (WT) and mutant (MUT) sequences of circ_0000419 (containing the binding sites to miR-580) were inserted into the pGL3 vector (Promega, Madison, WI, USA) to establish WT-circ_0000419 reporter and MUT-circ_0000419 reporter. The binding site of miR-580 to DNMT3B 3' UTR was predicted using the StarBase database (http://starbase.sysu.edu.cn/). The luciferase reporter gene plasmids containing WT-DNMT3B 3'UTR or MUT-DNMT3B 3'UTR were constructed using the same method. The above luciferase reporters and control miRNA mimics or miR-580 mimic were co-transfected into HEK-293T cells using Lipofectamine® 2000 (Invitrogen,

Table I. *Primer sequence used in this study*

Gene	Sequence
circ_0000419	F: 5'-TTCTGGAGGCTGTGGAAAAC-3'
	R: 5'-GACACGTCCTGTCCATTGTG-3'
DNMT3B	F: 5'-GTCATCCGACACCTCTTCGC-3'
	R: 5'-ACCTCCTGGGTCCTGGCTCT-3'
miR-580	F: 5'-GCCGAGTTGAGAATGATGAA-3'
	R: 5'-TGGTGTCGTGGAGTCGG-3'
GAPDH	F: 5'-GGAGCGAGATCCCTCCAAAAT-3'
	R: 5'-GGCTGTTGTCATACTTCTCATGG-3'
U6	F: 5'-ATTGGAACGATACAGAGAAGATT-3'
	R: 5'-GGAACGCTTCACGAATTTG-3'

Carlsbad, CA, USA). A dual-luciferase reporter detection kit measured the luciferase activity in HEK-293T cells (Promega, Madison, WI, USA).

RNA immunoprecipitation (RIP)

RIP experiment was executed using EZ-Magna RIP Kit (EMD Millipore, Billerica, MA, USA). First, HT29 and SW480 cells were lysed in RIP lysis buffer. Next, cell lysates were incubated with RIP buffer containing magnetic beads coupled with anti-Ago2 or anti-IgG antibodies (Millipore, Billerica, MA, USA). After that, proteinase K (Sigma, St. Louis, MO, USA) was utilized to incubate magnetic beads, and total RNA was isolated using TRIzol reagent (Invitrogen, Carlsbad, CA, USA). Subsequently, the purified RNA was obtained, and the abundance of circ_0000419 and miR-580 in the immunoprecipitate was measured using qRT-PCR.

RNA pull-down experiment

Briefly, HT29 and SW480 cells were transfected with biotinylated miR-580 probes or control probes (concentration: 50 nM). The cells were then rinsed with ice-cold PBS, collected, and lysed in the lysis buffer (Sigma, St. Louis, MO, USA) for 10 min on ice. The lysates were then centrifugated, and the supernatants were collected. Next, the supernatants were incubated with M-280 streptavidin magnetic beads (Sigma, St. Louis, MO, USA) for 3 h at 4°C and then thoroughly rinsed with the washing buffer. In order to detect RNA enrichment, the RNA in the immunoprecipitate was isolated, and then qRT-PCR was executed.

Western blot

Radio immunoprecipitation assay buffer (RIPA, Beyotime, Shanghai China) lysed cells, and the protein sample was obtained after centrifugation, and the protein concentration was quantified by a BCA kit (Beyotime, Shanghai, China). Protein extractions were dissolved by SDS-PAGE and transferred onto PVDF membranes (Sigma, St. Louis, MO, USA). After blocking with 5% skimmed milk for 1.5 h at room temperature, the membranes were incubated overnight at 4°C with the corresponding specific primary anti-DNMT3B antibody (ab79822, 1:500, Abcam, Cambridge, UK) and anti-GAPDH antibody (ab8245, 1: 3000, Abcam, Cambridge, UK). Next, the membranes were incubated with the appropriate secondary antibody (1:5000, Abcam, Cambridge, UK) for 1 h. After rinsing, an enhanced chemiluminescence kit (Millipore, Bedford, MA, USA) was added to the membranes, and the signals were detected with a chemiluminescence system (Bio-Rad, Hercules, VA, USA).

Statistical analysis

All the assays were executed at least in triplicate and repeated 3 times. Statistical analyses were performed using SPSS v22.0 (SPSS, Inc, Chicago, IL, USA). All measurement data were shown as "mean ± standard deviation". The Kolmogorov-Smirnov test measured the normality of the data. Comparisons between two groups and among multiple groups were made by student's *t*-test and one-way ANOVA with Dunnett's post-hoc test, respectively. Pearson's correlation test examined the linear relationships between circ_0000419, miR-580, DNMT3B. Finally, the categorical data were analyzed by the Chi-square test. Statistical significance was signified by $P<0.05$.

RESULTS

Crc_0000419 is up-regulated in CRC tissues and cell lines

The GEO2R tool was applied to analyze GSE138589 microarray data to identify the abnormally expressed circRNAs in CRC. The result indicated that there were 156 up-regulated circRNAs and 30 down-regulated circRNAs in CRC tissues (Fig. 1A), among which circ_0000419 was remarkably up-regulated and therefore selected as the target of the follow-up research (Fig. 1B, Supplementary Table 1&2). Moreover, qRT-PCR was performed to examine circ_0000419 expression in 93 pairs of CRC and paracancerous tissues. The data demonstrated that circ_0000419 expression was higher in CRC tissues than in normal tissues adjacent to cancer (Fig. 1C). Additionally, circ_0000419 expression was positively correlated with the T stage ($P<0.05$) and lymph node metastasis ($P<0.05$) of the patients (Fig. 1D&E). qRT-PCR data also suggested that circ_0000419 expression was remarkably up-regulated in CRC cell lines (HCT116, HT29, SW480, SW620, and LoVo) relative to normal colon epithelial cell line (NCM460) (Fig. 1F). Furthermore, circ 0000419 was observed to be primarily located in the cytoplasm of CRC cell lines, suggesting it could probably function as a competitive endogenous RNA (ceRNA) (Fig. 1G).

Notably, it was also found that increased expression of circ_0000419 was significantly associated with lymph node metastasis (P=0.002) and higher TNM stage (P=0.007) (Table II).

Knockdown of circ_0000419 restrains CRC growth and aggressiveness

Since circ 0000419 expression was relatively higher in HT29 and SW480 cells, three siRNAs targeting circ 0000419 (si-circ 0000419#1, si-circ 0000419#2, and si-circ 0000419#3) were transfected into HT29 and SW480 cells to establish the loss-of-function models. qRT-PCR experiments revealed that si-circ_0000419#1 had the most significant knockdown efficiency (Fig. 2A). Thus, si-circ_0000419#1 was selected for subsequent experiments. Next, the proliferation, migration, and invasion of CRC cells were examined by CCK-8 and Transwell experiment, respectively. The experimental data demonstrated that cell multiplication was remarkably decreased in si-circ_0000419 groups compared to control groups (Fig. 2B). Besides, both migration and invasion were markedly repressed in the si-circ_0000419 groups than in the control groups (Fig. 2C&D). The data indicated that the knockdown of circ_0000419 suppressed the malignant biological behaviours of CRC cells.

Circ_0000419 sponges miR-580 in CRC cells

The circular RNA Interactome database predicted miR-580 as a possible downstream target of circ_0000419 (Fig. 3A). A luciferase reporter gene experiment was performed to confirm the targeting relationship between circ 0000419 and miR-580, and the results revealed that miR-580 mimics significantly reduced luciferase activity of WT-circ 0000419 reporter. In comparison, miR-580 mimics had no significant effect on the luciferase activity of MUT-circ 0000419 reporter (Fig. 3B). RIP and pull-down experiments further verified that circ_0000419 could bind with miR-580 in HT29 and SW480 cells (Fig. 3C, D). Additionally, qRT-PCR indicated that miR-580 expression was markedly augmented in both HT29 and SW480 cells after knocking down circ_0000419 (Fig. 3E). Moreover, miR-580 was remarkably under-expressed in CRC tissues compared with normal tissues adjacent to cancer (Fig. 3F).

Table II. *Association between circ_0000419 expression and the clinical characteristics of 93 patients.*

Clinical characteristics	Total (n=93)	circ_0000419 expression		*P* value
		Low (47)	High (46)	
Age (years)				
≤65	51	29	22	0.178
>65	42	19	23	
Gender				
Male	48	27	21	0.255
Female	45	20	25	
Tumor site				
Colon	58	26	32	0.156
Rectum	35	21	14	
Tumor size (cm)				
≤5	65	30	35	0.197
>5	28	17	11	
Lymph node metastasis				
No	43	29	14	0.002**
Yes	50	18	32	
TNM stage				
I-II	35	24	11	0.007**
III-IV	58	23	35	

***P<0.01.*

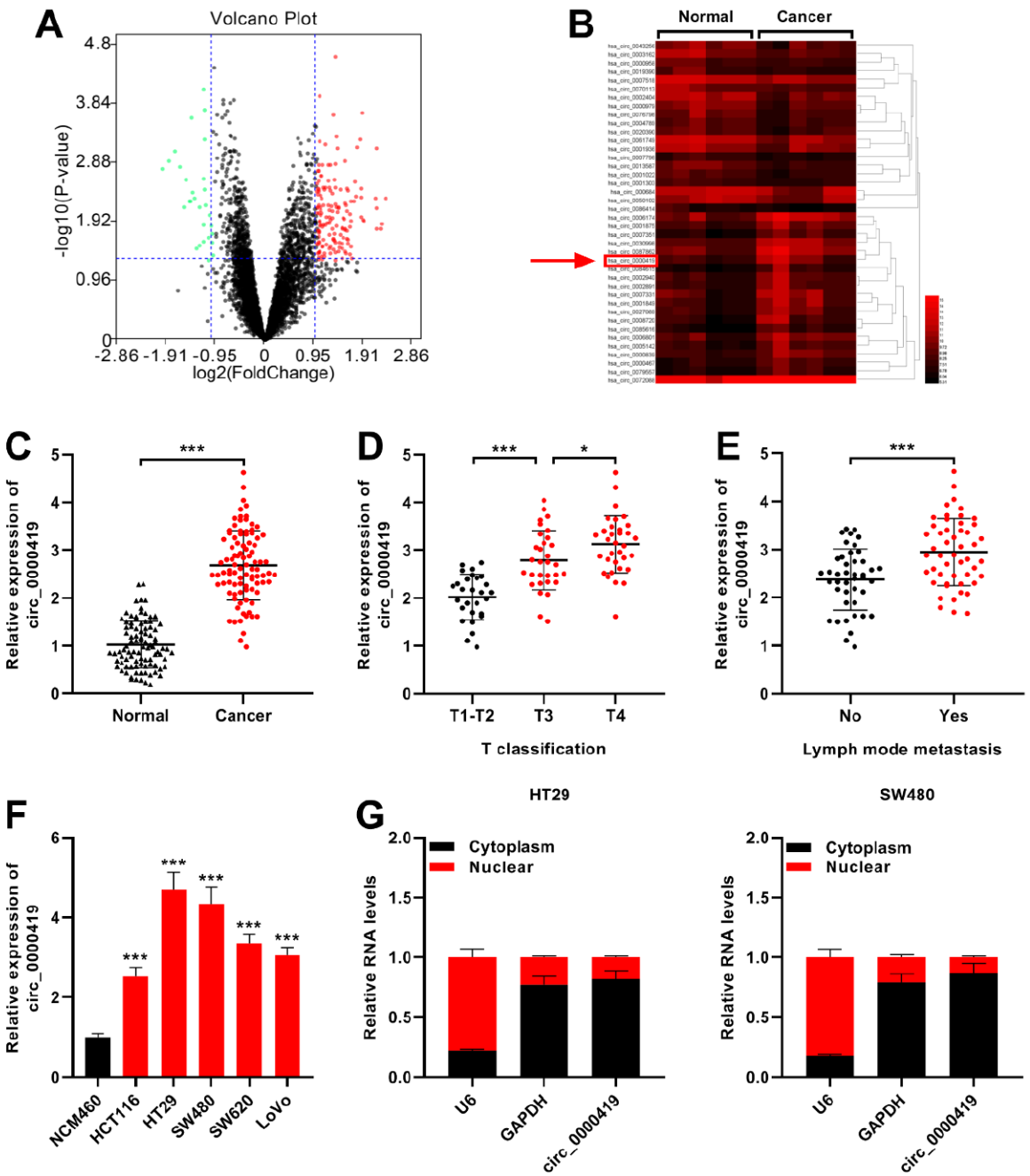


Fig. 1. *circ_0000419 is up-regulated in CRC.* ***A)*** *Differentially expressed circRNAs of GSE138589 in CRC tissues were presented in a volcano plot. The screening criteria: |log2FC| > 1 and P < 0.05.* ***B)*** *Cluster heatmap of top 20 up- and down-regulated differentially expressed circRNAs in GSE138589.* ***C)*** *qRT-PCR was utilized to detect circ_0000419 expression in 93 pairs of CRC tissues and adjacent tissues.* ***D)*** *qRT-PCR was applied to detect circ_0000419 expression in CRC tissues of different T stages.* ***E)*** *The expression of circ_0000419 in tumor tissues of CRC patients with and without lymph node metastasis was detected by qRT-PCR.* ***F)*** *qRT-PCR was adopted to detect circ_0000419 expression in normal colon epithelial cell line (NCM460) and CRC cell lines (HCT116, HT29, SW480, SW620, and LoVo).* ***G)*** *The cellular distribution of circ_0000419 was analyzed by cellular RNA fractionation assays. GAPDH was mostly enriched in the cytoplasm and U6 was mainly enriched in the nucleus, which were used as the controls. All experiments were performed in triplicate. * P < 0.05, *** P < 0.001.*

Furthermore, Pearson correlation analysis unveiled that miR-580 expression was negatively correlated with circ_0000419 expression (R^2 = 0.2499, P < 0.001) (Fig. 3G). These data implied that in CRC cells, circ_0000419 adsorbed miR-580 and negatively regulated its expression.

MiR-580 restrains the malignant biological behavior of CRC cells

Subsequently, the function of miR-580 in CRC was probed. MiR-580 was remarkably under-expressed in CRC cell lines compared with NCM460 cells (Fig. 4A). Then miR-580 mimics were transfected into HT29 and SW480 cells to construct miR-580 overexpression models (Fig. 4B). Cell proliferation and metastatic potential were then measured by CCK-8 and Transwell experiments, and a substantial decrease in the growth, migration and invasion of HT29 and SW480 cells was observed after up-modulation of miR-580 (Fig. 4C-E). The findings revealed that miR-580 restrained the malignant biological behaviours of CRC cells.

Circ_0000419 modulates the growth and metastasis of CRC cells via miR-580/DNMT3B axis

StarBase database predicted a complementary binding site between miR-580 and the 3'UTR of DNMT3B (Fig. 5A). The luciferase reporter gene experiment results revealed that miR-580 mimics significantly reduced the luciferase activity of WT-DNMT3B reporter, but miR-580 mimics had no significant effect on MUT-DNMT3B reporter (Fig. 5B). In CRC tissues, DNMT3B expression was significantly up-regulated, and its expression was negatively correlated with miR-580 expression (R^2=0.3469, P<0.001) and positively correlated with circ_0000419 expression (R^2=0.3716, P<0.001) (Fig. 5C, D, E). Moreover, miR-580 inhibitors were

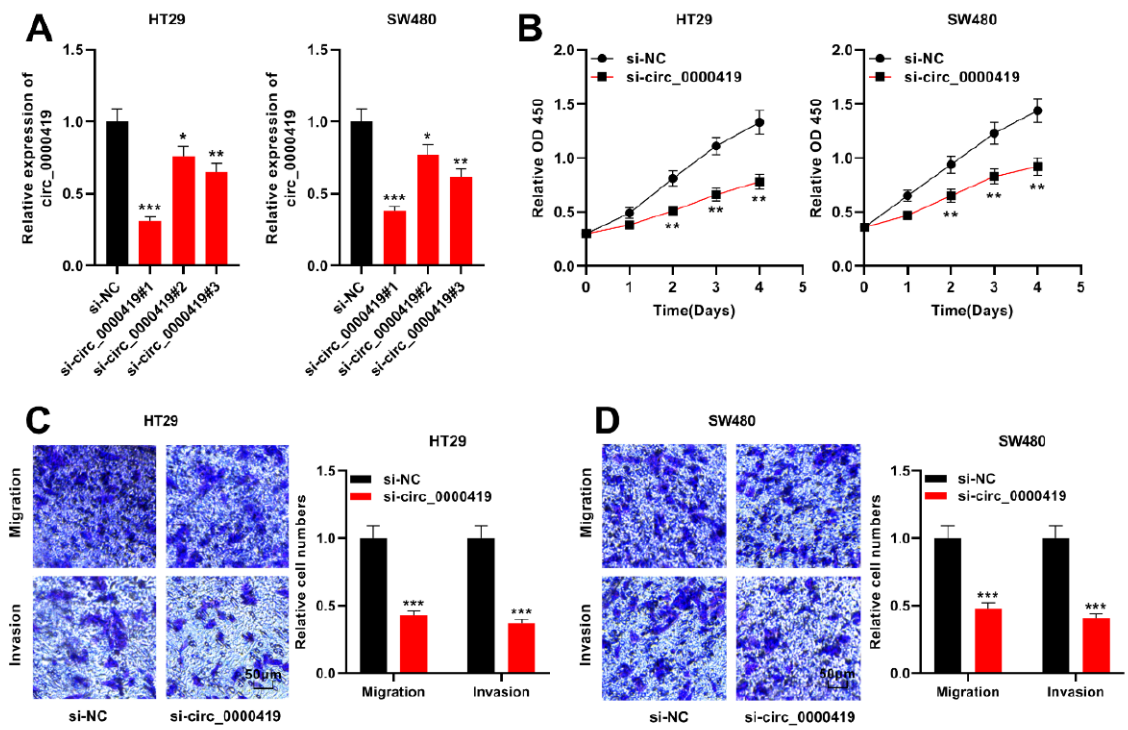


Fig. 2. *Knockdown of circ_0000419 impedes the proliferation, migration, and invasion of CRC cells.* ***A)*** *Three siRNAs against circ_0000419 (si-circ_0000419#1, si-circ_0000419#2 and si-circ_0000419#3) were transfected into HT29 and SW480 cells, and circ_0000419 expression was detected by qRT-PCR.* ***B)*** *CCK-8 experiment was executed to detect the proliferation of HT29 and SW480 cells transfected with si-circ_0000419.* ***C-D)*** *Transwell assay was implemented to detect the migration and invasion of HT29 cells transfected with si-circ_0000419. All experiments were performed in triplicate. * P < 0.05, ** P < 0.01, *** P < 0.001.*

transfected into transfected HT29 and SW480 cell lines with circ_0000419 knockdown for functional compensation experiments (Fig. 5F, Supplementary Fig. 2A). Western blot showed that DNMT3B expression was remarkably reduced in both HT29 and SW480 cells after knocking down circ_0000419, while DNMT3B expression in HT29 and SW480 cells was partially restored after co-transfection with miR-580 inhibitor (Fig. 5G). Consistent with this, knockdown of circ_0000419 remarkably impeded the proliferation, migration and invasion in both HT29 and SW480 cells, while the malignant biological behaviours of HT29 and SW480 cells were reversed after co-transfection with miR-580 inhibitor (Fig. 5H, I). For the exact role of DNMT3B in CRC, we also did a rescue experiment and found that overexpression of DNMT3B could reverse the effect of circ_ 0000419 knockdown on CRC progression (Supplementary Fig. 1, Supplementary Fig. 2B). The findings implied that DNMT3B was a direct target of miR-580; additionally, the suppressing effects of circ_0000419 knockdown on CRC cell proliferation, migration, and invasion could be partially attenuated by miR-580 down-modulation or DNMT3B overexpression.

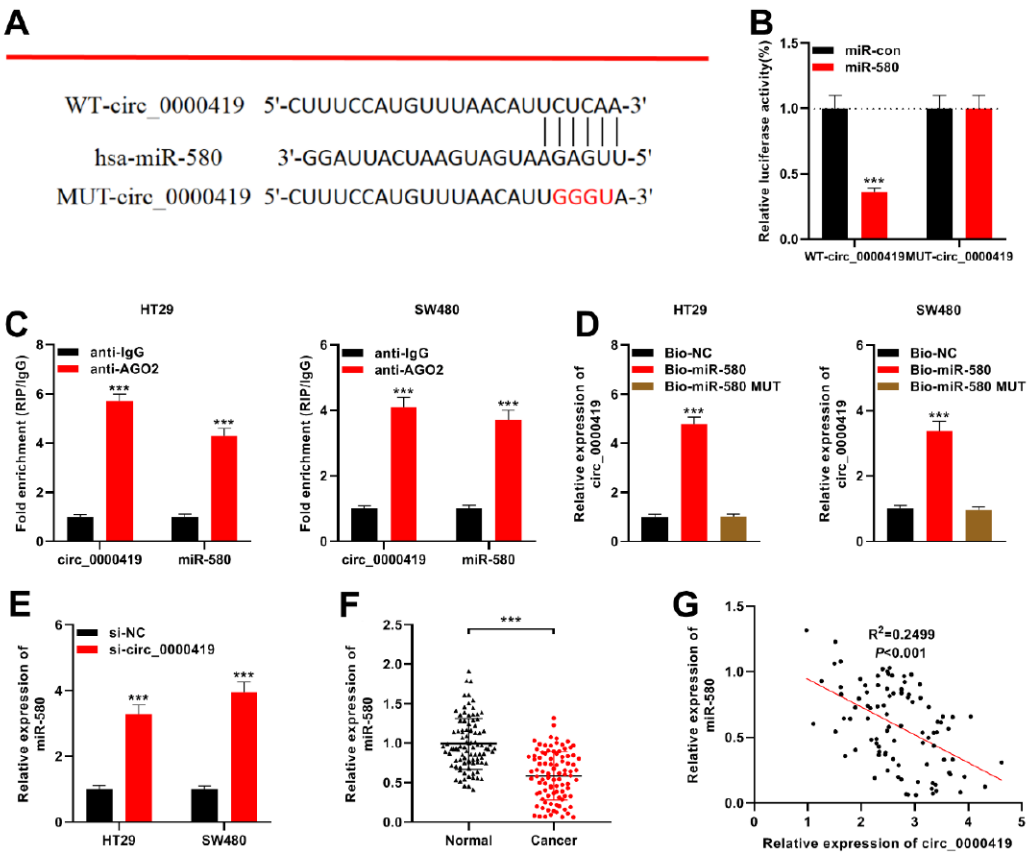


Fig. 3. *MiR-580 is a downstream target of circ_0000419.* ***A)*** *Bioinformatics analysis predicted that the sequence of miR-580 matched the sequences of circ_0000419.* ***B)*** *MiR-580 mimics or control mimics were co-transfected with WT-circ_0000419 or MUT-circ_0000419 respectively into HEK-293T cells, and the luciferase activity of each group was measured.* ***C)*** *The complex containing circ_0000419 and miR-580 in HT29 and SW480 cells was immunoprecipitated by anti-Ago2 antibody, and the interaction between circ_0000419 and miR-580 was verified.* ***D)*** *RNA pull-down assay was carried out to verify the interactions between circ_0000419 and miR-580.* ***E)*** *MiR-580 expression in HT29 and SW480 cells transfected with si-circ_0000419 was detected by qRT-PCR.* ***F)*** *qRT-PCR was conducted to examine miR-580 expression in 93 pairs of CRC tissues and adjacent tissues.* ***G)*** *Pearson's correlation analysis was utilized to evaluate the correlations between circ_0000419 and miR-580 expression in CRC tissues. All experiments were performed in triplicate. *** P < 0.001.*

DISCUSSION

Multiple circRNAs have been discovered to play a role in CRC progression (16). For instance, circ_0026344 expression is down-regulated in CRC tissues, and circ_0026344 expression is negatively linked to the prognosis of the patients (17). Additionally, circ_0004585 is overexpressed in both tissues and peripheral blood of CRC patients and is positively linked to the tumor size of the patients (18). In addition, the knockdown of circ_0071589 restrains CRC growth, invasion, and migration (19). In this work, circ_0000419 was observed to be overexpressed in CRC tissues and cell lines (P<0.05). Moreover, its overexpression was associated with the unfavourable pathological characteristics of CRC patients. Additionally, circ_0000419 knockdown repressed the multiplication, migration, and invasion of CRC cells. The results suggested that circ_0000419 may exert an oncogenic effect on CRC progression.

Reportedly, circRNAs can work as molecular sponges for miRNAs and repress miRNA expression (6). MiRNAs work as tumor suppressors or oncomiRs by modulating up to 60% of human protein-coding genes, which in turn are implicated in diverse biological processes in cancer development (20, 21). For instance, miR-466, which is remarkably down-regulated in CRC, is significantly linked to tumor size, lymph node metastasis, and distant metastasis; miR-466 overexpression represses the growth and metastasis of SW620 cells and induces G0/G1 arrest and apoptosis (22). MiR-580 is reported to be linked to the progression of melanoma, oesophagal squamous cell carcinoma and neuroblastoma (13, 14, 23). In addition, miR-580 overexpression restrains the growth of

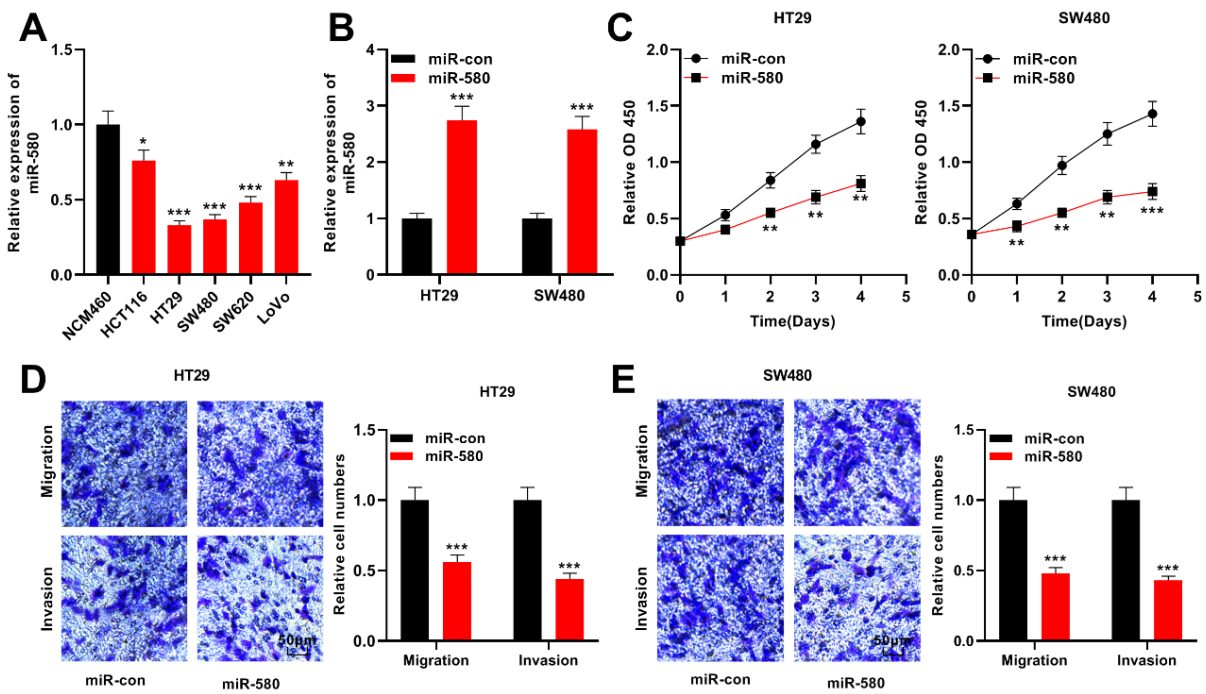


Fig. 4. *MiR-580 impedes the proliferation, migration, and invasion of CRC cells.* ***A)*** *qRT-PCR was employed to detect miR-580 expression in normal colon epithelial cell line (NCM460) and CRC cell lines (HCT116, HT29, SW480, SW620, and LoVo).* ***B)*** *MiR-580 mimics were transfected into HT29 and SW480 cells, and miR-580 expression was detected by qRT-PCR.* ***C)*** *CCK-8 assay was performed to detect the proliferation of HT29 and SW480 cells transfected with miR-580 mimics.* ***D-E)*** *Transwell assay was utilized to detect the migration and invasion of HT29 and SW480 cells transfected with miR-580 mimics. All experiments were performed in triplicate. * P < 0.05, ** P < 0.01, *** P < 0.001.*

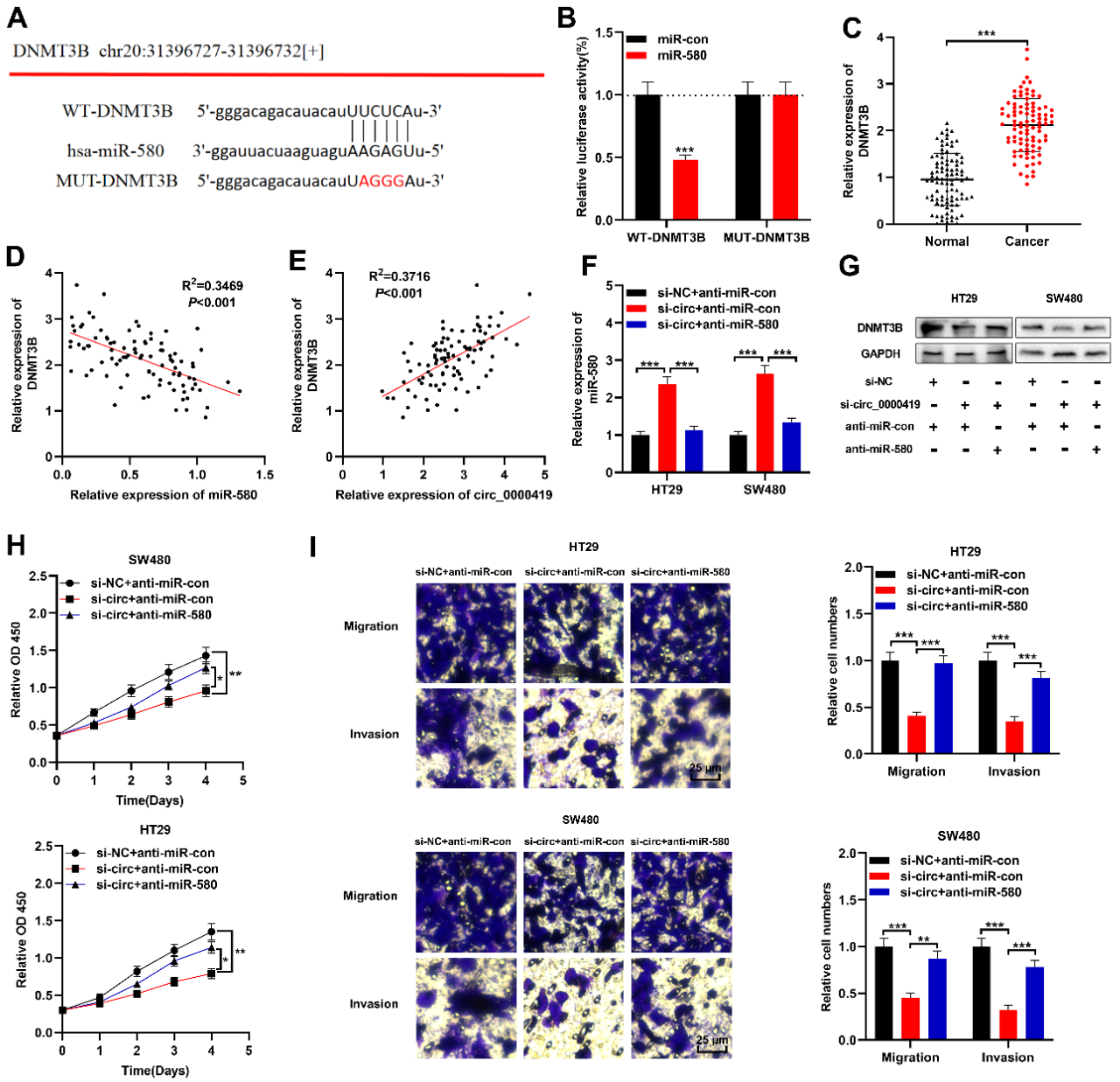
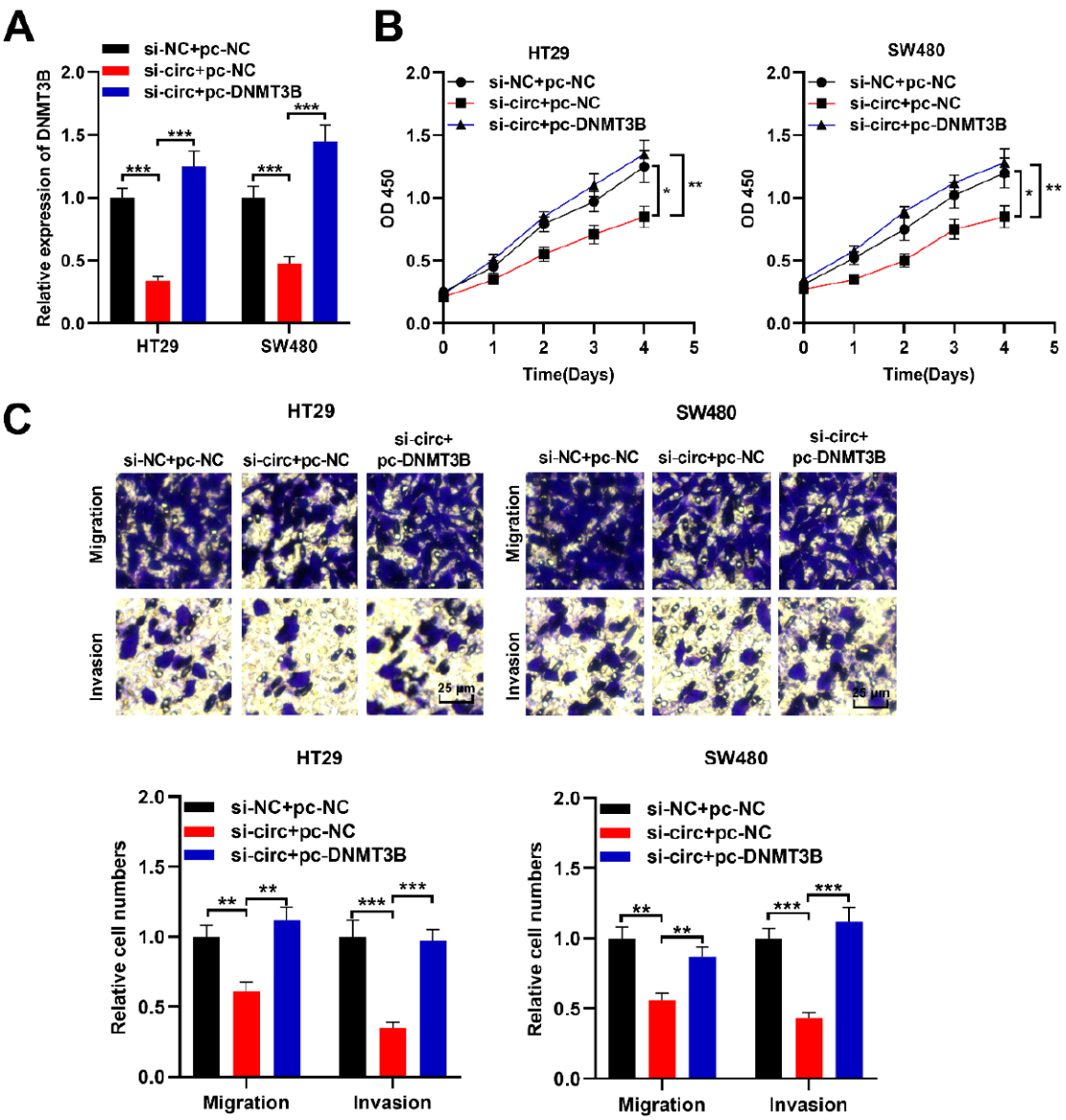


Fig. 5. *Circ_0000419 enhances the proliferation and metastasis of CRC cells via miR-580/DNMT3B axis.* ***A)*** *StarBase database predicted that the sequence of miR-580 matched the sequences of DNMT3B 3'UTR, and WT-DNMT3B and MUT-DNMT3B luciferase reporter gene vectors were constructed.* ***B)*** *MiR-580 mimics or miR control were co-transfected with WT-DNMT3B or MUT-DNMT3B, respectively, into HEK-293T cells, and the luciferase activity of each group was measured.* ***C)*** *qRT-PCR was conducted to examine DNMT3B mRNA expression in 93 pairs of CRC tissues and adjacent tissues.* ***D)*** *Pearson's correlation analysis was utilized to evaluate the correlations between DNMT3B and miR-580 expression in CRC tissues.* ***E)*** *Pearson's correlation analysis was utilized to evaluate the correlations between DNMT3B and circ_0000419 expression in CRC tissues.* ***F)*** *The miR-580 inhibitor was co-transfected with circ_0000419 siRNA1 into HT29 and SW480 cells, and miR-580 expression was detected by qRT-PCR.* ***G)*** *Western blot was utilized to detect DNMT3B protein expression in HT29 and SW480 cells after co-transfection.* ***H)*** *CCK-8 assay was conducted to detect the proliferation of HT29 and SW480 cells after co-transfection.* ***I)*** *Transwell assay was performed to detect the migration and invasion of HT29 and SW480 cells after co-transfection. All experiments were performed in triplicate. * $P < 0.05$, ** $P < 0.01$, *** $P < 0.001$.*

osteosarcoma cells (24). In the present study, miR-580 was shown to be under-expressed in CRC tissues and cell lines, and overexpression of miR-580 inhibited the proliferation and metastasis of CRC cells, implying that miR-580 has a tumour-suppressive role in CRC.

MiRNAs induce the degradation of mRNA and inhibit translation via binding with the 3'UTR of mRNA (25). In this work, DNMT3B was validated as a downstream target of miR-580. DNMT3B is a member of DNA methyltransferases that facilitates tumorigenesis through gene-specific *de novo* methylation and transcriptional silencing (26). Research has unearthed that total DNA



Supplementary Fig. 1. *DNMT3B overexpression counteracted the effects of circ_0000419 knockdown on CRC cells. **A)** HT29 and SW480 cells were transfected with si-NC, circ_0000419 siRNA + empty vector, or circ_0000419 siRNA + DNMT3B overexpression plasmid. qRT-PCR was employed to detect DNMT3B expression. **B)** The proliferation of CRC cells was measured by CCK-8 assay. **C)** The migration and invasion of CRC cells were measured by Transwell assay. All experiments were performed in triplicate. * P < 0.05, ** P < 0.01, *** P < 0.001.*

hypomethylation and regional hypermethylation frequently occur during tumorigenesis, suggesting that aberrant methylation substantially contributes to cancer progression (27, 28). DNMT3B, commonly considered as an oncogene, is reported to be overexpressed in diverse tumors and exerts an essential effect in tumor progression by hypermethylation cancer-related genes (29-31). For instance, DNMT3B is overexpressed in glioblastoma, and it is a promising biomarker for tumor staging and prognosis prediction (32). In NSCLC, DNMT3B activates Wnt/β-catenin signaling by silencing the tumor suppressor WIF-1 through the induction of promoter hypermethylation (33). In CRC, miR-124 and miR-506 suppress disease progression and increase sensitivity to chemotherapy by targeting DNMT3B and DNMT1 (34). The present work confirmed that circ_0000419 negatively regulated miR-580 while positively regulated DNMT3B expression. We also observed that the suppressive effect of circ 0000419 knockdown on CRC cell proliferation, migration, and invasion was partly counteracted by downregulation of miR-580 or overexpression of DNMT3B. These findings implied that circ_0000419 worked as a ceRNA to exert an oncogenic effect in CRC by modulating the miR-580/DNMT3B axis.

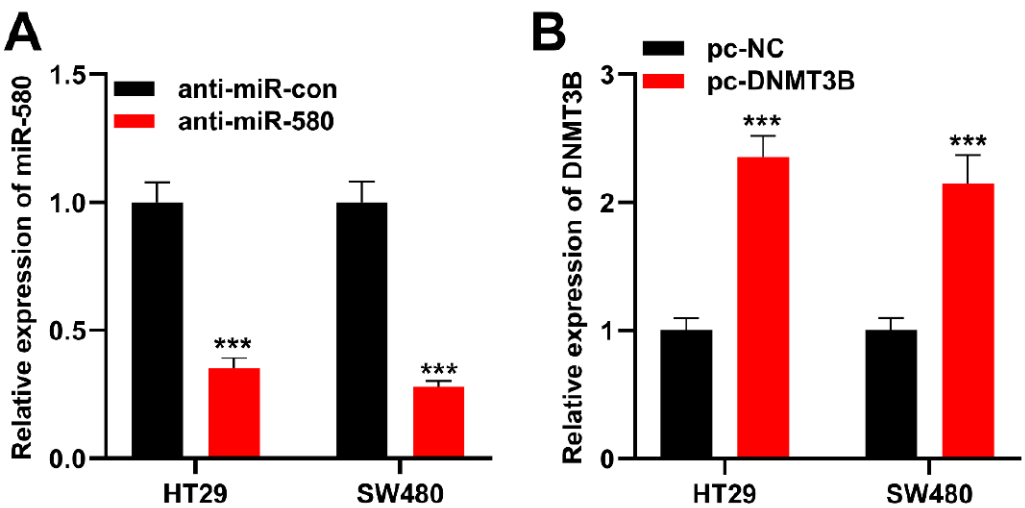
In summary, circ_0000419 is up-regulated, miR-580 is down-regulated in CRC tissues and cells, and circ_0000419 overexpression implies adverse prognosis of CRC patients. Besides, circ_0000419 knockdown or miR-580 overexpression suppresses the malignant biological behaviours of CRC cells, suggesting that circ_0000419 is an oncogenic circRNA and miR-580 is a tumor suppressor in CRC. Mechanistically, circ_0000419 participates in CRC development through regulating the miR-580/ DNMT3B axis. It may provide potential biomarkers and therapeutic targets for CRC diagnosis and treatment.

Conflict of interest:

The authors declare that they have no competing interests.

Funding:

This work was supported by a Grant-in-aid for Scientific Research from the National Natural Science Foundation for the Youth of China (No. 81704023).



Supplementary Fig. 2. *The expression of miR-580 and DNMT3B in HT29 and SW480.* ***A)*** *HT29 and SW480 cells were transfected with anti-miR-control or anti-miR-580. qRT-PCR was employed to detect miR-580 expression.* ***B)*** *HT29 and SW480 cells were transfected with empty vector (pc-NC), or DNMT3B overexpression plasmid (pc-DNMT3B). qRT-PCR was employed to detect DNMT3B expression. *** $P < 0.001$.*

Ethics statement:

The Ethics Review Board approved our study of the First Affiliated Hospital of the Central Hospital of Wuhan (Approval no. 2018-03-105).

Data Availability Statement:

The data used to support the findings of this study are available from the corresponding author upon request.

REFERENCES

1. Siegel RL, Miller KD, Jemal A. Cancer statistics, 2015. CA Cancer J Clin 2015; 65(1):5-29.
2. Siegel RL, Miller KD, Goding Sauer A, et al. Colorectal cancer statistics, 2020. CA Cancer J Clin 2020; 70(3):145-164.
3. Siegel RL, Miller KD, Fedewa SA, Ahnen DJ, Meester RGS, Barzi A, Jemal A. Colorectal cancer statistics 2017. CA Cancer J Clin 2017; 67(3):177-193.
4. Thanikachalam K, Khan G. Colorectal Cancer and Nutrition. Nutrients 2019; 11(1):164.
5. Chen L-L. The expanding regulatory mechanisms and cellular functions of circular RNAs. Nat Rev Mol Cell Biol 2020; 21(8):475-490.
6. Rajappa A, Banerjee S, Sharma V, Khandelia P. Circular RNAs: Emerging Role in Cancer Diagnostics and Therapeutics. Front Mol Biosci 2020; 7:577938.
7. Bachmayr-Heyda A, Reiner AT, Auer K, et al. Correlation of circular RNA abundance with proliferation--exemplified with colorectal and ovarian cancer, idiopathic lung fibrosis, and normal human tissues. Sci Rep 2015; 5:8057.
8. Xu H, Wang C, Song H, Xu Y, Ji G. RNA-Seq profiling of circular RNAs in human colorectal Cancer liver metastasis and the potential biomarkers. Mol Cancer 2019; 18(1):8.
9. Kramer MC, Liang D, Tatomer DC, Gold B, March ZM, Cherry S, Wilusz JE. Combinatorial control of Drosophila circular RNA expression by intronic repeats, hnRNPs, and SR proteins. Genes Dev 2015; 29(20):2168-82.
10. Lee H, Han S, Kwon CS, Lee D. Biogenesis and regulation of the let-7 miRNAs and their functional implications. Protein Cell 2016; 7(2):100-113.
11. Javanmardi S, Aghamaali MR, Abolmaali SS, Mohammadi S, Tamaddon AM. miR-21, An Oncogenic Target miRNA for Cancer Therapy: Molecular Mechanisms and Recent Advancements in Chemo and Radio-resistance. Curr Gene Ther 2017; 16(6):375-389.
12. Liu R, Shen L, Lin C, et al. MiR-1587 Regulates DNA Damage Repair and the Radiosensitivity of CRC Cells via Targeting LIG4. Dose Response 2020; 18(2):1559325820936906.
13. Zhang T, Zhao D, Wang Q, et al. MicroRNA-1322 regulates ECRG2 allele specifically and acts as a potential biomarker in patients with esophageal squamous cell carcinoma. Mol Carcinog 2013; 52(8):581-90.
14. Peng Q, Liu L, Pei H, Zhang J, Chen M, Zhai X. A LHFPL3-AS1/miR-580-3p/STAT3 Feedback Loop Promotes the Malignancy in Melanoma via Activation of JAK2/STAT3 Signaling. Mol Cancer Res 2020; 18(11):1724-1734.
15. Boyle J. Gene-Expression Omnibus integration and clustering tools in SeqExpress. Bioinformatics 2005; 21(10):2550-1.
16. Liu J, Li D, Luo H, Zhu X. Circular RNAs: The star molecules in cancer. Mol Aspects Med 2019; 70:141-152.
17. Yuan Y, Liu W, Zhang Y, Zhang Y, Sun S. CircRNA circ_0026344 as a prognostic biomarker suppresses colorectal cancer progression via microRNA-21 and microRNA-31. Biochem Biophys Res Commun 2018; 503(2):870-875.
18. Tian J, Xi X, Wang J, Yu J, et al. CircRNA hsa_circ_0004585 as a potential biomarker for colorectal cancer. Cancer Manag Res 2019; 11:5413-5423.
19. Yong W, Zhuoqi X, Baocheng W, Dongsheng Z, Chuan Z, Yueming S. Hsa_circ_0071589 promotes carcinogenesis via the miR-600/EZH2 axis in colorectal cancer. Biomed Pharmacother 2018; 102:1188-1194.
20. Friedman RC, Farh KKH, Burge CB, Bartel DP. Most mammalian mRNAs are conserved targets of microRNAs. Genome Res 2009; 19:92-105.
21. Di Leva G, Garofalo M, Croce CM. MicroRNAs in cancer. Annu Rev Pathol 2014; 9:287-314.
22. Tong F, Ying Y, Pan H, Zhao W, Li H, Zhan X. MicroRNA-466 (miR-466) functions as a tumor suppressor and prognostic factor in colorectal cancer

(CRC). Bosn J Basic Med Sci 2018; 18(3):252-259.
23. Ramraj SK, Aravindan S, Somasundaram DB, Herman TS, Natarajan M, Aravindan N. Serum-circulating miRNAs predict neuroblastoma progression in mouse model of high-risk metastatic disease. Oncotarget 2016; 7(14):18605-19.
24. Almog N, Ma L, Schwager C, et al. Consensus micro RNAs governing the switch of dormant tumors to the fast-growing angiogenic phenotype. PLoS One 2012; 7(8):e44001.
25. Bracken CP, Scott HS, Goodall GJ. A network-biology perspective of microRNA function and dysfunction in cancer. Nat Rev Genet 2016; 17:719–732.
26. Zhang W, Xu J. DNA methyltransferases and their roles in tumorigenesis. Biomark Res 2017; 5:1.
27. Jones PA, Laird PW. Cancer epigenetics comes of age. Nat Genet 1999; 21:163–7.
28. Baylin SB, Herman JG. DNA hypermethylation in tumorigenesis: epigenetics joins genetics. Trends Genet 2000; 16:168–74.
29. Rhee I, Bachman KE, Park BH, et al. DNMT1 and DNMT3b cooperate to silence genes in human cancer cells. Nature 2002; 416:552–556.
30. Roll JD, Rivenbark AG, Jones WD, Coleman WB. DNMT3b overexpression contributes to a hypermethylator phenotype in human breast cancer cell lines. Mol Cancer 2008; 7:15.
31. Esteller M. Cancer epigenomics: DNA methylomes and histone-modification maps. Nat Rev Genet 2007; 8(4):286-98.
32. Purkait S, Sharma V, Kumar A, et al. Expression of DNA methyltransferases 1 and 3B correlates with EZH2 and this 3-marker epigenetic signature predicts outcome in glioblastomas. Exp Mol Pathol 2016; 100(2):312-20.
33. Tan M, Wu J, Cai Y. Suppression of Wnt signaling by the miR-29 family is mediated by demethylation of WIF-1 in non-small-cell lung cancer. Biochem Biophys Res Commun 2013; 438:673–679.
34. Chen Z, Liu S, Tian L, et al. miR-124 and miR-506 inhibit colorectal cancer progression by targeting DNMT3B and DNMT1. Oncotarget 2015; 6(35):38139-50.

Sleep quality in partners with spouses and children affected by psoriasis and psoriatic arthritis: insights and implications from a pilot study

G. Damiani[1,2,3], K. Kridin[4], S. Garbarino[5], V. Chattu[6,7], H. Amital[8,9], M. Adawi[10], A. Watad[8,9], A. Pacifico[11], P. D.M. Pigatto[1,2], M. Del Fabbro[1,2], P. Malagoli[12], Young Dermatologists Italian Network[13] and N. L. Bragazzi[6]

Received July 5, 2021 – Accepted 10 February 2022

[1]Department of Biomedical, Surgical and Dental Sciences, University of Milan, Milan, Italy; [2]Clinical Dermatology, IRCCS Istituto Ortopedico Galeazzi, Milan, Italy; [3]PhD Degree Program in Pharmacological Sciences, Department of Pharmaceutical and Pharmacological Sciences, University of Padua, Padua, Italy; [4]Lübeck Institute of Experimental Dermatology, University of Lübeck, Lübeck, Germany; [5]Department of Neuroscience, Rehabilitation, Ophthalmology, Genetics and Maternal/ Child Sciences (DINOGMI), University of Genoa, Genoa, Italy; [6]Laboratory for Industrial and Applied Mathematics (LIAM), Department of Mathematics and Statistics, York University, Toronto, Canada; [7]Department of Psychiatry, University of Toronto, Toronto, Ontario, Canada; [8]Department of Medicine B and Zabludowicz Center for Autoimmune Diseases, Sheba Medical Center, Tel-Hashomer, Ramat-Gan, Israel; [9]Sackler Faculty of Medicine, Tel-Aviv University, Tel-Aviv, Israel; [10]Padeh and Ziv Hospitals, Azrieli Faculty of Medicine, Bar-Ilan University, Ramat Gan, Israel; [11]San Gallicano Dermatological Institute, IRCCS, Rome, Italy; [12]Dermatology Unit, Azienda Ospedaliera San Donato Milanese, Milan, Italy; [13]Study Centre of the Italian Group for Epidemiologic Research in Dermatology (GISED), Bergamo, Italy

Background: **Sleep disturbances are rather common in psoriasis (PsO) and psoriatic arthritis (PsA) patients; however, it is still unclear if they depend intrinsically on PsO/PsA or the predisposing comorbidities such as metabolic syndrome.**

Methods: **This is a multicenter cross-sectional assessing the sleep quality in partners of PsO/PsA patients. Patients and patients' partners were recruited consecutively. After a dermatological visit to the patient, the partner was interviewed to score his/her quality of sleep with Pittsburgh Sleep Quality Index (PSQI).**

Results: **A sample of 84 subjects (aged 45.38±8.55 years, 42 males and 42 females, with an average BMI of 25.24±1.75 kg/m^2) were included. Fifty-two (61.9%) of them developed PsO or PsA before starting the relationship. Although the average PSQI was 4.79±1.47, the prevalence rate of poor sleep raters (PSQI ≥5) was 42 (50.0%). At the multivariate regression, the best independent predictors of sleep quality were "having a PsO/PsA child" and "having a partner affected by PsO since before relationship". More in detail, the former predicted a worse sleep quality [OR 6.98 (95%CI 1.39-35.06)] and the latter a better sleep quality [OR 0.07 (95%CI 0.02-0.23)]. Specifically, performing a subgroup analysis among those who had a child and stratifying according to the presence of an affected child, no differences could be found for each parameter under study, except for PSQI, which was significantly higher in spouses with affected children (6.68±1.11 *versus* 4.35±1.11, p<0.001).**

Corresponding Author:
Dr Giovanni Damiani,
Clinical Dermatology,
IRCCS Galeazzi Orthopaedic Institute,
Via Riccardo Galeazzi 4,
20161, Milan, Italy
e-mail: dr.giovanni.damiani@gmail.com

0393-974X (2022)
Copyright © by BIOLIFE, s.a.s.
This publication and/or article is for individual use only and may not be further reproduced without written permission from the copyright holder.
Unauthorized reproduction may result in financial and other penalties
DISCLOSURE: ALL AUTHORS REPORT NO CONFLICTS OF INTEREST RELEVANT TO THIS ARTICLE.

Conclusions: **The present study showed that having a child significantly negatively impacted on sleep quality of the parent, whereas having a partner being affected by PsO since before the beginning of the relationship protected against poor sleep quality. Having a child affected by PsO was, instead, a risk factor.**

Keywords: sleep quality; psoriasis; psoriatic arthritis, child, spouses

Psoriatic disease, encompassing both psoriasis (PsO) and psoriatic arthritis (PsA), frequently coexist with metabolic syndrome, cardiovascular, and respiratory diseases (1-7), well-known predisposing factors of sleep disturbances (8). Sleep in PsO patients recently gained interest in the scientific community due to its modulatory effect on daily functionality and quality of life perception (9, 10). For instance, these patients have a higher risk of developing obstructive sleep apnea (OSA) with a prevalence rate of 36.0-81.8% *versus* 2.0-4.0% in the general population, as well as restless legs syndrome (15.1-18.0% *versus* 5.0-10.0%), whereas the burden of insomnia seems comparable with that of the general population (5.9-44.8% *versus* 10-35%) (11).

While it is well-established that PsO and PsA patients suffer from poor sleep quality (9, 10), there is a dearth of data about sleep quality in partners with spouses and children affected by PsO and PsA (11). Therefore, the present study was designed to fill in this knowledge gap.

MATERIAL AND METHODS

Study design and patients' recruitment

The present article is a cross-sectional multicenter observational study involving 3 referral hospitals in Italy (IRCCS Istituto Ortopedico Galeazzi, IRCCS San Donato, IRCCS San Gallicano). After obtaining IRB approval from the involved institutions, patient recruitment took place. Each patient signed an informed consent form.

Irrespective of medication (12-17) and diet (18-22), PsO and PsA patients who visited the clinics in August 2019 were asked to volunteer with their partners in the present study. Patients underwent a detailed dermatological assessment, whilst partners medical and pharmacological history were screened, ruling out conditions and drugs that may suggest or cause sleep disturbances.

In particular, the exclusion criteria in the pharmacological history were the habitual or occasional use of benzodiazepines, psychostimulant drugs and antihistamines. In addition, in medical history there were diagnoses of obstructive sleep apnea, narcolepsy, seizure, presence or history of brain tumor, restless leg syndrome, night works or jet-lag (23), a recent change of diet (18-22) and depression.

Clinical measurements

In the dermatological examination, PsO and PsA severity was determined using the "Psoriasis Area of Severity Index" (PASI) and the "Disease Activity in Psoriatic Arthritis" (DAPSA) (24) scores, respectively. DAPSA is a composite indicator that considers several parameters, including clinical symptoms (tender and swollen joints), laboratory findings (CRP) and patient-reported outcomes. Two independent board-certified dermatologists performed all these measurements and two independent board-certified rheumatologists.-Sleep quality measurement was conducted using the Pittsburgh Sleep Quality Index (PSQI) (25) in both partners and patients. The scale comprises 19 items, assessing seven components: namely, subjective sleep quality, sleep latency, sleep duration, habitual sleep efficiency, sleep disturbances, use of sleeping medications and daytime dysfunctions; scores in each domain of sleep quality range from 0 to 3 with the global PSQI ranging from 0 to 21. A total score equal to or greater than 5 has been considered poor sleep quality. All the measurements were collected only if the interobserver agreement were higher than 90%, and the final score was the result of the average between the two measurements.

Statistical analysis

Before starting any statistical processing (including data handling and manipulation), Fig.s were visually inspected for capturing any potential outlier. Normality of data distribution was verified by conducting the Shapiro-Wilk's test, which was preferred to other statistical tests given the small sample size (less than 100 subjects). Continuous data

were expressed as means ± standard deviation, whereas categorical parameters were computed as percentages, where appropriate.

Relevant socio-demographic (age, gender, marital status) and clinical (body mass index, BMI, familiarity for PsO, PASI, DAPSA, pharmacological treatment, and PSQI) information were extracted from clinical charts.

Both univariate (Student's t-test or its non-parametric version in case of violation of normal data distribution, and chi-squared test) and multivariate (multivariate regressions) analyses were conducted to shed light on the determinants of sleep quality among partners with spouses or children affected by PsO.

Figures with a p-value equal to or less than 0.05 were considered statistically significant. All statistical analyses were carried out using the commercial software "Statistical Package for Social Sciences" (SPSS version 24.0, IBM, Armonk, NY, USA). In addition, graphs were generated utilizing the commercial software MedCalc version 18.11.3 (MedCalc Software bvba, Ostend, Belgium).

Table I. *Main characteristics of the sample.*

Parameter	Value
Age (years; mean±standard deviation)	45.38±8.55
Sex (n; %)	
Male	42 (50.0%)
Female	42 (50.0%)
BMI (kg/m^2; mean±standard deviation)	25.24±1.75
Familiarity for PsO (n; %)	32 (38.1%)
PSQI (mean±standard deviation)	4.79±1.47
Poor sleeper (n; %)	42 (50.0%)
Marital status (n; %)	
Living together	25 (29.8%)
Legally married	59 (70.2%)
Relationship duration (years; mean±standard deviation)	12.18±6.99
Partner's age (years; mean±standard deviation)	45.68±8.97
Partner affected before relationship (n; %)	52 (61.9%)
Partner's familiarity for PsO (n; %)	26 (31.0%)
Partner's disease duration (mean±standard deviation)	13.86±8.42
Partner's PASI (mean±standard deviation)	4.99±2.73
Partner with PsA (n; %)	26 (31.0%)
Partner's DAPSA (mean±standard deviation)	5.26±8.39
Partner with past erythroderma (n; %)	24 (28.6%)
Partner 's pharmacological treatment (n; %)	
Adalimumab	17 (20.2%)
Apremilast	9 (10.7%)
Etanercept	22 (26.2%)
Golimumab	1 (1.2%)
Ixekizumab	3 (3.6%)
Metothrexate	9 (10.7%)
Secukinumab	12 (14.3%)
Ustekinumab	11 (13.1%)
With children (n; %)	68 (81.0%)
Affected children (n; %)	19 (27.9%)

BMI: Body Mass Index; DAPSA: Disease Activity Index for Psoriatic Arthritis; PsO: Psoriasis; PsA: Psoriatic Arthritis, PASI: Psoriasis Area Severity Index; PSQI: Pittsburgh Sleep Quality Index.

RESULTS

Characteristics of partners of PsO/PsA patients

We enrolled 84 subjects (42 males and 42 females) with an average age of 45.38±8.55 years and a BMI of 25.24±1.75 kg/m^2. Interestingly, thirty-two (38.1%) had a positive family history of psoriasis. In the cohort, 59 (70.2%) subjects were legally married, whereas 25 (29.8%) lived together, with a relationship lasting on average 12.18±6.99 years.

Characteristics of PsO/PsA patients

Fifty-two (61.9%) patients had been affected by PsO before starting the relationship with a disease duration of 3.86±8.42 years and a current severity quantifiable with PASI of 4.99±2.73. Slightly less than one-third of them (n=26; 31.0%) reported a family history of PsO. Twenty-six are also affected by PsA with a mean DAPSA of 5.26±8.39. From a therapeutic point of view, sixty-six (78.6%) patients were under biologics, 9 (10.7%) under small molecules and 9 (10.7%) on methotrexate. The great majority of the couples had children (n=68, 81.0%), and only 19 (27.9%) children display PsO and/or PsA (Table I).

Sleep evaluation of partners of PsO/PsA patients

Partners displayed an average PSQI of 4.79±1.47, with 50% classified as poor sleep quality subjects due to their PSQI ≥5 points. Comparing partners of patients that experienced PsO/PsA before starting or

Table II. *Characteristics of the recruited sample stratified according to whether the partner had been affected by psoriasis (PsO) already before the commencement of the relationship.*

Parameter	Partner affected before relationship		Statistical significance
	Yes (n=52)	No (n=32)	
Age	46.08±8.34	44.25±8.90	NS
Sex			NS
Male	26 (50.0%)	16 (50.0%)	
Female	26 (50.0%)	16 (50.0%)	
BMI	25.00±1.91	25.63±1.41	NS
Familiarity for PsO	19 (36.5%)	13 (40.6%)	NS
PSQI	4.37±1.46	5.47±1.24	p<0.001

BMI: *Body Mass Index;* ***PsO:*** *Psoriasis;* ***PSQI:*** *Pittsburgh Sleep Quality Index.*

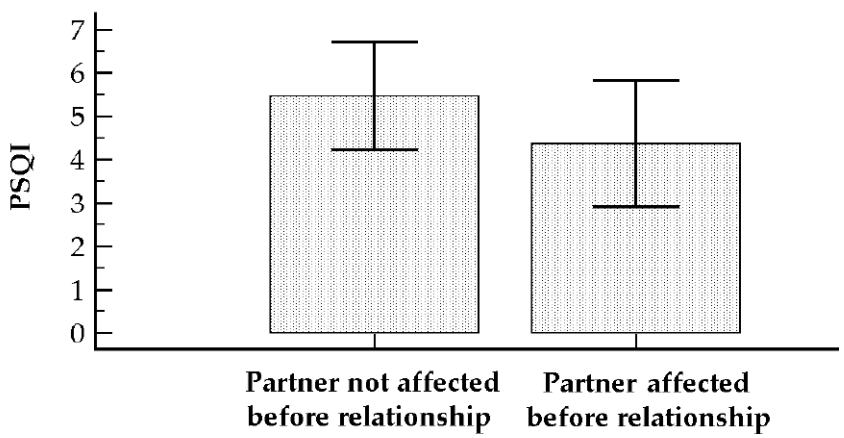


Fig. 1. *Impact of being affected before relationship on the global PSQI score. PSQI: Pittsburgh Sleep Quality Index.*

during the relationship, the PSQI was statistically different (4.37±1.46 vs 5.47±1.24, p<0.001) (Table II). Furthermore, subjects with partners being already affected before the relationship was found to be protected against poor sleep quality [crude OR 0.08 (95%CI 0.02-0.23)] (Fig. 1).

Stratifying according to the presence of a child (Table III), PsA prevalence (25.0% versus 56.2%, p=0.016), and severity (3.88±7.36 versus 11.13±10.10, p=0.002) in the affected, together with sleep quality (5.00±1.53 *versus* 3.88±0.72, p=0.004; Fig. 2) resulted statistically significant. Furthermore, having a child ends up being a risk factor for poor sleep quality [OR 5.83 (95%CI 1.52-22.35)].

At the multivariate regression, the most accurate predictors of sleep quality were "having a child" and "having a partner affected by PsO since before starting the relationship". More in detail, the former predicted a worse sleep quality [OR 6.98 (95%CI 1.39-35.06)] and the latter a better sleep quality [OR 0.07 (95%CI 0.02-0.23)].

Specifically, performing a subgroup analysis among those who had a child and stratifying according to the presence of an affected child (Table IV), no differences could be found for each parameter under study, except for PSQI, which was significantly higher in spouses with affected children (6.68±1.11 *versus* 4.35±1.11, p<0.001; Fig. 3). For further details, the reader is referred to Table III. At the multivariate regression analysis, adjusting for the confounding factors, the presence of an affected child remained statistically significant (regression coefficient=2.70, standard error=0.31, t=8.80, p<0.001, $r_{partial}$=0.77, $r_{semipartial}$=0.68).

Table III. *Characteristics of the recruited sample stratified according to the presence of a child.*

Parameter	With a child		Statistical significante
	Yes (n=68)	No (n=16)	
Age	45.79±8.47	43.63±8.94	NS
Sex			NS
Male	34 (50.0%)	8 (50.0%)	
Female	34 (50.0%)	8 (50.0%)	
BMI	25.22±1.75	25.31±1.82	NS
Familiarity for PsO	26 (38.2%)	6 (37.55%)	NS
Partner's age	46.37±8.61	42.75±10.12	NS
Partner's disease duration	14.04±8.37	13.06±8.84	NS
Partner affected before relationship	40 (58.8%)	12 (75.0%)	NS
Partner's PASI	5.29±2.69	3.69±2.55	NS
Partner's familiarity for PsO	23 (33.8%)	3 (18.8%)	NS
Partner with PsA	17 (25.0%)	9 (56.2%)	0.016
Partner's DAPSA	3.88±7.36	11.13±10.10	0.002
Partner with past erythroderma	21 (30.9%)	3 (18.8%)	NS
Relationship duration	12.88±7.22	9.19±5.02	NS
Marital status			
Legally married	49 (72.1%)	10 (62.5%)	NS
PSQI	5.00±1.53	3.88±0.72	0.004

BMI: *Body Mass Index;* ***DAPSA:*** *Disease Activity Index for Psoriatic Arthritis;* ***PsA:*** *Psoriatic arthritis;* ***PsO:*** *Psoriasis;* ***PSQI:*** *Pittsburgh Sleep Quality Index.*

DISCUSSION

The present study demonstrated that having a child and, specifically, a child affected by PsO negatively impacted the sleep quality of partners of PsO patients, whereas having a partner affected by PsO since before the beginning relationship protected against poor sleep quality.

In the existing scholarly literature, sleep is generally studied at the individual level and rarely from the dyadic (the couple, i.e., the two-bed partners) or triadic (partners and children) perspective (26). Moreover, according to Dittami and colleagues (27), co-sleeping is generally perceived as being more disturbing for women than for men, a finding that Troxel confirmed in a review study (28). However, we could not find any gender-related impact on sleep quality. We could, instead, replicate the so-called effect of social *zeitgebers*, such as children, who, besides the first months of life, dramatically impact sleep-wake rhythms and lifestyles (29).

The impact of having an affected partner/child, even though expected, has been overlooked in the literature, is limited to the impact of partners/children with snoring, OSA or other sleep disturbances (26, 30, 31). Few other diseases, such as diabetes or chronic pain, have been studied and family dynamics dissected (32-34). A recent study by Angelhoff and coworkers assessed using a qualitative approach sleep perceptions in a sample of 12 parents (11 mothers and 1 father) of children aged less than 2 years with atopic dermatitis. Authors found that parents had implemented different coping strategies and skills: namely, i) accepting to have an affected child and its consequence in terms of poor sleep quality and sleep loss, ii) modifying and changing one's lifestyles, and iii) needing support to manage one' sleep disturbances. Interestingly, the first coping strategy led to normalization of parental sleep quality and loss, which is in line with our findings (35). Furthermore, the fatherhood/motherhood wish among psoriatic patients is a complex issue since both the PsO heredity, sexual dysfunction and fertility (36-38) seem to heavily impact families with affected members, and this hardship may be reflected in partners poor sleep quality. In particular, besides the presence of psoriasis in social areas (face, scalp and hands) also, the itch (39, 40) is capable of triggering social stigmatization and impoverishing sleep quality, as recently suggested by Sommer et colleagues (41).

We observed, indeed, that spouses of partners affected before the commencement of the relationship had low PSQI scores and, as such, better sleep quality than their counterparts whose partner had developed PsO after the beginning of the relationship (42). Interestingly, other variables such as duration of the relationship, disease duration and activity/severity had no effect in our investigation, differently from the literature (43-45).

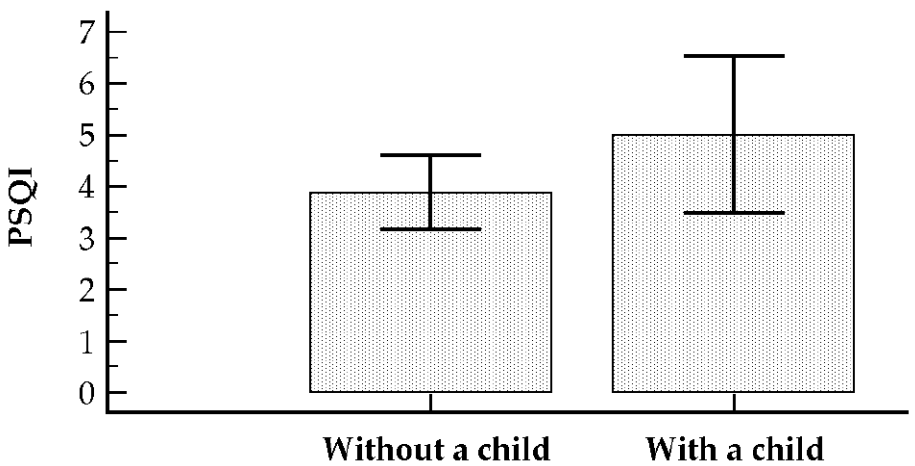


Fig. 2. *Impact of having a child on the global PSQI score. PSQI: Pittsburgh Sleep Quality Index.*

However, despite its novelty, our study is not without any limitations. The main shortcoming is the small sample size utilized in the present investigation. Another drawback is the cross-sectional study design, which does not capture the potential changes in the PSQI score throughout the time. Therefore, further longitudinal studies employing a larger sample size focusing on patient-reported outcomes (i.e. pruritus and pain) are urgently needed. In addition, these studies could investigate the relationship between partners/children affected and other variables/constructs, such as further sleep-related parameters (for example, chronotype, excessive daytime sleepiness and couple sleep concordance), mood, and generally, mental

Table IV. *Characteristics of the recruited sample stratified according to the presence of children affected.*

Parameter	Children affected		Statistical significance
	Yes (n=19)	No (n=49)	
Age	47.89±7.09	44.98±8.88	NS
Sex			NS
Male	7 (36.8%)	27 (55.1%)	
Female	12 (63.2%)	22 (44.9%)	
BMI	24.95±2.01	25.33±1.65	NS
Familiarity for PsO	8 (42.1%)	18 (36.7%)	NS
Partner's age	49.26±6.92	45.24±8.99	NS
Partner's disease duration	16.74±9.13	13.00±7.91	NS
Partner affected before relationship	13 (68.4%)	27 (55.1%)	NS
Partner's PASI	4.47±2.34	5.61±2.78	NS
Partner's familiarity for PsO	5 (26.3%)	18 (36.7%)	NS
Partner with PsA	7 (36.8%)	10 (20.4%)	NS
Partner's DAPSA	6.00±9.15	3.06±6.46	NS
Partner with past erythroderma	8 (42.1%)	13 (26.5%)	NS
Relationship duration	13.68±7.34	12.57±7.23	NS
Marital status			
Legally married	11 (57.9%)	38 (77.6%)	NS
PSQI	6.68±1.11	4.35±1.11	p<0.001

BMI: *Body Mass Index;* ***DAPSA:*** *Disease Activity Index for Psoriatic Arthritis;* ***PsA:*** *Psoriatic arthritis;* ***PsO:*** *Psoriasis;* ***PSQI:*** *Pittsburgh Sleep Quality Index.*

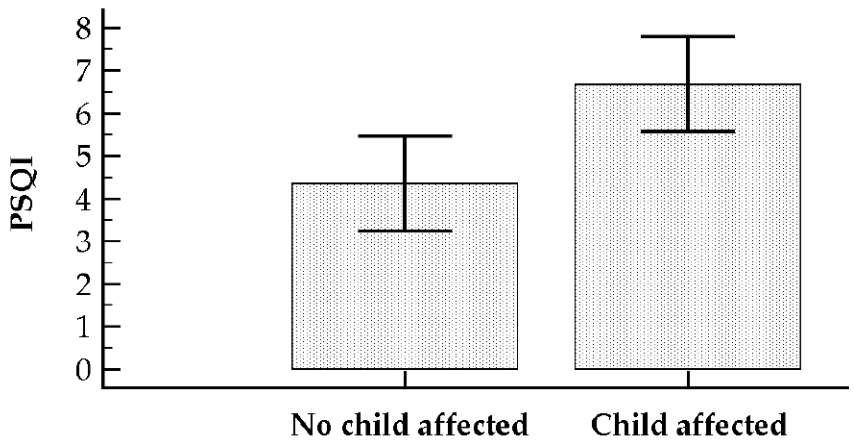


Fig. 3. *Impact of having a child affected by psoriasis on the global PSQI score. PSQI: Pittsburgh Sleep Quality Index.*

health, health-related quality of life, and relationship quality, among others.

This study suggests that having a child or a spouse with psoriasis deeply affects the sleep quality of both parents/partners. Furthermore, the child effect of parents' sleep quality is minimized if the partner developed psoriasis before the relationship. This is an interesting factor that should polarize clinicians' effort to sensitize the population with educative/informative campaigns focusing on psoriasis awareness. This aspect is even more important during the COVID-19 pandemic, in which psoriatic patients are more vulnerable (46-49) and may experience flares due to both SARS-CoV-2 (50) and COVID-19 vaccines (51, 52).

ACKNOWLEDGEMENTS

Funding sources: GD is supported by the P50 AR 070590 01A1 N ational Institute Of Arthritis And Musculoskeletal And Skin Diseases.

IRB status: Approved.

Conflict of interests:

There is no conflict of interest to declare.

REFERENCES

1. Damiani G, Bragazzi NL, Aksut CK, et al. The Global, Regional And National Burden Of Psoriasis: Results And Insights From The Global Burden Of Disease 2019 Study. Front Med (Lausanne) 2021; 8:743180.
2. Seth D, Ehlert AN, Golden JB, et al. Interaction of Resistin and Systolic Blood Pressure in Psoriasis Severity. J Invest Dermatol 2020; 140(6):1279-1282.e1.
3. Conic RR, Damiani G, Schrom KP, et al. Psoriasis and Psoriatic Arthritis Cardiovascular Disease Endotypes Identified by Red Blood Cell Distribution Width and Mean Platelet Volume. J Clin Med 2020; 9(1):186.
4. Damiani G, Radaeli A, Olivini A, et al. Increased airway inflammation in patients with psoriasis. Br J Dermatol 2016; 175(4):797-9.
5. Santus P, Rizzi M, Radovanovic D, et al. Psoriasis and Respiratory Comorbidities: The Added Value of Fraction of Exhaled Nitric Oxide as a New Method to Detect, Evaluate, and Monitor Psoriatic Systemic Involvement and Therapeutic Efficacy. Biomed Res Int 2018; 2018:3140682.
6. Damiani G, Pacifico A, Rizzi M, et al. Patients with psoriatic arthritis have higher levels of FeNO than those with only psoriasis, which may reflect a higher prevalence of a subclinical respiratory involvement. Clin Rheumatol 2020; 39(10):2981-2988.
7. Malerba M, Damiani G, Radaeli A, et al. Narrowband ultraviolet B phototherapy in psoriasis reduces proinflammatory cytokine levels and improves vitiligo and neutrophilic asthma. Br J Dermatol 2015; 173(6):1544-5.
8. Cappuccio FP, Miller MA. Sleep and Cardio-Metabolic Disease. Curr Cardiol Rep 2017; 19(11):110.
9. Nowowiejska J, Baran A, Flisiak I. Mutual Relationship Between Sleep Disorders, Quality of Life and Psychosocial Aspects in Patients With Psoriasis. Front Psychiatry 2021; 12:674460.
10. Nowowiejska J, Baran A, Lewoc M, Grabowska P, Kaminski TW, Flisiak I. The Assessment of Risk and Predictors of Sleep Disorders in Patients with Psoriasis-A Questionnaire-Based Cross-Sectional Analysis. J Clin Med 2021; 10(4):664.
11. Gupta MA, Simpson FC, Gupta AK. Psoriasis and sleep disorders: A systematic review. Sleep Med Rev 2016; 29:63-75.
12. Damiani G, Pacifico A, Chu S, Chi CC; Young Dermatologists Italian Network. Frequency of phototherapy for treating psoriasis: a systematic review. Ital J Dermatol Venerol 2021; doi: 10.23736/S2784-8671.21.06975-3.
13. Damiani G, Conic RRZ, Pigatto PDM, et al. Predicting Secukinumab Fast-Responder Profile in Psoriatic Patients: Advanced Application of Artificial-Neural-Networks (ANNs). J Drugs Dermatol 2020; 19(12):1241-1246.
14. Pacifico A, Damiani G, Iacovelli P, et al. Photoadaptation to ultraviolet B TL01 in psoriatic patients. J Eur Acad Dermatol Venereol 2020; 34(8):1750-1754.
15. Chiricozzi A, Burlando M, Caldarola G, et al. Ixekizumab Effectiveness and Safety in the Treatment of Moderate-to-Severe Plaque Psoriasis: A Multicenter, Retrospective Observational Study. Am J Clin Dermatol 2020; 21(3):441-447.

16. Damiani G, Conic RRZ, Pigatto PDM, et al. From randomized clinical trials to real life data. An Italian clinical experience with ixekizumab and its management. Dermatol Ther 2019; 32(3):e12886.
17. Damiani G, Conic RRZ, de Vita V, et al. When IL-17 inhibitors fail: Real-life evidence to switch from secukinumab to adalimumab or ustekinumab. Dermatol Ther 2019; 32(2):e12793.
18. Kocic H, Damiani G, Stamenkovic B, et al. Dietary compounds as potential modulators of microRNA expression in psoriasis. Ther Adv Chronic Dis 2019; 10:2040622319864805.
19. Asa'ad F, Fiore M, Alfieri A, et al. Saliva as a Future Field in Psoriasis Research. Biomed Res Int 2018; 2018:7290913.
20. Adawi M, Damiani G, Bragazzi NL, et al. The Impact of Intermittent Fasting (Ramadan Fasting) on Psoriatic Arthritis Disease Activity, Enthesitis, and Dactylitis: A Multicentre Study. Nutrients 2019; 11(3):601.
21. Damiani G, Watad A, Bridgewood C, et al. The Impact of Ramadan Fasting on the Reduction of PASI Score, in Moderate-To-Severe Psoriatic Patients: A Real-Life Multicenter Study. Nutrients 2019; 11(2):277.
22. Bragazzi NL, Sellami M, Salem I, et al. Fasting and Its Impact on Skin Anatomy, Physiology, and Physiopathology: A Comprehensive Review of the Literature. Nutrients 2019; 11(2):249.
23. Damiani G, Bragazzi NL, Garbarino S, et al. Psoriatic and psoriatic arthritis patients with and without jet-lag: does it matter for disease severity scores? Insights and implications from a pilot, prospective study. Chronobiol Int 2019; 36(12):1733-1740.
24. Smolen JS, Schoels M, Aletaha D. Disease activity and response assessment in psoriatic arthritis using the Disease Activity index for PSoriatic Arthritis (DAPSA). A brief review. Clin Exp Rheumatol 2015; 33(5 Suppl 93):S48-S50.
25. Buysse DJ, Reynolds CF 3rd, Monk TH, et al. The Pittsburgh Sleep Quality Index: a new instrument for psychiatric practice and research. Psychiatry Res 1989; 28(2):193-213.
26. Richter K, Adam S, Geiss L, Peter L, Niklewski G. Two in a bed: The influence of couple sleeping and chronotypes on relationship and sleep. An overview. Chronobiol Int. 2016; 33(10):1464-1472.
27. Dittami J, Keckeis M, Machatschke I. Sex differences in the reactions to sleeping in pairs versus sleeping alone in humans. Sleep Biol Rhythms 2007; 5:271–6.
28. Troxel WM. It's more than sex: Exploring the dyadic nature of sleep and implications for health. Psychosom Med 2010; 72:578–86.
29. Leonhard C, Randler C. In sync with the family: Children and partners influence the sleep-wake circadian rhythm and social habits of women. Chronobiol Int 2009; 26:510–25.
30. Luyster FS. Impact of Obstructive Sleep Apnea and Its Treatments on Partners: A Literature Review. J Clin Sleep Med 2017; 13(3):467-477.
31. Ondo W. Restless Legs Syndrome "Patient Odyssey" survey of disease burden on patient and spouses/ partners. Sleep Med 2018; 47:51-53.
32. Messina R, Due-Christensen M, Keller-Senn A, et al. Couples living with type 1 diabetes: An integrative review of the impacts on health and wellbeing. J Health Psychol 2021; 26(3):412-437.
33. Tracy EL, Berg CA, Baucom KJW, et al. Daily sleep quality and daily stressors in couples coping with type 1 diabetes. Health Psychol 2019; 38(1):75-83.
34. Song S, Graham-Engeland JE, Mogle J, Martire LM. The effects of daily mood and couple interactions on the sleep quality of older adults with chronic pain. J Behav Med 2015; 38(6):944-955.
35. Angelhoff C, Askenteg H, Wikner U, Edéll-Gustafsson U. "To Cope with Everyday Life, I Need to Sleep" - A Phenomenographic Study Exploring Sleep Loss in Parents of Children with Atopic Dermatitis. J Pediatr Nurs 2018; 43:e59-e65.
36. Filippi F, Odorici G, Conti A, et al. Biological therapy in psoriatic patients whishing fatherhood: a multi-centre italian experience in real life. J Eur Acad Dermatol Venereol 2020; 34(9):e468-e470.
37. De Simone C, Calabrese L, Balato A, et al. Psoriasis and its management in women of childbearing age: tools to increase awareness in dermatologists and patients. G Ital Dermatol Venereol 2020; 155(4):434-440.
38. Finelli R, Leisegang K, Finocchi F, et al. The impact of autoimmune systemic inflammation and associated medications on male reproductive health in patients with chronic rheumatological, dermatological, and gastroenterological diseases: A systematic review. Am J Reprod Immunol 2021; 85(5):e13389.
39. Damiani G, Cazzaniga S, Conic Rr, Naldi L, Psocare

Registry Network. Pruritus characteristics in a large Italian cohort of psoriatic patients. J Eur Acad Dermatol Venereol 2019; 33(7):1316-1324.
40. Damiani G, Kridin K, Pacifico A, et al. Antihistamines-refractory chronic pruritus in psoriatic patients undergoing biologics: aprepitant vs antihistamine double dosage, a real-world data. J Dermatolog Treat 2020; 2020:1-4.
41. Sommer R, Augustin M, Hilbring C, et al. Significance of chronic pruritus for intrapersonal burden and interpersonal experiences of stigmatization and sexuality in patients with psoriasis. J Eur Acad Dermatol Venereol 2021; 35(7):1553-1561.
42. Bragazzi NL, Chattu V, Pacifico A, et al. Sleep quality in parents with children affected by psoriasis, psoriatic arthritis, or atopic dermatitis: a multicenter cross-sectional study. J Biol Regul Homeost Agents. 2021; 35(6):1743-1753.
43. Chen JH, Waite LJ, Lauderdale DS. Marriage, Relationship Quality, and Sleep among U.S. Older Adults. J Health Soc Behav 2015; 56(3):356-77.
44. Roberson PNE, Shorter RL, Woods S, Priest J. How health behaviors link romantic relationship dysfunction and physical health across 20 years for middle-aged and older adults. Soc Sci Med 2018; 201:18-26.
45. Steptoe A, Fancourt D. Leading a meaningful life at older ages and its relationship with social engagement, prosperity, health, biology, and time use. Proc Natl Acad Sci U S A 2019; 116(4):1207-1212.
46. Kridin K, Schonmann Y, Solomon A, et al. Risk of COVID-19 Infection, Hospitalization, and Mortality in Patients with Psoriasis Treated by Interleukin-17 Inhibitors. J Dermatolog Treat 2021; 2021:1-28.
47. Gisondi P, Piaserico S, Naldi L, et al. Incidence rates of hospitalization and death from COVID-19 in patients with psoriasis receiving biological treatment: A Northern Italy experience. J Allergy Clin Immunol 2021; 147(2):558-560.e1.
48. Damiani G, Pacifico A, Bragazzi NL, Malagoli P. Biologics increase the risk of SARS-CoV-2 infection and hospitalization, but not ICU admission and death: Real-life data from a large cohort during red-zone declaration. Dermatol Ther 2020; 33(5):e13475.
49. Bragazzi NL, Riccò M, Pacifico A, et al. COVID-19 knowledge prevents biologics discontinuation: Data from an Italian multicenter survey during RED-ZONE declaration. Dermatol Ther 2020; 33(4):e13508.
50. Zhou Q, Vadakekolathu J, Watad A, et al. SARS-CoV-2 Infection Induces Psoriatic Arthritis Flares and Enthesis Resident Plasmacytoid Dendritic Cell Type-1 Interferon Inhibition by JAK Antagonism Offer Novel Spondyloarthritis Pathogenesis Insights. Front Immunol 2021; 12:635018.
51. Pacifico A, d'Arino A, Pigatto PDM, et al. COVID-19 vaccines do not trigger psoriasis flares in patients with psoriasis treated with apremilast. Clin Exp Dermatol 2021; 46(7):1344-1346.
52. Damiani G, Allocco F; Young Dermatologists Italian Network, Malagoli P. COVID-19 vaccination and patients with psoriasis under biologics: real-life evidence on safety and effectiveness from Italian vaccinated healthcare workers. Clin Exp Dermatol 2021; 46(6):1106-1108.

A DNA damage response mutation-related prognostic gene signature associated with survival outcomes and the immune microenvironment in patients with hepatocellular carcinoma

C. Guo[1#], H. Duan[2#], W. Fu[3], H. He[3], F. Xie[3], Z. Yang[4], M. Zheng[3*] and L. Zhang[5*]

[1]Department of Hepatobiliary Surgery, Hunan Provincial People's Hospital, The First Affiliated Hospital of Hunan Normal University, Changsha, Hunan Province, China; [2]Department of Oncology, Hunan Provincial People's Hospital, The First Affiliated Hospital of Hunan Normal University, Changsha, Hunan Province, China; [3]Department of Gastroenterology, The Second Affiliated Hospital of Kunming Medical University, Kunming, Yunnan, China; [4]The IVD Medical Marketing Department, 3D Medicines Inc., Shanghai, China; [5]Department of Hepatopancreatobiliary Surgery, The First People's Hospital of Yunnan Province, The Affiliated Hospital of Kunming University of Science and Technology, Kunming, Yunnan, China

Received November 23 2021 – Accepted February 9, 2022

[#]Co-first authors

Objective: **We aimed to investigate the key mechanism of the DNA damage response (DDR) mutation in hepatocellular carcinoma (HCC) and construct a prognostic signature for HCC.**

Methods: **Gene expression RNA-Seq data, somatic mutations, and clinical information were downloaded from The Cancer Genome Atlas-Liver Hepatocellular Carcinoma (TCGA-LIHC) dataset. Using survival analysis, stromal score correlation analysis, and DDR mutation-related differential analysis, the stromal prognostic differentially expressed mRNAs in the mutation vs no-mutation group were identified. Then immune infiltration analysis, functional enrichment analysis, and prognostic risk score model construction and evaluation were carried out. Moreover, a novel prognostic nomogram was established using the risk score and independent clinical prognostic factors.**

Results: **The proportions of resting dendritic cells and naïve CD4 T cells differed significantly between the DDR mutation and no-mutation groups. Moreover, the stromal differentially expressed genes (DEGs) in the mutation vs no-mutation group were significantly enriched in DNA replication, with a significant association with DDR. Furthermore, two stromal prognostic DEGs (SCML2 and CCDC134) were identified to construct a prognostic risk model, and the risk score was confirmed as an independent prognostic biomarker in patients with HCC. The established nomogram could predict survival probability at 1, 2, and 3 years.**

Conclusion: **Our data reveal that the DDR mutation-related stromal prognostic gene signature is associated with survival outcomes and the immune microenvironment in patients with HCC. The prognostic nomogram may help improve the clinical outcomes of patients with HCC undergoing personalized treatment.**

Keywords: Hepatocellular carcinoma; immune microenvironment; DNA damage response; mutation, prognosis

**Corresponding author:*
Dr Li Zhang
Department of Hepatopancreatobiliary Surgery, The First People's Hospital of Yunnan Province, The Affiliated Hospital of Kunming University of Science and Technology,
157 Jinbi Road, Xishan District, Kunming City, Yunnan Province, 650034, China.
E-mail: kmzhangli0909@126.com

0393-974X (2022)
Copyright © by BIOLIFE, s.a.s.
This publication and/or article is for individual use only and may not be further reproduced without written permission from the copyright holder.
Unauthorized reproduction may result in financial and other penalties
DISCLOSURE: ALL AUTHORS REPORT NO CONFLICTS OF INTEREST RELEVANT TO THIS ARTICLE.

Liver cancer has the sixth highest incidence and fourth highest mortality among all cancers worldwide, with 841,080 new cases and 781,631 deaths in 2018 (1). Hepatocellular carcinoma (HCC) accounts for approximately 85% of all primary liver cancers (2, 3). Tumor ablation, surgical resection, and liver transplantation have been confirmed as curative therapies for early-stage HCC. However, due to delayed screening for HCC, most patients are diagnosed late, precluding curative therapy and leading to poor prognosis (4, 5). Therefore, developing an effective prognostic model that can be used to identify HCC patients with a high risk of metastasis and recurrence will facilitate clinical management.

The DNA damage response (DDR) is the frontline barrier against spontaneous DNA damage accumulation under genotoxic stress conditions (6). DDR involves a complex network of genes that can sense, recognize, and respond to specific types of DNA damage and activate specific mechanisms to mediate DNA repair, apoptosis, and immune clearance (7, 8). Defects in DDR can lead to genomic instability in cells, contributing to cancer initiation and progression through mutation accumulation (9). Alterations in

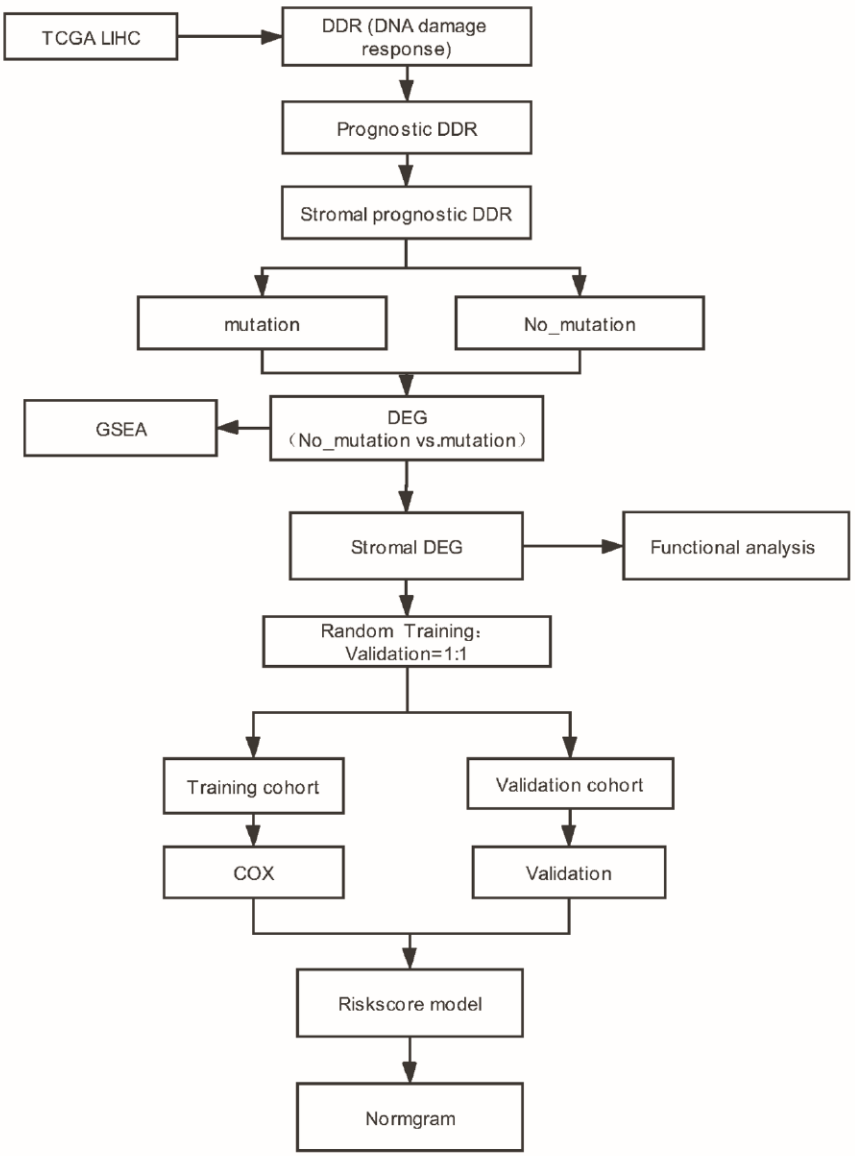


Fig. 1. *The workflow overview of this study.*

DDR pathways are emerging as promising targets for treating diverse cancer types (10-12). Accumulating evidence has revealed that dysregulation of DDR is one of the key mechanisms driving liver carcinogenesis (13, 14) and may lead to radioresistance and limit radiotherapy efficacy in HCC patients (15). In addition, alterations in DDR genes are associated with increased somatic tumor mutational burden (TMB), enhancing immunogenicity (16). A recent study has revealed the mutational landscape of DDR genes and the positive correlation between DDR mutations and TMB levels, suggesting a key role of DDR alterations in primary liver cancer (17). Therefore, elucidation of the key mechanism underlying DDR mutations will have broad prospects for interpreting the prognosis of patients with HCC.

In this study, we downloaded the RNA-Seq data, somatic mutations, and clinical information from The Cancer Genome Atlas Hepatocellular Carcinoma (TCGA-LIHC) database. Using survival analysis, stromal score calculation, correlation analysis and DDR mutation-related differential analysis, we identified differentially expressed mRNAs (DEGs) in the mutation vs the no-mutation group that had prognostic value and were correlated with the stromal score. Immune infiltration analysis, functional enrichment analysis, and prognostic risk score model construction and evaluation were then conducted. Our findings reveal that the DDR mutation-related risk model may be a promising prognostic marker for HCC.

MATERIALS AND METHODS

Data collection

Gene expression RNA-seq data, somatic mutations (SNPs and small INDELs), and clinical phenotype data were downloaded from TCGA-LIHC using the Genomic Data Commons tool. This dataset included 368 tumor samples and 56 adjacent non-tumor samples. Only 368 tumor samples were selected for the subsequent analyses. Ethical approval was not applicable because the data were downloaded from a publicly available database.

Data preprocessing

Based on the platform ID/gene mapping annotation information (hg38, V22) downloaded from the Gencod database (18), Ensembl_ID was converted to Symbol_ID. When multiple Ensembl_ IDs were mapped to the same Symbol_ID, the mean value of different Ensembl_ IDs was used.

Acquisition of DDR genes

Based on a previous study (19), 201 DDR genes were downloaded. Then, by matching with the TCGA dataset, the gene expression matrices of 188 DDR genes were obtained.

Identification of DDR genes related to prognosis

According to the median expression of each DDR gene, the tumor samples were classified into high- or low-expression groups using the survival package (version 3.2-7). Then, based on the survival information in TCGA, Kaplan-Meier (KM) survival curve analyses with log-rank tests were performed to compare the survival differences between the high- and low-expression groups. Differences were considered statistically significant at $p < 0.05$, and DDR genes related to prognosis were identified.

Selection of stromal prognostic DDR genes

The Stromal score was calculated using the Estimation of Stromal and Immune cells in Malignant Tumors using Expression data (ESTIMATE, version 1.0.13) (20) in the R package. Then, the stromal prognostic DDR genes were selected by analyses of the correlation between the stromal score and prognostic DDR genes using the Pearson correlation coefficient with the cor function in the R package. The cut-off value was set to $p < 0.05$.

Based on the somatic mutation (SNPs and small INDELs) data in TCGA, tumor samples were divided into mutation and no-mutation groups according to whether the stromal prognostic DDR genes were mutated or not. The sample with at least one gene mutation was placed in the mutation group; otherwise, it was placed in the no-mutation group. Then, the stromal score between the mutation and no-mutation groups was compared using the T-test, and a box plot was drawn using the Ggpubr package (version 0.2.2) in the R package.

Immune cell infiltration analysis of the mutation and no-mutation groups

The infiltration proportion of 22 immune cell types was analyzed in the mutation and no-mutation groups with cell type identification by estimating relative subsets of RNA

transcripts (CIBERSORT, R 4.0.2) algorithm (21) using the LM22 signature as a reference. The parameters were set as follows: perm = 100 and QN = F.

Differential analysis for the mutation and no-mutation groups

The DEGs between the mutation and no-mutation groups were analyzed using the limma package (version 3.10.3) (22) in R. The cut-off value was set to $p < 0.05$. The volcano plot for the DEGs was plotted using ggplot2.

Gene set enrichment analysis (GSEA)

To observe the pathway enrichment of the mutation and no-mutation groups, c2.cp.kegg.v7.2.symbols.gmt in MSigDB v7.2 (23) was used as the enrichment background. In addition, GSEA was performed using the GSEA algorithm in clusterProfiler (version: 3.16.0) (24) in R.

Functional enrichment analysis for stromal DEGs

The stromal DEGs were obtained by analysing the correlation between the stromal score and DEGs between the mutation and no-mutation groups using the Pearson correlation coefficient in the core function of R. The cut-off value was set to $p < 0.05$. Then, Kyoto Encyclopedia of Genes and Genomes (KEGG) pathway (25) and GO biological processes (GO-BP) (26) enrichment analyses for stromal DEGs were conducted using clusterProfiler (version: 3.16.0). The threshold value was $p < 0.05$ and count ≥ 2.

Construction of the prognostic risk score model

The samples were randomly divided into a training set (184 cases) and a validation set (184 cases). Univariate Cox regression analysis using the survival package was conducted based on the training set to screen the stromal DEGs whose expression levels were significantly associated with overall survival (OS). Candidate stromal DEGs ($p < 0.05$) were included in the multivariate Cox regression analysis to identify the stromal DEGs associated with independent prognosis. The significant factors were defined as $p < 0.05$. Based on the regression coefficient of stromal prognostic DEGs obtained from the multivariate Cox regression analysis and their expression level in the training set, the prognostic risk score model was constructed using the following formula: Risk Score = $\sum$ Coef (i) x Exp (i), where Coef (i) represents the estimated regression coefficient obtained from the multivariate Cox regression analysis, and Exp (i) represents the expression level of each stromal prognostic DEG in the training set.

Evaluation of the prognostic risk score model

The prognostic value of the risk score model was then evaluated in the training set, testing set, and entire set. The patients in the three datasets were all classified into high- or low-risk groups based on the median risk score in each dataset. Finally, KM survival curve analysis with a two-sided log-rank test was performed to evaluate the prognosis of the high- and low-risk patients.

Analysis of independent prognostic factors and establishment of a nomogram

In order to determine independent prognostic factors, univariate and multivariate Cox regression analyses were conducted by analyzing the risk score and other clinical variables, such as TNM stage, G stage, age, and sex. A log-rank of $p < 0.05$ indicated a significant result. A nomogram was constructed by integrating clinical variables that were significantly associated with the prognosis and risk score to analyze the probable 1-, 2-, and 3-year OS of patients.

RESULTS

Identification of prognostic DDR genes

Using KM survival analysis for 188 DDR genes, 80 prognostic DDR genes were obtained.

Selection of stromal prognostic DDR genes

By analyzing the correlation between the stromal score and prognostic DDR genes, 56 stromal prognostic DDR genes were identified. Based on the mutation status of the stromal prognostic DDR genes were mutated or not, there were 85 and 283 samples in the mutation and no-mutation groups, respectively. Moreover, the stromal score of the mutation group was significantly lower than that of the no-mutation group (Fig. 2).

Analysis of immune cell infiltration in the mutation and no-mutation groups

The infiltration proportion of 22 immune cell types was analyzed using the CIBERSORT algorithm to observe the difference in the abundance of immune

cell infiltration between the mutation and no-mutation groups (Fig. 3); only the proportion of resting dendritic cells and naïve CD4 T cells was significantly different between the two groups.

Analysis of DEGs between the mutation and no-mutation groups

With a cut-off value of p <0.05, a total of 1236 DEGs were acquired between the mutation and no-mutation groups, including 767 upregulated genes and 469 downregulated genes. The volcano plot of the DEGs is shown in Fig. 4.

GSEA results

GSEA showed that a total of 45 KEGG pathways associated with mutations were obtained, including 17 positively correlated pathways (*NES > 0)* and 28 negatively correlated pathways (*NES < 0)*. The top five

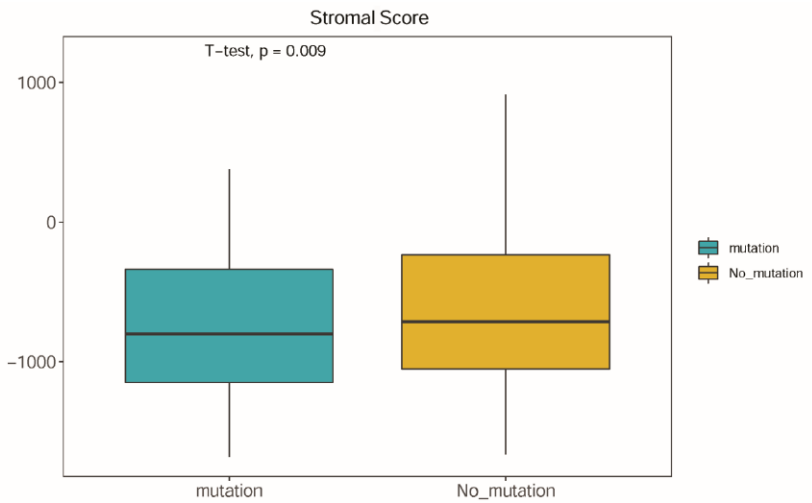


Fig. 2. *The stromal score of the mutation and no_mutation groups.*

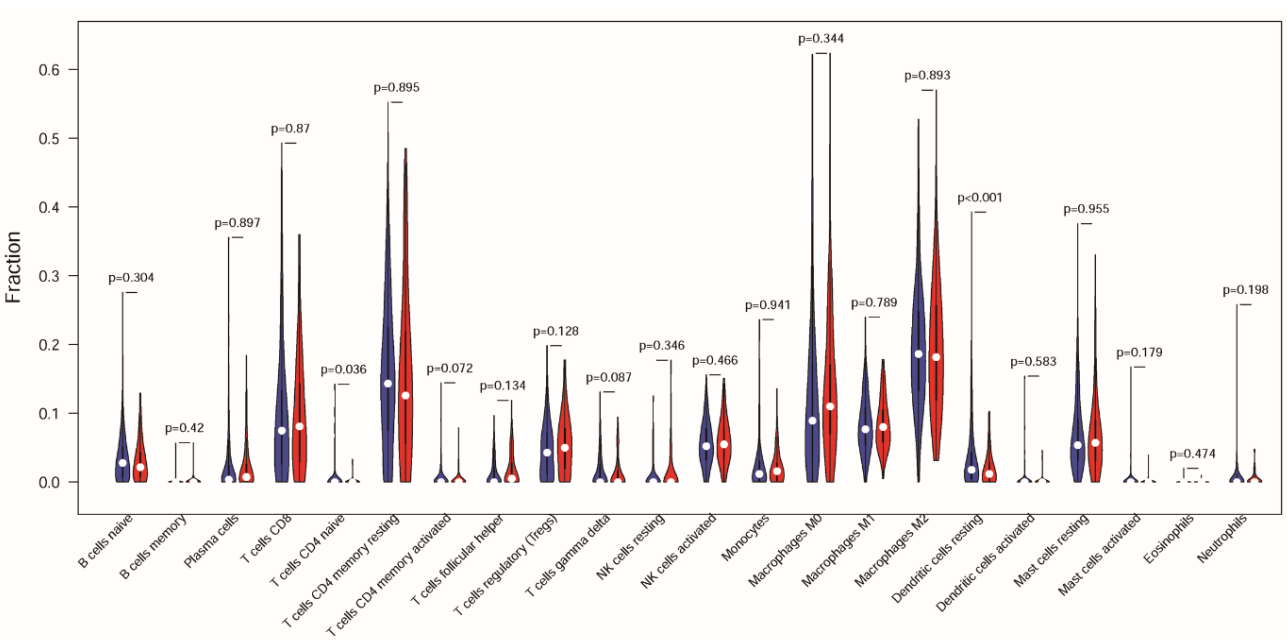


Fig. 3. *The infiltration proportion of 22 immune cell types in the mutation and no_mutation groups. Red indicates the mutation group and blue represents the no_mutation group.*

positively correlated pathways were DNA replication, peroxisome, proteasome, spliceosome, and steroid biosynthesis. The top five negatively correlated pathways were the B cell receptor signaling pathway, ECM receptor interaction, focal adhesion, Leishmania infection, and TGF beta signaling pathway (Fig. 5).

Functional enrichment analysis of the stromal DEGs

By analyzing the correlation between the stromal score and the DEGs between the mutation and no-mutation groups, 61 stromal DEGs were obtained. Further functional enrichment analysis revealed that the stromal DEGs were significantly enriched in one KEGG pathway, namely DNA replication [minichromosome maintenance complex component 7 (*MCM7*) and DNA polymerase delta 1, catalytic subunit (*POLD1*)] (Fig. 6A) and 53 GO-BP terms, such as DNA damage response and detection of

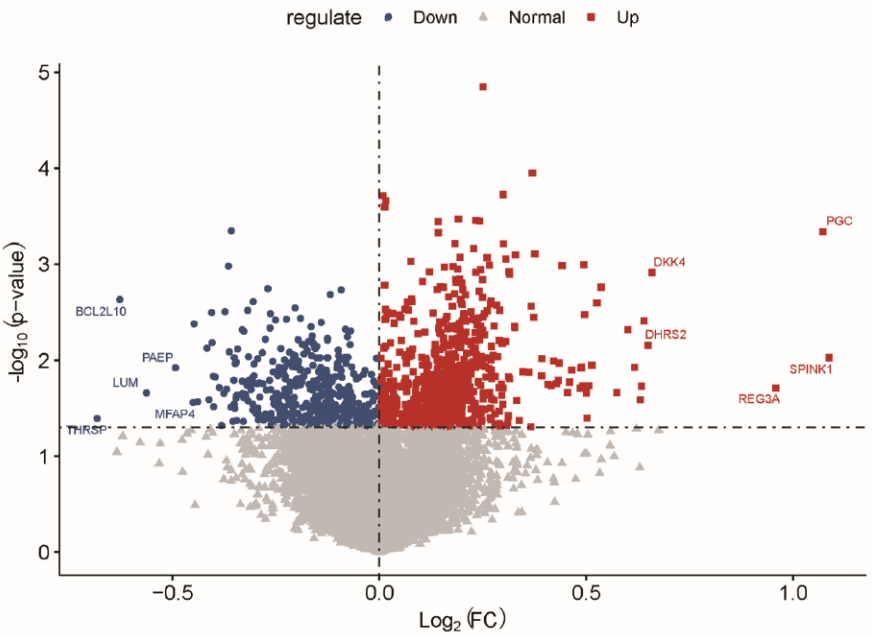


Fig. 4. *The volcano plot for the differentially expressed mRNAs (DEGs) between the mutation and no_mutation groups. The red node indicates upregulated genes, and the blue node indicates downregulated genes. DEGs, differentially expressed genes.*

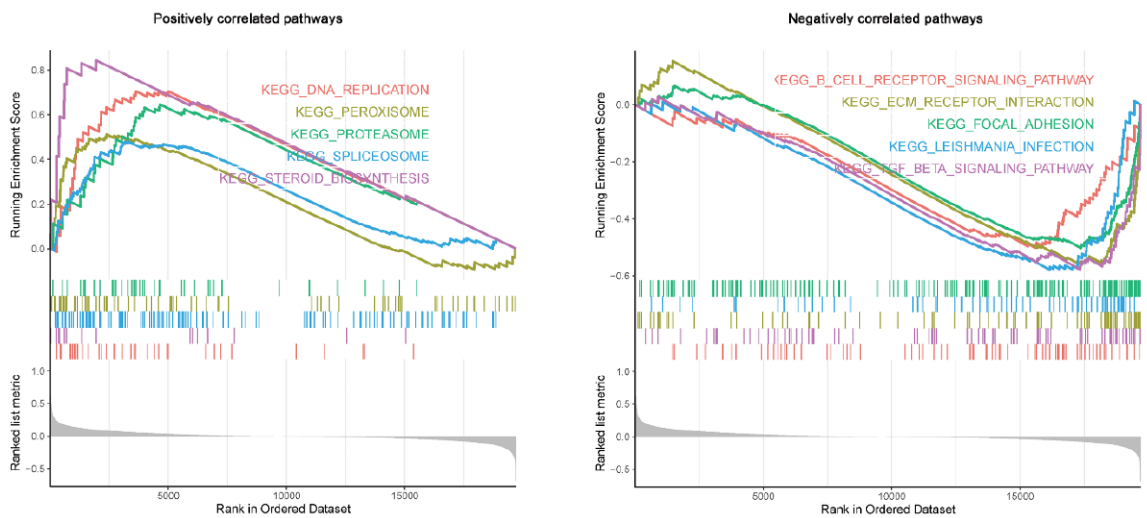


Fig. 5. *GSEA showed the top five positively and negatively correlated pathways associated with DDR mutation. GSEA, gene set enrichment analysis; DDR, DNA damage response.*

DNA damage [E3 ubiquitin-protein ligase RAD18 (*RAD18*) and *POLD1*]. The top 10 GO-BP terms are shown in Fig. 6B.

Construction and evaluation of the prognostic risk score model

Univariate Cox regression analysis was performed on the 61 stromal DEGs, 25 of which correlated significantly with OS. Further multivariate Cox regression analysis was conducted, and two stromal prognostic DEGs were confirmed, namely Scm polycomb group protein-like 2 (*SCML2*) and coiled-coil domain-containing 134 (*CCDC134*) (Fig. 7A). The final prognostic risk score formula was as follows: risk score = *(*0.863407 * expression level of *SCML2)* + *(*0.861212 * expression level of *CCDC134*). Further

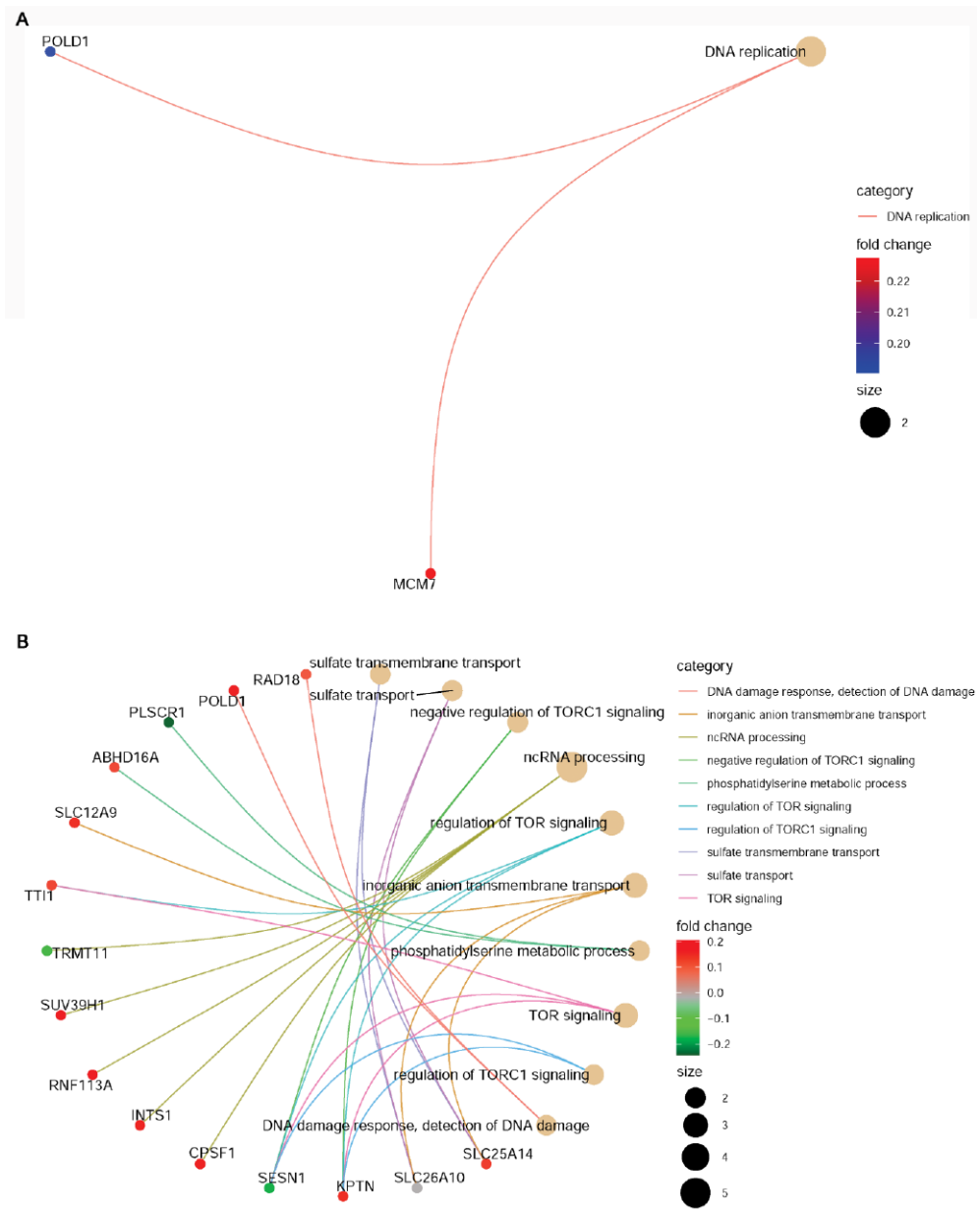


Fig. 6. *Functional enrichment analyses for stromal DEGs. A. KEGG results. B: The top 10 GO-BP terms and enriched genes. KEGG, Kyoto Encyclopedia of Genes and Genomes; GO-BP, Gene Ontology-biological process; DEGs, differentially expressed genes.*

KM survival analysis of the training set, testing set, and entire set yielded consistent results, which showed that the high-risk group had a significantly worse OS than the low-risk group (Fig. 7B).

Identification of independent prognostic factors and construction of a nomogram

The univariate Cox regression analysis results showed that the T stage, M stage, and risk score

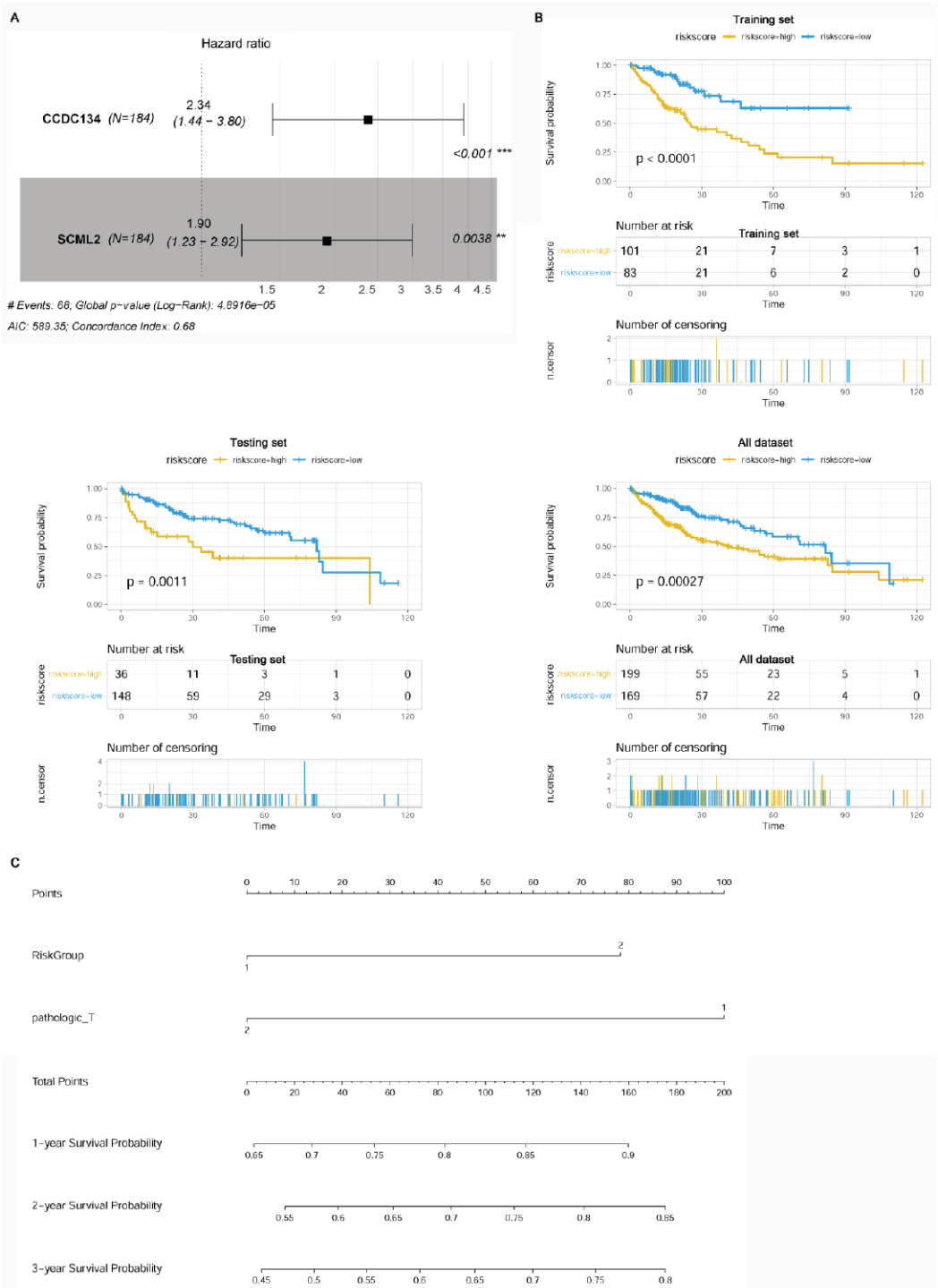


Fig. 7. *Construction and evaluation of the prognostic risk score model. A: The results of the multivariate Cox regression analysis. B: Kaplan-Meier survival analysis of the training set, testing set, and entire set. C: The nomogram established using independent prognostic factors (risk score and T stage).*

were significantly associated with OS. Subsequently, multivariate Cox regression analysis revealed that the T stage and risk score were independent prognostic factors (Table 1). A nomogram was then constructed using these independent prognostic factors; as a result, the established nomogram could be used to predict survival probability at 1, 2, and 3 years (Fig. 7C).

DISCUSSION

HCC remains a lethal disease with a poor prognosis. Due to the high heterogeneity and complex etiologic factors of HCC, it is challenging to predict the prognosis of HCC. However, it has been reported that deleterious DDR mutations are correlated with improved clinical outcomes in patients with lung cancer treated with PD-(L)1 blockade (27). Therefore, elucidation of the key mechanism underlying DDR mutations in HCC will improve patient prognosis. The present study found that the infiltration proportion of resting dendritic cells and naïve CD4T cells exhibited significant differences between the DDR mutation and no-mutation groups. Moreover, stromal DEGs in the mutation vs no-mutation group were significantly enriched in DNA replication, significantly related to DDR. Furthermore, we identified two stromal prognostic DEGs (SCML2 and CCDC134) to construct a prognostic risk model, and the nomogram established using the risk score and clinical factors could accurately predict the survival probability at 1, 2, and 3 years. These data suggest the key mechanisms mediating the role of DDR mutations in HCC and provide a new strategy for improving the prognosis of patients.

Tumor-infiltrating lymphocytes (TILs) are key components of the tumor microenvironment and have crucial effects on carcinogenesis and disease prognosis in many cancer types (28). An increasing number of studies have revealed that tumor-infiltrating lymphocytes are associated with the prognosis of patients with HCC (29). Shirabe et al. revealed that the presence of TILs in HCC is relatively rare, and HCC patients with marked TILs have a better prognosis than patients without TILs (30). In our study, resting dendritic cells and naïve CD4 T cells exhibited significant differences in the proportion of infiltration between the DDR mutation and no-mutation groups. In a previous study, the fraction of resting dendritic cells differed between the bone metastasis and non-bone metastasis groups, suggesting the critical role of resting dendritic cells in mesothelioma with bone metastasis (31). Furthermore, Su et al. indicated that the abundance of naïve CD4 T cells is correlated with poor prognosis in breast cancer patients (32). These data suggest that the resting tumor-infiltrating dendritic cells and naïve CD4 T cells may play a key role in HCC patients with DDR mutations.

Another important finding of our study was that stromal DEGs were significantly enriched in DNA replication. DNA replication is the basis for cellular proliferation, whose dysregulation is a driving force of oncogenesis, and exploiting replication stress may be a promising strategy for cancer treatment (33; 34). Our results showed that MCM7 and POLD1 were significantly enriched in DNA replication. It has been reported that MCM7 participates in initiating DNA replication and is suggested as a potential biomarker in various human malignancies (35; 36). In HCC, elevated MCM7 expression was significantly associated with intrahepatic metastasis, vascular invasion, and patient prognosis (37; 38). Furthermore, POLD1 is essential for proofreading and fidelity in DNA replication, and its mutation is associated with immunotherapy outcomes in diverse cancer types (39). Given the key role of MCM7 and POLD1 in DNA replication, we speculate that DDR mutations may contribute to HCC development by affecting the expression of MCM7 and POLD1 to regulate DNA replication.

Notably, our constructed prognostic risk score model showed strong prognostic, predictive capabilities. Our prognostic signature was composed of two stromal score- and DDR mutation-related genes, including SCML2 and CCDC134. SCML2 is one of the four homologs of Scm and is involved in several human tumors (40), including HCC (41). CCDC134 is a secreted protein that may function as an immune cytokine and contribute to cancer immunotherapy's CD8+ T cell effector functions (42). In addition, CCDC134 has been implicated in MAPK signal

transduction (43) and suppresses the migration and invasion of tumor cells through the MAPK pathway (44). Although the roles of SCML2 and CCDC134 in DDR have not been fully elucidated, we speculate that DDR mutations may regulate HCC development by increasing the expression of SCML2 and CCDC134. Our results also showed that the nomogram established by independent prognostic factors (T stage and risk score) could be used to predict the survival probability at 1, 2, and 3 years. Taken together, we confirmed that this prognostic signature could be used to accurately predict the survival outcomes of patients with high- and low-risk HCC.

This study had several limitations. First, the clinicopathological information of HCC patients extracted from TCGA was limited. Second, our prognostic model was constructed using public data from TCGA. Further validating the prognostic model in more real-world cohorts is warranted to verify its clinical utility. Lastly, the expression of key stromal prognostic DDR mutation-related genes has not yet been experimentally addressed. Given that all the analyses were based on public data in TCGA, the mechanism needs to be verified with cell and animal experimentation.

In conclusion, our study revealed that the DDR mutation may contribute to HCC development and affect patient prognosis by influencing tumor-infiltrating resting dendritic cells and naïve CD4 T cells and regulating DNA replication. The constructed prognostic signature can accurately predict the survival outcomes of HCC patients and distinguish them into high- and low-risk groups. Key DDR genes, such as MCM7, POLD1, SCML2, and CCDC134, may serve as potential therapeutic targets for HCC. Moreover, the constructed nomogram based on the prognostic signature and clinical parameters may help improve the clinical outcomes of patients with HCC undergoing personalized treatment.

ACKNOWLEDGEMENTS

This study was supported by an experimental study on allogeneic adoptive immunotherapy with dual targets of HCC tumor cells and the extracellular matrix (No. C0120180642).

Conflict of interest

The authors declare that they have no conflict of interest.

REFERENCES

1. Bray F, Ferlay J, Soerjomataram I, Siegel RL, Torre LA, Jemal A. Global cancer statistics 2018: GLOBOCAN estimates of incidence and mortality worldwide for 36 cancers in 185 countries. CA Cancer J Clin 2018; 68(6):394-424.
2. Harris PS, Hansen RM, Gray ME, Massoud OI, McGuire BM, Shoreibah MG. Hepatocellular carcinoma surveillance: An evidence-based approach. World J Gastroenterol 2019; 25(13):1550-9.
3. Rawat D, Shrivastava S, Naik RA, Chhonker SK, Mehrotra A, Koiri RK. An Overview of Natural Plant Products in the Treatment of Hepatocellular Carcinoma. Anticancer Agents Med Chem 2018; 18(13):1838-59.
4. Ko K-L, Mak L-Y, Cheung K-S, Yuen M-F. Hepatocellular carcinoma: recent advances and emerging medical therapies. F1000Res 2020; 9:F1000 Faculty Rev-620.
5. Francica G, Borzio M. Status of, and strategies for improving, adherence to HCC screening and surveillance. J Hepatocell Carcinoma 2019; 6:131-41.
6. Sy SM, Guo Y, Lan Y, Ng H, Huen MS. Preemptive Homology-Directed DNA Repair Fosters Complex Genomic Rearrangements in Hepatocellular Carcinoma. Transl Oncol 2020; 13(9):100796.
7. Ciccia A, Elledge SJ. The DNA damage response: making it safe to play with knives. Mol Cell 2010; 40(2):179-204.
8. McNally JP, Millen SH, Chaturvedi V, et al. Manipulating DNA damage-response signaling for the treatment of immune-mediated diseases. Proc Natl Acad Sci U S A 2017; 114(24):E4782-91.
9. Pilié PG, Tang C, Mills GB, Yap TA. State-of-the-art strategies for targeting the DNA damage response in cancer. Nat Rev Clin Oncol 2019; 16(2):81-104.
10. Mauri G, Arena S, Siena S, Bardelli A, Sartore-Bianchi A. The DNA damage response pathway as a land of therapeutic opportunities for colorectal cancer. Ann Oncol 2020; 31(9):1135-47.
11. Carrassa L, Damia G. DNA damage response

inhibitors: Mechanisms and potential applications in cancer therapy. Cancer Treat Rev 2017; 60:139-51.
12. Wengner AM, Scholz A, Haendler B. Targeting DNA Damage Response in Prostate and Breast Cancer. Int J Mol Sci 2020; 21(21):8273.
13. Nagahashi M, Matsuda Y, Moro K, et al. DNA damage response and sphingolipid signaling in liver diseases. Surg Today 2016; 46(9):995-1005.
14. Tahmasebi-Birgani M, Ansari H, Carloni V. Defective mitosis-linked DNA damage response and chromosomal instability in liver cancer. Biochim Biophys Acta Rev Cancer 2019; 1872(1):60-65.
15. Sun J, Zhu Z, Li W, et al. UBE2T-regulated H2AX monoubiquitination induces hepatocellular carcinoma radioresistance by facilitating CHK1 activation. J Exp Clin Cancer Res 2020; 39(1):222.
16. Mouw KW, Goldberg MS, Konstantinopoulos PA, D'Andrea AD. DNA Damage and Repair Biomarkers of Immunotherapy Response. Cancer Discov 2017; 7(7):675-93.
17. Lin J, Shi J, Guo H, et al. Alterations in DNA Damage Repair Genes in Primary Liver Cancer. Clin Cancer Res 2019; 25(15):4701-11.
18. Harrow J, Frankish A, Gonzalez JM, et al. GENCODE: the reference human genome annotation for The ENCODE Project. Genome Res 2012; 22(9):1760-74.
19. Wang Z, Zhao J, Wang G, et al. Comutations in DNA Damage Response Pathways Serve as Potential Biomarkers for Immune Checkpoint Blockade. Cancer Res 2018; 78(22):6486-96.
20. Yoshihara K, Shahmoradgoli M, Martínez E, et al. Inferring tumour purity and stromal and immune cell admixture from expression data. Nat Commun 2013; 4:2612.
21. Newman AM, Liu CL, Green MR, et al. Robust enumeration of cell subsets from tissue expression profiles. Nat Methods 2015; 12(5):453-7.
22. Smyth GK. 2005. Limma: Linear Models for Microarray Data. In Bioinformatics and Computational Biology Solutions Using R and Bioconductor, ed. R Gentleman, VJ Carey, W Huber, RA Irizarry, S Dudoit:397-420. New York, NY: Springer New York.
23. Liberzon A, Birger C, Thorvaldsdottir H, Ghandi M, Mesirov JP, Tamayo P. The Molecular Signatures Database Hallmark Gene Set Collection. Cell systems 2015; 1(6):417-25.
24. Yu G, Wang L, Han Y, He Q. clusterProfiler: an R package for comparing biological themes among gene clusters. OMICS 2012; 16(5):284-7.
25. Kanehisa M, Goto S. KEGG: Kyoto Encyclopedia of Genes and Genomes. Nucleic Acids Res 2000; 28(1):27-30.
26. Carbon S, Douglass E, Dunn N, et al. The Gene Ontology Resource: 20 years and still GOing strong. Nucleic Acids Res 2019; 47(D1):D330-D338.
27. Ricciuti B, Recondo G, Spurr LF, et al. Impact of DNA Damage Response and Repair (DDR) Gene Mutations on Efficacy of PD-(L)1 Immune Checkpoint Inhibition in Non-Small Cell Lung Cancer. Clin Cancer Res 2020; 26(15):4135-42.
28. Paijens ST, Vledder A, de Bruyn M, Nijman HW. Tumor-infiltrating lymphocytes in the immunotherapy era. Cell Mol Immunol 2021; 18(4):842-59.
29. Ding W, Xu X, Qian Y, et al. Prognostic value of tumor-infiltrating lymphocytes in hepatocellular carcinoma: A meta-analysis. Medicine (Baltimore) 2018; 97(50):e13301.
30. Shirabe K, Motomura T, Muto J, et al. Tumor-infiltrating lymphocytes and hepatocellular carcinoma: pathology and clinical management. Int J Clin Oncol 2010; 15(16):552-8.
31. Huang R, Wu J, Zheng Z, et al. The Construction and Analysis of ceRNA Network and Patterns of Immune Infiltration in Mesothelioma With Bone Metastasis. Front Bioeng Biotechnol 2019; 7:257.
32. Su S, Liao J, Liu J, et al. Blocking the recruitment of naive CD4(+) T cells reverses immunosuppression in breast cancer. Cell Res 2017; 27(4):461-82.
33. Ubhi T, Brown GW. Exploiting DNA Replication Stress for Cancer Treatment. Cancer Res 2019; 79(8):1730-9.
34. Kitao H, Iimori M, Kataoka Y, et al. DNA replication stress and cancer chemotherapy. Cancer Sci 2018; 109(2):264-71.
35. Toyokawa G, Masuda K, Daigo Y, et al. Minichromosome Maintenance Protein 7 is a potential therapeutic target in human cancer and a novel prognostic marker of non-small cell lung cancer. Mol Cancer 2011; 10:65.
36. Coli A, Asa SL, Fadda G, et al. Minichromosome maintenance protein 7 as prognostic marker of tumor aggressiveness in pituitary adenoma patients. Eur J Endocrinol 2016; 174(3):307-14.

37. Zhou YM, Zhang XF, Cao L, et al. MCM7 expression predicts post-operative prognosis for hepatocellular carcinoma. Liver Int 2012; 32(10):1505-9.
38. Qu K, Wang Z, Fan H, et al. MCM7 promotes cancer progression through cyclin D1-dependent signaling and serves as a prognostic marker for patients with hepatocellular carcinoma. Cell Death Dis 2017; 8(2):e2603.
39. Wang F, Zhao Q, Wang Y-N, Jin Y, He M-M, Liu Z-X, Xu R-H. Evaluation of POLE and POLD1 Mutations as Biomarkers for Immunotherapy Outcomes Across Multiple Cancer Types. JAMA Oncol 2019; 5(10):1504-6.
40. Yang J-J, Huang H, Xiao M-B, et al. Sex comb on midleg like-2 is a novel specific marker for the diagnosis of gastroenteropancreatic neuroendocrine tumors. Exp Ther Med 2017; 14(2):1749-55.
41. Qi L, Wang L, Huang J, et al. Activated amelogenin Y-linked (AMELY) regulation and angiogenesis in human hepatocellular carcinoma by biocomputation. Oncol Lett 2013; 5(3):1075-9.
42. Huang J, Xiao L, Gong X, et al. Cytokine-like molecule CCDC134 contributes to CD8+ T-cell effector functions in cancer immunotherapy. Cancer Res 2014; 74(20):5734-45.
43. Huang J, Shi T, Ma T, et al. CCDC134, a novel secretory protein, inhibits activation of ERK and JNK, but not p38 MAPK. Cell Mol Life Sci 2008; 65(2):338-49.
44. Zhong J, Zhao M, Luo Q, et al. CCDC134 is down-regulated in gastric cancer and its silencing promotes cell migration and invasion of GES-1 and AGS cells via the MAPK pathway. Mol Cell Biochem 2013; 372(1):1-8.

TTN-AS1 is altered during inhalation therapy in COPD patients and aggravates cigarette smoke extracts-induced lung epithelial cell injury via sponging miR-15b-5p

E. Guo[#], Y. Wu[#] and L. Zhang[*]

Department of Respiratory and Critical Care Medicine, Xiangyang Central Hospital, Affiliated Hospital of Hubei University of Arts and Science, Xiangyang, Hubei, China

Received July 8, 2021 – Accepted February 1, 2022

[#]These authors contributed equally.

Smoking has been found to contribute to the development of chronic obstructive pulmonary disease (COPD), with incompletely reversible airflow limitation. TTN-AS1 has been confirmed to modulate cell proliferation and apoptosis, but its expression in COPD patients and its function in lung bronchial epithelial cell injury remain elusive. The profiles of TTN-AS1 and miR-15b-5p in COPD patients and cigarette smoke extract (CSE)-induced 16HBE cells (*in vitro* COPD model) were examined by real-time quantitative PCR (RT-qPCR). We applied TTN-AS1 overexpression plasmids and miR-15b-5p mimics for gain-of-function assay. Cell proliferation was tested by the cell counting kit-8 (CCK-8) assay, while cell apoptosis was evaluated by flow cytometry (FCM), TdT-mediated dUTP nick end labeling (TUNEL) staining, and Western blot (WB), respectively. Meanwhile, the profiles of inflammatory cytokines were testified by enzyme-linked immunosorbent assay (ELISA), and the levels of COX2, iNOS and NF-κB were monitored by WB. Besides, the targeting correlation between TTN-AS1 and miR-15b-5p was predicted by the Starbase database. Moreover, the binding association between the two was further measured by the dual-luciferase reporter assay and RNA immunoprecipitation (RIP) method. Our findings showed that TTN-AS1 expression was dramatically strengthened, while miR-15b-5p profiles were curbed in CSE-treated 16HBE cells and serum of COPD patients (compared with healthy donors). Functionally, overexpressing TTN-AS1 aggravated CSE-induced cell viability inhibition and apoptosis and intensified inflammations in 16HBE. Furthermore, miR-15b-5p up-regulation eased CSE-mediated cell damage and inflammation and reversed the effects of TTN-AS1. Mechanically, TTN-AS1 targeted and repressed miR-15b-5p. In conclusion, TTN-AS1 and miR-15b-5p are promising diagnostic molecules for COPD, and TTN-AS1 aggravates CSE-induced human bronchial epithelial cell apoptosis by regulating miR-15b-5p.

Chronic obstructive pulmonary disease (COPD) is a frequent airway illness manifested as irreversible airflow restriction, recurrent airway inflammation and emphysematous destruction (1-2). Oxidative stress, epigenetics, cell senescence, cell death, chronic inflammation, environmental pollution, occupational chemical exposure and other factors have been reported to affect COPD progression (3). Among them, exposure to cigarette smoking (CS), whether active smoking or second-hand smoke, is the dominant

Keywords: chronic obstructive pulmonary disease; miR-15b-5p; TTN-AS1; Apoptosis; Inflammation

[*]*Corresponding Author:*
Dr Ling Zhang,
Department of Respiratory and Critical Care Medicine,
Xiangyang Central Hospital,
Affiliated Hospital of Hubei University of Arts and Science,
Xiangcheng District,
Xiangyang 441000, Hubei, China
e-mail: zhang_ling20@163.com

0393-974X (2022)
Copyright © by BIOLIFE, s.a.s.
This publication and/or article is for individual use only and may not be further reproduced without written permission from the copyright holder.
Unauthorized reproduction may result in financial and other penalties
DISCLOSURE: ALL AUTHORS REPORT NO CONFLICTS OF INTEREST RELEVANT TO THIS ARTICLE.

cause of COPD (4-5). The main influence of smoking on COPD is the direct activation of epithelial cells and macrophages and the release of cytokines and chemokines, leading to the recruitment of neutrophils and other inflammatory cells (6), which seriously aggravates COPD, lowers the quality of life and increases the social and economic burden. Hence, it's crucial to study the molecular mechanism of smoking-induced COPD for future prophylaxis and therapy.

Long non-coding RNAs (lncRNAs) are not translated into proteins, which regulate gene expression at the transcriptional and post-transcriptional levels and then contribute to the evolvement of various diseases (7). Growing research has reported that multiple types of lncRNAs are extensively involved in COPD development. For instance, some studies reveal that LINC00987 improves COPD by regulating the Let-7b-5p/SIRT1 axis to impede LPS-induced BEAS-2B cell apoptosis, oxidative stress, inflammation, and autophagy (8). Additionally, LncRNA MEG3 contributes to COPD by modulating pulmonary microvascular endothelial cell apoptosis (9). Also, Song J et al. state that LncRNA MIR155HG intensifies microvascular endothelial cell death and inflammation in smoke-related COPD by modulating miR-128-5p/BRD4 (10). TTN-AS1 is a lncRNA that has been demonstrated to have significant value in liver cancer (11), cutaneous melanoma (12), and other cancers. Nevertheless, its role in COPD has not been reported.

As another type of non-coding RNAs about 18-24 nt long, microRNAs (miRNAs) have been identified to participate in the pathological process of COPD. For instance, Liu X et al. have found that overexpressing miR-218 dampens CSE-induced bronchial epithelial cell apoptosis and inflammation by targeting BRD4 (13). Besides, miR-486-5p heightens COPD by targeting HAT1 to modulate TLR4-triggered inflammation in alveolar macrophages (14). As a miRNA, miR-15b-5p is involved in many diseases, including diabetic nephropathy (15), neutrophil extracellular trap formation during septic shock (16) and chemoresistance of colon cancer (17). However, its function in COPD remains unclear.

Here, we found that TTN-AS1 expression was heightened while miR-15b-5p profiles were restrained in COPD patients and CSE-treated 16HBE cells. Mechanically, TTN-AS1 targeted miR-15b-5p. This study reveals that TTN-AS1 aggravates CSE-induced human bronchial epithelial cell apoptosis and inflammation by impeding miR-15b-5p, which provides a referable molecular marker for clinical treatment and prognosis of COPD.

MATERIALS AND METHODS

Clinical samples

The serum samples of 69 patients (23 non-smokers, 23 smokers without COPD, and 23 smokers with COPD) who received treatment at Xiangyang Central Hospital, Affiliated Hospital of Hubei University of Arts and Science, were selected. Each participant signed informed consent. This study was authorized by the Medical Ethics Committee of Xiangyang Central Hospital, Affiliated Hospital of Hubei University of Arts and Science.

Cell culture

Human bronchial epithelial 16HBE cells were bought from the Shanghai Institute of Cell Biology, Chinese Academy of Sciences (Shanghai, China) and cultured in the RPMI1640 medium filled with 10% fetal bovine serum (Invitrogen Carlsbad, USA) at 37°C with 5% CO_2. Cigarette smoke extracts (CSE) at different concentrations (0.5%, 5%, and 10%) were applied to act on 16HBE cells for 12 hours.

Preparation of CSE

Smoke from 10 cigarettes (Yuxi, Hongta tobacco group, Yunnan, China) was cultured in 25 mL medium. The harvested suspension was titrated to reach a PH value of 7.4, filtered and disinfected (the concentration was regarded as100%). Then, the samples were diluted with PBS to respectively obtain CSE at concentrations of 0.5%, 5% and 10% and stored at -80°C.

Cell transfection

16HBE cells at the logarithmic growth stage were trypsinized, sub-cultured, and seeded into 6-well plates (5×10^6 per well). The transfection was made after cell growth was stable. Briefly, lncRNA TTN-AS1 overexpression plasmids, miR-15b-5p mimics and matched negative controls were transfected into 16HBE cells following the

FuGENEHD Transfection Reagent (Roche, Shanghai, China). Afterwards, the cells were incubated at 37℃ with 5% CO_2 and utilized for subsequent experiments 24 hours later.

Real-time quantitative PCR (RT-qPCR)

Total cellular RNA was separated with the TRIzol reagent. Then, it was transcribed into cDNA with the PrimeScript™ RT Reagent kit (Invitrogen, Shanghai, China) per the manufacturer's guidelines. RT-qPCR was implemented with the Bio-Rad CFX96 quantitative PCR system and SYBR. The reaction conditions were pre-denaturation at 95˚C for 5 min, denaturation at 95˚C for 15 s, and annealing at 60˚C for 30 s. GAPDH was the endogenous control of TTN-AS1, and U6 was that of miR-15b-5p. The $2^{(-\Delta\Delta Ct)}$ method was employed for statistical analysis. The qRT-PCR was made in triplicate. The primers were synthesized by Guangzhou Ribo Biotechnology Co. Ltd. (Table I).

Western blot (WB)

16HBE cells were harvested and rinsed by cold PBS 3 times and added to RIPA lysate (Beyotime Biotechnology, Shanghai, China). Next, they were dissociated in ice water with ultrasound, and the protein content was quantified by the Bradford method. The same amount of proteins was taken from each group for 10% SDS-PAGE, and the proteins on the gel were transferred to PVDF membranes (Millipore, Bedford, MA, USA). Then, the membranes were sealed at 4℃ for 1 hour and incubated at 4℃ overnight with the following primary antibodies (1:1000) of Bax (ab32503), Caspase3 (ab13847), Bcl2 (ab182858), COX2 (ab62331), iNOS (ab202417), P-NF-κB p50 (ab28849), and NF-κB p50 (ab220803). After washing the membranes twice with TBST, we incubated them at room temperature (RT) for 1 h with the fluorescein-labeled Goat-anti Rabbit IgG (ab6721, 1:2500). The above antibodies were all from Abcam (Cambridge, UK). After the membranes were rinsed three times, they were exposed with the ECL chromogenic agent (Millipore, Bedford, MA, USA) and visualized with a membrane scanner.

Table I. *Primer sequences of each gene*

Primer sequence of gene name (5'→3')
miR-15b-5p
F: UAAUACCGUCUUAAAACCGU
R: UUCUGGGAACGUGAAACCT
TTN-AS1
F: TACTTCCATGCTGTCCCTGG
R: AGAAGCCACCATTGAGACCA
U6
F: CTCGCTTCGGCAGCACA
R: AACGCTTCACGAATTTGCGT
GAPDH
F: TGATCTTCATGGTCGACGGT
R: CCACGAGACCACCACCTACAACT

Cell counting kit-8 (CCK-8) method

CCK-8 (Dojindo, Tokyo) was utilized to measure cell proliferation following the manufacturer's guidelines. Three thousand cells were seeded into 96-well plates. Then, each well was filled with 10 μL of CCK-8 solution. After 1 hour of incubation at 37℃, the absorbance at 450 nM was reviewed by Synergy 2 microplate reader (BioTek, Winooski, VT, USA).

Flow cytometry (FCM)

Cell apoptosis was measured by Annexin V-FITC double staining. After transfection for 24 h,16HBE cells were trypsinized, collected and planted in 6-well plates (2×10^6 cells/well). After further culture for 24 h, the supernatant was removed, and the cells were cleaned with precooled PBS and resuspended with 1×Binding buffer. AnnexinV-FITC (5 μL) and PI (5 μL) were added to the cell suspension, thoroughly mixed and maintained at RT for 15 min. The apoptotic rate was determined by FCM within 1 hour, which was calculated as the apoptotic cell number/(the apoptotic cell number + the normal cell number) ×100%. The determination was made according to the apoptosis kit (purchased from Yeasen Biotech Co., Ltd, Shanghai, China) instructions.

Enzyme-linked immunosorbent assay (ELISA)

The contents of inflammatory cytokines in the cell supernatant were evaluated by ELISA. Briefly, protein contents of inflammatory cytokines (IL-1β, IL-6 and

TNF-a) in the supernatant were measured by the ELISA kit (Elabscience, Wuhan, China). The determination was made at 450 nM with Centro LB 960 microplate luminometer (BERTHOLD, Germany).

Dual-luciferase reporter gene assay

The dual-luciferase reporter assay system (Promega, Madison, WI, USA) was utilized to detect luciferase reporter genes. The target fragments of wild-type and mutant TTN-AS1 were constructed and integrated into the pGL3 vectors (Promega, Madison, WI, USA) to construct pGL3-TTN-AS1-wild type (TTN-AS1-WT) and pGL3-TTN-AS1-mutant (TTN-AS1-MUT) reporter vectors.

TTN-AS1-WT/TTN-AS1-MUT and miR-15b-5p/negative control were transferred to 16HBE cells, respectively. The luciferase activity was determined 48 hours after transfection. We conducted all tests in triplicate and repeated them three times.

RNA immunoprecipitation (RIP) experiment

RIP was performed with the Magna RIP™ RNA-Binding protein immunoprecipitation kit (Millipore, Billerica, MA, USA). Cells were cracked in a complete RNA lysis buffer, and then the lysates were maintained with RIP buffer supplemented with magnetic beads coupled to human anti-Argonaute2 (AGO2) antibody (Millipore) or negative control mouse IgG (Millipore).

Fluorescence in situ hybridization (FISH) assay

The FISH assay was performed to investigate the co-location of lncRNA TTN-AS1 and miR-15b-5p. Briefly, 16HBE cells were inoculated in 24-well plates on the slides (1×10^5 cell per well). After a 24-h culturing in the incubator, the cells were fixed in 4% paraformaldehyde, permeabilized and blocked in 10% Triton X-100 (Solarbio, Beijing, China) and 10% BSA (Beyotime, Shanghai, China) for 1 hour. Next, the cells were treated with a Fluorescent In Situ Hybridization Kit (RiboBio, China), following the manufacturers' instructions. The FISH probes of TTN-AS1 and miR-15b-5p were purchased from GenePharma (GenePharma, Shanghai, China). The nucleus was stained by DAPI (Beyotime, Shanghai, China). The fluorescence signal was observed under confocal microscopy.

Statistical analysis

SPSS17.0 statistical software (SPSS Inc., Chicago, IL, USA) was adopted for analysis. The measurement data were presented as mean ± standard deviation (x±s). Student's *t*-test was adopted for pairwise comparison, and the data of multiple groups were compared by variance. Correlation analysis was made by Pearson analysis. The statistics were meaningful when $P < 0.05$.

RESULTS

To probe the capabilities of TTN-AS1 in COPD, we implemented RT-qPCR to examine the expression of related molecules in each group. The results revealed that the expression of TTN-AS1 was the lowest, and that of miR-15b-5p was the highest in the healthy non-smoking group. In addition, the expression of TTN-AS1 was the highest, and that of miR-15b-5p was the lowest in smokers with COPD. Besides, the relative expression of TTN-AS1 in lung tissues of smokers without COPD was elevated, and that of miR-15b-5p was attenuated (*vs* the healthy group) ($P <0.05$, Fig. 1A-B). Pearson analysis demonstrated that the profiles of TTN-AS1 and miR-15b-5p in the lung tissues of smokers with COPD were reversely correlated ($P <0.05$, Fig. 1C). These results testified that smoking heightened the relative profile of TTN-AS1 and hampered the relative level of miR-15b-5p in human lung tissues. 16HBE cells were further intervened by 0.5%, 5% and 10% CSE for 12 h, respectively. Then, the relative profiles of TTN-AS1 and miR-15b-5p were measured by RT-qPCR. As a result, with the increase of CSE concentration, the expression of TTN-AS1 increased while that of miR-15b-5p declined ($P <0.05$, Fig. 1D-E). It was confirmed that with the increase of CSE concentration, TTN-AS1 was up-regulated while miR-15b-5p was down-regulated.

The above experiments showed TTN-AS1 expression was boosted both in COPD lung tissues and CSE-induced 16HBE cells. To figure out the influence of TTN-AS1 on COPD evolvement, we transfected TTN-AS1 overexpression plasmids in CSE-induced 16HBE cells and examined the transfection validity by RT-qPCR ($P <0.05$, Fig. 2A). Then, the CCK-8 assay was adopted to measure cell viability, and FCM was applied to verify cell apoptosis. As a result, TTN-AS1 overexpression

resulted in weakened cell viability and enhanced cell apoptosis (P <0.05, Fig. 2B-C). Meanwhile, TUNEL assay results were consistent with those of FCM (P <0.05, Fig. 2D). WB results confirmed that the relative levels of pro-apoptotic proteins Bax and Caspase3 were increased while the relative profile of anti-apoptotic protein Bcl2 was decreased after overexpressing TTN-AS1 (P <0.05, Fig. 2E). To further probe the mechanism of TTN-AS1 in CSE-induced COPD, we monitored the contents of IL-1β, IL-6, TNFα and HMGB1 in each group by ELISA. It was discovered that compared with the CSE+NC group, the levels of the above inflammatory factors were signally up-regulated in the CSE+TTN-AS1 group (P <0.05, Fig. 2F). Moreover, the expression of pro-inflammatory proteins COX2, iNOS and NF-κB in 16HBE cells were measured by WB. The results illustrated that overexpressing TTN-AS1 significantly facilitated the expressions of these inflammatory proteins induced by CSE (P <0.05, Fig. 2G). These findings signified that overexpressing TTN-AS1 intensified CSE-induced 16HBE cell damage.

To study the downstream molecular mechanism of TTN-AS1, we analyzed the candidate targets of TTN-AS1 via the ENCORI database (http://starbase.sysu.edu.cn) and discovered that TTN-AS1 had a binding sequence to miR-15b-5p (Fig. 3A). The targeting association between the two was further ascertained by the dual-luciferase reporter assay and RIP assay, respectively. As a result, miR-15b-5p mimics hampered the luciferase activity of wild-type TTN-AS1, while it had no evident impact on mutant TTN-AS1 (P <0.05, Fig. 3B). Besides, after transfection of miR-15b-5p mimics, the amount of precipitated TTN-AS1 in the Ago2 antibody group was dramatically higher than that in the IGG group, confirming that TTN-AS1 was combined AGO2 via miR-15b-5p (P <0.05, Fig. 3C). The miR-15b-5p profile after TTN-AS1 overexpression was further evaluated by RT-qPCR, and it was revealed that overexpressing TTN-AS1 impeded the miR-15b-5p expression (P <0.05, Fig. 3D). The co-location of TTN-AS1 and miR-15b-5p was verified by FISH assay. The results indicated that both TTN-AS1 and miR-15b-5p were

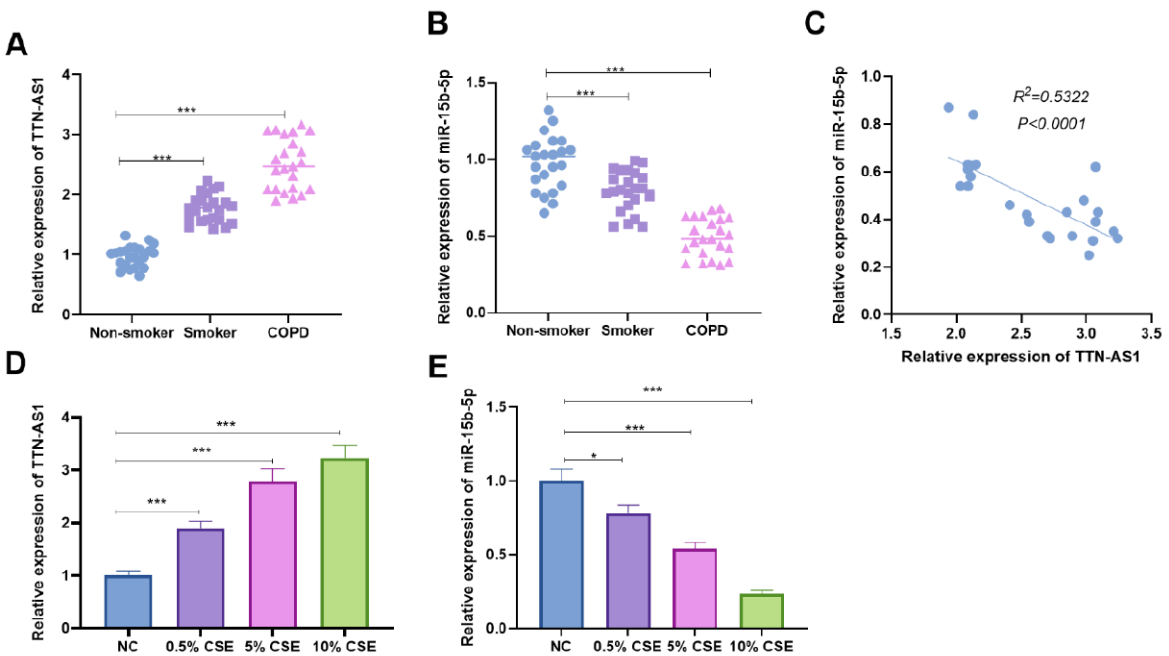


Fig. 1. *TTN-AS1 was expressed in COPD patients and CSE-treated 16HBE cells.* ***A-B****): The relative expression of TTN-AS1 and miR-15b-5p in lung tissues of the healthy non-smoking group, smoking group without COPD and smoking group with COPD was examined by RT-qPCR.* ***C****): The link between TTN-AS1 and miR-15b-5p in lung tissues of smokers with COPD was analyzed.* ***D-E****): Relative profiles of TTN-AS1 and miR-15b-5p in 16HBE cells intervened by different concentrations of CSE was monitored by RT-qPCR. * P <0.05, *** P <0.001. N=3.*

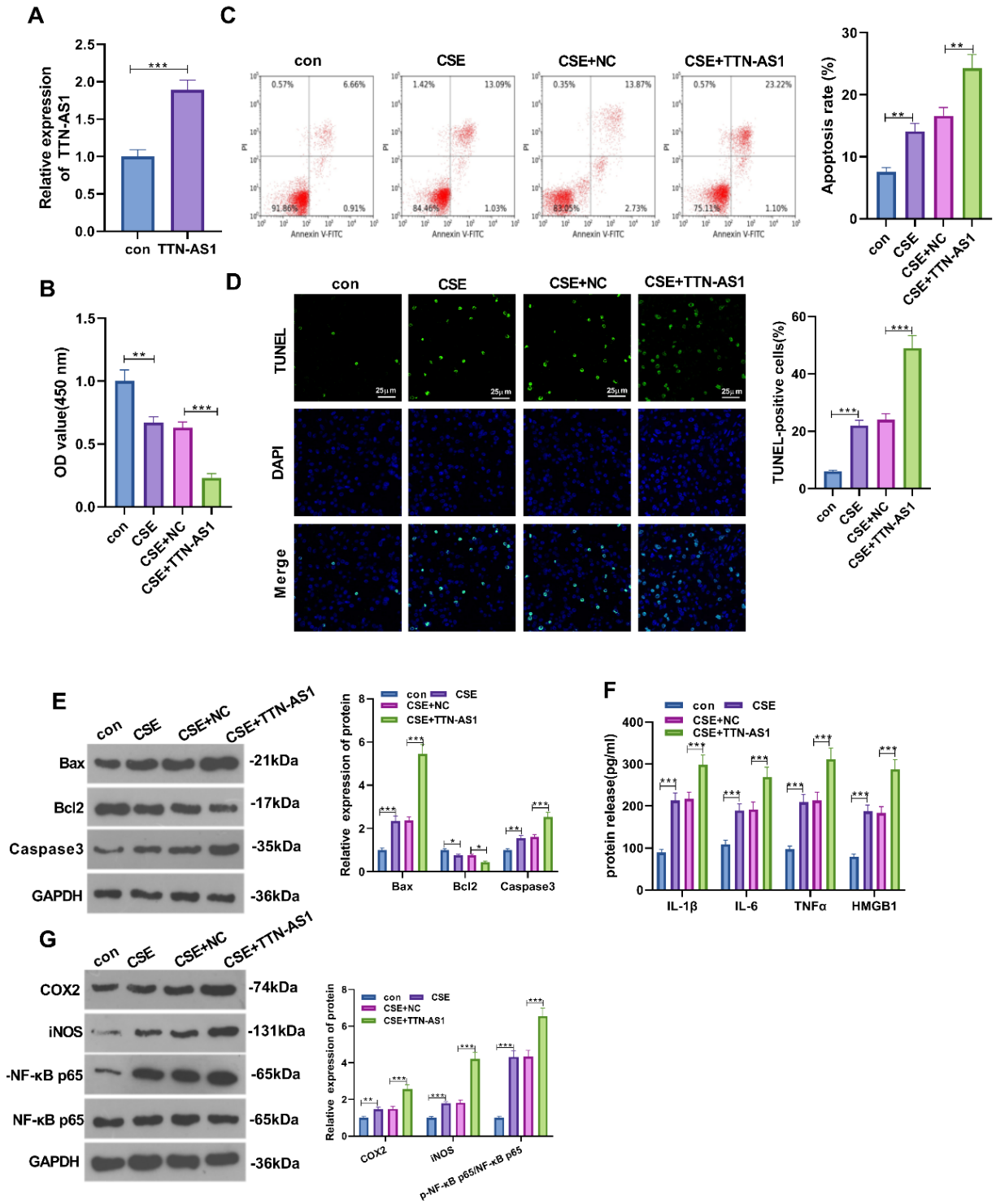


Fig. 2. *Overexpressing TTN-AS1 aggravated CSE-mediated cell apoptosis and inflammation. TTN-AS1 overexpression plasmids were transfected into CSE-treated 16HBE cells.* ***A****): The TTN-AS1 profile was examined by RT-qPCR.* ***B-C****): The CCK-8 method was applied to test cell viability, and FCM was applied to examine cell apoptosis.* ***D****): The TUNEL assay was utilized to monitor 16HBE cell apoptosis.* ***E****): The relative expression of Bax, Caspase3 and Bcl2 was assessed by WB.* ***F****) The contents of IL-1β, IL-6, TNFα and HMGB1 in each group were assayed by ELISA.* ***G****): WB was performed to test the levels of COX2, iNOS and NF-κB in 16HBE cells. **P <0.01, *** P <0.001. N=3.*

mainly located at the cytoplasm of 16HBE cells, and they were co-located in the cytoplasm (Fig. 3E). These findings signified that TTN-AS1 targeted and repressed miR-15b-5p profile.

In the previous experiments, we concluded that miR-15b-5p expression was curbed in both COPD lung tissues and CSE-induced 16HBE cells. To further probe the influence of miR-15b-5p on COPD progression, we transfected miR-15b-5p mimics in CSE-induced 16HBE cells and examined the miR-15b-5p profile by RT-qPCR. The results testified that miR-15b-5p was up-regulated after miR-15b-5p overexpression (P <0.05, Fig. 4A). The CCK-8 assay and FCM were conducted to assay cell proliferation and apoptosis, respectively. Results illustrated that overexpressing miR-15b-5p heightened cell viability while decreasing cell apoptosis (P <0.05, Fig. 4B-C). Meanwhile, the results of the TUNEL assay were consistent with those of FCM (P <0.05, Figure 4D). WB results exhibited that after miR-15b-5p overexpression, the profiles of Bax and Caspase3 were impeded, while Bcl2 expression was facilitated (P <0.05, Fig. 4E). To further clarify the mechanism of miR-15b-5p in CSE-induced COPD, we monitored the levels of IL-1β, IL-6, TNFα and HMGB1 in each group by ELISA. As expected, the contents of the

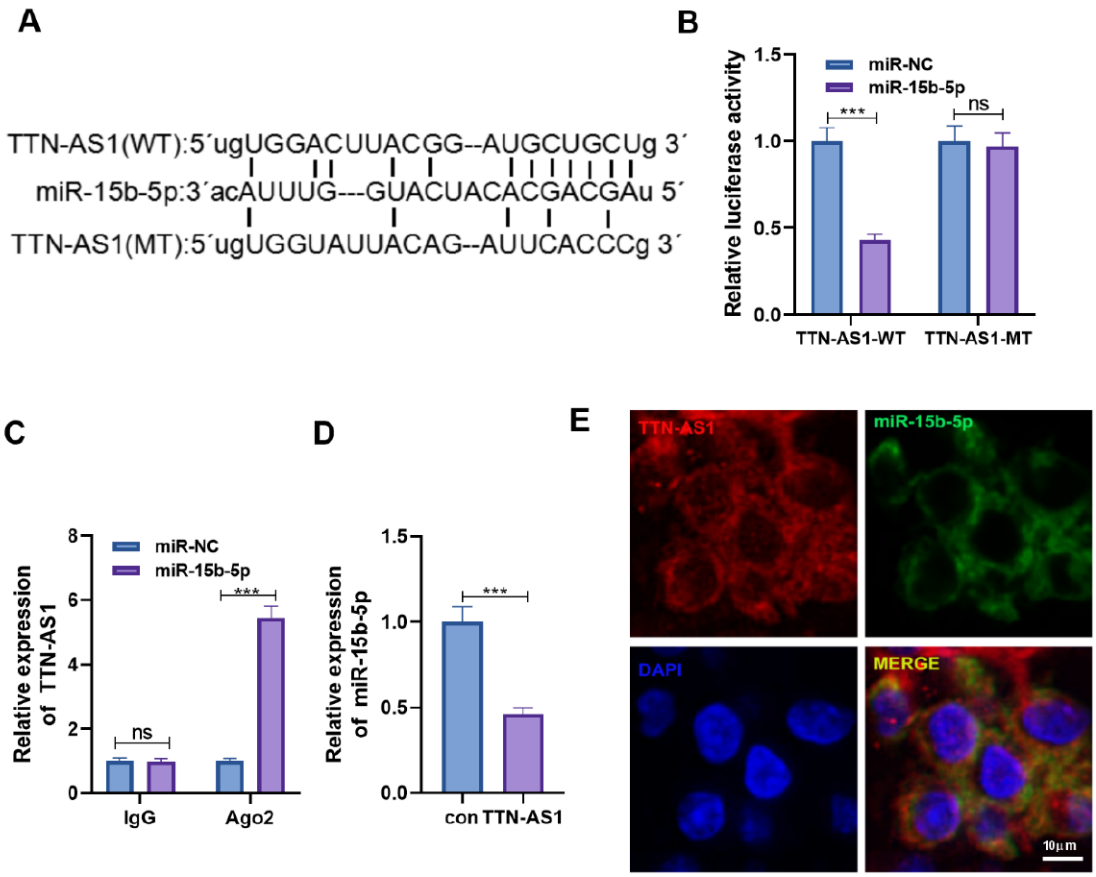


Fig. 3. *TTN-AS1 targeted miR-15b-5p.* ***A****): Candidate targets of TTN-AS1 were analyzed via the ENCORI database (http://starbase.sysu.edu.cn/). The data suggested that miR-15b-5p contained binding sites on TTN-AS1.* ***B-C****): The targeting association between TTN-AS1 and miR-15B-5p was ascertained by the dual-luciferase reporter assay and the RIP experiment, respectively.* ***D****): The miR-15B-5p profile in 16HBE cells after TTN-AS1 overexpression was checked by RT-qPCR. E. FISH assay was used for detecting the co-location of TTN-AS1(red) and miR-15b-5p (green) in 16HBE cells. NS P >0.05, *** P <0.001. N=3.*

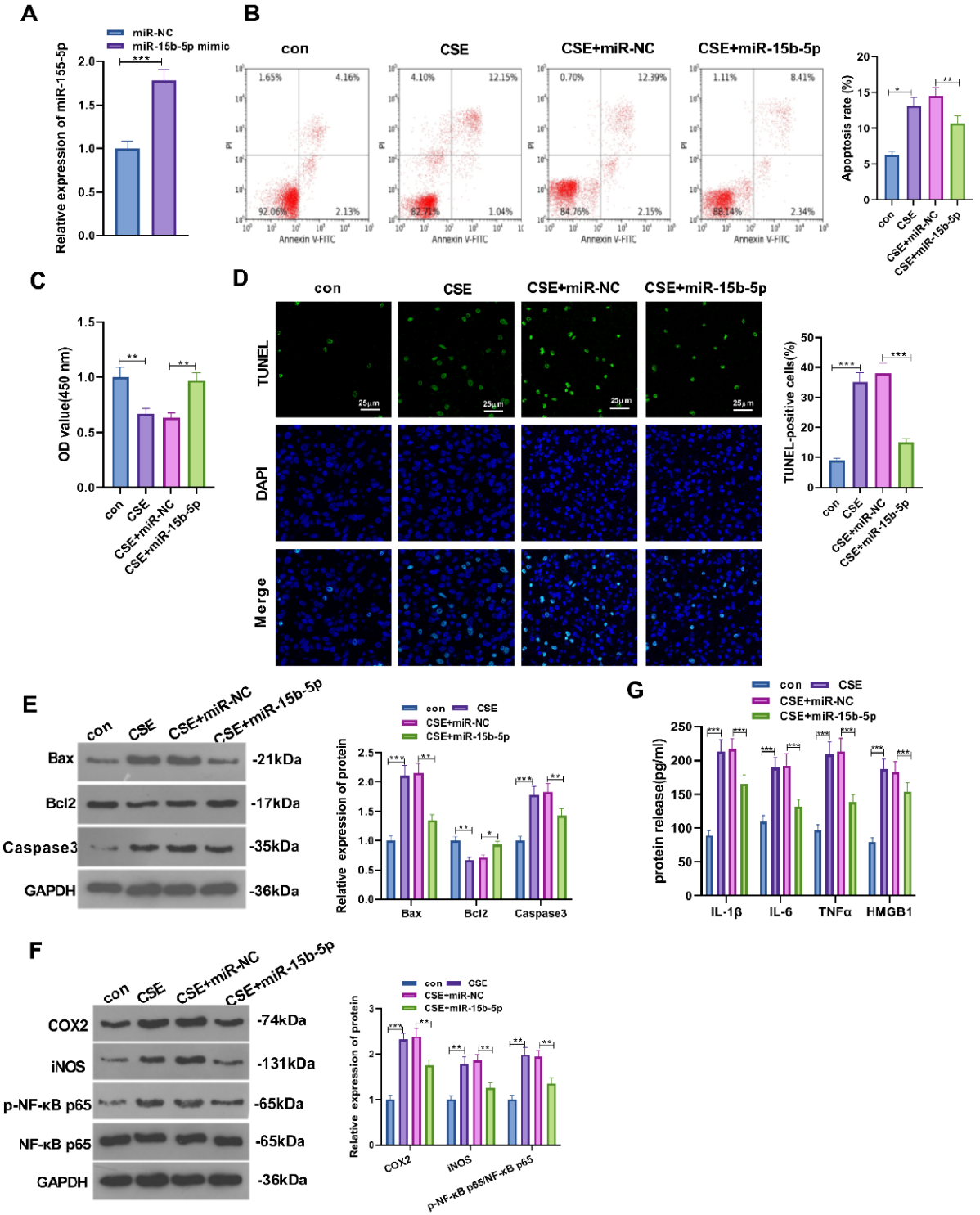


Fig. 4. *Overexpressing miR-15b-5p alleviated CSE-mediated cell injury and inflammation. miR-15b-5p mimics were transfected into CSE-induced 16HBE cells.* ***A****): The miR-15b-5p profile was tested by RT-qPCR.* ***B-C****): Cell proliferation and apoptosis were examined by the CCK-8 method and FCM, respectively.* ***D****): Cell apoptosis was measured by the TUNEL assay.* ***E****): The relative profiles of Bax, Caspase3 and Bcl2 were checked by WB.* ***F****): The contents of IL-1β, IL-6, TNFα and HMGB1 in each group were monitored by ELISA.* ***G****): WB was applied to gauge the expression of COX2, iNOS and NF-κB in 16HBE cells. ** P <0.01, *** P <0.001.N=3.*

above inflammatory factors in the CSE+miR-15b-5p group were significantly repressed (*vs* the CSE+miR-NC group) (P <0.05, Fig. 4F). The contents of COX2, iNOS and NF-κB in 16HBE cells were monitored by WB. The results manifested that overexpressing miR-15b-5p dampened the expression of these inflammatory proteins induced by CSE (P <0.05, Fig. 4G). The above experiments unveiled that the transfection of miR-15b-5p mimics hampered CSE-induced 16HBE cell damage.

To probe the impact of miR-15b-5p on TTN-AS1 damage in 16HBE cells, we transfected TTN-AS1 overexpression plasmids and/or miR-15b-5p mimics in CSE-induced 16HBE cells. First, the expression of TTN-AS1 and miR-15b-5p was tested by RT-qPCR. The results manifested that compared with the CSE group, TTN-AS1 overexpression up-regulated TTN-AS1 and down-regulated miR-15b-5p. In contrast, the results were opposite after miR-15b-5p mimic transfection (P <0.05, Fig. 5A-B). CCK-8 assay and FCM results demonstrated that overexpressing TTN-AS1 decreased cell viability and facilitated cell apoptosis (*vs* the CSE group). However, compared with the CSE+TTN-AS1+miR-NC group, the results in the CSE+TTN-AS1+ miR-15b-5p group were completely opposite (P <0.05, Fig. 5C-D). Besides, the results of the TUNEL assay were consistent with those of FCM (P <0.05, Fig. 5E). WB marked that Bax and Caspase3 were up-regulated, and Bcl2 was down-regulated after overexpressing TTN-AS1. Nevertheless, the

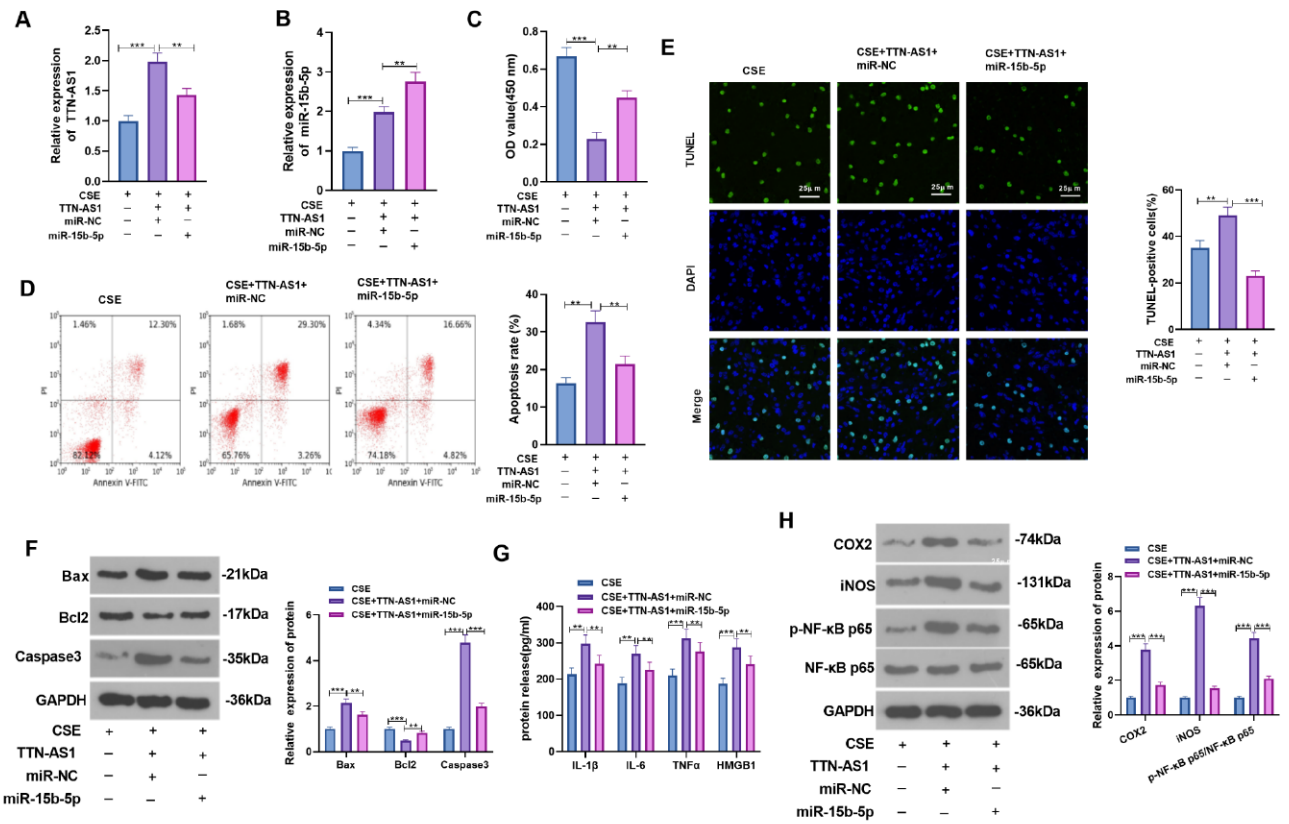


Fig. 5. *Overexpressing miR-15b-5p suppressed the effect of TTN-AS1 in 16HBE cells. TTN-AS1 overexpression plasmids and/or miR-15b-5p mimics were transfected in CSE-induced 16HBE cells.* ***A-B****): The levels of TTN-AS1 and miR-15b-5p were checked by RT-qPCR.* ***C-D****): The CCK-8 method was utilized to measure cell viability, and cell apoptosis was determined by FCM.* ***E****): The TUNEL assay was utilized to test cell apoptosis.* ***F****): The relative expression of Bax, Caspase3 and Bcl2 was compared by WB.* ***G****): The contents of IL-1β, IL-6, TNFα and HMGB1 in each group were checked by ELISA.* ***H****): The expression of COX2, iNOS and NF-κB in 16HBE cells was assessed by WB. * P <0.05, ** P <0.01, *** P <0.001.N=3.*

miR-15b-5p mimic transfection exerted the opposite function (P <0.05, Fig. 5F). The profiles of IL-1β, IL-6, TNFα and HMGB1 in each group were monitored by ELISA, and the results exhibited that the levels of these inflammatory cytokines were facilitated in the CSE+TTN-AS1+miR-NC group (vs the CSE group). In contrast, compared with the CSE+TTN-AS1+miR-NC group, the levels of the above inflammatory factors were lessened in the CSE+TTN-AS1+ miR-15b-5p group (P <0.05, Fig. 5G). The profiles of COX2, iNOS and NF-κB in 16HBE cells were measured by WB. The results illustrated that overexpressing TTN-AS1 significantly heightened their expression induced by CSE. Nevertheless, the results were completely reversed after miR-15b-5p mimic transfection (P <0.05, Fig. 5H). These findings enunciated that overexpressing TTN-AS1 aggravated CSE-mediated apoptosis and inflammation in 16HBE cells, while miR-15b-5p mimic transfection significantly attenuated TTN-AS1-mediated damage.

DISCUSSION

COPD is manifested as partially reversible airflow obstruction, airway inflammation, and other systemic symptoms (18). COPD is not only a lesion limited to the lungs but also a systemic disease that leads to low nutrition, skeletal muscle, body weight, and immune function in the body, with adverse effects on the cardiovascular system and the nervous system (19-20). It is the primary reason for morbidity and mortality and the third leading killer worldwide (21). In the last few decades, growing reports have claimed that lncRNAs contribute to COPD pathogenesis. Also, the profiles of lncRNAs in lung tissues from non-smokers and smokers with or without COPD have been revealed (22). For example, lncRNA miR155HG regulates GM-CSF-mediated M1/M2 polarization of macrophages during the progression of COPD (23). In addition, LncRNA COPDA1 increases calcium transport in human bronchial smooth muscle cells (HBSMCs) by up-regulating MS4A1, thus promoting the proliferation of COPD airway smooth muscle cells as well as airway remodeling (24). As a common lncRNA, TTN-AS1 has been shown to have significant values in osteosarcoma (25), lung adenocarcinoma (26), glioblastoma (27), etc. The study of Feng H et al. also has manifested that TTN-AS1 aggravates breast cancer by modulating miR-524-5p/RRM2 (28).

This article revealed that TTN-AS1 was up-regulated in smokers, especially in those with COPD. Meanwhile, we treated 16HBE cells with CSE to construct an *in vitro* COPD model and discovered that TTN-AS1 expression was heightened in 16HBE cells, and the relative expression of TTN-AS1 was gradually facilitated with the elevation of CSE concentration. Subsequently, to ascertain the biological role of TTN-AS1 in COPD development, we implemented gain-of-function experiments, which testified that overexpressing TTN-AS1 aggravated CSE-mediated apoptosis and inflammation. These results demonstrate the potential regulatory role of TTN-AS1 in COPD.

A growing body of evidence manifests that lncRNAs serve as competitive endogenous RNA or miRNA sponges to modulate COPD progression. As reported, lncRNA SNHG5 is lowly expressed in COPD tissues and CSE-treated 16HBE cells, and SNHG5 suppresses the COPD evolvement and inflammation by regulating miR-132/PTEN (29). Additionally, LncRNA RP11-86H7.1 activates the NF-κB pathway in human bronchial epithelial cells as a ceRNA for miR-9-5p, thereby facilitating the TRAPM2.5-induced inflammation in COPD (30). Comprehending the exact molecular mechanism by which lncRNAs function heightens the evolvement of lncRNA-mediated diagnostics and therapeutics for COPD. To probe the specific molecular mechanisms of TTN-AS1, we identified and confirmed possible targets regulated by TTN-AS1 through bioinformatics analysis. Here, the dual-luciferase reporter assay and RIP assay results exhibited that TTN-AS1 targeted miR-15b-5p, and miR-15b-5p expression was signally attenuated in smokers with COPD and CSE-treated 16HBE cells. Functional analysis implied that overexpressing miR-15b-5p evidently impeded CSE-mediated cell damage and the contents of IL-6, TNF-α, IL-1β, and HMGB1, suggesting that miR-15b-5p protected against CSE-induced COPD. Interestingly, a previous study has revealed that miR-15b-5p exerts anti-inflammatory and anti-apoptotic effects. For example, miR-15b-5p mitigates apoptosis, oxidative

stress, and inflammatory responses induced by high glucose on podocytes. The underlying mechanism is that miR-15b-5p targets and inhibits Sema3A (31). In another study, hsa-miR-15b-5p was found significantly altered in Influenza A patients and had high correlations to IL-6, IL-15, IL-17A, IL-1β, and monocyte chemoattractant protein-1 (MCP-1) (32). Finally, the results of the compensation experiment illustrated that miR-15b-5p overexpression in 16HBE cells attenuated the damaging effect of TTN-AS1. These results demonstrated that TTN-AS1 intensified CSE-induced 16HBE cell apoptosis and inflammation by modulating miR-15b-5p, which exacerbated COPD progression (Fig. 6).

Overall, the results of this study confirmed that TTN-AS1 expression was elevated, and miR-15b-5p was down-regulated in COPD patients and CSE-treated 16HBE cells. Meanwhile, TTN-AS1 expedited CSE-induced epithelial cell injury by hampering the miR-15b-5p profile, which aggravated COPD (Figure 6). These findings provide new insights into the pathogenesis and treatment options of COPD. Although some valuable results have been obtained in this study, some limitations, such as small sample size, may lead to poor statistical effects. Therefore, it is indispensable to study more data of COPD patients to further explore the pathogenesis and molecular characteristics of COPD.

Author contribution

Conceived and designed the experiments: LZ; Performed the experiments: EG, YW; Statistical analysis: EG, YW; Wrote the paper: EG, YW, LZ. The authors declare that they have no conflict of interest.

Ethics statement

This study was authorized by the Medical Ethics Committee of Xiangyang Central Hospital, Affiliated Hospital of Hubei University of Arts and Science.

Data Availability Statement

The data sets used and analyzed during the current study are available from the corresponding author on reasonable request.

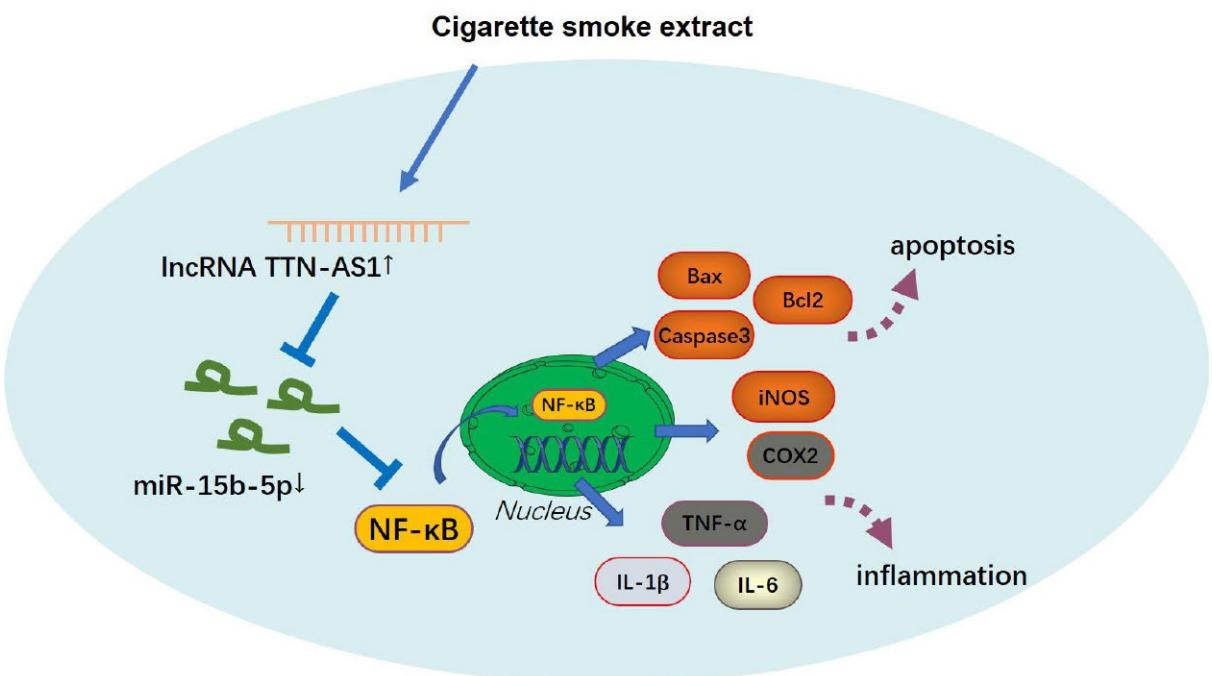


Fig. 6. *The mechanism diagram. TTN-AS1 is up-regulated in cigarette smoke extract (CSE)-induced 16HBE cells. TTN-AS1 aggravates CSE-mediated apoptosis and inflammation via targeting miR-15b-5p.*

REFERENCES

1. Bagdonas E, Raudoniute J, Bruzauskaite I, et al. Novel aspects of pathogenesis and regeneration mechanisms in COPD. Int J Chron Obstruct Pulmon Dis 2015; 10:995-1013.
2. Raherison C, Girodet PO. Epidemiology of COPD. Eur Respir Rev 2009; 18(114):213-21.
3. Rabe KF, Watz H. Chronic obstructive pulmonary disease. Lancet 2017; 389(10082):1931-1940.
4. Salimian J, Mirzaei H, Moridikia A, et al. Chronic obstructive pulmonary disease: MicroRNAs and exosomes as new diagnostic and therapeutic biomarkers. J Res Med Sci 2018; 23:27.
5. Chen Y, Luo H, Kang N, et al. Beraprost sodium attenuates cigarette smoke extract-induced apoptosis in vascular endothelial cells. Mol Biol Rep 2012; 39(12):10447-57.
6. Kirby M, Tanabe N, Tan WC, et al. Total Airway Count on Computed Tomography and the Risk of Chronic Obstructive Pulmonary Disease Progression. Findings from a Population-based Study. Am J Respir Crit Care Med 2018; 197(1):56-65.
7. Sun Q, Hao Q, Prasanth KV. Nuclear Long Noncoding RNAs: Key Regulators of Gene Expression. Trends Genet 2018; 34(2):142-157.
8. Wang Y, Chen J, Chen W, et al. LINC00987 Ameliorates COPD by Regulating LPS-Induced Cell Apoptosis, Oxidative Stress, Inflammation and Autophagy Through Let-7b-5p/SIRT1 Axis. Int J Chron Obstruct Pulmon Dis 2020; 15:3213-3225.
9. Bi H, Wang G, Li Z, et al. Long Noncoding RNA (lncRNA) Maternally Expressed Gene 3 (MEG3) Participates in Chronic Obstructive Pulmonary Disease through Regulating Human Pulmonary Microvascular Endothelial Cell Apoptosis. Med Sci Monit 2020; 26:e920793.
10. Song J, Wang Q, Zong L. LncRNA MIR155HG contributes to smoke-related chronic obstructive pulmonary disease by targeting miR-128-5p/BRD4 axis. Biosci Rep 2020; 40(3):BSR20192567.
11. Huang Y, Chu P, Bao G. Silencing of Long Non-coding RNA TTN-AS1 Inhibits Hepatocellular Carcinoma Progression by the MicroRNA-134/ITGB1 Axis. Dig Dis Sci 2021; 66:3916-3928.
12. Wang Y, Li D, Lu J, et al. Long non-coding RNA TTN-AS1 facilitates tumorigenesis and metastasis by maintaining TTN expression in cutaneous skin melanoma. Cell Death Dis 2020; 11(8):664.
13. Liu X, Wang J, Luo H, et al. MiR-218 Inhibits CSE-Induced Apoptosis and Inflammation in BEAS-2B by Targeting BRD4. Int J Chron Obstruct Pulmon Dis 2020; 15:3407-3416.
14. Zhang J, Xu Z, Kong L, et al. miRNA-486-5p Promotes COPD Progression by Targeting HAT1 to Regulate the TLR4-Triggered Inflammatory Response of Alveolar Macrophages. Int J Chron Obstruct Pulmon Dis 2020; 15:2991-3001.
15. Tsai YC, Kuo MC, Hung WW, et al. High Glucose Induces Mesangial Cell Apoptosis through miR-15b-5p and Promotes Diabetic Nephropathy by Extracellular Vesicle Delivery. Mol Ther 2020; 28(3):963-974.
16. Jiao Y, Li W, Wang W, et al. Platelet-derived exosomes promote neutrophil extracellular trap formation during septic shock. Crit Care 2020; 24(1):380.
17. Zhao C, Zhao Q, Zhang C, et al. miR-15b-5p resensitizes colon cancer cells to 5-fluorouracil by promoting apoptosis via the NF-κB/XIAP axis. Sci Rep 2017; 7(1):4194.
18. Decramer M, Janssens W, Miravitlles M. Chronic obstructive pulmonary disease. Lancet 2012; 379(9823):1341-51.
19. Smid DE, Franssen FME, Gonik M, et al. Redefining Cut-Points for High Symptom Burden of the Global Initiative for Chronic Obstructive Lung Disease Classification in 18,577 Patients With Chronic Obstructive Pulmonary Disease. J Am Med Dir Assoc 2017; 18(12):1097.e11-1097.e24.
20. Adeloye D, Chua S, Lee C, et al. Global Health Epidemiology Reference Group (GHERG). Global and regional estimates of COPD prevalence: Systematic review and meta-analysis. J Glob Health 2015; 5(2):020415.
21. Elbehairy AF, Ciavaglia CE, Webb KA, et al. Pulmonary Gas Exchange Abnormalities in Mild Chronic Obstructive Pulmonary Disease. Implications for Dyspnea and Exercise Intolerance. Am J Respir Crit Care Med 2015; 191(12):1384-94.
22. Bi H, Zhou J, Wu D, et al. Microarray analysis of long non-coding RNAs in COPD lung tissue. Inflamm Res 2015; 64(2):119-26.

23. Li N, Liu Y, Cai J. LncRNA MIR155HG regulates M1/M2 macrophage polarization in chronic obstructive pulmonary disease. Biomed Pharmacother 2019; 117:109015.
24. Zheng M, Hong W, Gao M, et al. Long Noncoding RNA COPDA1 Promotes Airway Smooth Muscle Cell Proliferation in Chronic Obstructive Pulmonary Disease. Am J Respir Cell Mol Biol 2019; 61(5):584-596.
25. Fu D, Lu C, Qu X, et al. LncRNA TTN-AS1 regulates osteosarcoma cell apoptosis and drug resistance via the miR-134-5p/MBTD1 axis. Aging 2019; 11(19):8374-8385.
26. Jia Y, Duan Y, Liu T, et al. LncRNA TTN-AS1 promotes migration, invasion, and epithelial mesenchymal transition of lung adenocarcinoma via sponging miR-142-5p to regulate CDK5. Cell Death Dis 2019; 10(8):573.
27. Tang W, Wang D, Shao L, et al. LINC00680 and TTN-AS1 Stabilized by EIF4A3 Promoted Malignant Biological Behaviors of Glioblastoma Cells. Mol Ther Nucleic Acids 2020; 19:905-921.
28. Feng H, Wang Q, Xiao W, et al. LncRNA TTN-AS1 Regulates miR-524-5p and RRM2 to Promote Breast Cancer Progression. Onco Targets Ther 2020; 13:4799-4811.
29. Shen Q, Zheng J, Wang X, et al. LncRNA SNHG5 regulates cell apoptosis and inflammation by miR-132/PTEN axis in COPD. Biomed Pharmacother 2020; 126:110016.
30. Zhao J, Pu J, Hao B, et al. LncRNA RP11-86H7.1 promotes airway inflammation induced by TRAPM2.5 by acting as a ceRNA of miRNA-9-5p to regulate NFKB1 in HBECS. Sci Rep 2020; 10(1):11587.
31. Fu Y, Wang C, Zhang D, et al. miR-15b-5p ameliorated high glucose-induced podocyte injury through repressing apoptosis, oxidative stress, and inflammatory responses by targeting Sema3A. J Cell Physiol 2019; 234(11):20869-20878.
32. Othumpangat S, Lindsley WG, Beezhold DH, et al. Differential Expression of Serum Exosome microRNAs and Cytokines in Influenza A and B Patients Collected in the 2016 and 2017 Influenza Seasons. Pathogens 2021;10(2):149.

Effects of 5-azacytidine on Th cell Differentiation and IFN-γ, IL-4, GATA3, ROR-γ, and Foxp3 Cytokine Expression in Allergic Rhinitis

H.L. Jia[1], R. Zhang[1], Q.Q. Liang[1], X.F. Jiang[2*]

[1]Department of College of Traditional Chinese Medicine, Xinjiang Medical University, Xinshi District, Urumqi, China; [2]Department of Central Laboratory, Xinjiang Medical University, Xinshi District, Urumqi, China

Received September 17, 2021 – Accepted 20 January, 2022

Background: **Allergic rhinitis (AR) is a commonly diagnosed disease worldwide, which seriously compromises people's quality of life and health. The imbalance of T helper (Th) cell differentiation and dysregulation of related cytokine expression underlay the immunological basis of AR. 5-azacytidine (5-aza) is a pyrimidine nucleoside analogue that can inhibit the secretion of pro-inflammatory factors and improve the transcription of anti-inflammatory factors. This study explored the effects of 5-aza on the differentiation of Th1/Th2 and Th17/regulatory T cells (Treg) cell subsets and the expressions of related cytokines in AR. Objective: To investigate the effects of 5-aza on $CD4^+$ T lymphocyte Th1/Th2 and Th17/Treg cell subsets and cytokines IFN-γ, IL-4, GATA3, ROR-γ, and Foxp3 in AR patients and rats.**

Materials and methods: **98 normal controls and 88 AR patients were recruited for the isolation of $CD4^+$ T lymphocytes. The mRNA expressions of IFN-γ, IL-4, GATA3, ROR-γ, and Foxp3 were detected by using RT-qPCR. A rat model of AR was established. The mRNA and protein expressions of cytokines IFN-γ, IL-4, GATA3, ROR-γ, and Foxp3 in AR rats were detected using RT-qPCR and Western blotting. ELISA was used to detect the levels of IFN-γ, IL-4, GATA3, ROR-γ, and Foxp3 cytokines in the serum of rats. Flow cytometry was performed to detect the differentiation ratio of Th1, Th2, Th17, and Treg cell subsets.**

Results: **The mRNA expressions of IFN-γ, IL-4, GATA3, and ROR-γ were increased and Foxp3 was decreased in AR patients and AR rats. The protein expressions of IFN-γ, IL-4, GATA3, and ROR-γ were increased and Foxp3 was decreased in AR rats. 5-aza intervention decreased the mRNA and protein expressions of IFN-γ, IL-4, GATA3, and ROR-γ and increased the mRNA and protein expression of Foxp3 in AR rats. The number of Th1, Th2, and Th17 cell subsets was increased and Treg was decreased in AR rats, while the number of Th1, Th2, and Th17 cell subsets was decreased and Treg was increased significantly after 5-aza intervention.**

Conclusions: **The number and relative expressions of Th1, Th2, and Th17 cell subsets were increased in AR, while the Treg cell subset was decreased. Methyltransferase inhibitor 5-aza downregulated the number of Th1, Th2, and Th17 cell subsets and upregulated the Treg cell subset. The expressions of cytokines IFN-γ, IL-4, GATA3, ROR-γ, and Foxp3 were regulated by methyltransferase inhibitor 5-aza.**

Allergic rhinitis (AR) is an immunoglobulin E (IgE)-mediated respiratory hypersensitivity characterized by nasal mucosal eosinophil (EOS) infiltration and elevated T helper (Th) 2 cytokine secretion, with an increasing prevalence rate year by year (1). The clinical symptoms of AR mainly

Key words: allergic rhinitis; T lymphocytes; Th cell; 5-aza; DNA methylation

*Corresponding Author:
Dr X.F. Jiang
Department of Central Laboratory,
Xinjiang Medical University,
Xinshi District, Urumqi, 830054, China
Tel: +86 13609983280
e-mail: jxf@xjmu.edu.cn

0393-974X (2022)
Copyright © by BIOLIFE, s.a.s.
This publication and/or article is for individual use only and may not be further reproduced without written permission from the copyright holder.
Unauthorized reproduction may result in financial and other penalties
DISCLOSURE: ALL AUTHORS REPORT NO CONFLICTS OF INTEREST RELEVANT TO THIS ARTICLE.

include nasal itching, nasal congestion, runny nose, and sneezing. Approximately 10% ~ 40% of adults and 2% ~ 25% of children suffer from AR worldwide (2), which seriously compromises people's quality of life and consumes huge social medical resources (3). The pathogenesis of AR is complex. It is reported that the imbalanced differentiation of $CD4^+$ T lymphocyte subsets Th1/Th2 and Th17/regulatory T cells (Treg) and the abnormal expression of related cytokines may contribute to the occurrence and development of AR.

5-azacytidine (5-aza) is a pyrimidine nucleoside analogue that commonly serves as a DNA methyltransferase (DNMT) inhibitor. It can bind to the DNA or RNA of high proliferating cells, consume DNMT1, and alter methylation (4), thereby participating in the regulation of cell cycle, signal transduction, and the occurrence and development of human malignancies. Drugs that induce hypomethylation can increase the number of Treg cells, and reduce the production of pro-inflammatory factors (5), and also participate in autoimmune diseases by regulating the expression of $CD4^+$ T lymphocytes (6). It has been reported that 5-aza can reduce the expression of pro-inflammatory Th1 and Th17 cytokines by functioning as a DNMT inhibitor (7). In ovalbumin (OVA)-induced rats, 5-aza treatment can alleviate airway hyperresponsiveness and eosinophil (EOS) infiltration, reduce IgE level, and inhibit Th2 cytokine secretion (8). Moreover, 5-aza has been demonstrated to reduce inflammatory responses by inhibiting Foxp3 methylation and reconstructing the balance of Th17/Treg cell subsets (9). As a DNMT inhibitor, 5-aza plays an important role in autoimmune diseases, but the role of 5-aza in AR has not been thoroughly elucidated. Therefore, we conducted in vitro and in vivo experiments to explore the effects of 5-aza on the differentiation of Th1/Th2 and Th17/Treg cell subsets and the expression of related cytokines in AR.

MATERIALS AND METHODS

Our study was approved by the Ethics Committee of the Xinjiang Medical University. All subjects signed informed consent prior to the participation. The animal experiments were approved by the Experimental Animal Ethics Committee of the Xinjiang Medical University. All experimental procedures were strictly conform with the International Code of Ethics and the National Health Guideline for the Care and Use of Laboratory Animals (Certificate number: SCXK2011-0004).

Patients

Eighty-eight AR patients (18-60 years old) were recruited from the First Affiliated Hospital of Xinjiang Medical University and the Traditional Chinese Medicine Hospital of Xinjiang Uygur Autonomous Region from December 2013 to November 2017. The diagnosis of AR was in accordance with the Allergic Rhinitis and its Impact on Asthma (ARIA) Guideline (10) and based on the disease history (more than one year), nasal symptoms, clinical examination, skin prick test, and/or specific IgE measurement. Ninety-eight people of similar age with no history of allergic disease were enrolled as the normal control group. The subjects with the following conditions were excluded from the study: history of vasomotor rhinitis, nasopharyngeal carcinoma, respiratory diseases, cancer, diabetes, hypertension, blood diseases, and other immune diseases; use of β-receptor blocker and histamine H1 antagonist within the past 1 month.

Sample collection and $CD4^+$T cells isolation

The peripheral blood of subjects was collected under sterile conditions and lymphocytes were separated by using the HISTOPAQUE®-1077 (RNBF2219, Sigma, USA). The isolated lymphocytes were treated with a 500 μL phosphate-buffered saline (PBS) culture medium and mixed with a 45 μL magnetic bead antibody (557787, BD, USA) to obtain the $CD4^+$T cells. $CD4^+$T cells were stored at -80°C for qPCR measurement.

Animal grouping and modeling

Thirty male-specific pathogen-free Sprague-Dawley rats (5-week-old, 180-200 g) were purchased from the Animal Experiment Center of Xinjiang Medical University (Urumchi, China). All rats were housed in the clean barrier environment under standard conditions (12-hours light/dark cycles, 18-22°C, and 50-60% humidity), with food and water provided ad libitum. The rats were divided randomly into three groups (10 rats in each group): I) normal control group (NC group); II) ovalbumin (OVA, A5503, Sigma, USA) and aluminium hydroxide (Alum, 239186, Sigma,

USA)-induced AR group (AR group); III) 5-azacytidine (5-aza, 5 mg/kg, A2385, Sigma, USA) intervention group (AR + 5-aza group). For the modeling, rats were injected intraperitoneally with 1 mL physiological saline containing 1 mg OVA and 10 mg Alum on days 1, 8, and 15. From day 22 to 28, rats received a daily intranasal stimulation with 25 μL of 10 mg/mL OVA per nostril. The rats in the AR + 5-aza group were additionally treated with 5-aza reagents 30 min before OVA intranasal challenge. The rats in the NC group were injected with PBS intranasally using the same schedule. Rats were sacrificed by 2% pentobarbital injection on the next day of the last nasal challenge. Blood was taken from the abdominal aorta, and nasal mucosa was collected for subsequent experiments (Fig. 1).

Rats were intraperitoneally sensitized with OVA and Alum on days 1, 8, and 15. All groups of rats received intranasal challenge OVA from day 22 to day 28, while rats injected with PBS were used for the NC. In addition to sensitization and challenge, rats in the AR + 5-aza group were intraperitoneally injected with 5-aza 30 min before an intranasal challenge from day 22 to day 28.

Reverse transcription-quantitative real-time polymerase chain reaction (RT-qPCR)

Total RNA was extracted from $CD4^+$T cells of patients and nasal mucosa of rats using TRIzol (15596018, Thermo, USA) according to the manufacturer's instructions. Then, the extracted RNA (2μg) was reverse transcribed into complementary DNA (cDNA) using PrimeScript™ RT reagent Kit with gDNA Eraser (RR047A, Takara, Tokyo, Japan). RT-qPCR was performed using TB Green® Premix Ex Taq™ II (RR820A, Takara, Tokyo, Japan), with the QuantStudio6 Flex PCR system used for amplification analysis. GAPDH was used as the internal reference, and the experiment was repeated in triplicate. The relative expression of genes was measured by using the $2^{-\Delta\Delta CT}$ method. The primer sequences are listed in Table I.

Western Blot

Total proteins were obtained from the nasal mucosa of rats using RIPA lysing buffer (R0010, Solarbio, Beijing, China) and quantified by using a BCA protein assay kit (PC0020, Solarbio, Beijing, China). Equal amounts of protein samples were separated by 10% SDS-PAGE and transferred onto PVDF membranes. After being sealed with 5% skim milk for 2 hours at 25°C, the membranes were incubated with primary antibodies (GAPDH, ab8245, Abcam, USA, 1:10000; IFN-γ, BM4939,

Table I. *Detailed Information about Primer Sequence*

Gene		Primer sequences (5'-3')
IFN-γ	Forward	AACCCACAGATCCAGCACAAAGC
	Reverse	TACCCCAGAATCAGCACCGACTC
IL-4	Forward	CAAGGAACACCACGGAGAACGAG
	Reverse	CTTCAAGCACGGAGGTACATCACG
GATA3	Forward	CTCTTCCCTCCCAGCAGCCTAC
	Reverse	AGTACCATCTCGCCGCCACAG
ROR-γ	Forward	GCAGCAAGGACGGCACCAAG
	Reverse	GCCAGCAACTCCCGAGATGTTC
Foxp3	Forward	TGTGGTGGAGAGTAGTGCTCAGAG
	Reverse	GAGGTGGCGATACTCAGCAAGAAG
GAPDH	Forward	ACGGCAAGTTCAACGGCACAG
	Reverse	CGACATACTCAGCACCAGCATCAC

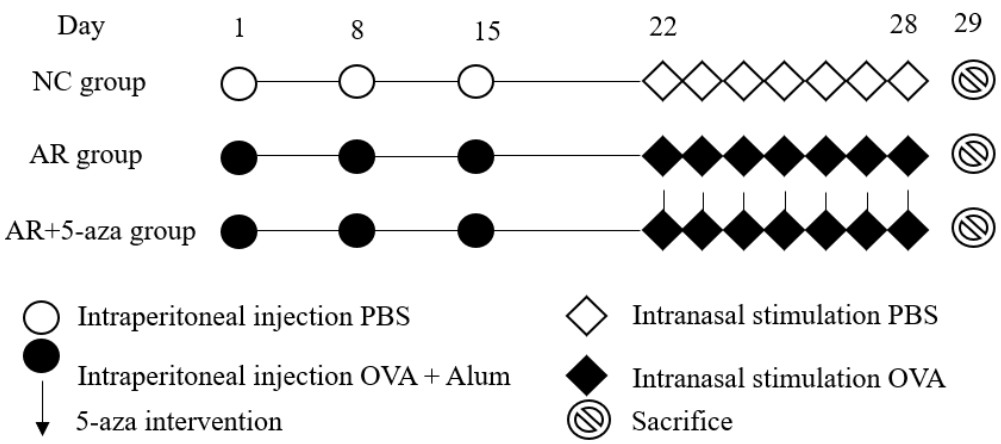


Fig. 1. *Schematic representation of AR rat modeling and intervention experiments*

Boster Biological Technology Co., Ltd, Wuhan, China, 1:500; IL-4, AF5142, Affinity Biosciences. OH. USA, 1:500; GATA3, PB0195, Boster Biological Technology Co., Ltd, Wuhan, China, 1:500; ROR-γ, DF3196, Affinity Biosciences. OH. USA, 1:500; Foxp3, AF6544, Affinity Biosciences. OH. USA, 1:500) overnight at 4°C. On the next day, the membranes were washed three times with 1×TBST and incubated with the secondary antibody (HRP-IgG, ZB-2301, ZSGB-BIO, Beijing, China, 1:40000) for 1 hour at 25°C. After washing three times with 1×TBST, the protein bands were developed using enhanced chemiluminescence (ECL, BL520A, Biosharp, Shanghai, China) chromogenic substrates with a gel imaging system. The experiments were repeated in triplicate, and the grey values were analyzed using Image J software.

Enzyme-linked immunosorbent assay (ELISA)

The serum of rats was centrifuged at 500 g for 30 minutes and stored at -20°C. The levels of IFN-γ, IL-4, GATA3, ROR-γ, and Foxp3 in the serum of rats were measured by using ELISA kits (J&l Biological, Shanghai, China). The absorbance at the wavelength of 450 nm was measured by a microplate reader and the standard curve was made.

Flow cytometry (FCM)

The fresh blood of rats was collected in EDTA tubes, and peripheral blood mononuclear cells (PBMCs) were isolated by using the HISTOPAQUE®-1077. PBMCs were added with 4μL Leukocyte Activation Cocktail with BD GolgiPlug™ (550583, Becton, Dickinson and Company, USA) and cultured at 37°C with 5% CO_2 for 4 hours. Then, PBMCs were stained with Anti-Rat CD4-PE-Cy™7 (B280481, Clone: W3/25, Biolegend®) and Anti-Rat CD25-PE (B302343, Clone: OX-39, Biolegend®). The Fixation/Permeabilization Solution Kit (554714, Becton, Dickinson and Company, USA) was used to fix and permeabilize cells. Finally, except for the control cells, PBMCs were stained with Anti-Rat IFN-γ-FITC (B315221, Clone: DB-1, Biolegend®), Anti-Rat IL-4-eFluor 660 (2252118, Clone: OX81, eBioscience™), Anti-Rat IL-17A-PE (2261900, Clone: eBio17B7, eBioscience™), and Anti-Rat FOXP3-PE-Cyanine5 (2275289, Clone: FJK-16s, eBioscience™). The expression frequency of cytokines IFN-γ, IL-4, IL-17A, and Foxp3 on gated $CD4^+$ and $CD25^+$ cells were measured using a flow cytometer (Beckman Dxflex), and the number of Th1/Th2 and Th17/Treg cell subsets was analyzed.

Statistical analysis

The statistical analysis was performed using SPSS 25.0 Software (IBM Crop., New York, USA) and GraphPad Prism 9.0 (GraphPad Software Inc., San Diego, USA). All data are presented as mean ± standard deviation (SD). The differences between the two groups were compared using an unpaired *t*-test and the differences among multiple groups were compared using one-way analysis of variance (ANOVA). A value of $P < 0.05$ was considered statistically significant.

RESULTS

mRNA expression patterns of IFN-γ, IL-4, GATA3, ROR-γ, and Foxp3 in AR patients

The mRNA expressions of IFN-γ, IL-4, GATA3, ROR-γ, and Foxp3 in the NC group and AR patient group were determined using RT-qPCR. As shown in Table II, the mRNA expressions of IFN-γ ($P < 0.01$), IL-4 ($P < 0.01$), GATA3 ($P < 0.01$), ROR-γ ($P < 0.01$) in AR patients were significantly higher than those in the controls, while the mRNA expression of Foxp3 ($P < 0.05$) in AR patients was lower than that in the controls (Fig. 2).

mRNA expression patterns of IFN-γ, IL-4, GATA3, ROR-γ, and Foxp3 in AR rats

To investigate the effects of 5-aza on AR, we detected the mRNA expressions of IFN-γ, IL-4, GATA3, ROR-γ, and Foxp3 of rats in the NC group, AR group, AR + 5-aza group by using RT-qPCR. As shown in Table III, the mRNA expressions of IFN-γ ($P < 0.05$), IL-4 ($P < 0.01$), GATA3 ($P < 0.05$), and ROR-γ ($P < 0.01$) of rats in the AR group was higher than those in the NC group, while the expressions of IFN-γ ($P < 0.05$), IL-4 ($P < 0.01$), GATA3 ($P < 0.01$), and ROR-γ ($P < 0.01$) of rats were reduced in the AR + 5-aza group. The mRNA expression of Foxp3 ($P < 0.05$) of rats in the AR group was lower than that in the NC group, while the expression of Foxp3 ($P < 0.01$) of rats was increased in the AR + 5-aza group (Fig. 3).

Protein expression patterns of IFN-γ, IL-4, GATA3, ROR-γ, and Foxp3 in AR rats

Similarly, we detected the protein expressions of IFN-γ, IL-4, GATA3, ROR-γ, and Foxp3 of rats using Western blotting and ELISA. Our results showed that

Table II. *mRNA expression in the NC group and AR patient group ($\bar{X}$±S, %)*

Group	IFN-γ	IL-4	GATA3	ROR-γ	Foxp3
NC group	1.69±0.26	1.79±0.12	2.04±0.29	1.55±0.75	3.62±0.98
AR patient group	3.91±0.49**	4.27±0.88**	5.31±0.28**	4.70±0.94**	1.30±0.34*

*Note: *P<0.05 vs. NC group, **P<0.01 vs. NC group, the difference was statistically significant.*

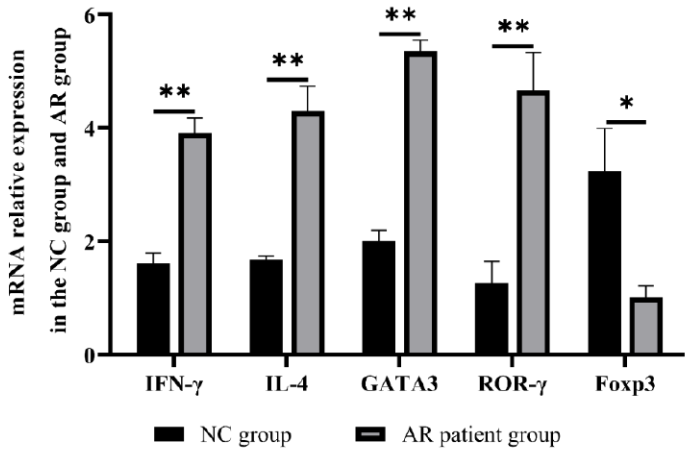


Fig. 2. *mRNA relative expressions of IFN-γ, IL-4, GATA3, ROR-γ, and Foxp3 in the NC group and AR patient group. GAPDH was used as the internal reference. The statistical results were expressed as X±S. *P < 0.05 vs. NC group, **P < 0.01 vs. NC group.*

Table III. *mRNA relative expression in AR rats ($\bar{X}$±S, %)*

Group	NC group	AR group	AR+5-aza group
IFN-γ	1.37±0.52	3.05±1.05*	1.42±0.53$^{\#}$
IL-4	1.00±0.02	2.54±0.20**	0.33±0.35$^{\#\#}$
GATA3	1.03±0.28	1.70±0.30*	0.42±0.35$^{\#\#}$
ROR-γ	1.05±0.39	2.21±0.18**	0.44±0.10$^{\#\#}$
Foxp3	1.00±0.08	0.35±0.15*	1.13±0.35$^{\#\#}$

*Note: *P<0.05 vs. NC group, **P<0.01 vs. NC group, #P<0.05 vs. AR group, ##P<0.01 vs. AR group, the difference was statistically significant.*

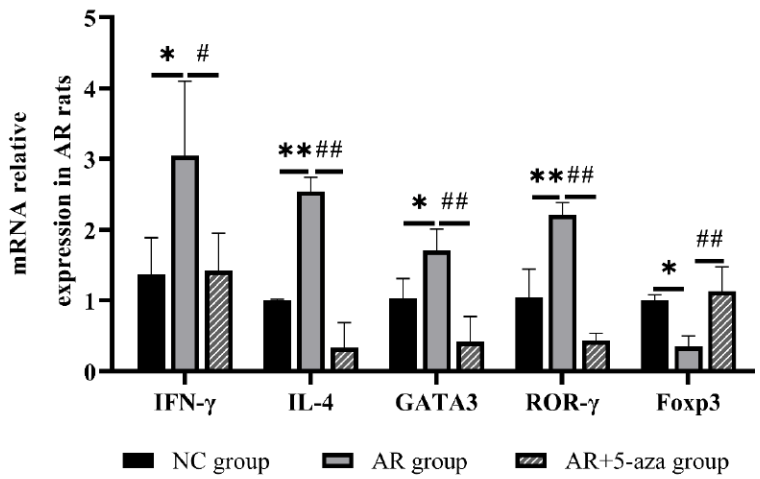


Fig. 3. *mRNA relative expressions of IFN-γ, IL-4, GATA3, ROR-γ, and Foxp3 in rats in the NC group, AR group, and AR + 5-aza group. GAPDH was used as the internal reference. The statistical results were expressed as X±S. *P < 0.05 vs. NC group, **P < 0.01 vs. NC group, #P < 0.05 vs. AR group, ##P <0 .01 vs. AR group.*

the protein expressions of IFN-γ ($P < 0.01$), IL-4 ($P < 0.01$), GATA3 ($P < 0.01$), and ROR-γ ($P < 0.05$) of rats in the AR group were significantly higher than those in the NC group, while the protein expressions of IFN-γ ($P<0.01$), IL-4 ($P < 0.01$), GATA3 ($P < 0.01$), and ROR-γ ($P < 0.05$) of rats in the AR + 5-aza group were reduced. The protein expression of Foxp3 ($P < 0.01$) of rats in the AR group was significantly lower than that in the NC group, while the protein expression of Foxp3 ($P < 0.01$) of rats in the AR + 5-aza group was increased (Fig. 4).

As shown in Table IV, the levels of IFN-γ, IL-4, GATA3, ROR-γ, and Foxp3 in the serum of rats were measured using ELISA kits. The levels of IFN-γ ($P < 0.01$), IL-4 ($P < 0.01$), GATA3 ($P < 0.01$), and ROR-γ ($P < 0.01$) in the serum of rats in the AR group were significantly higher than those in the NC group, while their levels in the serum of rats in the AR + 5-aza group were decreased significantly; the serum level of cytokine Foxp3 ($P < 0.01$) of rats in the AR group was significantly lower than that in the NC group, while the serum level of Foxp3 of rats in the AR+5-aza group was increased significantly (Fig. 5).

The ratio of Th1/Th2 and Th17/Treg cell subsets in AR rats

FCM analysis revealed the ratio of Th1/Th2 and Th17/Treg cell subsets of rats in the NC group, AR group, and AR + 5-aza group. As shown in Table V, the ratio of Th1, Th2, and Th17 cell subsets of rats in the AR group were significantly higher than that in the NC group ($P < 0.01$), while the ratio of Th1, Th2, and

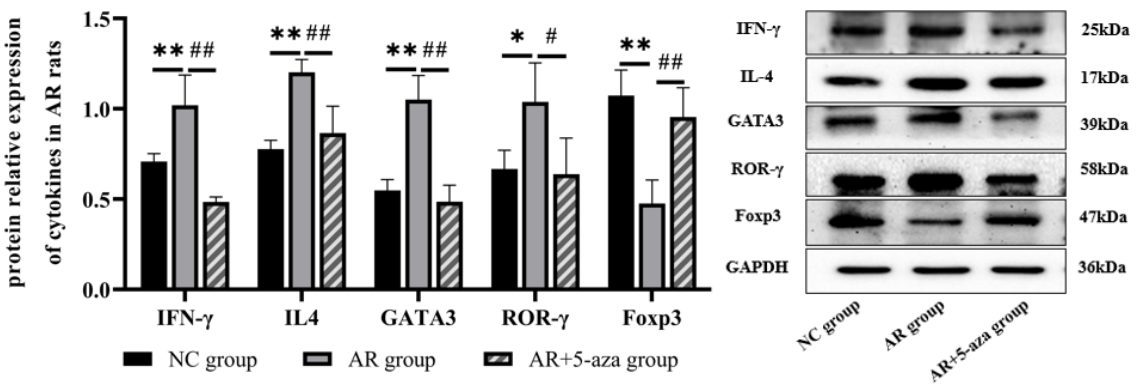


Fig. 4. *Protein relative expressions of IFN-γ, IL-4, GATA3, ROR-γ, and Foxp3 of rats in the NC group, AR group, and AR + 5-aza group. GAPDH was used as the internal reference. The statistical results were expressed as X±S. *P < 0.05 vs. NC group, **P < 0.01 vs. NC group, #P < 0.05 vs. AR group, ##P < 0.01 vs. AR group.*

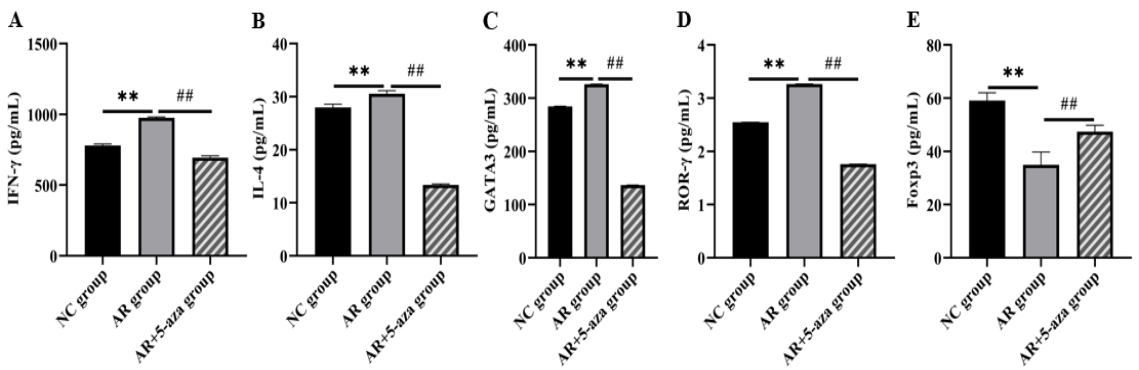


Fig. 5. *Serum levels of IFN-γ (A), IL-4 (B), GATA3 (C), ROR-γ (D), and Foxp3 (E) of rats in the NC group, AR group, and AR + 5-aza group were measured using ELISA assay. The statistical results were expressed as X±S. **P < 0.01 vs. NC group, ##P < 0.01 vs. AR group.*

Th17 cell subsets were decreased significantly in the AR + 5-aza group ($P < 0.01$). The ratio of the Treg cell subset of rats in the AR group was significantly lower than that in the NC group ($P < 0.01$), while its ratio was increased significantly in the AR + 5-aza group ($P < 0.01$) (Fig. 6).

DISCUSSION

Abnormal differentiation of $CD4^+$ Th lymphocytes is the immunological basis of AR. According to the different cytokines secreted by Th0, Th cells can be divided into four subsets: Th1, Th2, Th17, and Treg. Th1 participates in cellular immunity and mainly secretes cytokines such as IFN-γ. IFN-γ is a specific cytokine that inhibits the production of characteristic factors of Th2 cells and regulates the activation, differentiation, and recruitment of EOSs. Th2 participates in humoral immunity and mainly secretes cytokines such as IL-4 and GATA3. IL-4 is a specific cytokine that can promote the differentiation of Th0 into Th2 cells, maintain the proliferation of Th2 cells, induce the production of IgE, promote the maturation of EOSs and mast cells, trigger airway hyperresponsiveness, and produce a large amount of mucus. GATA-3 is a specific transcription factor that induces the production of Th2 cytokine IL-4 and promotes Th2 regeneration. Th17 cells can secrete specific cytokines such as IL-17 and ROR-γ with pro-inflammatory effects, promote T cell activation, promote the recruitment of neutrophils and monocytes, and induce allergic inflammation (11). ROR-γ is a specific transcription factor that induces the gene encoding the IL-17 cytokine and promotes its expression. Treg cell is a special subtype of T cells, which inhibits the differentiation of Th0 cells into Th2 and alleviates airway allergic inflammation (12). Foxp3, a specific transcription factor of Treg, can upregulate the Th1 cytokine signal pathway and is highly expressed in Treg cells (13).

Under normal conditions, Th cells maintain immune homeostasis. AR attack induces the imbalance of Th1/Th2 and Th17/Treg differentiation. Therefore, maintaining the balance of Th1/Th2 and

Table IV. *Relative cytokine protein expression in AR rats ($\bar{X}$±S, %)*

Group	NC Group	AR Group	AR+5-aza Group
IFN-γ	781.15±9.37	975.92±6.56**	694.82±11.8##
IL-4	27.98±0.60	30.54±0.61**	13.35±0.19##
GATA3	284.34±0.61	326.14±0.20**	136.44±0.53##
ROR-γ	2.55±0.00	3.26±0.00**	1.76±0.00##
Foxp3	59.07±2.96	35.00±4.77**	47.43±2.41##

*Note: **P<0.01 vs. NC group, ##P<0.01 vs. AR group, the difference was statistically significant.*

Table V. *Ratio of Th1/Th2 and Th17/Treg cell subsets in AR rats ($\bar{X}$±S, %)*

Group	NC group	AR group	AR+5-aza group
Th1	0.57±0.33	1.49±0.74**	0.16±0.09##
Th2	0.87±0.41	1.49±0.57**	0.33±0.13##
Th17	0.24±0.12	0.48±0.24**	0.20±0.05##
Treg	13.71±3.09	4.33±0.67**	9.00±1.69##

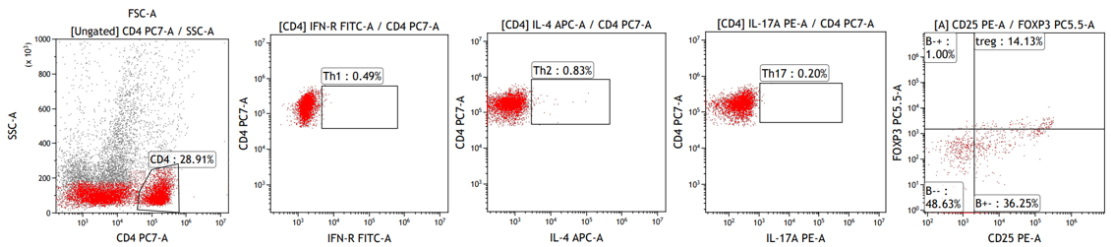
*Note: **P<0.01 vs NC group, ##P<0.01 vs AR group, the difference was statistically significant*

*Note: **P<0.01 vs. NC group, ##P<0.01 vs. AR group, the difference was statistically significant.*

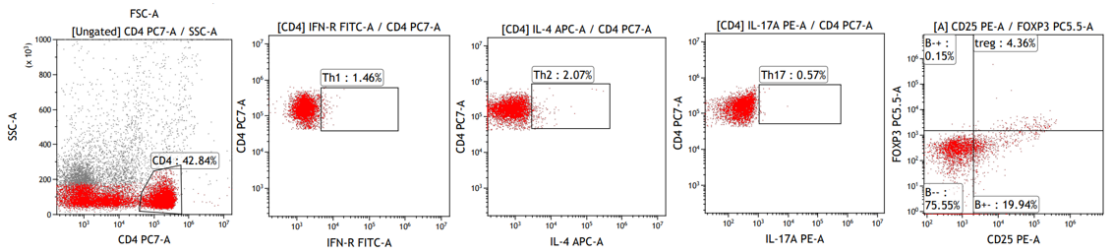
Th17/Treg and regulating the expressions of Th cell subset cytokines can weaken inflammatory responses in AR, which may represent an effective entry point for the treatment of AR and airway sensitivity.

Previous studies have shown the elevated mRNA and protein expressions of IFN-γ in AR patients and animal models of asthma (14, 15). IL-4 and GATA3 expressions in AR rats are significantly higher than those in the control rats (16). The expression of ROR-γ is demonstrated to be elevated in AR animal models (17). Previous studies have also reported the reduction of Foxp3 expression in AR animal models. In our study, the expressions of IFN-γ, IL-4, GATA3, and ROR-γ were increased in AR patients, and the expression of Foxp3 was decreased in AR patients. These results were consistent in animal models. Therefore, this study indicates that when AR occurs, the regulatory trends of inflammatory factors and anti-inflammatory factors in humans and animals are roughly the same, which lays a foundation for further better exploring the relationship between AR and Th-related cytokines in animal models.

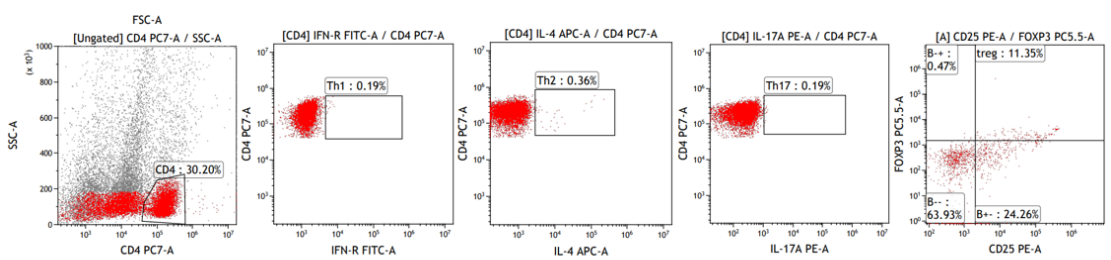
DNA methylation is one of the most abundant and well-studied epigenetic modifications, which regulates gene expression without changing DNA sequence (18). DNA methylation can alter gene transcription, which may increase the risk of allergic airway diseases (19). 5-aza can reduce inflammatory responses (20) and play an important role in allergic diseases as a DNMT inhibitor. The expression of Th2 cytokine IL-4 is decreased significantly after 5-aza intervention (21). Also, the reduction of IL-4 is observed in plasma and $CD4^+$ splenocytes after 5-aza intervention



A: The ratio of Th1/Th2 and Th17/Treg cell subsets in the NC group



B: The ratio of Th1/Th2 and Th17/Treg cell subsets in the AR group



C: The ratio of Th1/Th2 and Th17/Treg cell subsets in the AR+5-aza group

Fig. 6. *Ratio of Th1/Th2 and Th17/Treg cell subsets of rats in the NC group (**A**), AR group (**B**), and AR+5-aza group (**C**) were measured using FCM. The statistical results were expressed as X±S. **P < 0.01 vs. NC group, ##P < 0.01 vs. AR group.*

(22). The expression of ROR-γ is decreased and Foxp3 is increased in OVA-induced rats after 5-aza intervention (23). 5-aza can upregulate the transcription level of anti-inflammatory cytokine Foxp3 and downregulate the mRNA expressions of pro-inflammatory mediators (24). In this study, the mRNA and protein expressions of IFN-γ, IL-4, GATA3, and ROR-γ were increased in AR rats but decreased significantly after 5-aza treatment; the ratio of Th1, Th2, and Th17 cell subsets in AR rats was significantly higher than that in the control rats, while 5-aza intervention led to an opposite trend. The mRNA and protein expressions of Foxp3 were decreased in AR rats and increased significantly after 5-aza treatment; the number of Treg cell subsets in AR rats was lower than that in the control rats, while the ratio of Treg cell subset was increased significantly after 5-aza intervention. At present, the role of 5-aza in human models of AR has not been studied, but our findings indicated that 5-aza could regulate the differentiation of Th cell subsets and the expressions of relevant inflammatory factors in animal models, laying a foundation for future human experiments.

In summary, the number and relative expressions of Th1, Th2, and Th17 cell subsets and cytokines were increased in AR, while Treg cell subset and cytokine were decreased. Methyltransferase inhibitor 5-aza downregulated the number of Th1, Th2, and Th17 cell subsets and upregulated Treg cell subsets. The expressions of cytokines IFN-γ, IL-4, GATA3, ROR-γ, and Foxp3 were regulated by methyltransferase inhibitor 5-aza. However, the regulatory mechanisms of IFN-γ and GATA3 in AR, the safe concentration of DNMT inhibitors, and the regulatory relationship between Th1, Th2, Th17, and Treg cell subsets have not been fully clarified, which needs further exploration.

Funding

This study was supported by a grant from the National Natural Science Foundation of China (No. 81760182).

Conflicts of interest

The authors declare that they have no conflict of interest.

REFERENCES

1. Leth-Moller KB, Skaaby T, Linneberg A. Allergic rhinitis and allergic sensitization are still increasing among Danish adults. Allergy 2020; 75(3): 660-668.
2. Zhang Y, Zhang L. Increasing Prevalence of Allergic Rhinitis in China. Allergy Asthma Immunol Res 2019; 11(2): 156-169.
3. Cheng L, Zhou W, Liu M. [Highlights of the Chinese guideline on sublingual immunotherapy for allergic rhinitis and asthma.] (English edition) J Clin Otorhin Head Neck Surg 2020; 34(4): 292-295.
4. Kordella C, Lamprianidou E, Kotsianidis I. Mechanisms of Action of Hypomethylating Agents: Endogenous Retroelements at the Epicenter. Front Oncol 2021; 11:650473.
5. Fagone P, Mazzon E, Chikovani T, et al. Decitabine induces regulatory T cells, inhibits the production of IFN-gamma and IL-17 and exerts preventive and therapeutic efficacy in rodent experimental autoimmune neuritis. J Neuroimmunol 2018; 321(41-48).
6. Wang Q, Wang P, Zhou H, et al. 5-Azacytidine specifically inhibits the NIH-3T3 PCD process induced by TNF-alpha and cycloheximide via affecting BCL-XL. J Cell Biochem 2018; 119(2): 1501-1510.
7. Petralia MC, Mazzon E, Basile MS, et al. Effects of Treatment with the Hypomethylating Agent 5-aza-2 ‘-deoxycytidine in Murine Type II Collagen-Induced Arthritis. Pharmaceuticals (Basel) 2019; 12(4):174.
8. Wu CJ, Yang CY, Chen YH, et al. The DNA methylation inhibitor 5-azacytidine increases regulatory T cells and alleviates airway inflammation in ovalbumin-sensitized mice. Int Arch Allergy Immunol 2013; 160(4): 356-64.
9. Jiang T, Zhang HW, Wen YP, et al. 5-Aza-2-deoxycytidine alleviates the progression of primary biliary cholangitis by suppressing the FoxP3 methylation and promoting the Treg/Th17 balance. Int Immunopharmacol 2021; 96:107820.
10. Brozek JL, Bousquet J, Baena-Cagnani CE, et al. Allergic Rhinitis and its Impact on Asthma (ARIA) guidelines: 2010 Revision. J Allergy Clin Immulol 2010; 126(3): 466-476.
11. Jia YH, Wei YY. Modulators of MicroRNA Function in the Immune System. Int J Mol Sci 2020; 21(7):2357.
12. Luo Y, Deng Y, Tao Z, et al. Regulatory effect of

microRNA-135a on the Th1/Th2 imbalance in a murine model of allergic rhinitis. Exp Ther Med 2014; 8(4): 1105-10.
13. Park BS, Hong G U, Ro J Y. Foxp3(+)-Treg Cells Enhanced by Repeated Low-Dose Gamma-Irradiation Attenuate Ovalbumin-Induced Allergic Asthma in Mice. Radiat Res 2013; 179(5): 570-583.
14. Wang J, Yin J, Peng H, et al. MicroRNA-29 mediates anti-inflammatory effects and alleviation of allergic responses and symptoms in mice with allergic rhinitis. Allergy Asthma Clin Immunol 2021; 17(1):24.
15. Brand S, Kesper D A, Teich R, et al. DNA methylation of TH1/TH2 cytokine genes affects sensitization and progress of experimental asthma. J Allergy Clin Immunol 2012; 129(6):1602-10.
16. Luo YY, Deng YQ, Tao ZZ, et al. Regulatory effect of microRNA-135a on the Th1/Th2 imbalance in a murine model of allergic rhinitis. Exp Ther Med 2014; 8(4): 1105-10.
17. Shi Z, Jiang W, Chen X, et al. Chlorogenic acid ameliorated allergic rhinitis-related symptoms in mice by regulating Th17 cells. Biosci Rep 2020; 40(11).
18. Feil R, Fraga MF. Epigenetics and the environment: emerging patterns and implications. Nat Rev Genet 2012; 13(2): 97-109.
19. Hollingsworth JW, Maruoka S, Boon K, et al. In utero supplementation with methyl donors enhances allergic airway disease in mice. J Clin Invest 2016; 126(5):2012.
20. Landman S, van der Horst C, van Erp PEJ, et al. Immune responses to azacytidine in animal models of inflammatory disorders: a systematic review. J Transl Med 2021; 19(1):11.
21. Wang X, Cao Q, Yu L, et al. Epigenetic regulation of macrophage polarization and inflammation by DNA methylation in obesity. JCI Insight 2016; 1(19): e87748.
22. Xia Y, Yang J, Wang G, et al. Age-Related Changes in DNA Methylation Associated with Shifting Th1/Th2 Balance. Inflammation 2016; 39(6): 1892-1903.
23. Wang C, Wang D, Zhao H, et al. Traffic-related PM2.5 and diverse constituents disturb the balance of Th17/Treg cells by STAT3/RORgammat-STAT5/Foxp3 signaling pathway in a rat model of asthma. Int Immunopharmacol 2021; 96:107788.
24. Mangano K, Fagone P, Bendtzen K, et al. Hypomethylating agent 5-aza-2'-deoxycytidine (DAC) ameliorates multiple sclerosis in mouse models. J Cell Physiol 2014; 229(12): 1918-25.

Investigation of key ubiquitination-related genes associated with cervical cancer

C. Shi, H. Xu, and H. Ding*

Department of Obstetrics and Gynecology, The Affiliated Huaian No. 1 People's Hospital of Nanjing Medical University, Huai'an, Jiangsu P. R. China

This study investigated key ubiquitination-related genes associated with cervical cancer. We downloaded standardized gene expression profiles (GSE39001, GSE63514, GSE52903, GSE9750, GSE6791, and GSE7803) to analyze differentially expressed genes (DEGs) between the tumor and normal samples. By comparing with ubiquitination-related genes downloaded from hUbiquitome, key ubiquitination-related DEGs (*BRCA1, CCNE2, HLTF, ICAM1, KIF15, PCNA,* and *PTTG1)* were identified, followed by mutation and copy number alteration (CNA), immune infiltration, methylation, and protein expression analyses. Based on The Cancer Genome Atlas (TCGA) data of cervical cancer, prognosis and gene set enrichment analysis were conducted. *BRCA1* was mainly subjected to somatic mutation. *ICAM1* expression was positively correlated with the abundance of neutrophils and dendritic cells. In different CNA groups of *HLTF* and *PTTG1*, the abundance of more immune cells exhibited a significant difference. *HLTF* and *ICAM1* were negatively correlated with more methylation sites. High *BRCA1*, *PCNA*, and *ICAM1* expression were associated with favorable survival. *BRCA1* was significantly enriched in mismatch repair and homologous recombination; *ICAM1* was enriched in chemokine signaling pathway and cell adhesion molecules, and *PCNA* was involved in DNA replication and cell cycle. Our findings reveal that these key ubiquitination-related genes may affect cervical cancer development and prognosis.

Cervical cancer is the fourth most common cancer in women globally, resulting in a great economic and medical burden on society (1). In 2018, an estimated 570,000 patients were diagnosed with cervical cancer, and the disease caused 311,000 deaths worldwide (2). Cervical cancer treatment mainly includes surgery, radiotherapy, and chemotherapy, but treatment strategies remain insufficient (3). Despite significant advances in early detection and treatment modalities, tumor metastases still occur and have a negative impact on the survival of patients diagnosed with early-stage cervical cancer (4). Furthermore, the overall prognosis remains poor for patients with advanced or recurrent cervical cancer, with a median survival of 8–13 months (5, 6). Therefore, a deeper understanding of the molecular mechanisms underlying cervical cancer will foster the development of new therapeutic strategies.

Ubiquitination, a conserved post-translational modification in eukaryotic organisms, is achieved via sequential action of E1 and E2 enzymes and E3 ligases. The ubiquitin-proteasome pathway, which combines ubiquitination with the proteasome complex, is a core component of the cellular protein degradation machinery and has important functions in homeostasis, including protection against misfolded or deleterious protein accumulation (7). Accumulating evidence has revealed that the ubiquitin-proteasome pathway plays a significant role in multiple biological processes, such as cell metabolism, gene transcription

Keywords: cervical cancer; ubiquitination; immune infiltration; prognosis; pathway

*Corresponding author:
Dr Hongyan Ding
Department of Obstetrics and Gynecology,
The Affiliated Huaian No. 1 People's Hospital of Nanjing Medical University, 1 Huanghe Road West, Huai'an,
Jiangsu 223300, P. R. China
e-mail: matedoor916@163.com

0393-974X (2022)
Copyright © by BIOLIFE, s.a.s.
This publication and/or article is for individual use only and may not be further reproduced without written permission from the copyright holder.
Unauthorized reproduction may result in financial and other penalties
DISCLOSURE: ALL AUTHORS REPORT NO CONFLICTS OF INTEREST RELEVANT TO THIS ARTICLE.

and translation, and epigenetic regulation (8, 9). Dysregulation of the ubiquitin-proteasome pathway is involved in the tumorigenesis and progression of various cancers, including cervical cancer (10, 11). It has been shown that ubiquitin-specific protease 7 plays a key role in sustaining DNA damage response and promoting cervical carcinogenesis (12); furthermore, the ubiquitin-conjugating enzyme E2-EPF is associated with tumor growth and cervical cancer cell invasiveness (13). In addition, many oncoproteins are subjected to ubiquitination-dependent degradation, and enhancing ubiquitination or targeting deubiquitinating enzymes may result in destabilization or functional inactivation of crucial oncoproteins, such as MYC and β-catenin (14, 15). Inhibiting the ubiquitin pathway and targeting the pathway components represent promising strategies to overcome anti-cancer drug resistance (16). However, the ubiquitination-related genes that play an important role in cervical cancer have not been fully explored.

In the present study, we combined multiple cervical cancer gene expression datasets with data from the hUbiquitome database to investigate key ubiquitination-related genes associated with cervical cancer and their corresponding regulatory mechanisms. Our analysis provides novel insights into cervical cancer pathogenesis.

MATERIALS AND METHODS

Data acquisition

Six standardized cervical cancer gene expression profiles were downloaded from the Gene Expression Omnibus (GEO) (17) database, including GSE39001 (43 tumor and 12 normal samples; platform, Affymetrix Human HG-Focus Target Array), GSE63514 (28 tumors and 24 normal samples; platform, Affymetrix Human Genome U133 Plus 2.0 Array), GSE52903 (55 tumors and 17 normal samples; platform, Affymetrix Human Gene 1.0 ST Array), GSE9750 (33 tumors and 24 normal samples; platform, Affymetrix Human Genome U133A Array), GSE6791 (20 tumors and 8 normal samples; platform, Affymetrix Human Genome U133 Plus 2.0 Array), and GSE7803 (31 tumors and 10 normal samples; platform, Affymetrix Human Genome U133A Array). The gene expression RNA sequencing and clinical data of cervical squamous cell carcinoma and endocervical adenocarcinoma (CESC) were downloaded from The Cancer Genome Atlas (TCGA) database.

Differential expression analysis

Based on the six datasets from the GEO database, differentially expressed genes (DEGs) between the tumor and normal samples were analyzed using the limma package (version 3.34.0) (18) in R3.6.1. The cut-off value was set as false discovery rate < 0.05, and $|\log2 \text{ fold change}| > 0.5$. Overlapping DEGs were then obtained by intersection analysis of the six DEG sets.

Identification of ubiquitination-related DEGs

Human ubiquitination-related genes were obtained from hUbiquitome (19), a database of human ubiquitination sites and cascades, including 1 E1, 12 E2, and 136 E3 enzymes, 283 substrates, and 17 deubiquitinating enzymes. The ubiquitination-related DEGs were identified by intersecting overlapping DEGs.

Mutation and copy number alteration (CNA) analysis

Mutation and CNA analyses of ubiquitination-related DEGs were performed using the cBioPortal (20) database.

Immune infiltration analysis

The abundance of six immune cell types, including CD4+ T cells, B cells, CD8+ T cells, macrophages, neutrophils, and dendritic cells, was calculated using the Tumor Immune Estimation Resource (21) algorithm based on CESC sample expression level data. The correlation of ubiquitination-related DEGs with immune infiltrate abundance was analyzed. Meanwhile, the difference in immune infiltrate abundance between different CNA groups of ubiquitination genes was analyzed.

Methylation analysis

The correlation between ubiquitination-related DEGs and their corresponding methylation sites was analyzed using the MEXPRESS (22) tool.

Analysis of the protein expression level of ubiquitination-related DEGs

The protein expression of ubiquitination-related DEGs in the tumor and normal samples were analyzed based on immunohistochemistry results in the Human Protein Atlas (HPA) (23) database (version 18).

Prognosis analysis of ubiquitination-related DEGs

Based on clinical data from the TCGA database, survival analysis of ubiquitination-related DEGs was conducted using the Gene Expression Profiling Interactive Analysis (24) online database. Ubiquitination related DEGs associated with prognosis were then identified for subsequent analysis.

Gene set enrichment analysis (GSEA)

Based on the CESC whole-genome expression level data obtained from the TCGA database, Kyoto Encyclopedia of Genes and Genomes (KEGG) pathways associated with prognostic ubiquitination-related DEGs were screened using GSEA (25). The q-value < 0.05 was selected as the screening threshold for the significantly enriched KEGG pathway.

RESULTS

Identification of ubiquitination-related DEGs by comprehensive analysis of multiple datasets

Based on the gene expression data in GSE39001, GSE63514, GSE52903, GSE9750, GSE6791, and GSE7803, 1520 (657 down- and 863 up-regulated), 4187 (787 down- and 3400 up-regulated), 2498 (1424 down- and 1074 up-regulated), 3254 (2237 down- and 1017 up-regulated), 3907 (267 down- and 3640 up-regulated), and 1826 (619 down- and 1027 up-regulated) DEGs were identified between the tumor and control samples, respectively. A subsequent Venn analysis revealed that 214 overlapping DEGs were obtained from the six DEG sets (Fig. 1). By comparing the 214 overlapping DEGs with ubiquitination-related genes downloaded from hUbiquitome, seven ubiquitination-related DEGs were identified, including BRCA1 DNA repair associated (*BRCA1*), cyclin E2 (*CCNE2*), helicase like transcription factor (*HLTF*), intercellular adhesion molecule 1 (*ICAM1*), kinesin family member 15 (*KIF15*), proliferating cell nuclear antigen (*PCNA*), and PTTG1 regulator of sister chromatid separation, securin (*PTTG1*), all of which were significantly up-regulated in all datasets.

Mutation and CNA analysis

Mutation and CNA analyses of seven ubiquitination-related DEGs were performed using the cBioPortal database (Fig. 2A). The results showed that different genes had different variation patterns. For instance, *BRCA1* was mainly subjected to somatic mutations, while *CCNE2*, *HLTF*, *PCNA*, *KIF15*, and *ICAM1* were mainly subjected to CNA (Fig. 2A). Moreover, the gene variation patterns varied

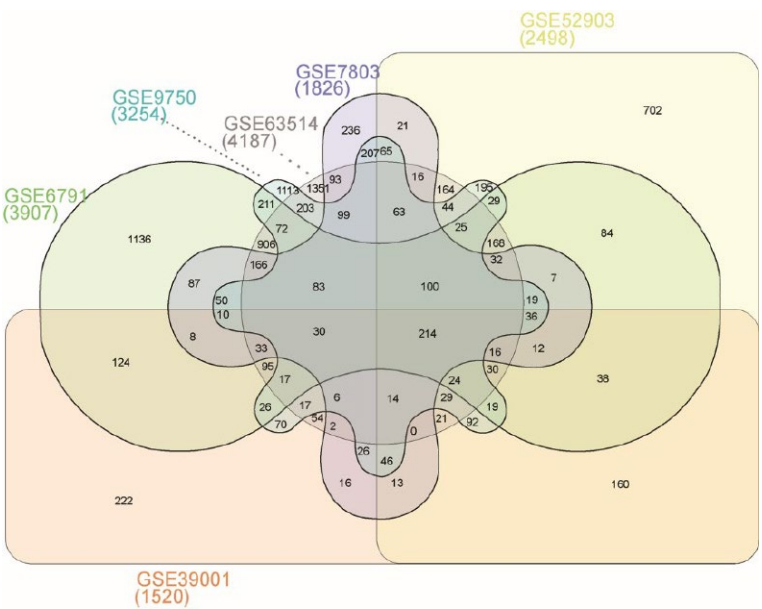


Fig. 1. *Venn diagram showing the overlapping differentially expressed genes (DEGs) of six datasets.*

between different pathological subtypes of cervical cancer. All seven genes showed variations in the cervical squamous cell carcinoma subtype (Fig. 2A). In addition, gene expression distribution in different CNA groups showed that the expression of the seven genes increased continuously with copy number changes from deletion to amplification, confirming a positive correlation between gene expression and CNA (Fig. 2B).

Immune infiltration analysis

It has been reported that ubiquitination-related enzymes are important tumor micro-environment components (26). Moreover, tumour-infiltrating immune cells are highly relevant to cervical cancer development (27). Therefore, immune infiltration analysis was conducted to elucidate the association between ubiquitination-related enzymes and immune cell infiltration in cervical cancer. Based on CESC sample expression level data, the abundance of six immune cell types was calculated, and their correlation with the expression of the seven ubiquitination-related DEGs was analyzed. Among the seven ubiquitination-related DEGs, only *ICAM1* expression was negatively associated with tumor purity and positively correlated with neutrophil and dendritic cell abundance (Fig. 3A).

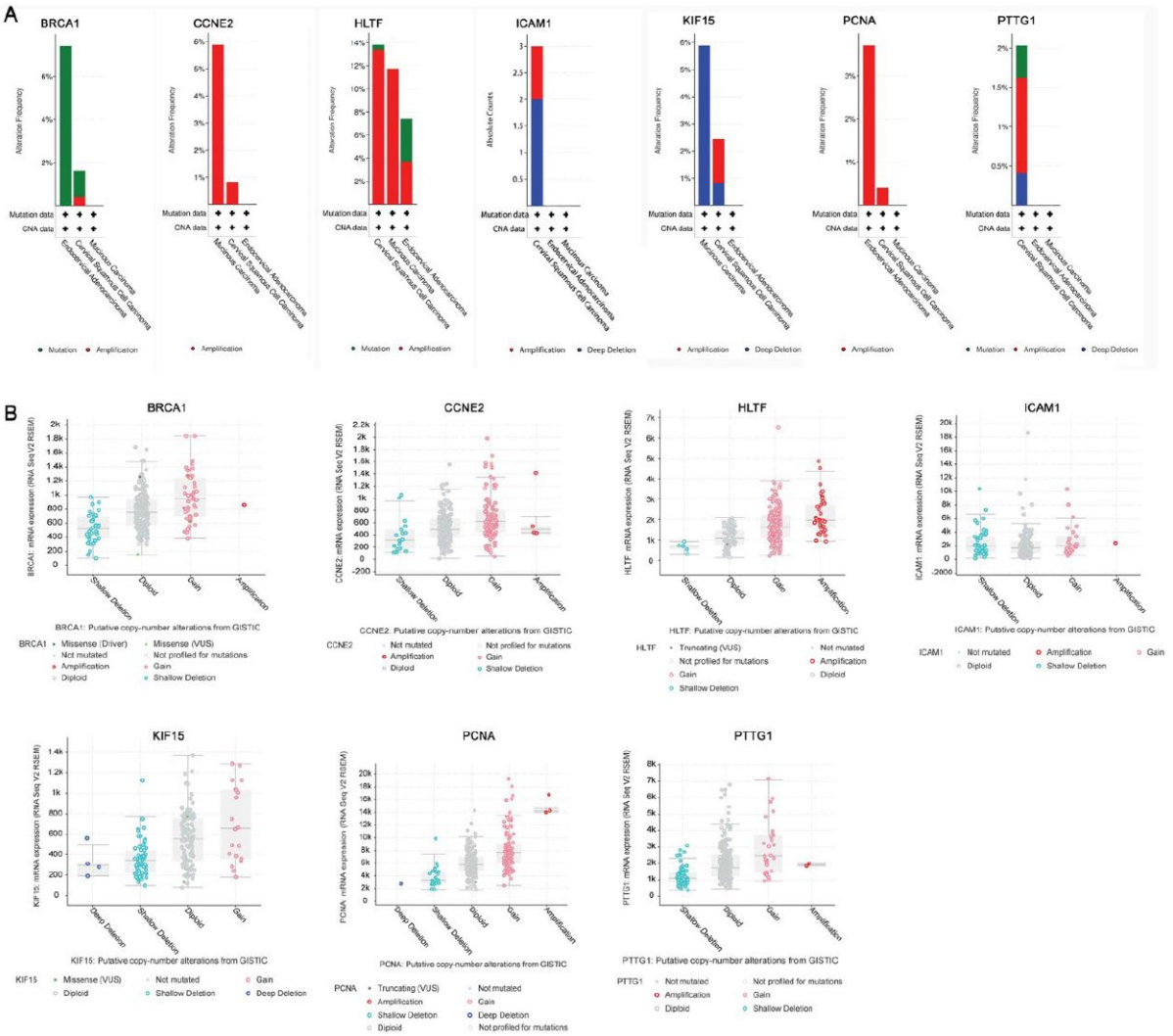


Fig. 2. *Mutation and copy number alteration (CNA) analysis of seven ubiquitination-related differentially expressed genes (DEGs).* ***A****: Mutation sample distribution of the seven ubiquitination-related DEGs in different cervical squamous cell carcinoma and endocervical adenocarcinoma (CESC) subtypes;* ***B****: Distribution of the expression of the seven ubiquitination-related DEGs in different mutation types.*

Moreover, there was no significant correlation between the expression of the six other ubiquitination-related DEGs and immune infiltrate abundance (Supplementary Fig. 1). In addition, the difference in immune infiltrate abundance between different CNA groups of the seven ubiquitination-related DEGs was analyzed. The abundance of more immune cell types significantly varied between different *HLTF* and *PTTG1* CNA groups (Fig. 3B) (Supplementary Fig. 2).

Methylation analysis

The MEXPRESS tool analysed the correlation between ubiquitination-related DEGs and their corresponding methylation sites. The results showed that *HLTF* (Fig. 4A) and *ICAM1* (Fig. 4B) were negatively correlated with more methylation sites, suggesting that *HLTF* and *ICAM1* were susceptible to methylation. However, other ubiquitination-related DEGs correlated with fewer methylation sites (Supplementary Fig. 3).

Analysis of the protein expression level of ubiquitination-related DEGs

Based on the information from the HPA database, immunohistochemistry results confirmed that the expression levels of BRCA1, ICAM1, and PCNA were significantly increased in cervical cancer (Fig. 5).

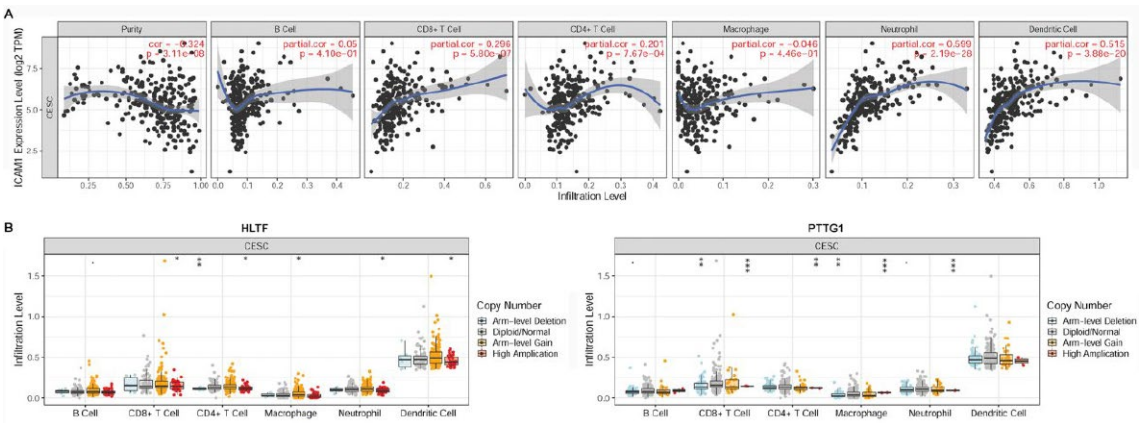


Fig. 3. *Immune infiltration and correlation analyses.* ***A****: Correlation between ICAM1 and the abundance of six immune cell types including CD4+ T cells, B cells, CD8+ T cells, macrophages, neutrophils, and dendritic cells;* ***B****: Abundance distribution of the six immune cell types in different copy number alteration (CNA) groups of HLTF and PTTG.*

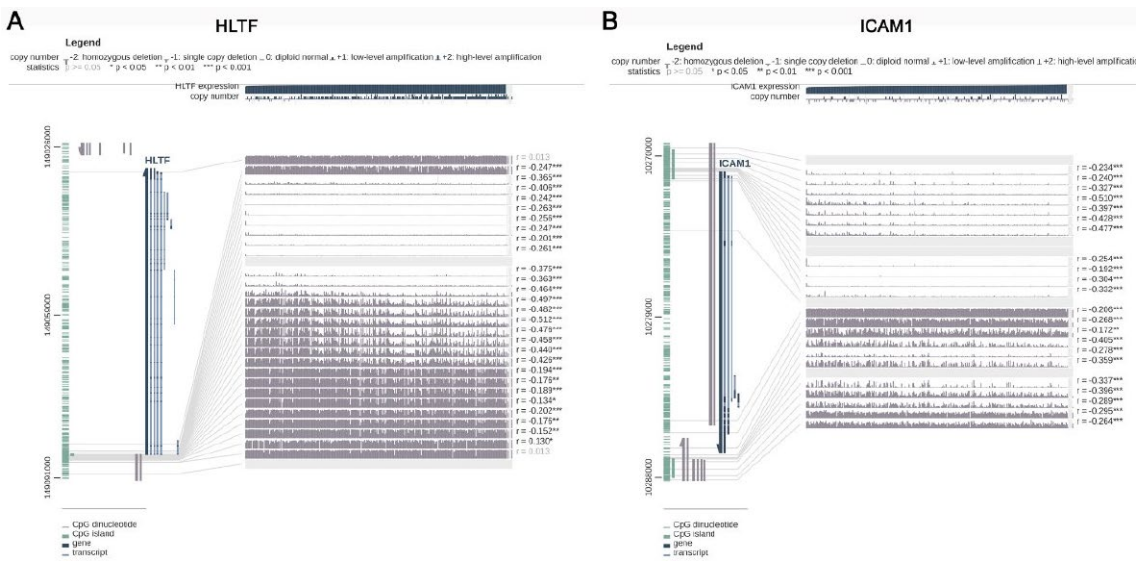


Fig. 4. *Methylation analysis results for HLTF (****A****) and ICAM1 (****B****) obtained using the MEXPRESS tool.*

Prognosis analysis of ubiquitination-related DEGs

Based on the clinical data, survival analysis of ubiquitination-related DEGs was conducted. High BRCA1 and PCNA expression levels were significantly associated with favorable overall survival, and high *ICAM1* expression significantly correlated with favorable disease-free survival (Fig. 6).

Notably, *BRCA1*, *PCNA*, and *ICAM1* were up-regulated in the tumor samples; however, their expression was highest in stage 1 samples and gradually

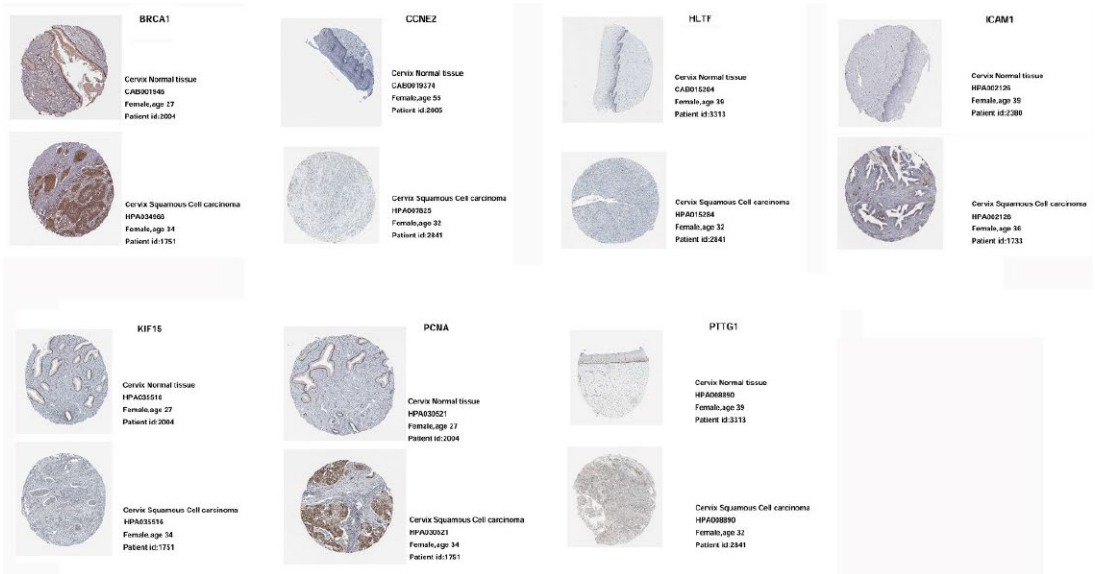


Fig. 5. *Validation of the protein expression levels of seven ubiquitination-related differentially expressed genes (DEGs) using the Human Protein Atlas (HPA) database.*

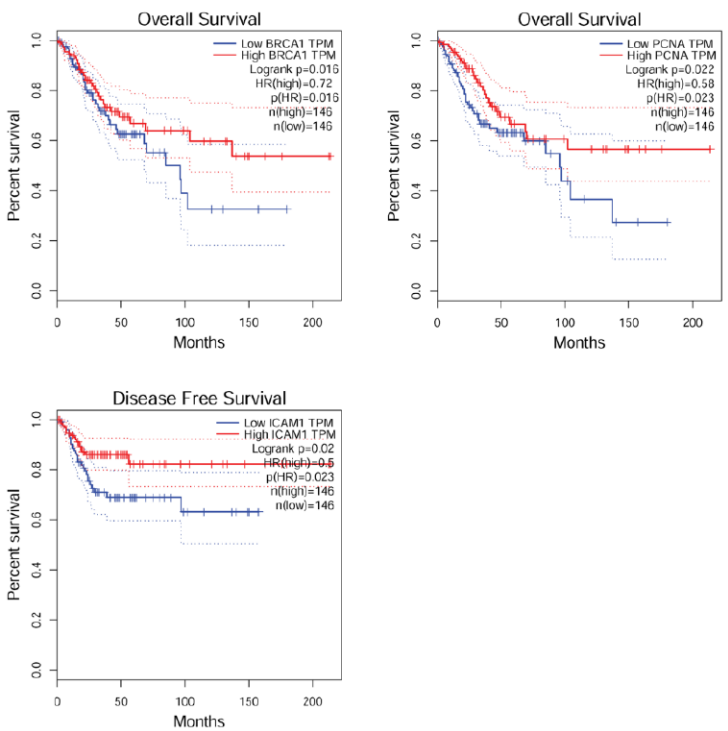


Fig. 6. *Kaplan–Meier survival analysis of ubiquitination-related differentially expressed genes (DEGs), including BRCA1, PCNA, and ICAM1.*

decreased in stage 2–4. Moreover, *BRCA1* and *ICAM1* in the N1 stage was lower than that in the N0 stage, and *PCNA* expression in the G1 grade was higher than that in G2–4 grades (Supplementary Fig. 4). These data might explain the positive correlation between high gene expression and favorable prognosis.

GSEA of the three prognostic ubiquitination-related DEGs

According to GSEA, *BRCA1*, *PCNA*, and *ICAM1* were significantly enriched in 18, 21, and 20 KEGG pathways, respectively. For instance, *BRCA1* was significantly enriched in mismatch repair and homologous recombination; *ICAM1* was markedly enriched in the chemokine signaling pathway and CAMs, and *PCNA* was mainly involved in DNA replication and the cell cycle (Fig. 7).

DISCUSSION

The ubiquitination pathway plays a pivotal

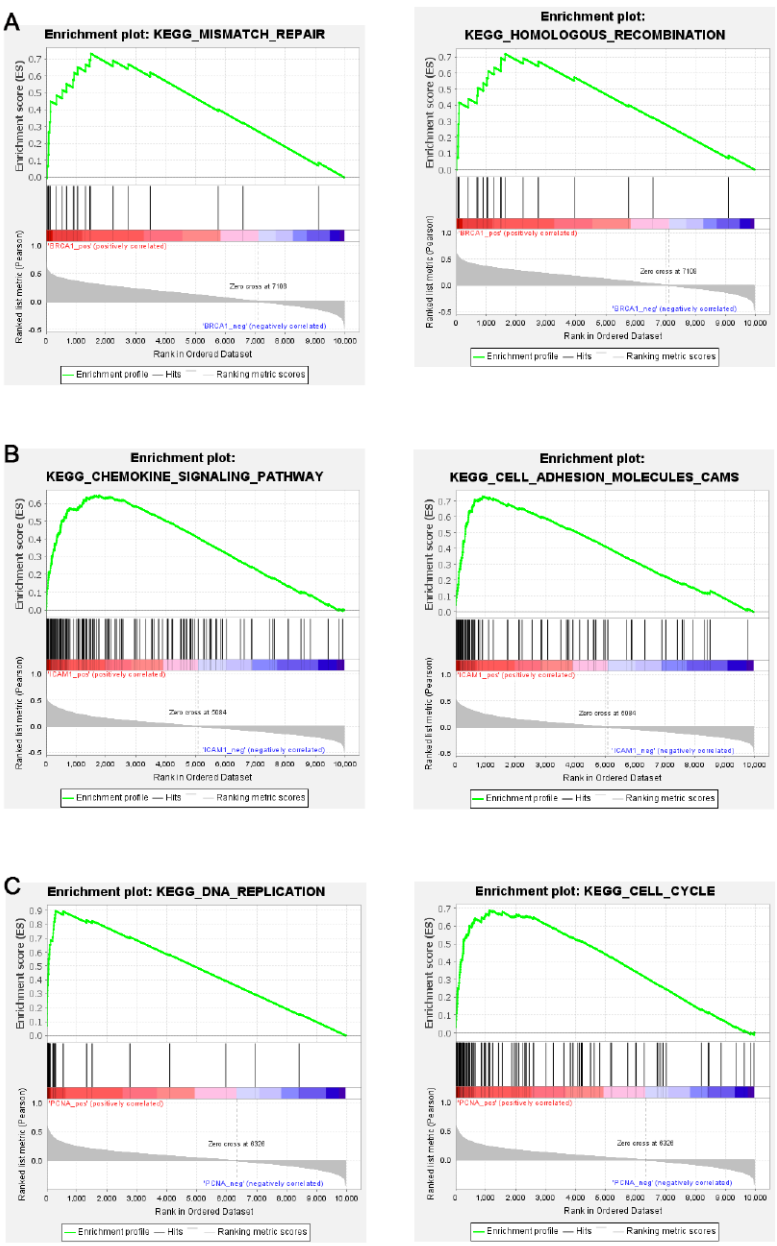


Fig. 7. *Gene set enrichment analysis (GSEA) showed the pathways significantly enriched by prognostic ubiquitination-related differentially expressed genes (DEGs). Significant pathways enriched by **A**: BRCA1, **B**: ICAM1, **C**: PCNA.*

role in the occurrence and development of human cancers. Unfortunately, cervical cancer prognosis is poor, and treatment strategies are insufficient. Therefore, exploring key ubiquitination-related genes can help elucidate the molecular mechanism of tumor progression. In the present study, seven ubiquitination-related DEGs were identified, among which high *BRCA1*, *PCNA*, and *ICAM1* expression levels were significantly associated with favorable prognosis. In addition, *BRCA1* was mainly subjected to somatic mutations. Further, *ICAM1* expression was negatively associated with tumor purity and positively correlated with neutrophils and dendritic cell abundance. Moreover, *BRCA1* was significantly enriched in mismatch repair and homologous recombination, *ICAM1* was markedly enriched in the chemokine signaling pathway and CAMs, and *PCNA* was mainly involved in DNA replication and the cell cycle. These data merit further discussion.

The E3 ubiquitin ligase BRCA1 is a crucial regulator in genomic stability maintenance and is subjected to ubiquitin-dependent degradation (28). In addition, *BRCA1* can promote DNA double-strand break repair by homologous recombination and plays a key role in DNA replication (29). Furthermore, *BRCA1* contains multiple functional domains that can interact with various molecules, such as oncogenes (c-myc), tumor suppressors (p53), cell cycle regulators (cyclins), and DNA damage repair proteins (RAD51), thus playing a significant role in multiple biological pathways involved in tumor evolution, cell-cycle progression, and DNA damage repair (30, 31). Reduced *BRCA1* expression caused by mutations or epigenetic inactivation results in an increased risk of breast cancer development (32). A meta-analysis also confirmed that *BRCA1* mutations are associated with an increased risk of colorectal cancer (33). Our study found that *BRCA1* was mainly subjected to somatic mutations in cervical cancer samples and was significantly enriched in pathways such as mismatch repair and homologous recombination. Therefore, we speculate that *BRCA1* mutations may contribute to cervical cancer via dysregulation of mismatch repair and homologous recombination.

Additionally, *PCNA* is an essential component of the replication machinery and plays a key role in DNA replication. PCNA-ubiquitination protects fork integrity and enhances BRCA-deficient cell resistance to poly adenosine diphosphate-ribose polymerase inhibitors (34). Moreover, lncRNA *CCHE1* can promote the cell proliferation of cervical cancer by regulating *PCNA*, suggesting the potential role of *PCNA* in cervical cancer (35). Our results showed that *PCNA* was mainly involved in DNA replication and the cell cycle. Thus, *PCNA* may affect cervical cancer proliferation by DNA replication and the cell cycle.

ICAM1, a transmembrane glycoprotein member of the immunoglobulin superfamily, plays a significant role in promoting adhesion at the inflammation site, regulating immune response, and manipulating tumor metastasis and progression (36). Accumulating evidence has revealed that ICAM-1 is implicated in the development and progression of various cancer types, such as breast cancer (37) and prostate cancer (38). *ICAM-1* gene polymorphisms are associated with susceptibility to various cancers, including cervical cancer (39). Notably, it has been reported that ICAM-1 stability could be controlled by the E3 ligase FBXO4 during ubiquitin-mediated proteasomal degradation, and alterations in ICAM1 stability can affect therapeutic outcomes in metastatic cancer (40). Our results showed that ICAM1 was a key substrate during the ubiquitination process.

Moreover, *ICAM1* was markedly enriched in the chemokine signaling pathway and CAMs, which are associated with inflammation. These data indicate that ICAM1 may be regulated by ubiquitination, and ubiquitination-mediated ICAM1 alteration might be involved in cervical cancer via the regulation of the chemokine signaling pathway and CAMs. Furthermore, *ICAM1* expression positively correlated with neutrophil and dendritic cell abundance. Tumor-associated neutrophils have pro-tumorigenic functions, such as enhancing tumor metastasis and inhibiting antitumor immune surveillance (41). Circulating neutrophils may play a role in the host response to cervical cancer (42). Elevated neutrophil levels have been confirmed as prognostic factors for cervical cancer recurrence (43).

Additionally, dendritic cells play a significant role in immune response initiation and regulation (44). Manickam et al. confirmed the immunological role

of dendritic cells in cervical cancer (45). Therefore, it can be concluded that *ICAM1* may affect cervical cancer development and prognosis by affecting the infiltration of neutrophils and dendritic cells.

However, our study has certain limitations. First, our results are limited to the analysis of several published datasets. Second, experiments did not validate the deregulated ubiquitination-related genes and their corresponding pathways. Finally, there was no in-depth research of the mechanisms involved. Further experimental and mechanistic studies are required to validate our findings.

In conclusion, key ubiquitination-related genes, such as *BRCA1*, *PCNA*, and *ICAM1*, may affect the development and prognosis of cervical cancer.

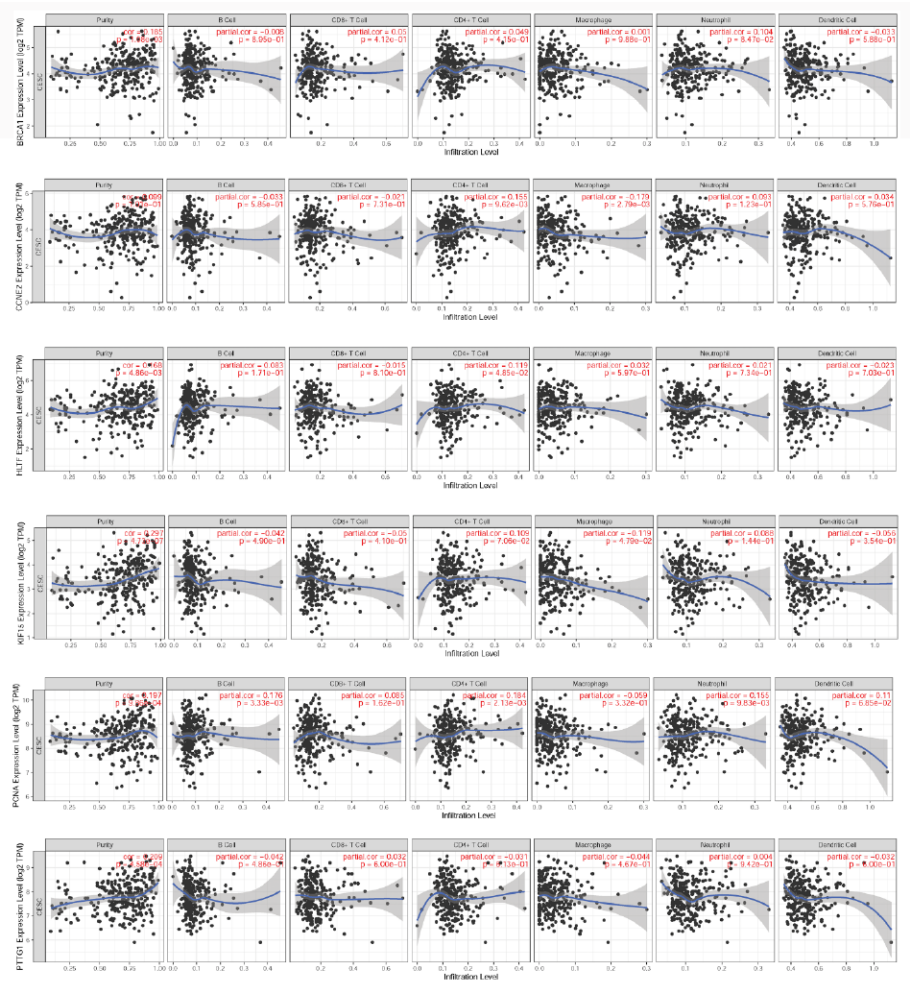
Data availability statement:

The data supporting the findings of this study are available in the article and its supplementary materials.

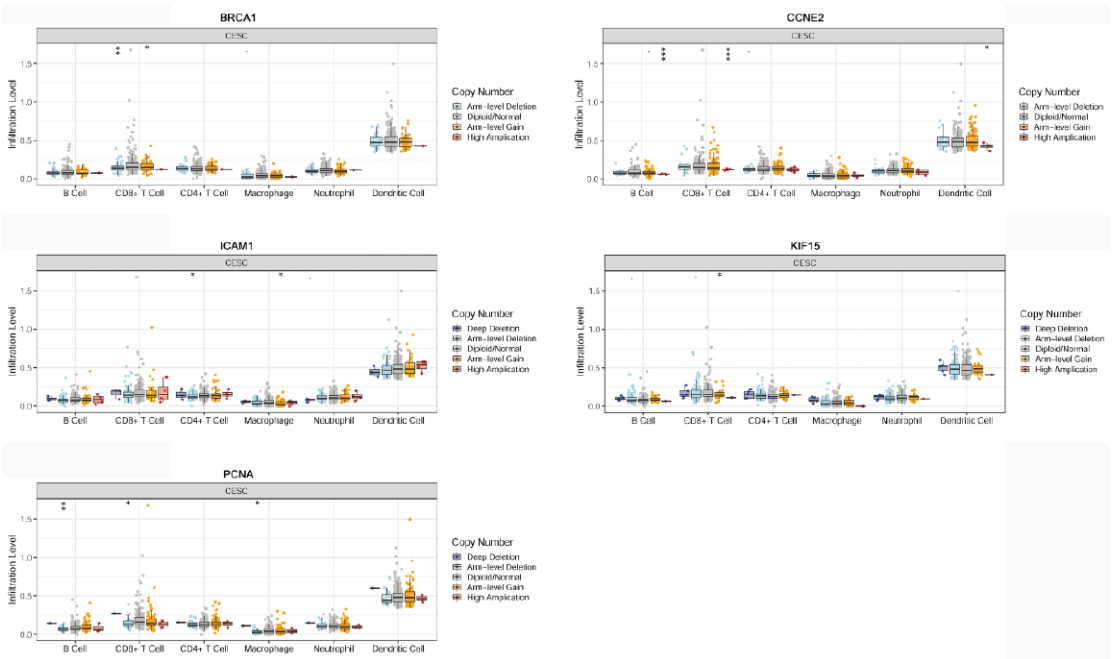
Authors' contributions:

CS conceived and designed the research, participated in data acquisition, and drafted the manuscript. HX conducted the analysis and interpretation of the data. HD performed the statistical analysis and revised the manuscript for important intellectual content. All authors read and approved the final manuscript. The authors declare that they have no competing interests.

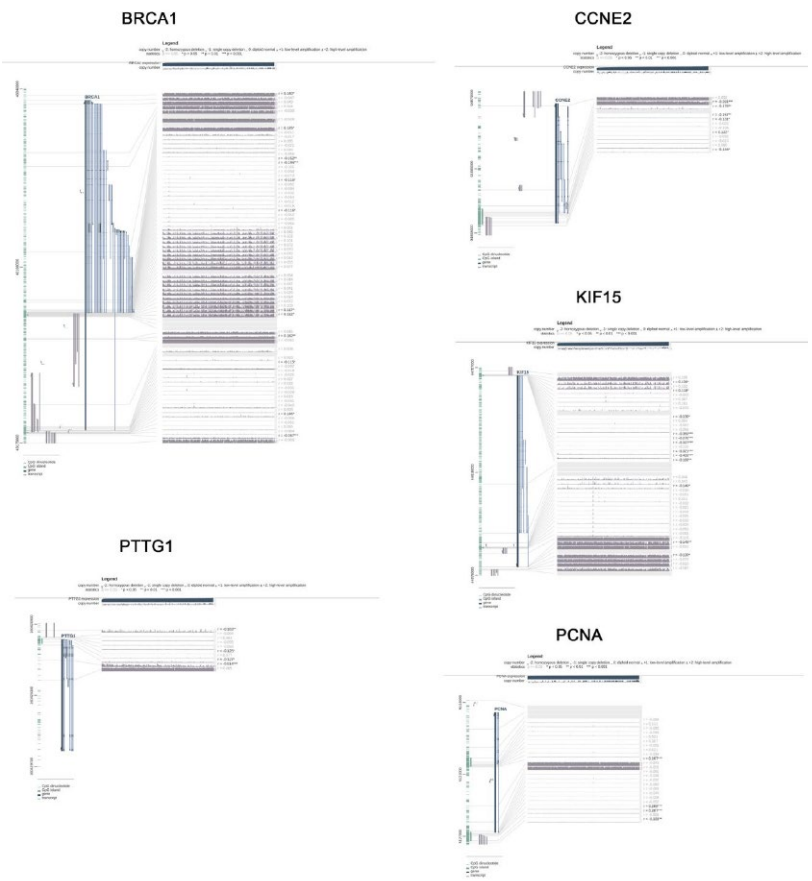
Supplementary figures



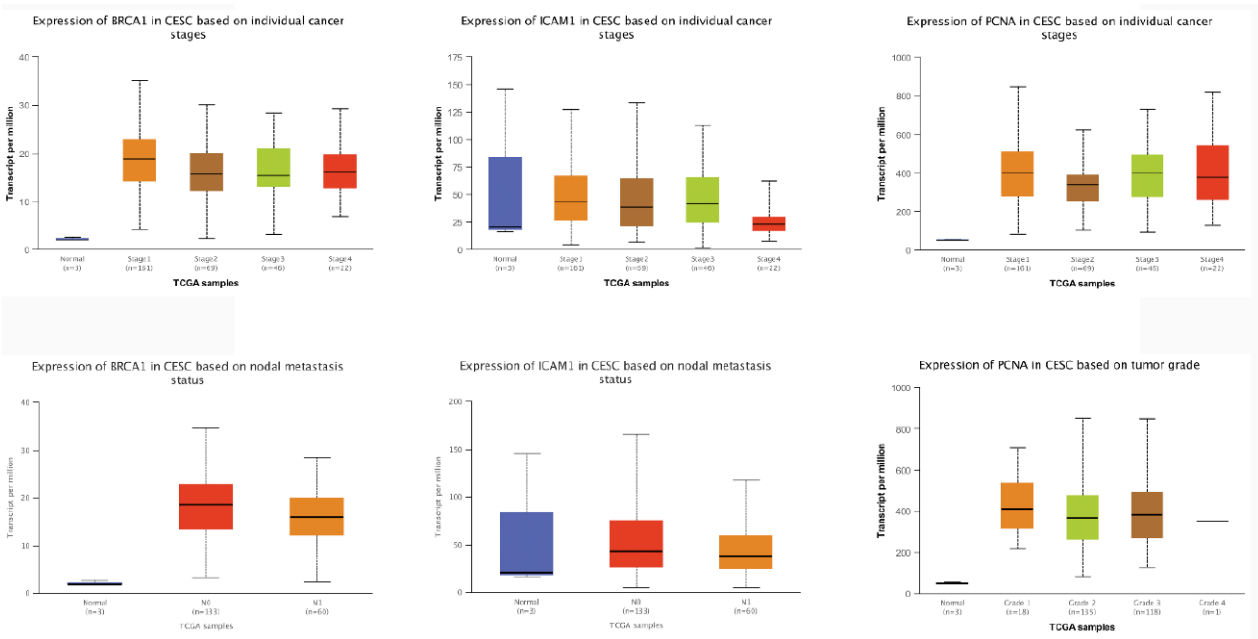
Supplementary Fig. 1. *Correlation between six ubiquitination-related differentially expressed genes (DEGs; BRCA1, CCNE2, HLTF, KIF15, PCNA, and PTTG1) and the abundance of six immune cell types (CD4+ T cells, B cells, CD8+ T cells, macrophages, neutrophils, and dendritic cells).*



Supplementary Fig. 2. *Abundance distribution of six immune cell types in different copy number alteration (CNA) groups of five ubiquitination-related differentially expressed genes (DEGs; BRCA1, CCNE2, ICAM1, KIF15, and PCNA).*



Supplementary Fig. 3. *Methylation analysis results for BRCA1, CCNE2, KIF15, PCNA, and PTTG1 obtained using the MEXPRESS tool.*



Supplementary Fig. 4. *BRCA1, PCNA, and ICAM1 expression in different clinical stages, nodal metastasis status, and tumor grade.*

REFERENCES

1. Small W Jr., Bacon MA, Bajaj A, et al. Cervical cancer: A global health crisis. Cancer 2017; 123:2404-12.
2. Arbyn M, Weiderpass E, Bruni L, de Sanjosé S, Saraiya M, Ferlay J, Bray F. Estimates of incidence and mortality of cervical cancer in 2018: a worldwide analysis. Lancet Glob Health 2020; 8:e191-e203.
3. Naga Ch P, Gurram L, Chopra S, Mahantshetty U. The management of locally advanced cervical cancer. Curr Opin Oncol 2018; 30:323-9.
4. Fleming ND, Frumovitz M, Schmeler KM, et al. Significance of lymph node ratio in defining risk category in node-positive early stage cervical cancer. Gynecol Oncol 2015; 136:48-53.
5. Cohen PA, Jhingran A, Oaknin A, Denny L. Cervical cancer. Lancet 2019; 393:169-82.
6. Menderes G, Black J, Schwab CL, Santin AD. Immunotherapy and targeted therapy for cervical cancer: an update. Expert Rev Anticancer Ther 2016; 16:83-98.
7. Manasanch EE, Orlowski RZ. Proteasome inhibitors in cancer therapy. Nat Rev Clin Oncol 2017; 14:417-33.
8. Yerlikaya A, Kanbur E, Stanley BA, Tümer E. The Ubiquitin-Proteasome Pathway and Epigenetic Modifications in Cancer. Anti-cancer Agents Med Chem 2021; 21:20-32.
9. Ding F, Xiao H, Wang M, Xie X, Hu F. The role of the ubiquitin-proteasome pathway in cancer development and treatment. Front Biosci 2014; 19:886-95.
10. Ge Z, Leighton JS, Wang Y, et al. Integrated Genomic Analysis of the Ubiquitin Pathway across Cancer Types. Cell Rep 2018; 23:213-26.
11. Ren CC, Yang L, Liu L, Chen YN, Cheng GM, Zhang XA, Liu H. Effects of shRNA-mediated silencing of PSMA7 on cell proliferation and vascular endothelial growth factor expression via the ubiquitin-proteasome pathway in cervical cancer. J Cell Physiol 2019; 234:5851-62.
12. Su D, Ma S, Shan L, et al. Ubiquitin-specific protease 7 sustains DNA damage response and promotes cervical carcinogenesis. J Clin Invest 2018; 128:4280-96.
13. Liang J, Nishi H, Bian ML, Higuma C, Sasaki T, Ito H, Isaka K. The ubiquitin-conjugating enzyme E2-EPF is overexpressed in cervical cancer and associates with tumor growth. Oncol Rep 2012; 28:1519-25.
14. Salami J, Crews CM. Waste disposal-An attractive

strategy for cancer therapy. Science 2017; 355:1163-7.
15. Xiao Z, Zhang P, Ma L. The role of deubiquitinases in breast cancer. Cancer Metastasis Rev 2016; 35:589-600.
16. Narayanan S, Cai CY, Assaraf YG, et al. Targeting the ubiquitin-proteasome pathway to overcome anti-cancer drug resistance. Drug Resist Updat 2020; 48:11.
17. Edgar R, Domrachev M, Lash AE. Gene Expression Omnibus: NCBI gene expression and hybridization array data repository. Nucleic Acids Res 2002; 30:207-10.
18. Ritchie ME, Phipson B, Wu D, Hu Y, Law CW, Shi W, Smyth GK. limma powers differential expression analyses for RNA-sequencing and microarray studies. Nucleic Acids Res 2015; 43:20.
19. Du Y, Xu N, Lu M, Li T. hUbiquitome: a database of experimentally verified ubiquitination cascades in humans. Database 2011; 30.
20. Gao J, Aksoy BA, Dogrusoz U, et al. Integrative analysis of complex cancer genomics and clinical profiles using the cBioPortal. Sci Signal 2013; 6:2004088.
21. Li T, Fan J, Wang B, et al. TIMER: A Web Server for Comprehensive Analysis of Tumor-Infiltrating Immune Cells. Cancer Res 2017; 77:e108-e10.
22. Koch A, De Meyer T, Jeschke J, Van Criekinge W. MEXPRESS: visualizing expression, DNA methylation and clinical TCGA data. BMC Genomics 2015; 16:015-1847.
23. Miura K, Ishida K, Fujibuchi W, Ito A, Niikura H, Ogawa H, Sasaki I. Differentiating rectal carcinoma by an immunohistological analysis of carcinomas of pelvic organs based on the NCBI Literature Survey and the Human Protein Atlas database. Surg Today 2012; 42:515-25.
24. Tang Z, Li C, Kang B, Gao G, Zhang Z. GEPIA: a web server for cancer and normal gene expression profiling and interactive analyses. Nucleic Acids Res 2017; 45:W98-W102.
25. Subramanian A, Tamayo P, Mootha VK, et al. Gene set enrichment analysis: a knowledge-based approach for interpreting genome-wide expression profiles. Proc Natl Acad Sci U S A 2005; 102:15545-50.
26. Zou R, Xu H, Li F, Wang S, Zhu L. Increased expression of UBE2T predicting poor survival of epithelial ovarian cancer: based on comprehensive analysis of UBE2s, clinical samples, and the GEO database. DNA Cell Biol 2021; 40(1):36-60.
27. Wang J, Li Z, Gao A, Wen Q, Sun Y. The prognostic landscape of tumor-infiltrating immune cells in cervical cancer. Biomed Pharmacother 2019; 120:109444.
28. Lu Q, Zhang FL, Lu DY, Shao ZM, Li DQ. USP9X stabilizes BRCA1 and confers resistance to DNA-damaging agents in human cancer cells. Cancer Med 2019; 8:6730-40.
29. Tarsounas M, Sung P. The antitumorigenic roles of BRCA1-BARD1 in DNA repair and replication. Nat Rev Mol Cell Biol 2020; 21:284-99.
30. Deng CX, Brodie SG. Roles of BRCA1 and its interacting proteins. Bioessays 2000; 22:728-37.
31. Deng CX. BRCA1: cell cycle checkpoint, genetic instability, DNA damage response and cancer evolution. Nucleic Acids Res 2006; 34:1416-26.
32. Romagnolo AP, Romagnolo DF, Selmin OI. BRCA1 as target for breast cancer prevention and therapy. Anti-cancer Agents Med Chem 2015; 15:4-14.
33. Oh M, McBride A, Yun S, et al. BRCA1 and BRCA2 Gene Mutations and Colorectal Cancer Risk: Systematic Review and Meta-analysis. J Natl Cancer Inst 2018; 110:1178-89.
34. Thakar T, Leung W, Nicolae CM, Clements KE, Shen B, Bielinsky A-K, Moldovan G-L. Ubiquitinated-PCNA protects replication forks from DNA2-mediated degradation by regulating Okazaki fragment maturation and chromatin assembly. Nat Commun 2020; 11:2147.
35. Yang M, Zhai X, Xia B, Wang Y, Lou G. Long noncoding RNA CCHE1 promotes cervical cancer cell proliferation via up-regulating PCNA. Tumour Biol 2015; 36:7615-22.
36. Bui TM, Wiesolek HL, Sumagin R. ICAM-1: A master regulator of cellular responses in inflammation, injury resolution, and tumorigenesis. J Leukoc Biol 2020; 108:787-99.
37. Figenschau SL, Knutsen E, Urbarova I, et al. ICAM1 expression is induced by proinflammatory cytokines and associated with TLS formation in aggressive breast cancer subtypes. Sci Rep 2018; 8:018-29604.
38. Yu HS, Lin TH, Tang CH. Involvement of intercellular adhesion molecule-1 up-regulation in bradykinin promotes cell motility in human prostate cancers. Int J Mol Sci 2013; 14:13329-45.
39. Feng Y, Li X, Ma Q, et al. Intercellular Adhesion

Molecule-1 Gene Polymorphisms and Susceptibility to Cervical Cancer in the Northern Chinese Han Population. Front Genet 2021; 12.

40. Kang J-H, Choi M-Y, Cui Y-H, et al. Regulation of FBXO4-mediated ICAM-1 protein stability in metastatic breast cancer. Oncotarget 2017; 8(47):83100-13.
41. Kim J, Bae JS. Tumor-Associated Macrophages and Neutrophils in Tumor Microenvironment. Mediators Inflamm 2016; 2016:6058147.
42. Fernandes PC Jr, Garcia CB, Micheli DC, Cunha FQ, Murta EF, Tavares-Murta BM. Circulating neutrophils may play a role in the host response in cervical cancer. Int J Gynecol Cancer 2007; 17(5):1068-74.
43. Kim YH, Chung HH, Kim JW, Park NH, Song YS, Kang SB. Prognostic significance of neutropenia during adjuvant concurrent chemoradiotherapy in early cervical cancer. J Gynecol Oncol 2009; 20:146-50.
44. Wculek SK, Cueto FJ, Mujal AM, Melero I, Krummel MF, Sancho D. Dendritic cells in cancer immunology and immunotherapy. Nat Rev Immunol 2020; 20:7-24.
45. Manickam A, Sivanandham M, Tourkova IL. Immunological role of dendritic cells in cervical cancer. Adv Exp Med Biol 2007; 601:155-62.

Wilms' tumor 1-associated protein facilitates the progression of CC by silencing BRCA1

X-P. Xu[1], M. Shi[1] and H. Huang[2*]

[1]Department of Laboratory Medicine, The Third Affiliated Hospital of Soochow University, Changzhou, P.R. China; [2]Department of Blood Transfusion, The Third Affiliated Hospital of Soochow University, Changzhou, P.R. China

Received December 21, 2020 – Accepted May 20, 2021

Cervical cancer (CC) is one of the most common female malignancies, and cisplatin-based chemotherapy is routinely utilized in patients with locally advanced stage. Exploration of the pathogenesis and molecular mechanism of CC is pivotal for the development of effective treatments for this disease. N6-Methyladenosine (m6A) modification, the most prevalent modification of eukaryotic messenger RNA (mRNA), is involved in the progression of various tumours, however, as the key component of m6A methylation, Wilms' tumor 1-associated protein (WTAP) has not been well studied in CC. WTAP is a nuclear protein that is ubiquitously expressed in many tissues, therefore this study investigated the biological role and underlying mechanism of WTAP in CC. Western blot, RT-qPCR, and immunofluorescence techniques were used to detect the expression of WTAP in CC tumour tissues, adjacent tissues, and CC cell lines. We clarified the effects of WTAP on CC cells using cell proliferation assays and colony formation experiments. We then applied RNA sequencing combined with Gene Expression Omnibus data to screen for candidate targets of WTAP. The results demonstrated that in CC cell lines and tissues, WTAP was significantly overexpressed and exerted a pro-oncogenic influence. We determined that WTAP regulated breast Cancer Susceptibility Protein-1 (BRCA1) expression, thereby affecting the proliferation of CC cells.

Cervical cancer (CC) in China accounts for 12% of the worldwide CC incidence (1) and 11% of CC deaths (2). It has been reported that more than 529,800 new cases and approximately 275,100 deaths occur each year 1 (3). Infection with human papillomaviruses (HPVs) is the main cause of the disease development (4), however, the possibility that some other genes may affect the initiation and progression of CC cannot be ruled out. One study reported the expression of CCAT1 in CC and the molecular mechanism of CCAT1 in the progression of CC (5). Several studies have revealed that the miR-195-5p/YAP1 axis plays a key role in the pathogenesis of the malignant progression of CC (6). A recent proteomic analysis of CC cell line secretomes indicated an association of an impaired NRF2-mediated oxidative stress response with cervical carcinogenesis (7). Thus, CC is a multi-step process involving the deregulation of multiple genes; therefore, it is necessary to identify the molecular mechanisms underlying the initiation and development of CC.

Wilms' tumor 1-associated protein (WTAP) is a component of the m6A methyltransferase complex (8) and is a conserved nuclear protein that acts as a partner of Wilms' tumor 1 (9). Removal of WTAP has been indicated to be embryonic lethal, which

Key words: WTAP; CC; BRCA1; proliferation

**Corresponding Author:*
Dr Hui Huang,
Department of Blood Transfusion,
The Third Affiliated Hospital of Soochow University,
No.185 Ju Qian Street, Changzhou,
Jiangsu 213003, P.R. China
Tel.: +86 13656120262 - Fax: +86 0519-6887000
e-mail: huanghui167@yeah.net

0393-974X (2022)
Copyright © by BIOLIFE, s.a.s.
This publication and/or article is for individual use only and may not be further reproduced without written permission from the copyright holder.
Unauthorized reproduction may result in financial and other penalties
DISCLOSURE: ALL AUTHORS REPORT NO CONFLICTS OF INTEREST RELEVANT TO THIS ARTICLE.

indicates the vital biological role of this protein in the development of vertebrates (10). WTAP has been suggested to function as a structural scaffold that regulates the localization and catalytic activity of the complex in cells (11). WTAP does not have MTase activity but is required for efficient RNA methylation *in vivo* and for localization of METTL3 and METTL14 to nuclear speckles in tumour cells (12). Moreover, accumulating evidence suggests that WTAP contributes to aggressive features of numerous cancers. For instance, overexpression of WTAP facilitates renal cell carcinoma by stabilizing the CDK2 transcript and promotes the invasiveness of glioblastoma cells by enhancing the activity of EGFR (13, 14). In addition, WTAP is an oncogene in both AML and diffuse large B-cell lymphoma, in which it associates with heat shock protein 90 (15). WTAP increases the aggressiveness of cholangiocarcinoma by stimulating the expression of the metastasis-related markers MMP7 and MMP28 (15, 16). However, no research has yet reported the biological role of WTAP relevant to m6A modification in CC.

In this study, the effect was evaluated of WTAP for the first time in CC. WTAP expression was significantly increased in tumour tissues compared with paired adjacent normal tissues. Functional analysis showed that WTAP-silenced CC cells exhibited significant suppression of the proliferative capacity. Mechanistically, WTAP-mediated m6A modification led to epigenetic silencing of BRCA1, which was subsequently validated as a tumour suppressor in tumours. Further research confirmed that BRCA1 also functions as a potential tumour suppressor by blocking tumour growth.

MATERIALS AND METHODS

Patients and specimens

Tissue samples were collected from patients diagnosed with CC who underwent surgery at The Third Affiliated Hospital of Soochow University. All patients provided signed consent for the use of their samples in research. This study was reviewed and approved by The Third Affiliated Hospital of Soochow University prior to participant recruitment (Approval No: 2020-1124). The pathological features of CC are summarized in Table I.

Cell culture and transfection

CC cell lines and HUVECs were purchased from the Chinese Academy of Sciences Center for Type Culture Collection, Shanghai, China. These cells were grown in Dulbecco's modified Eagle's medium (DMEM, Gibco, USA) supplemented with 10% foetal bovine serum (HyClone,USA), 10 mg/ml antibiotics (penicillin and streptomycin) and 200 mM L-glutamine at 37°C under 5% carbon dioxide and saturated humidity conditions.

RNA extraction and RT-qPCR

RNA extraction was performed using an RNA extraction kit according to the manufacturer's instructions. After DNase treatment, complementary DNA (cDNA) was synthesized using HiScript II Q RT SuperMix (Vazyme Biotech, R223-01). Messenger RNA expression was analysed by quantitative real-time PCR (RT–PCR) using SYBR Green in a Bio-Rad QX100 Droplet Digital PCR System (USA), and relative RNA amounts were calculated by the $2^{\Delta\Delta Ct}$ method with normalization to GAPDH. All primers were obtained from Tsingke Biological Technology (Beijing, China). The primer sequences were as follows: WTAP: Forward-GAACCCAGCCTATAATAGA, Reverse-TTGGATCAAGGAGAACCC;

BRCA1: Forward-CAATACGCAACTACAACCA, Reverse-AGGGTGCAGGTCAG

TCAGGACG; GAPDH: Forward-ACCCACTCCTCCACCTTTG, Reverse- CACCA CCCTGTTGCTGTAG.

Western blotting

Cells were washed three times with cold PBS and lysed on ice for 30 min; the lysate was then centrifuged at 3500 rpm for 3 h at 4°C, and the supernatant was extracted as total protein. Briefly, frozen tissues were homogenized, the homogenate was centrifuged for 10 min at 4°C, and the supernatant was collected. The protein concentration was measured by a bicinchoninic acid (BCA) kit (Sigma). In preparation for SDS-PAGE, the samples were then mixed with loading buffer, boiled at 100**°C** for 5 min, and loaded on the prepared SDS gel for protein separation. After separation, the proteins were transferred from the gel to a the PVDF membrane, and the membrane was incubated with the primary antibody at 4°C overnight. The next day, the primary antibody was washed off for 1 h, and the membrane was then incubated with the labelled

secondary antibody for 1 h. The fluorescent secondary antibody was then washed off. Detection was performed with electrochemiluminescence (ECL) reagents, and the densities of relevant bands were quantified by densitometry using the accompanying computerized image analysis program (Amercontrol Biosciences, USA).

RNA interference

Small interfering RNAs (siRNAs) targeting WTAP and BRCA1, as well as negative control RNAs (siNCs), were synthesized by GenePharma Company (Shanghai, China). Transient transfection was performed with a jetPRIME Polyplus kit (France) in accordance with the standard protocol. Cells were harvested after 48 h for qRT-PCR analysis or after 72 h for immunoblot analysis and functional study.

Cell proliferation assay

Cells in logarithmic growth phase were seeded into a 96-well plate at a density of 5x104 cells/mL. After successful transfection for 48 h, the cells were incubated for 0, 12, 24, 36, and 48 h prior to the addition of 20 µl of CCK-8 reagent per well. A Synergy H4 Hybrid microplate reader (Bio Tek, Winooski, VT) was used to measure the absorbance at 450 nm.

Colony formation assay

After cells were successfully transfected, they were inoculated into a 6-well plate at 200 cells per well and cultured for 15 days. The cells were fixed with 10% paraformaldehyde for 10 min and stained with 0.1% crystal violet for 15 min. Finally, the number of colonies formed was determined under a microscope.

RNA sequencing

Total RNA was extracted with an ESscience RNA-Quick Purification Kit (YiShan Biotech, Shanghai, China). Then, library construction and RNA sequencing (RNA-seq) were performed at Shanghai Sinomics Corporation (Shanghai, China) with the Illumina NovaSeq 6000 platform (Illumina, USA), followed by computational analysis by the same company. The criteria for differential gene expression were established as a P value < 0.01 and fold change > 1.5 or < 0.5.

Immunofluorescence assay

Fixed tissues were embedded in paraffin. After dewaxing with water and a graded alcohol series, sodium citrate was added for antigen retrieval, and tissues were incubated with primary antibodies against WTAP (Abcam, 1:100) and BRCA1 (Abcam, 1:200) at 4°C overnight. The tissues were then incubated with secondary antibodies at room temperature for 30 min, and DAPI was applied to stain nuclei. Immunofluorescence (IF) images were acquired via confocal microscopy (Olympus, Japan).

Statistical analysis

The data were analysed using GraphPad Prism 8 software. Data from two groups were compared using unpaired Student's *t*-test. One-way ANOVA with the Bonferroni correction was used for comparisons among multiple groups. The *in-vitro* experiments were repeated at least three times, and the data are presented as the means ± standard deviations (SDs) from at least three independent experiments. P values <0.05 were considered significant for all analyses.

RESULTS

Overexpression of WTAP was associated with poor survival in CC

To determine the functional role of WTAP in CC, we first analysed the mRNA expression of WTAP in human CC samples. The results indicated that WTAP expression was higher in tumour tissues than in adjacent normal tissues (Fig. 1A). Similarly, WTAP protein expression was found to be significantly higher in CC tissues (Fig. 1 B, C). The immunofluorescence (IF) staining results further confirmed the results of RT-PCR and Western blotting (Fig. 1 D, E). Moreover, we investigated the relationship between WTAP expression and clinicopathological features in 84 CC patients. Kaplan-Meier analysis revealed that higher WTAP expression levels were associated with poorer overall patient survival (Fig. 1F).

WTAP promoted CC cell proliferation in vitro

The expression of WTAP in CC lines was examined before functional experiments were conducted (Fig. 2A). Overexpression and knockdown of WTAP were carried out in SiHa cells and HeLa/HCC94/MS751 cells, respectively. The CCK-8 and colony formation assay results indicated that

PROOF

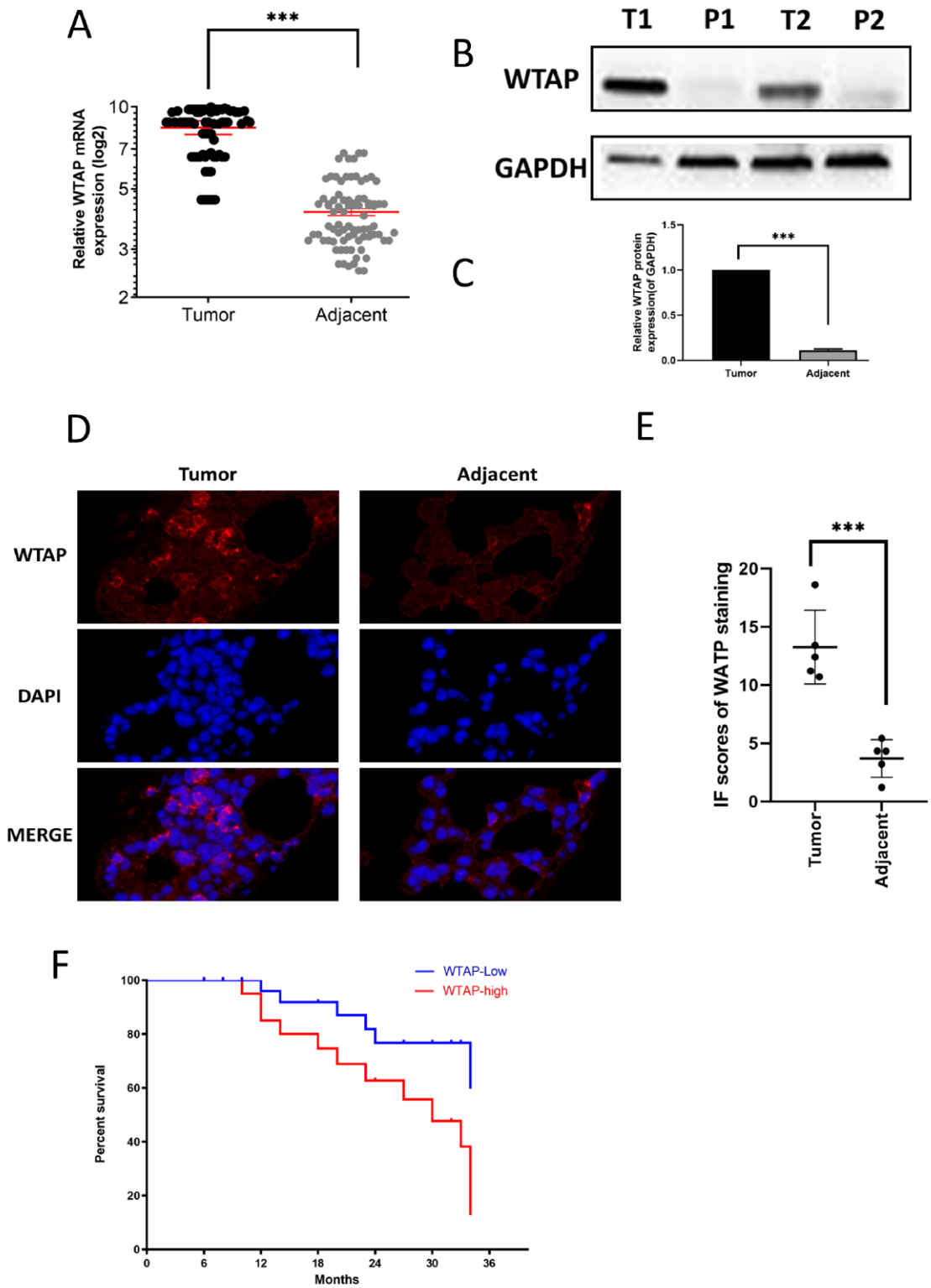


Fig. 1. *Positive WTAP expression correlates with the poor prognosis of CC patients.* ***A****) WTAP mRNA expression in 73 CC samples.* ***B, C****) WTAP protein expression levels in 73 CC samples were determined via western blotting (T: tumour; P: peri-tumour).* ***D, E****) Representative immunofluorescence images and quantitative analysis of WTAP staining (scale bar, 50 μm).* ***F****) Survival analysis of 73 CC patients by the Kaplan-Meier method (***P<0.001).*

WTAP deficiency reduced the proliferation ability of all three knockdown cell lines (Fig. 2 C-E), and the opposite results were found in the cell line with WTAP overexpression (Fig. 2B).

BRCA1 was identified as a potential target of WTAP in CC

To understand the underlying mechanism by which WTAP exerts tumour-promoting effects in CC, we employed transcriptome sequencing to show the transcriptional alterations in WTAP knockdown cells. Hierarchical clustering indicated 1243 upregulated genes and 498 downregulated genes after deletion of WTAP (Fig. 3A). To filter the downstream targets, we integrated the GEO data to elucidate the transcripts regulated by WTAP in order to establish the overlap of the gene sets. A total of 11 overlapping genes were revealed by the Venn diagram (Fig. 3B). RT-qPCR was then carried out to evaluate the impact of WTAP on the expression of each candidate gene. Among the candidate genes, BRCA1 and PRPT1 were consistently significantly upregulated after WTAP silencing, and both were moderately downregulated when WTAP was overexpressed (Fig. 3 C-F). However, notably, Western blot analyses revealed that inactivation of WTAP led to the elevation of BRCA1 expression at the protein level (Fig. 3G).

BRCA1 served as a tumour suppressor in CC

The expression of BRCA1 in tumour tissues was identified to be lower than that in paracancerous tissues in patients with CC (Fig. 4 A-C). This result was further validated by immunofluorescence staining (Fig. 4 D, E). A high level of BRCA1 implied a better prognosis, according to analysis of TCGA data (Fig. 4F). Functional validation by *in-vitro* experiments, including CCK-8 assays, demonstrated that knockdown of BRCA1 enhanced the proliferation ability of HeLa and HCC94 cells (Fig. 4 G, H); however, overexpressing BRCA1 suppressed the proliferation of SiHa and MS751cells (Fig. 4 I, J). Hence, inactivation of BRCA1 may lead to the progression of CC via the WTAP-BRCA1 axis.

DISCUSSION

CC is a common female malignancy (17), and screening is the most effective method for the early detection and treatment of precancerous cervical lesions and for reducing the mortality (18). Screening programmes have greatly reduced the relative deaths in developed countries in recent decades by detecting cancer early when it can be treated; however, preventing cervical carcinogenesis is preferred (19). Therefore, exploring the molecular mechanisms of tumorigenesis is conducive to developing new therapeutics for cervical carcinoma.

As the most prevalent internal modification of RNA, m6A modification regulates many biological processes of RNA, including its decay, splicing, translation and transport (20). Studies indicate the possibility that m6A methylation might modulate the substrate specificity of m6A demethylases by finely tuning the conformation of the modified RNA (21). For example, METTL3 regulates m6A modification of LINC00958, thus affecting its stability (22, 23). In recent years, remarkable advancements have been made in recognizing the role of m6A modification in regulating all stages of the RNA life cycle in tumour cells (24, 25). Accumulating evidence indicates that dysregulation of m6A profoundly contributes to the pathogenesis of various diseases, including HCC (26). WTAP is an important m6A methyltransferase in tumours, and previous studies have suggested that WTAP may be a novel oncogene (27). In addition, a large number of studies have suggested that WTAP, as a novel oncogenic protein, plays a vital role in AML and is also a crucial factor in the poor prognosis of malignant glioma (28). It has been established that WTAP facilitates the progression of hepatocellular carcinoma via m6A-HuR-dependent epigenetic silencing of ETS1 (15). However, the role of WTAP has not been reported in CC.

The present study found that the expression of WTAP was elevated in CC tissues compared with normal cervical tissues. In addition, the expression of WTAP was significantly correlated with the survival prognosis of patients. CC patients with high expression of WTAP had a poor recurrence-free survival rate. The effect of gain or loss of WTAP expression through ectopic overexpression or RNA interference-mediated knockdown in CC cell lines was also investigated and found that WTAP enhances

PROOF

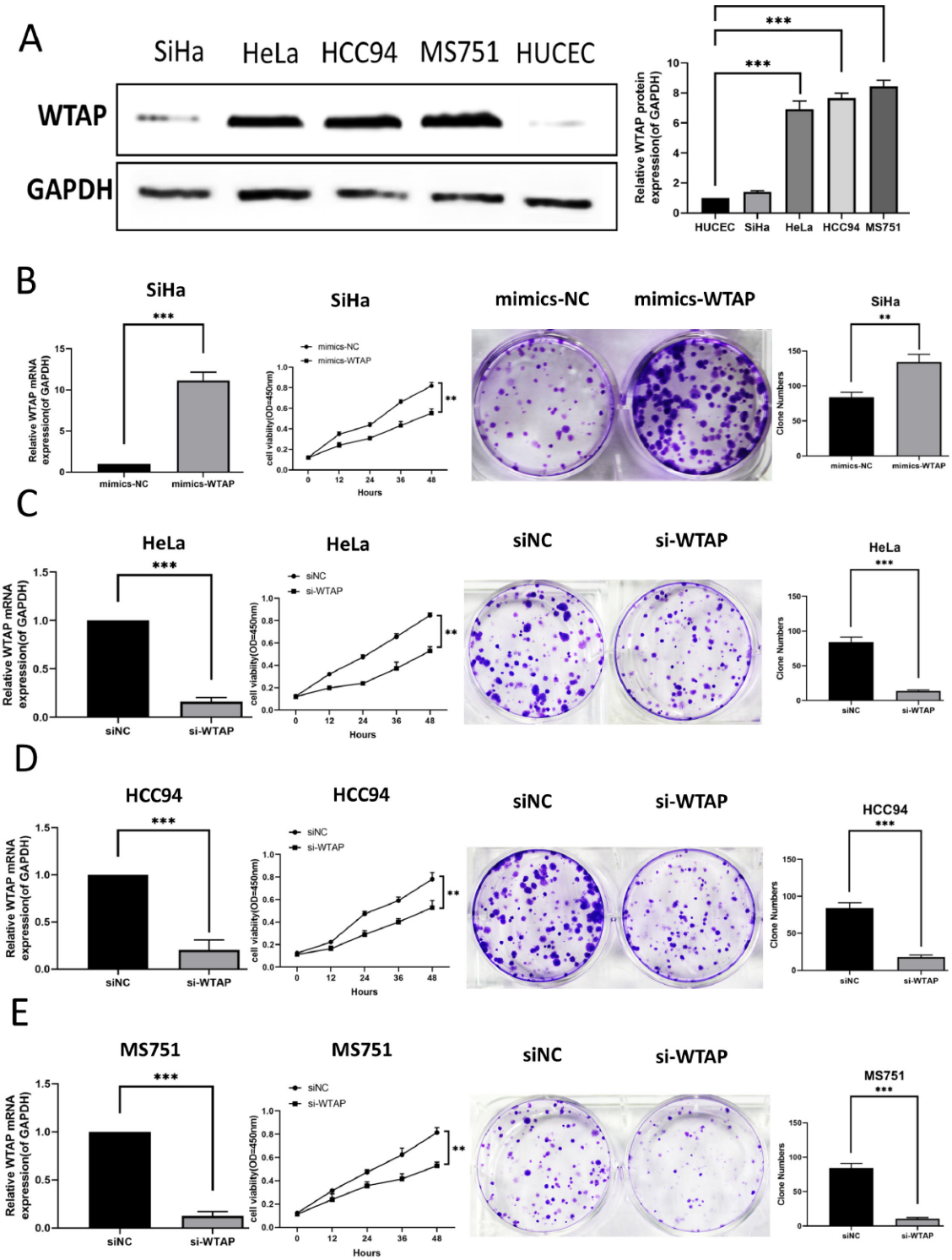


Fig. 2. *WTAP promotes the growth of CC cells in vitro.* ***A****) The expression of WTAP protein was analysed by western blotting in CC cells.* ***B****) SiHa cells were transfected with mimic-NC or mimic-WTAP. The overexpression efficiency was assessed, and the proliferation ability was evaluated by CCK-8 and colony formation assays, with bar charts showing colony counts.* ***C-E****) Negative control siRNA or siWTAP was transfected into HeLa (C), HCC94 (D) and MS751 (E) cells. The knockdown efficiency was assessed, and the proliferation ability was evaluated by CCK-8 and colony formation assays, with bar charts showing colony counts (**P<0.01, ***P<0.001).*

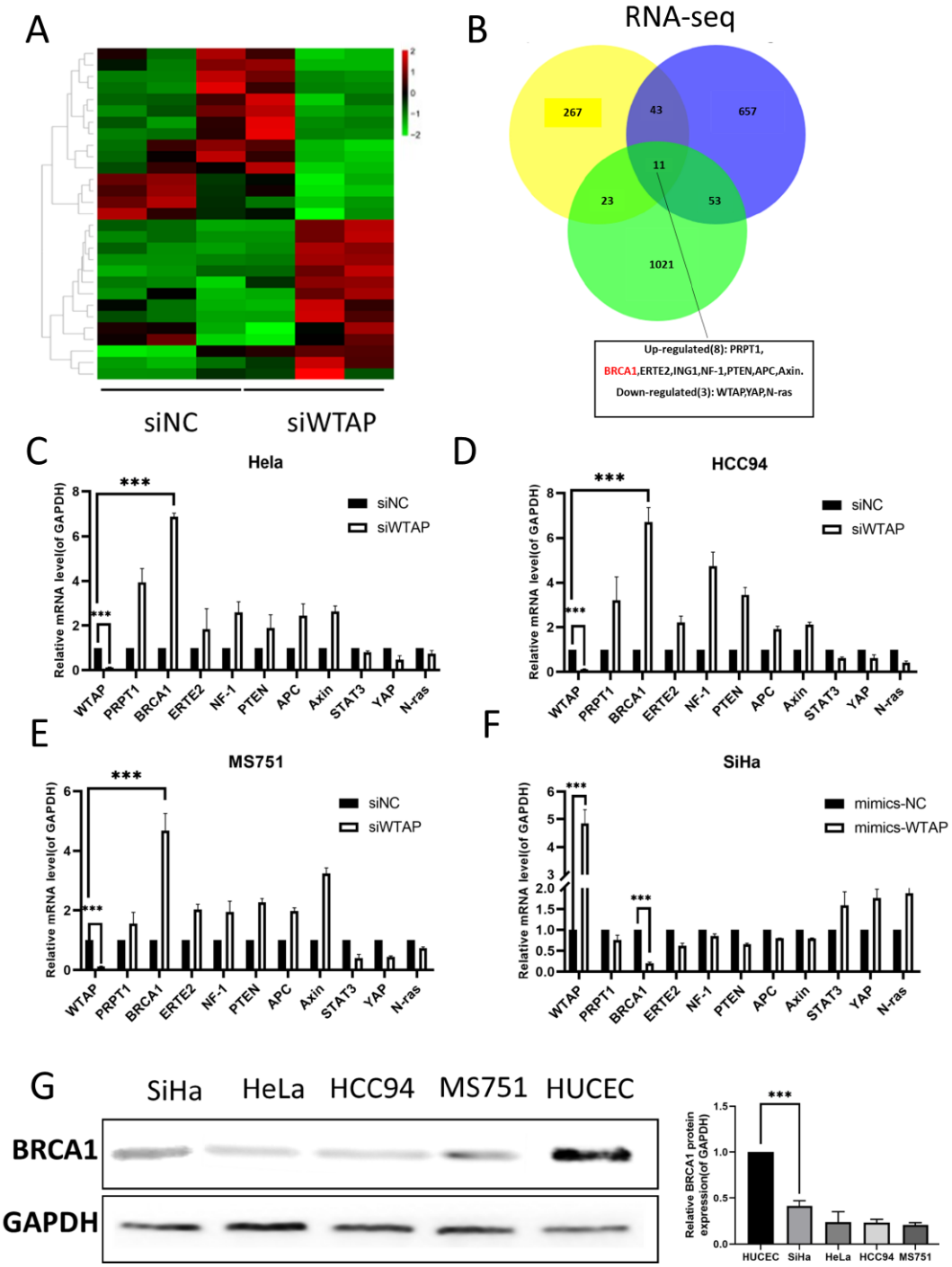


Fig. 3. *Identification of BRCA1 as a direct target of WTAP through high-throughput sequencing. **A**) Transcriptome profiles of HeLa cells transfected with WTAP siRNA or negative control siRNA (both in triplicate) are shown. Red, black and green bands in the heat map indicate high, moderate and low expression, respectively. **B**) A Venn diagram was generated with the gene sets enriched for transcripts with substantially altered levels after WTAP silencing (RNA-seq data), along with those enriched with m6A-modified transcripts and those enriched with WTAP-bound transcripts. A total of 11 genes were selected according to the overlap of these gene sets. **C-F**) RT-qPCR was performed in HeLa (C), HCC94 (D) and MS751 (E) cells with WTAP silencing and in HeLa (F) cells with WTAP overexpression to validate the overlapping genes. The variation in BRCA1 was consistent with that of the 11 genes in the above four cell lines. **G**) The protein expression of BRCA1 in CC cells was analysed by western blotting (***P<0.001).*

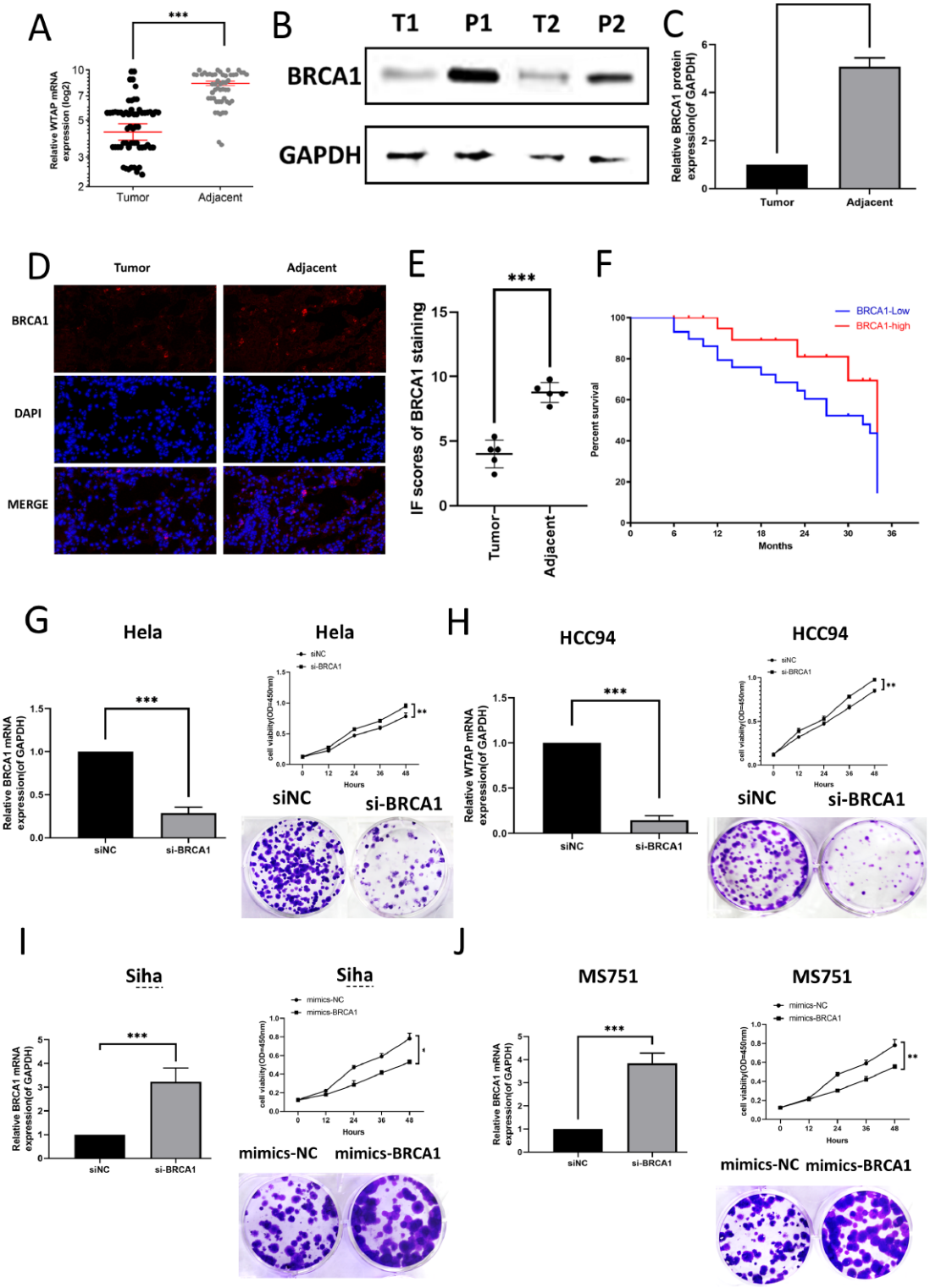


Fig. 4. *BRCA1 plays a tumour-suppressive role in CC.* ***A)*** *BRCA1 mRNA expression in 73 CC samples.* ***B, C)*** *BRCA1 protein expression levels in 73 CC samples were determined via western blotting (T: tumour; P:peri-tumour).* ***D, E)*** *Representative immunofluorescence images and quantitative analysis of BRCA1 staining (scale bar, 50 μm).* ***F)*** *Survival analysis of 73 CC patients by the Kaplan-Meier method.* ***G, H)*** *Negative control siRNA or siBRCA1 was transfected into HeLa (G) and HCC94 (H) cells.* ***I, J)*** *Negative control or mimic-BRCA1 was transfected into SiHa (I) and MS751 (J) cells (**P<0.01, ***P<0.001).*

the proliferation of CC cells. This study showed for the first time that WTAP enhances CC development.

To further address the role of WTAP, we combined the RNA-seq data to reveal that BRCA1 is the downstream target of WTAP. Thus, WTAP may function by impairing BRCA1 and be involved in the development of CC. It was further confirmed in the subsequent verification experiments that BRCA1 expression was significantly increased when WTAP expression was silenced.

BRCA1 is a tumour suppressor gene that encodes a protein involved in DNA repair (29). In addition, a reduced BRCA1 level is associated with sporadic cancers; loss of BRCA1 function has been implicated in the development of breast and ovarian cancer (30). However, few studies have attempted to identify the biological role of BRCA1 in CC. In our study, lower expression of BRCA1 was detected in tumour tissues than in normal tissues, and BRCA1 was markedly upregulated in noncancerous lesions compared with CC lesions, which emphasized the unique role of BRCA1 in CC tumorigenesis. Consistent with this finding, lower expression of BRCA1 was found in CC tissues from patients with worse overall survival outcomes.

In summary, the study confirmed that WTAP, a critical m6A methyltransferase, plays an oncogenic role in CC. As the first attempt to elucidate the role of WTAP in CC, this work provides insights into the tumour-suppressive function of m6A and the potential underlying molecular mechanisms. The present data open a novel avenue to investigate the molecular mechanism of CC progression and to develop potential therapeutic strategies for CC.

REFERENCES

1. Xie H, Li J, Ying Y, Yan H, et al. METTL3/YTHDF2 m 6 A axis promotes tumorigenesis by degrading SETD7 and KLF4 mRNAs in bladder cancer. Cell Mol Med 2020; 24 (7):4092-104.
2. Liu Y, Fan P, Yang Y, et al. Human papillomavirus and human telomerase RNA component gene in CC progression. Sci Rep 2019; 9(1):15926-30.
3. Jin X, Chen X, Hu Y, et al. Lncrna-tcons_00026907 is involved in the progression and prognosis of CC through inhibiting mir-143-5p. Cancer Med 2017; 6(6):1409-23.
4. Taguchi A, Hara K, Tomio J, et al. Multistate Markov model to predict the prognosis of high-risk human papillomavirus-related cervical lesions. Cancers (Basel) 2020; 12(2):1423-7.
5. Shen H, Wang L, Xiong J, et al. Long non-coding RNA ccat1 promotes CC cell proliferation and invasion by regulating the mir-181a-5p/mmp14 axis. Cell Cycle 2019; 18(10):1110-21.
6. Liu X, Zhou Y, Ning YE, Gu H, Tong Y, Wang N. Mir-195-5p inhibits malignant progression of CC by targeting yap1. Onco Targets Ther 2020; 13:931-44.
7. Wang M, Xue Y, Shen L, et al. Inhibition of sgk1 confers vulnerability to redox dysregulation in CC. Redox Biol 2019; 24(12):101225.
8. Kuai Y, Gong X, Ding L, et al. Wilms' tumor 1-associating protein plays an aggressive role in diffuse large b-cell lymphoma and forms a complex with bcl6 via hsp90. Cell Commun Signal 2018; 16(1):50-5.
9. Li H, Su Q, Li B, Lan L, et al. High expression of WTAP leads to poor prognosis of gastric cancer by influencing tumour-associated t lymphocyte infiltration. Cell Mol Med 2020; 24(8):4452-65.
10. Horiuchi K, Umetani M, Minami T, et al. Wilms' tumor 1-associating protein regulates g2/m transition through stabilization of cyclin a2 mRNA. Proc Natl Acad Sci U S A 2006; 103(46):17278-83.
11. Kretschmer J, Rao H, Hackert P, Sloan KE, Hobartner C, Bohnsack MT. The m(6)a reader protein YTHDC2 interacts with the small ribosomal subunit and the 5'-3' exoribonuclease XRN1. RNA 2018; 24(10):1339-50.
12. Sledz P, Jinek M. Structural insights into the molecular mechanism of the m(6)A writer complex. Elife 2016; 5(12):1243-6.
13. Tang J, Wang F, Cheng G, et al. Wilms' tumor 1-associating protein promotes renal cell carcinoma proliferation by regulating cdk2 mrna stability. Exp Clin Cancer Res 2018; 37(1):40-6.
14. Jin DI, Lee SW, Han ME, et al. Expression and roles of Wilms' tumor 1-associating protein in glioblastoma. Cancer Sci 2012; 103(12):2102-9.
15. Chen Y, Peng C, Chen J, et al. WTAP facilitates progression of hepatocellular carcinoma via m6a-

PROOF

HuR-dependent epigenetic silencing of ETS1. Mol Cancer2019; 18(1):127-31.
16. Jo HJ, Shim HE, Han ME, et al. WTAP regulates migration and invasion of cholangiocarcinoma cells. Gastroenterol 2013; 48(11):1271-82.
17. Su M, Gao Y, Ye X, et al. Clinical value of apatinib as a salvage treatment in patients with chemo-refractory advanced CC. Onco Targets 2019; 12(11):9707-13.
18. Mitiku I, Tefera F. Knowledge about CC and associated factors among 15-49 year old women in Dessie town, northeast Ethiopia. Plos One 2016; 11(9):e163136.
19. Ogilvie G, Anderson M, Marra F, et al. A population-based evaluation of a publicly funded, school-based HPV vaccine program in British Columbia, Canada: parental factors associated with HPV vaccine receipt. Plos med 2010; 7(5):e1000270.
20. Xu J, Chen Q, Tian K, et al. M6a methyltransferase METTL3 maintains colon cancer tumorigenicity by suppressing SOCS2 to promote cell proliferation. Oncol Rep 2020; 44(3):973-86.
21. Zou S, Toh JD, Wong KH, Gao YG, Hong W, Woon EC. N(6)-methyladenosine: a conformational marker that regulates the substrate specificity of human demethylases FTO and ALKBH5. Sci Rep 2016; 6(10):25677-81.
22. Zuo X, Chen Z, Gao W, et al. M6a-mediated upregulation of linc00958 increases lipogenesis and acts as a nanotherapeutic target in hepatocellular carcinoma. Hematol Oncol 2020; 13(1):5-10.
23. Chen ZH, Chen TQ, Zeng ZC, et al. Nuclear export of chimeric mRNAs depends on an lncRNA-triggered autoregulatory loop in blood malignancies. Cell Death Disease 2020; 11(7):566-72.
24. Zhen XL, Li ML, Sun HL, Liu SM. Link Between m6A Modification and Cancers. Front Bioeng Biotechnol 2018; 13(1):5-9.
25. Huang Y, Su R, Sheng Y, et al. Small-molecule targeting of oncogenic FTO demethylase in acute myeloid leukemia. Cancer Cell 2019; 35(4):677-91.
26. Wang S, Chai P, Jia R, Jia R. Novel insights on m(6)a RNA methylation in tumorigenesis: a double-edged sword. Mol Cancer 2018; 17(1):101-11.
27. Li BQ, Huang S, Shao QQ, et al. Wt1-associated protein is a novel prognostic factor in pancreatic ductal adenocarcinoma. Oncol Lett 2017; 13(4):2531-8.
28. Guan K, Liu X, Li J, Ding Y, Li J, Cui G, Cui X. Expression status and prognostic value of m6a-associated genes in gastric cancer. Cancer 2020; 11(10):3027-40.
29. Wu J, Li S, Ma R, et al. Tumor profiling of co-regulated receptor tyrosine kinase and chemoresistant genes reveal different targeting options for lung and gastroesophageal cancers. Am Transl Res 2016; 8(12):5729-5740.
30. Kim S, Jin H, Seo HR, Lee HJ, Lee YS. Regulating brca1 protein stability by cathepsin s-mediated ubiquitin degradation. Cell Death Differ 2019; 26(5):812-825.

Ang 1-7 increases nitric oxide synthesis by modulating endothelial nitric oxide synthase -caveolin-1 interaction in rat vascular smooth muscle cells

Y. Xu[1,2], C. Li[2], G. Liu[1], H. Zhang[3], S. Tian[1], H. Hao[2] and Y. Hao[2*]

[1]First Department of Endocrinology, Tangshan Gongren Hospital, Tangshan City, Hebei Province, China; [2]Department of Endocrinology, Second Hospital of Hebei Medical University, Shijiazhuang City, Hebei Province, China; [3]Second Department of Radiotherapy and Chemotherapy, Tangshan Gongren Hospital, Tangshan City, Hebei Province, China

Background: **We aimed to explore the potential protective effect of angiotensin (Ang) 1-7 in rat vascular smooth muscle cells (VSMCs) following exposure to high glucose and the mechanism of its effect on nitric oxide (NO) synthesis.**

Methods: **Rat VSMCs were cultured with/without high glucose, Ang 1-7, and methyl-β-cyclodextrin (MβCD). The expression levels of caveolin-1 (Cav-1), inducible nitric oxide synthase (iNOS), and endothelial nitric oxide synthase (eNOS)/phosphorylated eNOS (Ser1177) were evaluated by western blotting and immunofluorescence staining. NO, superoxide dismutase (SOD), malondialdehyde (MDA) and peroxynitrite ($ONOO^-$) levels in cell culture supernatants were measured by enzyme-linked immunosorbent assay. Intracellular calcium content was determined by flow cytometry.**

Results: **VSMCs cultured with high glucose exhibited striking increases in Cav-1, MDA, iNOS, $ONOO^-$, and intracellular Ca2+, as well as reductions in eNOS phosphorylation, SOD, and NO production. Ang 1-7 treatment reversed the effects of high glucose in these cells.**

Conclusion: **Ang 1-7 increases NO synthesis by regulating Cav-1 expression, Cav-1–eNOS interaction, oxidative stress, and intracellular Ca2+ levels in rat VSMCs cultured in high glucose.**

Patients with diabetes mellitus are at high risk of micro- and macro-vascular complications, including ischemic heart disease, peripheral vascular disease, atherosclerosis, and renal disease (1-3). In addition, experimental evidence suggests that hyperglycemia-induced diastolic dysfunction, decreased local nitric oxide (NO), and oxidative stress are particularly pertinent to the occurrence and development of vascular disease (4-6).

Extensive studies have established the protective effects of the NO signaling pathway in the vascular system (7, 8). Overexpression of endothelial nitric oxide synthase (eNOS) can boost NO production and lead to a reduction of vascular tone (9), this NO reduction enhances platelet aggregation, increases monocyte adhesion to vascular endothelium, and stimulates the proliferation of smooth muscle cells, all of which are essential contributing factors to vascular injury (10, 11). Intracellular calcium homeostasis is another indispensable condition in maintaining the contractile function of muscle cells, and previous studies have demonstrated that high glucose-induced intracellular calcium signaling mediates smooth muscle contraction (12).

It has been demonstrated that angiotensin (Ang)1-7, a member of the renin-angiotensin (RAS) family,

Keywords: Ang 1-7; Caveolin-1; inducible nitric oxide synthase; endothelial nitric oxide synthase; NO

**Corresponding author:*
Dr Yongmei Hao,
Department of Endocrinology,
Second Hospital of Hebei Medical University,
Shijiazhuang City, Hebei Province, China
e-mail: hb2yhym@163.com

0393-974X (2022)
Copyright © by BIOLIFE, s.a.s.
This publication and/or article is for individual use only and may not be further reproduced without written permission from the copyright holder. Unauthorized reproduction may result in financial and other penalties
DISCLOSURE: ALL AUTHORS REPORT NO CONFLICTS OF INTEREST RELEVANT TO THIS ARTICLE.

can reduce the levels of reactive oxygen species (ROS), increase NO synthesis, and relax renal blood vessels (13, 14). Treatment with Ang 1-7 has been shown to protect against fibrosis and improve erectile function (15). Ang 1-7 can also increase NO levels to induce artery relaxation through the NO-cGMP-PKG pathway in a spontaneously hypertensive rat model (16). Ang 1-7 also offers protective effects against ischemia-reperfusion (I/R) induced arrhythmias and contractile dysfunction, which are related to disturbance of intracellular calcium homeostasis (12).

Caveolin-1 (Cav-1) is a membrane protein usually implicated in caveolae's biogenesis and is thus frequently used as a caveolar marker protein. It has been confirmed that Cav-1 can bind to the calmodulin domain of eNOS to inhibit its activity and negatively regulate the production of NO in endothelial cells (17, 18), and caveolin-1 belongs to one of the key regulators of the intracellular calcium homeostasis (19). At the same time, an endogenous receptor for Ang1-7, Mas, has been shown to colocalize with Cav-1 (20). Therefore, we speculated that Ang 1-7 might competitively bind to Cav-1 to abrogate its effect on NO synthesis inhibition. In the present study, we investigated the mechanisms underlying the protective role of Ang 1-7 on NO synthesis in vascular smooth muscle cells (VSMCs).

MATERIALS AND METHODS

Cell culture conditions

Rat thoracic aortic smooth muscle cells (A7R5) were obtained from iCell Bioscience Inc. (Shanghai, China) and cultured under standard conditions (humidified 5% CO_2/95% air at 37°C) in Dulbecco's Modified Eagle's Medium (DMEM) containing 5.5 mM glucose supplemented with 10% fetal bovine serum (FBS), 100 μg/ml penicillin, and 100 μg/ml streptomycin. The cells used for all experiments had been passaged fewer than 10 times.

Drug treatment

Ang 1-7 (Bachem, Switzerland) was used at a concentration of 10 μM (15), and methyl-β-cyclodextrin (MβCD, Sigma, USA), which is a cholesterol dissolving agent that can specifically destroy caveolae structure without affecting the integrity of the cell membrane, was used as an antagonist of Cav-1 function at a concentration of 10 μg/mL (21). For high-glucose stimulation, cells were treated with a high-glucose medium for 48 h.

Western blot analysis

Samples of target cells were obtained after the indicated treatments. The protein concentration in each sample was determined with the BCA method. Western blot analysis was carried out to assess the levels of eNOS, phosphorylated eNOS (p-eNOS), inducible nitric oxide synthase (iNOS) and Cav-1 following standard procedures. The following primary antibodies were used: eNOS (ab7619, Abcam, USA), p-eNOS (Ser1177) (AF3247, Affinity, USA), iNOS (ab15323, Abcam, USA) and Cav-1 (GTX108807, GeneTex, USA). The protein expression levels were normalized to that of β-actin (Proteintech, China), and p-eNOS expression was normalized to its total protein. Band intensity was quantified and analyzed using ImageJ software (NIH, USA).

Measurement of NO, superoxide dismutase (SOD), malondialdehyde (MDA) and peroxynitrite ($ONOO^-$) levels

The cell culture supernatant was collected, and the levels of indexes about oxidative stress were detected using enzyme-linked immunosorbent assay (ELISA) kits: NO (Jiancheng Bioengineering Institute, China), SOD (Jiancheng Bioengineering Institute, China), MDA (Jiancheng Bioengineering Institute, China), $ONOO^-$ (BestBio Biotechnology, Shanghai, China) according to the instructions of the manufacturers.

Immunofluorescence microscopy

VSMCs were grown on glass coverslips and then fixed in 4% paraformaldehyde. In addition, 0.05% Triton X-100 was used for permeabilization, and 3% bovine serum albumin was employed to block nonspecific binding. As mentioned above, the following primary antibodies were used: eNOS, p-eNOS (Ser1177), iNOS, and Cav-1. The coverslips were incubated with secondary antibodies for 1 h at room temperature and then mounted in DAPI for 20 min. Following standard procedures, laser scanning confocal microscopy was used to view and photograph the coverslips.

Cellular calcium ions

The harvested VSMCs were transferred to a 15-mL

centrifuge tube, and the supernatant was discarded after centrifugation. Then cells were washed with phosphate-buffered saline three times, followed by the addition of Fluo-3/AM working solution for incubation at 37 °C for 30 min. The cells were then suspended in 1 ml PBS solution, and the concentration of Ca^{2+} was calculated through fluorescence-activated cell sorting (FACS) analysis (Thermo Fisher, USA).

Statistical analysis

SPSS 18.0 statistical software (IBM, USA) was used for data analysis. Measurement data are expressed as the mean ± standard deviation (± SD), and multiple-group comparisons were performed by one-way analysis of variance (ANOVA). Values of $p<0.05$ were considered statistically significant.

RESULTS

High glucose-induced Cav-1 expression inhibits eNOS activity

To investigate the potential involvement of Cav-1 in a diabetes mellitus rat model, we first measured the expression of Cav-1 in VSMCs following high glucose incubation. Compared with the control group, Cav-1 expression was significantly elevated after high glucose treatment (Fig. 1, $p<0.05$). However, this upregulation was largely diminished after treatment with MβCD (Fig. 1, $p<0.05$), implicating the role of oxidative stress in the high glucose-induced expression of Cav-1. Furthermore, consistent with the studies showing that Cav-1 can negatively regulate

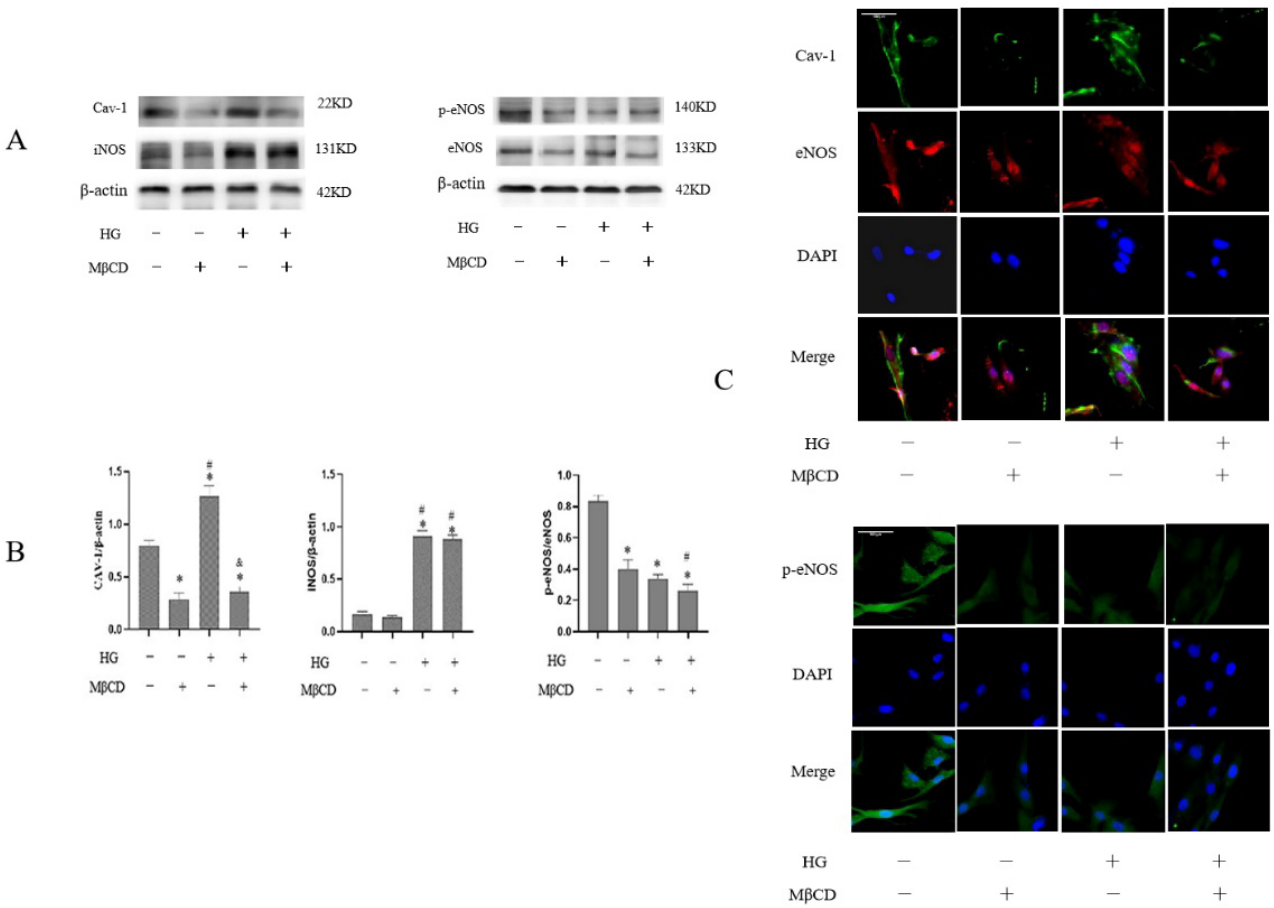


Fig. 1. *High glucose increases Cav-1 expression and downregulates the phosphorylation of eNOS. Cells in the high-glucose (HG) + MβCD group were preincubated with MβCD for 30 min and then cultured with high glucose for another 48h. a, Western blotting was applied to measure the expression levels of Cav-1, iNOS, eNOS and p-eNOS. b, Quantification of the protein band intensities for Cav-1, iNOS, eNOS and p-eNOS. *p<0.05 vs. control group, #p<0.05 vs. MβCD group, and &p<0.05 vs. HG group. c, Colocalization of Cav-1 (green) and eNOS (red), expression and cellular localization of iNOS and p-eNOS protein in VSMCs. Scale bar: 100 μm.*

eNOS activity, we observed a corresponding decrease in eNOS phosphorylation following high glucose treatment, which could also be abrogated by MβCD treatment (Fig. 1b, $p<0.05$), suggesting the effect of Cav-1 on eNOS activity. By comparison, the high glucose-induced iNOS increase (Fig. 1, $p<0.05$) in VSMCs was not significantly reduced by MβCD (Fig. 1, $p>0.05$). We further confirmed the association of Cav-1 and eNOS in cultured VSMCs using microscopy (Fig. 1c). As expected, Cav-1 colocalized with eNOS under basal conditions in its considerabe phosphorylated form, but high glucose treatment dramatically increased colocalization and eNOS was predominantly dephosphorylated. MβCD treatment likewise reversed the effect of high glucose.

eNOS activity inhibition by Cav-1 results in reduced NO production

As eNOS phosphorylation is critical for NO production, we measured NO level in the supernatant of cultured VSMCs. Indeed, we observed a significant reduction in NO production after high glucose treatment (Fig. 2a, $p<0.05$). High glucose treatment also resulted in a decrease in SOD and an increase in MDA (Fig. 2b and 2c, $p<0.05$), two biomarkers of oxidative stress. Together with the effect of MβCD (Fig. 2, $p<0.05$), these findings suggest the essential role of oxidative stress in the NO production decrease following high glucose treatment. However, MβCD had little effect on the synthesis of $ONOO^-$ (Fig. 2d, $p>0.05$), indicating that Cav-1 had little effect on the cellular nitrification stress.

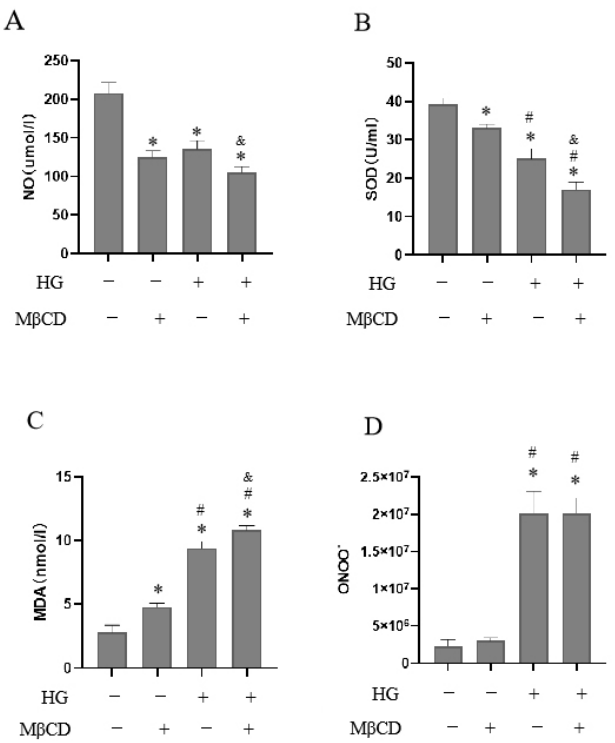


Fig. 2. *Cav-1 takes part in oxidative stress. ELISA detection of oxidative stress indicators NO, SOD, MDA and $ONOO^-$ in the culture supernatant. *p<0.05 vs. control group, #p<0.05 vs. MβCD group, and &p<0.05 vs. HG group.*

Cav-1 overexpression induced by high glucose increases the intracellular calcium ion level

Compared with the control group, high glucose treatment caused a robust increase in calcium ion levels (Fig. 3, $p<0.05$), indicating that Cav-1 may have a pertinent effect on the intracellular calcium ion level. However, the effect of MβCD was minimal (Fig. 3).

Ang 1-7 decreases Cav-1 expression induced by high glucose in VSMCs

To investigate whether the Ang 1-7–induced NO production could be attributed, at least in part, to Cav-1 and could reverse the effect of high glucose, we tested the expression of Cav-1 following high glucose treatment and addition of Ang1-7. Ang 1-7 abolished the increase in Cav-1 expression induced by high glucose, an effect that MβCD further augmented (Fig. 4, $p<0.05$). A similar effect was observed in the expression of iNOS, except for MβCD treatment, which had no additional effect on iNOS expression. In the case of eNOS, whereas Ang 1-7 could rescue the eNOS phosphorylation inhibition by high glucose as expected, MβCD almost completely blocked the protective effect of Ang 1-7 (Fig. 4, $p<0.05$), indicating that Ang 1-7 might rebalance eNOS activity by regulating CAV-1 expression. Our microscopy observations recapitulated the potential protective effect of Ang 1-7 against high glucose. Both the disruption of eNOS–Cav-1 colocalization and eNOS phosphorylation inhibition by high glucose were restored by Ang 1-7 treatment (Fig. 4c and 4d).

Ang 1-7 suppresses oxidative stress induced by high glucose in VSMCs

Following incubation in high glucose, the levels

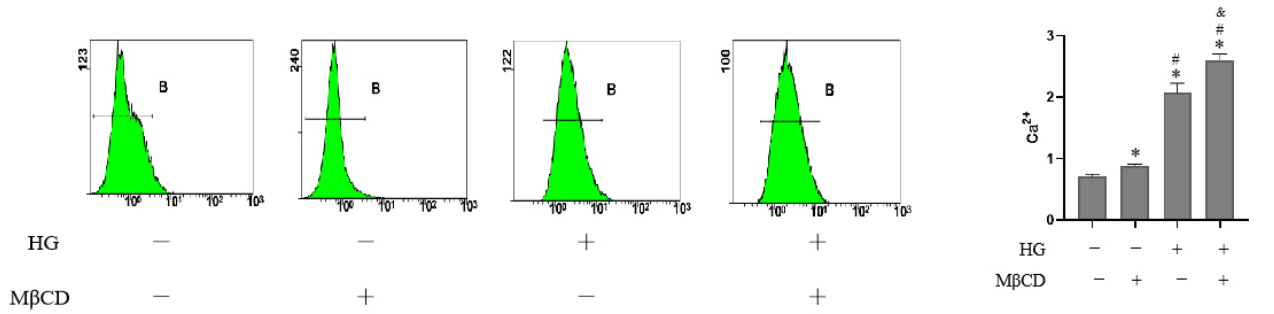


Fig. 3. *Cav-1 overexpression induced by high glucose increases the intracellular calcium ion level. *p<0.05 vs. control group, #p<0.05 vs. MβCD group, and &p<0.05 vs. HG group.*

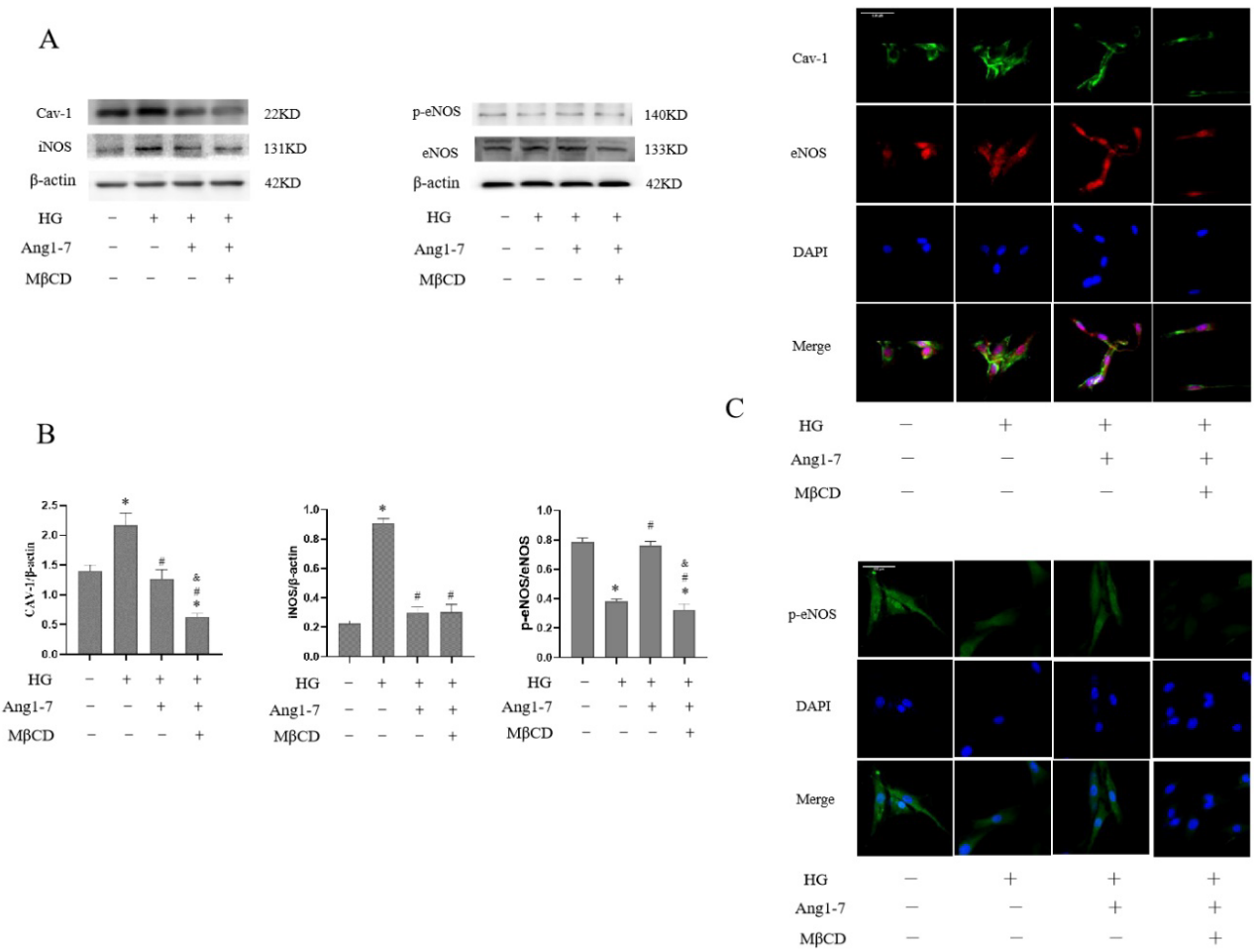


Fig. 4. *Ang 1-7 decreases Cav-1 expression induced by high glucose and rebalances the phosphorylation of eNOS in VSMCs. The cells in the HG + Ang1-7 + MβCD group were preincubated with MβCD for 30 min and then incubated with high glucose with the addition of Ang1-7 for another 48h. a, Western blotting was applied to measure the expression levels of Cav-1, iNOS, eNOS and p-eNOS. b, Quantification of the protein band intensities for Cav-1, iNOS, eNOS and p-eNOS. *p<0.05 vs. control group, #p<0.05 vs. HG group, and &p<0.05 vs. HG with Ang1-7 treatment group. c, Colocalization of Cav-1 (green) and eNOS (red), and expression and cellular localization of iNOS and p-eNOS protein in VSMCs. Scale bar: 100 μm.*

of NO and SOD were significantly lower, while the MDA and $ONOO^-$ levels were significantly higher in VSMCs than in controls (Fig. 5, $p<0.05$). Ang 1-7 treatment significantly increased NO and SOD levels while decreasing $ONOO^-$ and MDA levels (Fig. 5, $p<0.05$), indicating that Ang 1-7 might be able to stimulate NO synthesis and promote the relaxation of smooth muscle cells while at the same time downregulating nitrification stress in VSMCs.

MβCD treatment counteracted most of the effect of Ang 1-7 on NO synthesis and partially inhibited its effects on SOD and MDA, while the $ONOO^-$ level was only minimally affected, indicating that the function of Ang 1-7 in rebalancing the NO disorder induced by high glucose might depend largely on the normal expression of Cav-1.

Ang 1-7 reduces the intracellular calcium ion level induced by high glucose

High glucose treatment led to a significantly increased calcium ion level in VCSMCs compared with controls (Fig. 6, $p<0.05$), and this effect was dramatically diminished by Ang 1-7 treatment (Fig. 6, $p<0.05$). MβCD caused a statistically significant increase in the calcium ion level compared with that seen in the Ang 1-7 group (Fig. 6, $p>0.05$), indicating that the reduction in the calcium ion level by Ang 1-7 might partially rely on the normal expression of caveolae structural protein.

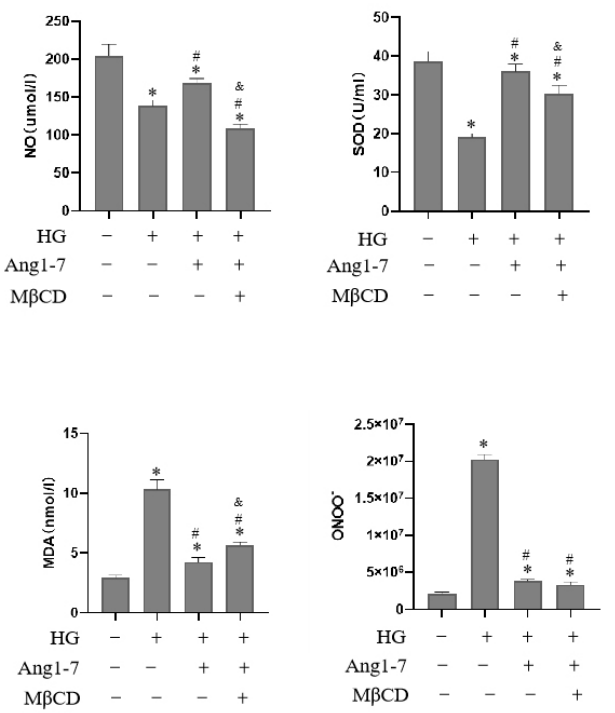


Fig. 5. *Ang1-7 suppresses oxidative stress induced by high glucose in VSMCs. ELISA detection of oxidative stress indicators NO, SOD, MDA and $ONOO^-$. *p<0.05 vs. control group, #p<0.05 vs. HG group, &p<0.05 vs. HG with Ang1-7 treatment group.*

DISCUSSION

In recent years, Ang 1-7 has been frequently studied as an effective vasodilator peptide. Its roles include anti-hypertensive vasodilation, inhibition of smooth muscle cell proliferation, amelioration of oxidative stress and inhibition of myocardial remodelling, most of which rely on the regulation of NO synthesis (16, 22). Studies have found that Ang-1-7 stimulates eNOS activation and increases NO synthesis in human aortic endothelial cells (23). Also, Ang1-7 effectively regulates the phosphorylation of eNOS to enhance the synthesis of NO and prevent oxidative stress in db/db mice (14). In addition, it has been well documented that the Ang 1-7/Max axis is necessary for long-term maintenance of normal calcium handling in cardiac cells (24).

Caveolae, a structure widely seen in mammalian cells, are involved in various cellular functions. Cav-1, as a scaffolding protein in the cell membrane, is entrapped with caveolae in endothelial cells and VSMCs and is involved in multiple biological activities, such as smooth muscle cell contraction, cell metabolism, and proliferation (25, 26). It is widely accepted that the interaction of Cav-1 and eNOS has an inhibitory role on NO generation (27). Penta decapeptide BPC 157 can dissociate Cav-1 and eNOS to increase nitric oxide production and thus promote vessel relaxation (28). H_2S treatment can attenuate the renovascular damage induced by hyperhomocysteinemia through dehomocysteinylating eNOS and reducing Cav-1 to increase eNOS availability (29).

The present study built on the previous findings that eNOS binding to Cav-1 is Ca^{2+}/calmodulin dependent, and its activity is regulated by its interaction with Cav-1. This study aimed to explore the role of Cav-1 in Ang 1-7–induced synthesis of NO in VSMCs. The major findings of our study are as follows: 1) Ang 1-7

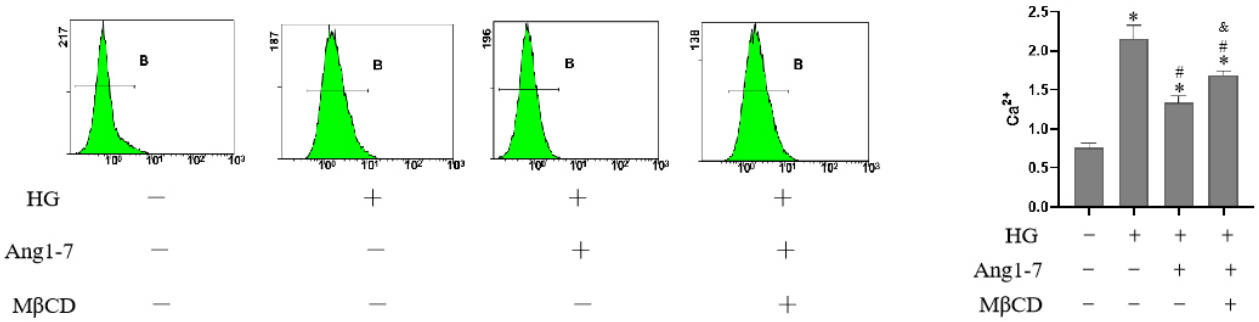


Fig. 6. *Ang1-7 treatment reduces the intracellular calcium ion level induced by high glucose. *p<0.05 vs. control group, #p<0.05 vs. HG group, and &p<0.05 vs. HG with Ang1-7 treatment group.*

regulates NO synthesis in cultured VSMCs under high glucose; 2) the Cav-1/eNOS pathway is involved in Ang 1-7–induced NO synthesis in VSMCs; 3) the reduction of oxidative stress is essential in the protective effect of Ang 1-7; and 4) the intracellular calcium ion level plays a role in Ang 1-7–induced synthesis of NO.

The high glucose-induced increase in Cav-1 expression seen in the present study agrees with previous research (30, 31), this also explains the decreased eNOS availability due to the interplay between eNOS of Cav-1. Cav-1 overexpression is involved in both oxidative stress and intracellular calcium ion increase, leading to a decrease in the diastolic function of VSMCs. Furthermore, Cav-1 has been shown to act as a potential regulator of Ca^{2+} influx via store-operated Ca^{2+} entry (29, 30). Increased Cav-1 expression in smooth muscle cells from patients with idiopathic pulmonary artery hypertension is associated with increased Ca^{2+} entry (31). In our study, we observed that Cav-1 overexpression inhibited NO synthesis and induced oxidative stress and increased the intracellular calcium ion. These findings confirm that Cav-1 plays an important role in the homeostasis of VSMCs.

In addition, our study further explored the role of Cav-1 in the antagonistic effect of Ang 1-7 in response to high glucose. The results showed that Ang 1-7 could partially balance the oxidative stress response by normalizing Cav-1 expression, and MβCD, as a Cav-1 inhibitor, restrained the protective effect of Ang 1-7 on NO synthesis and the intracellular calcium ion level. These findings demonstrate a critical role of Cav-1 in the protective effects of Ang 1-7 against damage caused by high glucose; together, these findings suggest that Cav-1/eNOS is involved in NO synthesis as well as oxidative stress in VSMCs and further clarify a role for Cav-1 in the process of Ang 1-7–mediated vascular protection. Our study provides convincing evidence that new therapies for preventing or treating diabetic angiopathies should incorporate antioxidant treatment and improve Cav-1/eNOS signaling.

Funding:

This study was supported by the Scientific Research Fund of the Hebei Health Commission (20201491).

Authors' contributions:

All authors contributed to the study. YH conceived the study; YX designed the experiments, analyzed the data, and wrote the manuscript; CL, HZ and HH carried out the experiments and contributed to sample collection; GL helped with the experiment design. The authors declare no conflicts of interest.

ACKNOWLEDGMENTS

We gratefully acknowledge the Department of Pathology, Hebei Medical University, for the equipment and technical assistance.

REFERENCES

1. Forster RB, Garcia ES, Sluiman AJ, et al. Retinal venular tortuosity and fractal dimension predict incident retinopathy in adults with type 2 diabetes: the

Edinburgh Type 2 Diabetes Study. Diabetologia 2021; 64(5):1103-12.
2. Reddy SSK. Diagnosis of Diabetes Mellitus in Older Adults. Clin Geriatr Med 2020; 36(3):379-84.
3. Reusch JE, Wang CC. Cardiovascular disease in diabetes: where does glucose fit in? J Clin Endocrinol Metab 2011; 96(8):2367-76.
4. Yao Y, Song Q, Hu C, et al. Endothelial cell metabolic memory causes cardiovascular dysfunction in diabetes. Cardiovasc Res 2022; 118(1):196-211.
5. Chen NX, Moe SM. Arterial calcification in diabetes. Curr Diab Rep 2003; 3(1):28-32.
6. Murugan DD, Zain ZM, Choy KW, et al. Edible Bird's Nest Protects Against Hyperglycemia-Induced Oxidative Stress and Endothelial Dysfunction. Front Pharmacol 2020; 10:1624.
7. Ghalayini IF. Nitric oxide-cyclic GMP pathway with some emphasis on cavernosal contractility. Int J Impot Res 2004; 16(6):459-69.
8. Klinger JR, Kadowitz PJ. The Nitric Oxide Pathway in Pulmonary Vascular Disease. Am J Cardiol 2017; 120(8):S71-S79.
9. Ertuna E, Loot AE, Fleming I, Yetik-Anacak G. The role of eNOS on the compensatory regulation of vascular tonus by H2S in mouse carotid arteries. Nitric Oxide 2017; 69:45-50.
10. Smiljic S, Nestorovic V, Savic S. Modulatory role of nitric oxide in cardiac performance. Med Pregl 2014; 67(9-10):345-52.
11. Monti M, Solito R, Puccetti L, et al. Protective Effects of Novel Metal-Nonoates on the Cellular Components of the Vascular System. J Pharmacol Exp Ther 2014; 351(3):500-9.
12. Lam DS, Zhao J, Chen LJ, et al. Adjunctive effect of acupuncture to refractive correction on anisometropic amblyopia: one-year results of a randomized crossover trial. Ophthalmology 2011; 118(8):1501-11.
13. Benter IF, Yousif MH, Cojocel C, Al-Maghrebi M, Diz DI. Angiotensin-(1-7) prevents diabetes-induced cardiovascular dysfunction. Am J Physiol Heart Circ Physiol 2007; 292(1):H666-72.
14. Papinska AM, Rodgers KE. Long-Term Administration of Angiotensin (1–7) to db/db Mice Reduces Oxidative Stress Damage in the Kidneys and Prevents Renal Dysfunction. Oxid Med Cell Longev 2018; 2018:1-10.
15. Singh N, Vasam G, Pawar R, Jarajapu YP. Angiotensin-(1-7) reverses angiogenic dysfunction in corpus cavernosum by acting on the microvasculature and bone marrow-derived cells in diabetes. J Sex Med 2014; 11(9):2153-63.
16. Zhang F, Tang H, Sun S, et al. Angiotensin-(1-7) induced vascular relaxation in spontaneously hypertensive rats. Nitric Oxide 2019; 88:1-9.
17. Cassuto J, Dou H, Czikora I, et al. Peroxynitrite disrupts endothelial caveolae leading to eNOS uncoupling and diminished flow-mediated dilation in coronary arterioles of diabetic patients. Diabetes 2014; 63(4):1381-93.
18. Lian X, Matthaeus C, Kaßmann M, Daumke O, Gollasch M. Pathophysiological Role of Caveolae in Hypertension. Front Med (Lausanne) 2019; 6:153.
19. Agervi P, Kugelberg U, Kugelberg M, Zetterström C. Two-year follow-up of a randomized trial of spectacles alone or combined with Bangerter filters for treating anisometropic amblyopia. Acta Ophthalmol 2013; 91(1):71-7.
20. Gironacci MM, Adamo HP, Corradi G, Santos RA, Ortiz P, Carretero OA. Angiotensin (1-7) induces MAS receptor internalization. Hypertension 2011; 58(2):176-81.
21. Qin L, Yang Yb, Yang Yx, et al. Ezetimibe suppresses cholesterol accumulation in lipid-loaded vascular smooth muscle cells in vitro via MAPK signaling. Acta Pharmacol Sin 2014; 35(9):1129-36.
22. Dobrocsyova V, Slamkova M, Krskova K, et al. AVE0991, a Nonpeptide Angiotensin 1-7 Receptor Agonist, Improves Glucose Metabolism in the Skeletal Muscle of Obese Zucker Rats: Possible Involvement of Prooxidant/Antioxidant Mechanisms. Oxid Med Cell Longev 2020; 2020:6372935.
23. Oliveira Sampaio W, Souza dos Santos RA, Faria-Silva R. Angiotensin-(1-7) through receptor Mas mediates endothelial nitric oxide synthase activation via Akt-dependent pathways. Hypertension 2007; 49(1):185-92.
24. Gomes ERM, Lara AA, Almeida PWM, et al. Angiotensin-(1-7) Prevents Cardiomyocyte Pathological Remodeling Through a Nitric Oxide/ Guanosine 3′,5′-Cyclic Monophosphate–Dependent Pathway. Hypertension 2010; 55(1):153-60.
25. Oliviera SDS, Chen J, Castellon M, et al. Injury-

Induced Shedding of Extracellular Vesicles Depletes Endothelial Cells of Cav-1 (Caveolin-1) and Enables TGF-β (Transforming Growth Factor-β)-Dependent Pulmonary Arterial Hypertension. Arterioscler Thromb Vasc Biol 2019; 39(6):1191-1202.

26. Samarakoon R, Higgins SP, Higgins CE, Higgins PJ. The TGF-β1/p53/PAI-1 Signaling Axis in Vascular Senescence: Role of Caveolin-1. Biomolecules 2019; 9(8):341.
27. Srivastav RK, Ansari TM, Prasad M, Vishwakarma VK, Bagga P, Ahsan F. Caveolins; An Assailant or An Ally of Various Cellular Disorders. Drug Res 2019; 69(08):419-27.
28. Hsieh M-J, Lee C-H, Chueh H-Y, Chang G-J, Huang H-Y, Lin Y, Pang J-HS. Modulatory effects of BPC 157 on vasomotor tone and the activation of Src-Caveolin-1-endothelial nitric oxide synthase pathway. Sci Rep 2020; 10(1):17078.
29. Pushpakumar S, Kundu S, Sen U. Hydrogen Sulfide Protects Hyperhomocysteinemia-Induced Renal Damage by Modulation of Caveolin and eNOS Interaction. Sci Rep 2019; 9(1):2223.
30. Van Krieken R, Krepinsky JC. Caveolin-1 in the Pathogenesis of Diabetic Nephropathy: Potential Therapeutic Target? Curr Diab Rep 2017; 17(3):19.
31. Elçioğlu KH, Kabasakal L, Çetinel Ş, Conturk G, Sezen SF, Ayanoğlu-Dülger G. Changes in caveolin-1 expression and vasoreactivity in the aorta and corpus cavernosum of fructose and streptozotocin-induced diabetic rats. Eur J Pharmacol 2010; 642(1-3):113-20.

A rare case of ST-elevation myocardial infarction caused by thrombotic occlusion of a coronary artery aneurysm in the left anterior descending artery

L. Wang, F. Wang, G. Su and G-H. Su*

Department of Cardiology, Central Hospital Affiliated to Shandong First Medical University, Jinan, Shandong Province, China

Background: **Coronary artery aneurysm (CAA) is a rare condition in 0.3-4.9% of patients undergoing coronary angiography (CAG). Effort angina is the most common clinical manifestation in patients with CAA, along with dyspnea, arrhythmias, acute myocardial infarction (MI), congestive heart failure, cardiac arrest, or unstable angina. Its treatment options mainly include medical therapy, surgical resection, coronary artery bypass grafting (CABG), and percutaneous coronary intervention (PCI).**

Case report: **This case report summarizes our experience of treating MI caused by a thrombotic CAA. A 54-year-old woman presented with an acute ST-elevation myocardial infarction (STEMI) caused by thrombotic occlusion of a CAA in the left anterior descending (LAD) artery. She was treated with percutaneous transluminal coronary angioplasty (PTCA) and was subsequently referred to our institution due to recurrence of chest pain and persistence of ST-wave changes. The patient's clinical symptoms resolved after 10 days of anticoagulation (enoxaparin) and dual antiplatelet therapy (aspirin, clopidogrel). However, repeat CAG revealed recanalization and a fusiform aneurysm with thrombosis in the LAD. The patient was discharged in good physical condition with an indication for continuous anticoagulation (enoxaparin) and dual antiplatelet therapy (aspirin and clopidogrel).**

Conclusion: **In the setting of acute MI, PTCA of an aneurysmal vessel followed by long-term anticoagulation may be associated with good clinical outcomes and could be considered a reasonable treatment choice. Additionally, intravascular ultrasound (IVUS) assessment remains extremely useful as a diagnostic tool and guide for treatment.**

As a rare disorder, coronary artery aneurysm (CAA) is defined as dilating the coronary artery that exceeds half of the reference vessel diameter (1, 2). It occurs in approximately 0.3–5.3% of patients who have undergone coronary angiography (CAG) and in 1.4% of postmortem examinations (3). Atherosclerosis is the most common cause of CAA, associated with over 50% of all aneurysms diagnosed in adults (4). In addition, CAA may complicate coronary angioplasty with stent implantation, especially in those that use drug-eluting stents (DES) (5, 6). Coronary dissection, oversizing, and stent malaposition are the main mechanisms associated with stent-related CAA (7-9). Recently, with the widespread use of DES, a growing number of studies have reported that stents can result in CAAs months or even years after interventional treatment (10).

The right coronary artery (RCA) is the most common site of CAAs, which is followed by the left circumflex artery (LCX) and the left anterior descending (LAD) artery. Although rare, aneurysms

Keywords: coronary artery aneurysm; myocardial infarction; anticoagulation; dual antiplatelet therapy

*Corresponding author:
Dr Guohai Su
Department of Cardiology,
Central Hospital Affiliated to Shandong First Medical University,
No. 105 Jiefang Road, Lixia District,
Jinan, Shandong Province, 250013, China
e-mail: sghjn65@126.com

0393-974X (2022)
Copyright © by BIOLIFE, s.a.s.
This publication and/or article is for individual use only and may not be further reproduced without written permission from the copyright holder.
Unauthorized reproduction may result in financial and other penalties
DISCLOSURE: ALL AUTHORS REPORT NO CONFLICTS OF INTEREST RELEVANT TO THIS ARTICLE.

may lead to thrombosis and require spontaneous dissection, which can cause acute myocardial infarction (MI) (11). Currently, effort angina is the most common manifestation in CAA patients and occurs along with dyspnea, arrhythmias, acute MI, congestive heart failure, cardiac arrest, or unstable angina (12). Several reports showed that CAA might be a rare cause of acute coronary syndrome (ACS) and MI, and low blood flow in the aneurysm capsule may easily form thrombosis that can lead to distal embolism (13, 14).

The treatment of choice for CAA remains unclear. Treatment options mainly consist of medical therapy, surgical resection, coronary artery bypass grafting (CABG), and percutaneous coronary intervention (PCI) (15-22). Notably, most of these clinical suggestions are based only on small case series or anecdotal evidence (15), making the clinical decision-making process more complicated. In light of this, Kawsara *et al*. (23) highlighted the need for collaborative studies, with clear definitions of disease phenotypes and clinical endpoints, to find the most optimal approach to managing CAA.

In this report, we present a rare case of CAA in the LAD artery with acute ST-elevation myocardial infarction (STEMI) and explore the management of CAA, providing evidence for its clinical treatment.

CASE REPORT

The Ethics Committee approved this case report of Jian Central Hospital, Shandong University (Approval No. 2020-165-01), and informed consent was obtained from the patient accordingly.

A 54-year-old woman with no history of diabetes, hypertension, and rheumatism was admitted to the local hospital because of precordial pain radiating to the left upper limb, chest tightness, and nausea that have been persistent for 3 h. Her electrocardiogram showed acute STEMI (Fig. 1A). The emergency CAG showed an aneurysm complicated by massive acute thrombosis in the proximal LAD artery, with a length of 59.33 mm by intravascular ultrasound (IVUS) (Fig. 1B). Percutaneous transluminal coronary angioplasty (PTCA) was performed, and the infarct-related artery (IRA) was temporarily opened and then occluded again due to a high-burden thrombus (Supplementary File 1 available on request). The patient was then transferred to our centre (Jinan Central Hospital, Shandong University) for further diagnosis and treatment.

Upon arrival in our centre, the patient had an initial heart rate of 84 bpm and an initial blood pressure of 120/79 mmHg. Physical examination demonstrated clear chest sounds and distant heart sounds, and laboratory workup showed elevated troponin T (2910 ng/L, normal range: 0–14 ng/L) and natriuretic peptide type B (BNP) (1295 pg/ml, normal range: 0–100 pg/ml). Further workup showed that the patient's renal function, liver function, complete hemogram, electrolyte level, C-reactive protein level, and erythrocyte sedimentation rate were normal. However, the patient still complained of chest pain with her ECG showing persistence of ST-elevation in the anterior leads from V1 to V5 (Fig. 2A).

Her clinical symptoms resolved after 10 days of anticoagulation (1 mg/kg enoxaparin twice a day) and dual antiplatelet therapy (0.1 g aspirin per day, 90 mg clopidogrel twice a day). Repeat CAG was performed, revealing recanalization and a fusiform aneurysm with thrombosis in the LAD artery (Fig. 2B; Supplementary file 2 available on request). The LCA and RCA arteries were also normal (Supplementary file 3 available on request). Moreover, IVUS showed a large-sized fusiform aneurysm with thrombosis in the LAD artery (Fig. 2C-D); we also obtained IVUS images showing the LAD distal artery with thrombosis (Fig. 2E-F). The patient was started on 15 mg rivaroxaban per day and 75 mg clopidogrel per day. Before discharge, the resolution of chest pain, chest tightness, and other symptoms were observed.

The patient was generally in good condition during the one-month follow-up with an oral intake of 15 mg rivaroxaban combined with 75 mg clopidogrel daily except for her slightly impaired left ventricular function. After one year, her ECG showed her previous MI in the anterior leads (Fig. 3A), and her CAG reexamination showed that her coronary arteries were unobstructed (Fig. 3B; Supplementary file 4 available on request).

Moreover, IVUS showed that only turbulent flow was found in the aneurysm with no thrombus detected anywhere (Fig. 3C-D). Finally, the patient was maintained on 15 mg rivaroxaban combined with 75 mg clopidogrel daily for life.

DISCUSSION

Morgagni first described CAA in 1761, and most coronary aneurysms are currently found by CAG or computed tomographic angiography (CTA) in clinical practice (11). Despite the low overall incidence of CAA, ranging from 0.3-5.3%, and a pooled analysis suggesting an average incidence of 1.65%, the true burden of CAA and ectasia may be underestimated (24); some patients remain asymptomatic throughout their lives. The aetiology of CAA has yet to be fully understood, and multiple causes of CAA have been proposed in recent years. Among them, atherosclerosis is the most common in adults, accounting for 50% of all cases; Kawasaki disease and Takayasu arteritis, among others, are the other major etiologies for pediatric CAA (25). Rare causes include drugs (e.g., Cocaine, protease inhibitor, amphetamine, etc.) and infections (e.g., HIV, bacteria) (25). More importantly, since the advent of the interventional era, increasing attention has been paid to the occurrence of CAA after the treatment of atherosclerotic coronary artery disease (ACAD) by the percutaneous coronary intervention (PCI), including balloon angioplasty, stent implantation (26. 27), and especially the use of DES (10, 28).

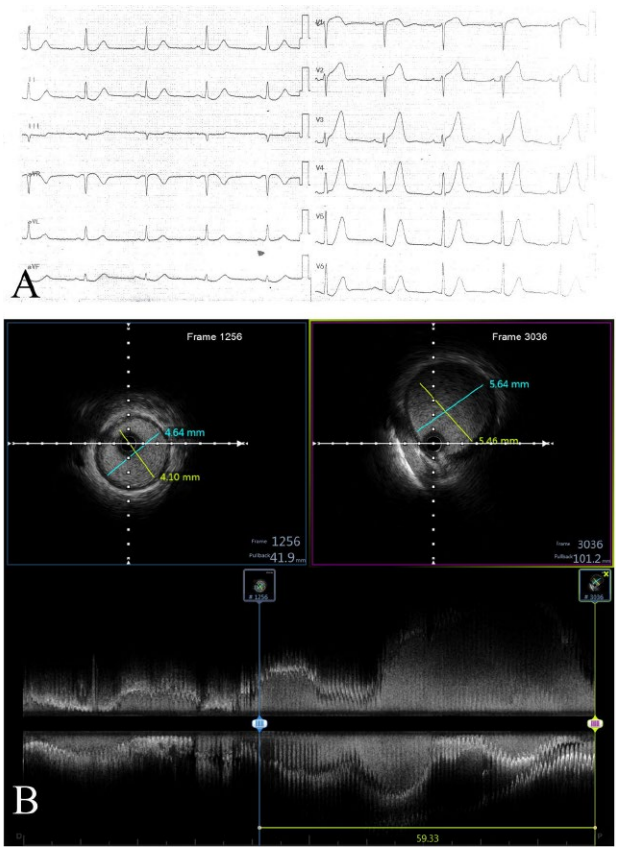


Fig. 1. *Electrocardiogram and intravascular ultrasound of the patient during first admission. (A) Electrocardiogram showing ST-segment elevation; (B) Intravascular ultrasound showing an aneurysm with acute thrombosis and a length of 59.33 mm.*

During this patient's admission, the immune index, blood sedimentation rate, C-reactive protein (CRP), and other indicators were evaluated, which were negative; thus, rheumatic diseases were excluded, with the patient also denying any history of Kawasaki disease or immune-related diseases; considering the patient's age, the possibility of coronary atherosclerosis was initially suspected. Therefore, IVUS was conducted, which showed a thrombus in the aneurysm and a distal embolus; previous literature has never reported this. In the current case, the cause of the infarction did not appear to be related to atherosclerotic stenotic lesions. Instead, the thrombus in the aneurysm was thought to be associated with unsmooth intima and blood flow turbulence. A previous case report has shown that the risk of thrombi in the aneurysm will significantly increase if the aneurysm exceeds 5 mm (29). In this case, the diameter of the LAD aneurysm was 8.85 mm, so we infer that the patient's MI was related to the aneurysm. Another cause of the MI may be the sluggish and turbulent blood flow in the ectatic vessel wherein the thrombus fell off and caused distal vascular thrombosis after PTCA.

Due to the low incidence of coronary aneurysms and the lack of large-scale randomized controlled trials, no guideline references and individualized treatment strategies currently exist. There remains no consensus on the optimal management of CAAs. As discussed, surgery, percutaneous intervention, and drug therapy are the main treatment options for CAAs

(24). CAA management varies according to aetiology, size, and symptoms. Generally, small asymptomatic aneurysms without coronary artery disease are managed conservatively (30). Pericardial tamponade caused by aneurysm rupture (31) and aneurysms caused by infection (32) is usually managed by surgical exclusion via ligation, resection, or coronary bypass. Fusiform or saccular aneurysms that involve a major side branch can be managed with a balloon or stent-assisted coil embolization (15).

Nevertheless, none of the above conditions and their corresponding treatments applies to the presented case due to condition limitation as well as patient acceptance. For patients with acute MI caused by thrombosis in coronary aneurysms, as seen in this case, coronary interventional therapy is needed to restore TIMI-III blood flow; this includes thrombus aspiration and PTCA. The risk of rupture or embolism should be assessed in asymptomatic patients by detecting the CAA's morphology, extent, and size (15). There are also no specific guideline references or high-quality evidence for or against the use of antithrombotic or antiplatelet agents in patients with CAAs. Some studies have suggested using antithrombotic therapy for aneurysms (33, 34), while others hold the opposite view (35, 36). The possible association between inflammatory cytokines and matrix metalloproteinases (MMPs) with CAAs may also suggest a role for statins and the inhibition of the renin-angiotensin system (37); however, no studies have supported these hypotheses so far. If thrombosis and/or embolism occur, long-term antiplatelet and anticoagulant therapies should be considered (35). Conservative management using dual antiplatelet therapy (aspirin, clopidogrel) was undertaken in our case. The patient was initially treated with dual antiplatelets and anticoagulation with enoxaparin as part of the ACS regiment. After it was concluded that the MI was most likely caused by thrombus embolization, the patient was discharged and maintained on rivaroxaban and clopidogrel only. During the one-month follow-up period, the patient was in good condition with the off-label use of rivaroxaban and clopidogrel, provided that it is

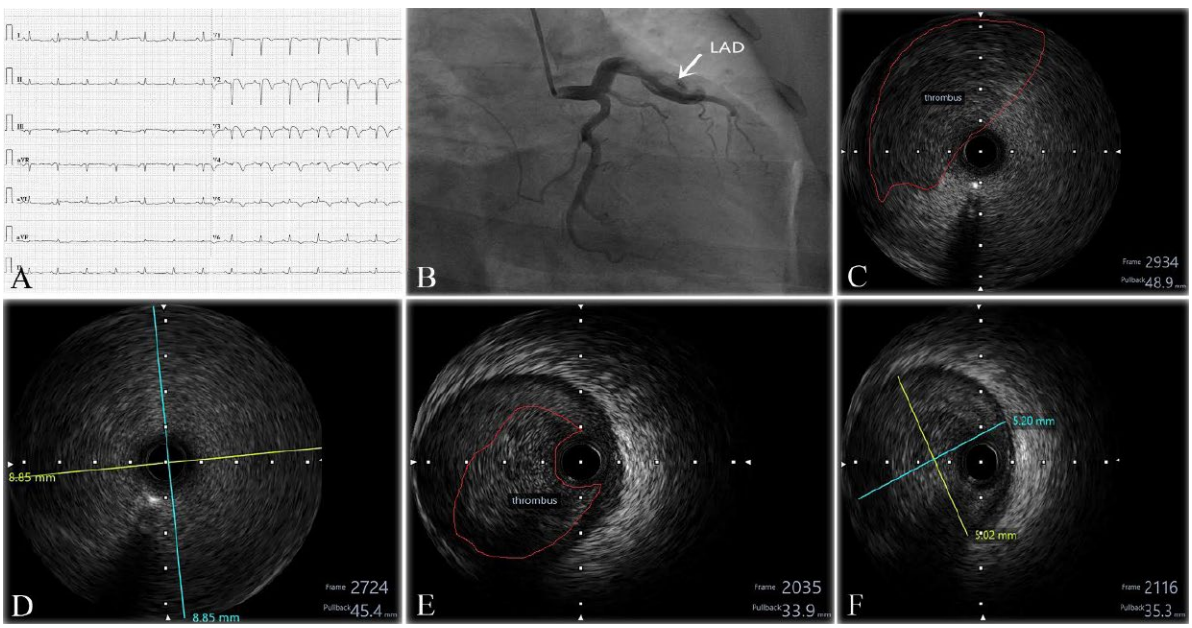


Fig. 2. *Coronary angiogram, electrocardiogram, and intravascular ultrasound of the patient early during admission. (A) Electrocardiogram showing ST-segment elevation in V1–5; (B) Left coronary angiogram showing total occlusion of the left anterior descending (LAD) artery and a large fusiform aneurysm (arrowheads); (C-D) Intravascular ultrasound showing a large fusiform aneurysm in the LAD with a thrombus and its widest segment of about 8.85 mm; (E-F) Intravascular ultrasound showing the LAD distal artery with a thrombus and its widest segment of about 5.2 mm.*

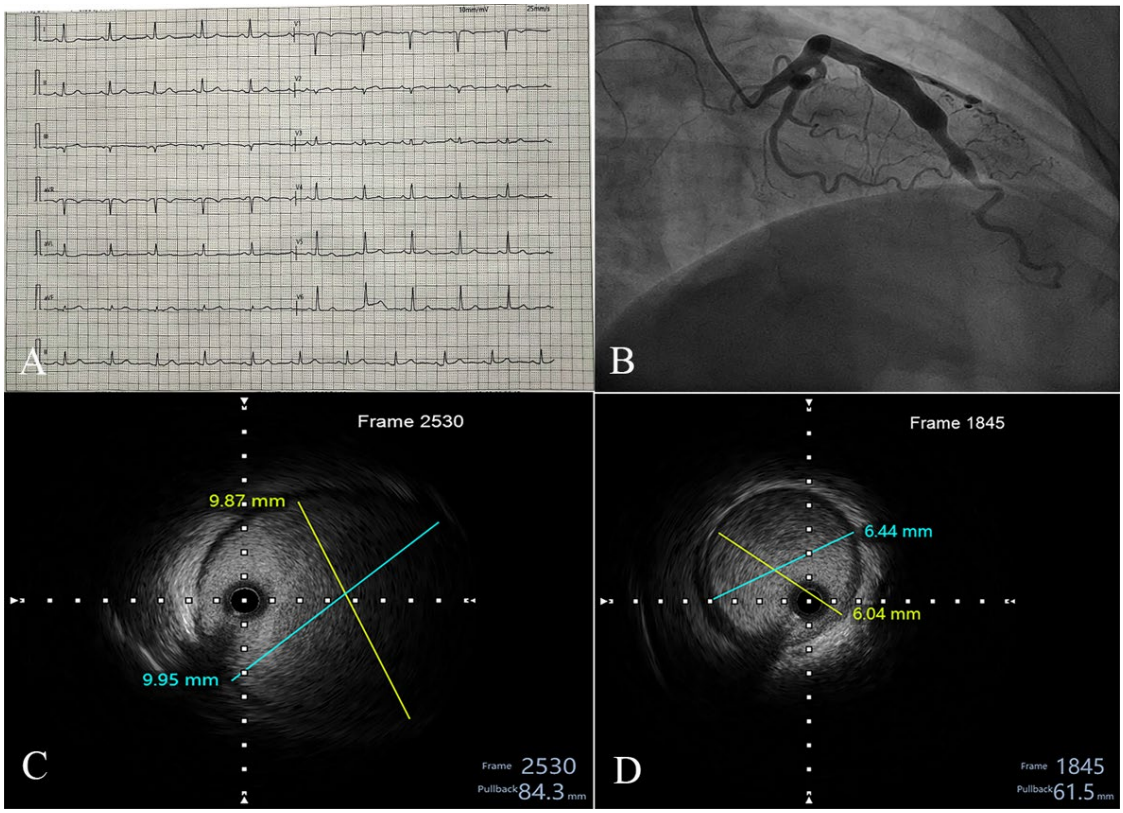


Fig. 3. *Coronary angiogram, electrocardiogram, and intravascular ultrasound of the patient in the 1-year follow-up period. (A) The electrocardiogram findings were normal; (B) Left coronary angiogram revealed that the occluded coronary artery has been recanalized; (C) Intravascular ultrasound showed a large fusiform aneurysm in the left anterior descending (LAD) artery without a thrombus and a widest segment of about 9.87 mm; (D) Intravascular ultrasound showed a coronary artery aneurysm in the LAD distal artery with no thrombus and a widest segment of about 6.44 mm.*

not licensed to manage coronary aneurysms; this indicated that the treatment measures performed were valuable in improving the patient's symptoms.

This case report has some limitations. For instance, because of the short follow-up time, the long-term effects of the therapeutic regimen were not obtained.

A rare case of STEMI caused by thrombotic occlusion of a CAA in the LAD artery was successfully treated with anticoagulant and antiplatelet therapy. Our results showed that a CAA is a potential aetiology of infarction, and CAG and IVUS both play important roles in diagnosing and treating such cases.

Ethics approval and consent to participate

The Ethics Committee approved this case report of Central Hospital Affiliated to Shandong First Medical University (Approval No. 2020-165-01), and informed consent was obtained from the patient.

Author contributions

LW contributed to the diagnoses, data curation, and manuscript writing. FW and GYS contributed to the diagnoses data curation. GHS contributed to the conceptualization and reviewed the manuscript. All authors have read and approved the final manuscript. The authors declare that they have no conflict of interest.

Availability of data and materials

The supplementary files and the datasets used and analyzed during the current study are available from the corresponding author on request.

REFERENCES

1. Falsetti HL, Carrol RJ. Coronary artery aneurysm. A review of the literature with a report of 11 new cases. Chest 1976; 69:630-6.
2. Matta AG, Yaacoub N, Nader V, Moussallem N, Carrie D, Roncalli J. Coronary artery aneurysm: A review. World J Cardiol 2021; 13:446-55.
3. Sheikh AS, Hailan A, Kinnaird T, Choudhury A, Smith D. Coronary Artery Aneurysm: Evaluation, Prognosis, and Proposed Treatment Strategies. Heart Views 2019; 20:101-8.
4. Bjelobrk M, Dodic S, Miljkovic T, et al. Asymptomatic Giant Aneurysm of the Left Anterior Descending Coronary Artery: A Case Report and Review of the Literature. J Tehran Heart Cent 2020; 15:178-82.
5. Gadepalli R, Rayidi G, Pramod G, Srivastava SK, Venkata Balakrishna SN. A case of early development of giant coronary artery aneurysms after drug-eluting stents implantation: An unpredictable menace. Interv Med Appl Sci 2017; 9:47-50.
6. Timmers L, Lim YC, Tan HC, Low AF. Coronary aneurysm without malapposition after bioresorbable vascular scaffold implantation. EuroIntervention 2016; 12:60.
7. Bell MR, Garratt KN, Bresnahan JF, Edwards WD, Holmes DR, Jr. Relation of deep arterial resection and coronary artery aneurysms after directional coronary atherectomy. J Am Coll Cardiol 1992; 20:1474-81.
8. Regar E, Klauss V, Henneke KH, Werner F, Theisen K, Mudra H. Coronary aneurysm after bailout stent implantation: diagnosis of a false lumen with intravascular ultrasound. Cathet Cardiovasc Diagn 1997; 41:407-10.
9. Oshima T, Minatsuki S, Myojo M, et al. Coronary Artery Aneurysm Caused by a Stent Fracture. Int Heart J 2018; 59:203-8.
10. Hong SJ, Kim H, Ahn CM, et al. Coronary Artery Aneurysm after Second-Generation Drug-Eluting Stent Implantation. Yonsei Med J 2019; 60:824-31.
11. Jiang LC, Cao JY, Chen M. Coronary artery aneurysm combined with other multiple aneurysms at multiple locations: A case report and systematic review. Medicine (Baltimore) 2017; 96:e9230.
12. Zhu X, Zhou Q, Tong S, Zhou Y. Challenges and strategies in the management of coronary artery aneurysms. Hellenic J Cardiol 2021; 62:112-20.
13. Cotter R, Krantz M, Hogan S, Holland M. Exclusion of a Giant Coronary Artery Aneurysm With Covered Stents Using a Long Drug-Eluting Stent Scaffold. Clin Med Insights Case Rep 2019; 12:1179547619828689.
14. Ma W, Li C, Zhang W, Ji Z, Li Y. Anterior wall myocardial infarction in a 16-year-old man caused by coronary artery aneurysm during the outbreak of COVID-19. BMC Cardiovasc Disord 2020; 20:314.
15. Kawsara A, Nunez Gil IJ, Alqahtani F, Moreland J, Rihal CS, Alkhouli M. Management of Coronary Artery Aneurysms. JACC Cardiovasc Interv 2018; 11:1211-23.
16. Seguy B, Osborn EA, Pernot M, Gerbaud E. A giant coronary artery aneurysm and recurrent ST-segment elevation myocardial infarction: A management dilemna. Cardiol J 2019; 26:212-4.
17. Boyer N, Gupta R, Schevchuck A, et al. Coronary artery aneurysms in acute coronary syndrome: case series, review, and proposed management strategy. J Invasive Cardiol 2014; 26:283-90.
18. Myler RK, Schechtmann NS, Rosenblum J, et al. Multiple coronary artery aneurysms in an adult associated with extensive thrombus formation resulting in acute myocardial infarction: successful treatment with intracoronary urokinase, intravenous heparin, and oral anticoagulation. Cathet Cardiovasc Diagn 1991; 24:51-4.
19. Szalat A, Durst R, Cohen A, Lotan C. Use of polytetrafluoroethylene-covered stent for treatment of coronary artery aneurysm. Catheter Cardiovasc Interv 2005; 66:203-8.
20. Dutary J, Zakhem B, CB DEL, Paulo M, Gonzalo N, Alfonso F. Treatment of a giant coronary artery aneurysm: intravascular ultrasound and optical coherence tomography findings. J Interv Cardiol 2012; 25:82-5.
21. Kim TH, Marfatia R, Lee J, Azrin M. Giant coronary aneurysm management with Viabahn covered stent. Cardiovasc Revasc Med 2017; 18:56-9.
22. Boi A, Sanna F, Rossi A, Loi B. Exclusion of a giant saphenous vein graft pseudo-aneurysm with a "double-layer bridging" technique. Cardiovasc Revasc Med 2018; 19:8-12.
23. Kawsara A, Núñez Gil IJ, Alqahtani F, Moreland J, Rihal CS, Alkhouli M. Management of Coronary Artery Aneurysms. JACC Cardiovasc Interv 2018; 11:1211-23.

24. Abou Sherif S, Ozden Tok O, Taskoylu O, Goktekin O, Kilic ID. Coronary Artery Aneurysms: A Review of the Epidemiology, Pathophysiology, Diagnosis, and Treatment. Front Cardiovasc Med 2017; 4:24.
25. Pham V, Hemptinne Q, Grinda JM, Duboc D, Varenne O, Picard F. Giant coronary aneurysms, from diagnosis to treatment: A literature review. Arch Cardiovasc Dis 2020; 113:59-69.
26. Zhang HP, Yu X, Ji FS, Sun FC. Coronary artery aneurysm formation after drug-coated balloon treatment of de novo lesions: Two case reports. Medicine (Baltimore) 2018; 97:e13208.
27. Garcia-Guimaraes M, Cuesta J, Alvarado T, Rivero F, Bastante T, Benedicto A, Alfonso F. Coronary artery aneurysm formation following implantation of a bioresorbable vascular scaffold for in-stent restenosis. Rev Port Cardiol 2017; 36:473.e1-4.
28. Joo HJ, Woong Yu C, Choi R, et al. Clinical outcomes of patients with coronary artery aneurysm after the first generation drug-eluting stent implantation. Catheter Cardiovasc Interv 2018; 92:E235-45.
29. Daniels LB, Tjajadi MS, Walford HH, et al. Prevalence of Kawasaki disease in young adults with suspected myocardial ischemia. Circulation 2012; 125:2447-53.
30. Usuku H, Kojima S, Kuyama N, et al. Multiple Giant Coronary Artery Aneurysms. Intern Med 2017; 56:1973-6.
31. Kondo T, Takahashi M, Nakagawa K, et al. Rupture of massive coronary artery aneurysm resulting in cardiac tamponade. Leg Med (Tokyo) 2015; 17:388-90.
32. Aggarwal P, Saxena P, Bhan A. Successful management of a giant unruptured mycotic coronary artery aneurysm after coronary angioplasty. Indian Heart J 2016; 68 Suppl 2:S44-S6.
33. Chen T, Li J, Xu Q, Li X, Lv Q, Wu H. Antithrombotic Therapy of a Young Adult with Giant Left Main Coronary Artery Aneurysm. Int Heart J 2020; 61:601-5.
34. Peng H, Wu Z, Liu Y, Li L, Kong S, Wu J, Liu Y. Low-dose antithrombotic treatment in coronary thrombosis of Kawasaki disease. Pediatr Cardiol 2015; 36:503-8.
35. Warisawa T, Naganuma T, Tomizawa N, et al. High prevalence of coronary artery events and non-coronary events in patients with coronary artery aneurysm in the observational group. Int J Cardiol Heart Vasc 2016; 10:29-31.
36. Kuroda H, Mochizuki T, Shimizu S, Kumabe T. Rupture of Thrombosed Cerebral Aneurysm During Antithrombotic Therapy for Ischemic Stroke: Case Report and Literature Review. World Neurosurg 2019; 126:468-71.
37. Nichols L, Lagana S, Parwani A. Coronary artery aneurysm: a review and hypothesis regarding etiology. Arch Pathol Lab Med 2008; 132:823-8.

CASE REPORT

Vitamin B12 deficiency in type 1 diabetes patient with thalassemia trait: the challenge of early diagnosis

G. Zirilli[1], G. Salzano[1], F. Galletta[1], P. Basile[1], F. Caime[1], U. Cucinotta[1], M. Licciardello[2], S. Passanisi[1], G. Russo[2] and F. Lombardo[1].

[1]Department of Human Pathology in Adult and Developmental Age "G. Barresi", University of Messina, Messina, Italy; [2]Pediatric Oncohematology Unit, Department of Clinical and Experimental Medicine, School of Medicine, University of Catania, Catania, Italy

Received September 1, 2021 – Accepted January 18, 2022

Anaemia may frequently occur in patients with type 1 diabetes (T1D) due to several factors such as iron deficiency or autoimmune diseases (e.g. autoimmune gastritis and pernicious anaemia) (1), leading to vitamin B12 deficiency. Causes of vitamin B12 deficiency include impaired gastric or intestinal absorption and reduced intake in cases of vegan diet or malnutrition (2). To date, there are no national or international clear guidelines on the advisability of vitamin B12 deficiency screening in pediatric patients with T1D and, therefore, this disorder often remains underestimated and under-recognized by clinicians (3). An early diagnosis of vitamin B12 deficiency is crucial to start prompt treatment, thus preventing the development of severe symptoms and complications.

Glycated haemoglobin (HbA1c) measurement, which is a known marker for the development of long-term complications in patients with diabetes, is influenced by clinical conditions that increase or shorten the life of erythrocytes. Therefore, a careful evaluation of HbA1c may be indicative of abnormalities in the diabetic patients' haematological status.

We hereby report a case of a patient with T1D who progressively developed pancytopenia caused by vitamin B12 deficiency.

Case report

A 17-year-old boy has suffered from T1D since the age of two and has been treated with multiple daily insulin injections. At the age of fourteen, he started to use continuous glucose monitoring (CGM) system. His glycemic control was suboptimal as demonstrated by the last year mean value of HbA1c that was 50 mmol/mol. Annual screening for associated autoimmune diseases were negative. No microvascular or macrovascular diabetes-related complications were present. His past medical history was also characterized by the recurrence of haemoglobin value within the normal lower limits and reduced mean corpuscular volume (MCV). At the age of ten, hemoglobin electrophoresis by high-pressure liquid chromatography showed a pattern suggestive of beta thalassemia trait.

During a follow-up visit, he reported recurrent episodes of fatigue, nausea and vomiting. His anthropometric parameters revealed a significant weight loss compared to the preceding visit. On physical examination, he had mild scleral jaundice, liver and splenic enlargement of 1 cm below the subcostal margin, with no lymphadenopathy. Laboratory tests showed haemoglobin 8.2 g/L, red blood cell (RBC) count 2.43 x 10^{12}/L, reticulocyte

Key words: continuous glucose monitoring; glycated haemoglobin; pancytopenia; pernicious anaemia

Corresponding Author:
Dr. Stefano Passanisi,
Department of Human Pathology in Adult and Developmental Age,
G. Barresi University of Messina, Messina, Italy
Tel.: +39 0902213023
e-mail: stepassanisi@unime.it

0393-974X (2022)
Copyright © by BIOLIFE, s.a.s.
This publication and/or article is for individual use only and may not be further reproduced without written permission from the copyright holder.
Unauthorized reproduction may result in financial and other penalties
DISCLOSURE: ALL AUTHORS REPORT NO CONFLICTS OF INTEREST RELEVANT TO THIS ARTICLE.

count 1.9%, MCV 97 fl, white blood cell count 2.5 × 10^9/L with mild neutropenia (0.8 x 10 10^9/L), platelet count 101 × 10^9/L. Transaminases, lactate dehydrogenase, and serum iron levels were elevated. Coagulation profile, bilirubin, and ferritin were within the normal ranges for our laboratory. His stools and urine were normochromic. Coombs test and autoantibodies to intrinsic factor (AIF) and parietal cells (APC) were negative. Noteworthy, HbA1c was higher 67 mmol/mol than three months earlier (vs 53 mmol/mol). His CGM data reported satisfactory percentage time within the ideal range of glucose between 70 and 180 mg/dl and percentage time above 180 mg/dl (72% and 25%, respectively). Thus, pancytopenia was further investigated.

Peripheral blood smear confirmed the presence of leukopenia, moderate anaemia and thrombocytopenia. A discrete amount of virocytes was also detected. To rule out infectious causes of pancytopenia, serology for Epstein Barr virus, cytomegalovirus, Parvovirus B19 was tested and all resulted negative for recent infections. The patient underwent bone marrow aspirate and threphine biopsy. Morphological and cytofluorimetric evaluation excluded neoplastic elements and showed an hypercellular marrow with increased and megaloblastic erythropoiesis (Fig. 1).

To classify megaloblastic anaemia, further laboratory tests were performed. Low values of vitamin B12 (136 pg/ml), hyperhomocysteinemia (58.5 mml/L) and abundant urinary excretion of methylmalonic acid were found. Folic acid was within the normal values (5.2 ng/ml). Finally, re-evaluation of patient's blood count values over the last 3 years revealed progressive increase of MCV, gradually rising from 69 fl in 2017 to 97 fl in 2020 (Table I). A detailed specific nutritional history revealed a strictly selective diet since the age of fifteen, based on low intake of animal proteins. Such inadequate eating habits could be the leading cause of vitamin B 12 deficiency.

Replacement therapy with vitamin B12 was immediately started at the dose of 1000 mcg/die for 4 days, then once a week for 1 month. During the subsequent days we recorded a progressive improvement in his general condition. Blood tests showed a progressive normalization of haemoglobin and other cell lines, with elevated circulating reticulocytes (19%). A progressive decrease of homocysteinemia and methylmalonic acid urinary excretion was also detected. Furthermore, a relevant improvement of HbA1c value was noticed after three months (Fig. 2). Written informed consent was

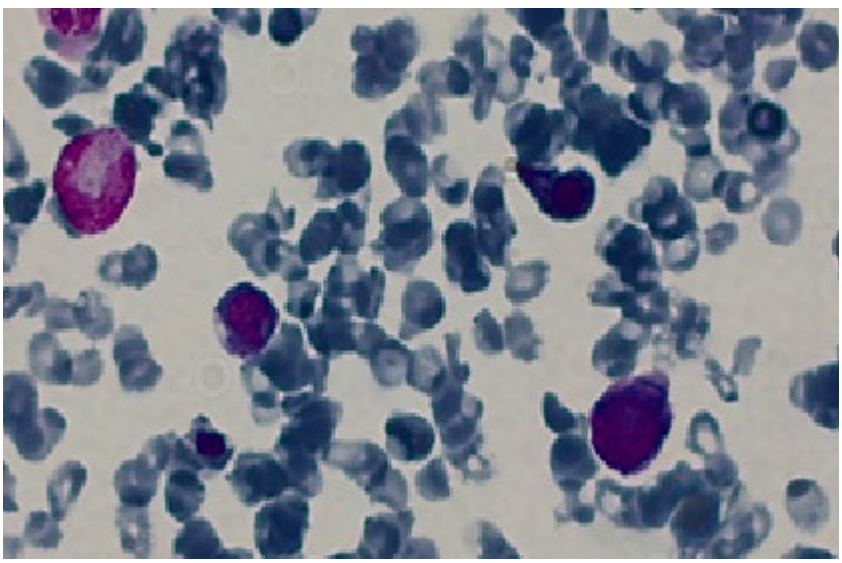


Fig. 1. *Bone marrow aspirate revealed large, oval shaped erythroblasts containing an immature, lacy nucleus*

obtained from the patient's parents for the publication of this case report.

DISCUSSION

Vitamin B12 deficiency in T1D patients is a potential comorbidity that is often overlooked (4), since typical symptoms such as clinical signs of anaemia, neurological symptoms, atrophic glossitis, and stomatitis may occur later (2). Moreover, classical haematological finding of vitamin B12 deficiency, such as macrocytic red blood cells (mean corpuscular volume MCV > 100 fl), can be blunted by concomitant iron deficiency or thalassemia trait (5, 6).

As known, HbA1c reflects average glucose of the last 2-3 months, but it doesn't identify the magnitude and frequency of intra- and inter-day glucose variation (7). Conditions such as anaemia, haemoglobinopathies, iron or vitamin B12 deficiency, can falsify HbA1c values (5,8). Therefore, an adequate interpretation of the HbA1c measurement also requires the knowledge of patient's haematological status. Typically, clinical conditions that increase the life of erythrocytes or associated with decreased turnover rate of RBCs prolong the exposure of cells to glucose and result in elevated HbA1c levels. Iron deficiency anaemia,

Table I. *Complete blood count cell and other biochemical data before, at the time of diagnosis, and after the start of replacement therapy. The progressive increase of mean corpuscular value and decrease of all cell lines is typical of vitamin B 12 deficiency. Replacement therapy led to a normalization of complete blood count cell.*

Complete blood count and other biochemical data	Previously to the clinical presentation	At the onset of symptoms	One month after vitamin B12 therapy	Three months after vitamin B12 therapy
Erythrocyte count	6.18×10^{12}/L	**2.43×10^{12}/L**	4.70×10^{12}/L	5.60×10^{12}/L
Hemoglobin(g/L)	10	**8.2**	11.7	12
Mean corpuscolar volume (fL)	59	**97**	80	69
Mean corpuscolar hemoglobin (pg)	16.1	**33.6**	24.9	21.5
Mean corpuscolar hemoglobin concentration	27	**34.5**	31.1	31
Red cell distribution width (%)	17.6	**20.9**	17.1	18.9
Total leucocyte count	6.34 x 10^9/L	**2.50 x 10^9/L**	5.80 x 10^9/L	5.40 x 10^9/L
Neutrophils (%)	50	**32**	60	66
Eosinophilis (%)	2	**5**	2	3
Lymphocytes(%)	43	**58**	34	25
Platelets	366 x 10^9/L	**101 x 10^9/L**	231 x 10^9/L	242 x 10^9/L
Reticulocytes(%)	/	**1.9**	1.4	1.2
Sideremia (μg/dl)	17	**223**	22	26
Ferritin (ng/ml)	/	**120**	/	/
Vitamin B12 (pg/ml)	/	**136**	359	310

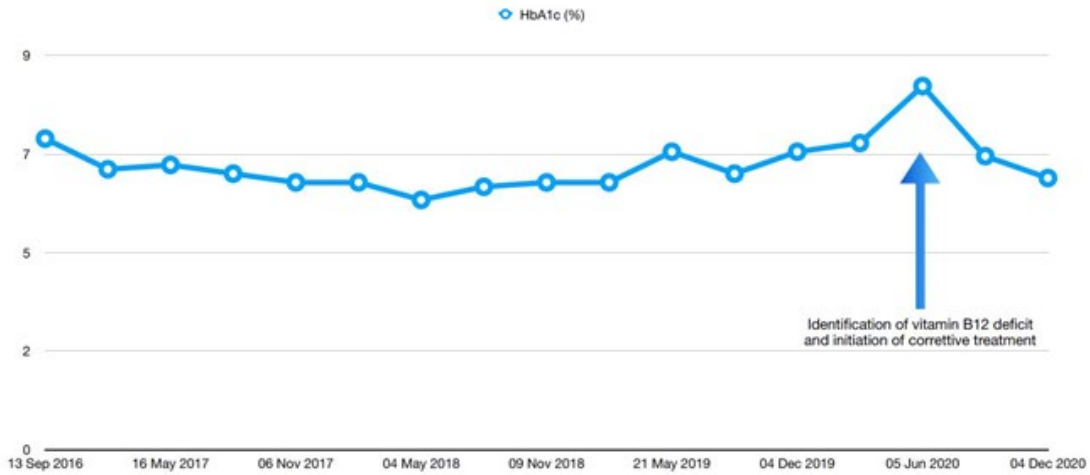


Fig. 2. *Clinical conditions that cause changes in the life of erythrocytes prolong the exposure of cells to glucose and result in falsely elevated HbA1c levels, as demonstrated by the sudden increase in our patient. HbA1c value decreased immediately after replacement therapy*

vitamin B12 and folate deficiency are associated with spuriously elevated HbA1c levels in patients with or without diabetes (9). Conversely, disorders such as haemoglobinopathies, which make RBCs more prone to haemolysis, decreased the time for glycosylation and produce false low HbA1c values (8).

Finally, beta thalassemia trait does not seem to affect HbA1c concentrations (10). HbA1c could also be an important marker of changes in the erythrocyte population when therapy is practiced (5,8). Gram-Hansen et al. reported a significant decrease in HbA1c concentration after therapy with iron and cobalamin together with significant changes in the erythrocyte indices, as we observed in our patient (11). Nowadays, in diabetic patients using CGM systems, other glucose metrics such as time within range, time below range, time above range, and coefficient of variation are recognized as appropriate and useful clinical targets that complement HbA1c in the evaluation of glycemic control (12). Our case highlights how unexpected and sudden changes in HbA1c levels, especially if not related to the worsening of CGM metrics, should be considered red flags to suspect potential haematological diseases in patients with T1D.

Author's contributions

GF wrote the paper with the help of BP, CF, and CU; ZG and SG had been in charge the patient; LM and RG performed bone marrow aspirate and threphine biopsy, PS contributed to discussion, FL contributed to discussion and reviewed the paper. The paper has been read and approved by all the authors and each author considers that the paper represents their honest work.

Competing interests

The authors declare that they have no competing interests.

REFERENCES

1. Rusak E, Rotarska-Mizera A, Adamczyk P, et al. Markers of Anemia in Children with Type 1 Diabetes. J Diabetes Res. 2018; 2018:5184354.
2. Kibirige D, Mwebaze R. Vitamin B12 deficiency among patients with diabetes mellitus: is routine screening and supplementation justified? J Diabetes Metab Disord. 2013; 12:17.
3. Stabler SP. Vitamin B12 deficiency. N Engl J Med. 2013; 368:2041-2.
4. Koshy AS, Kumari SJ, Ayyar V, Kumar P. Evaluation of serum vitamin B12 levels in type 1 diabetics attending a tertiary care hospital: A preliminary cross - sectional study. Indian J Endocrinol Metab. 2012;16 Suppl 1:S79-82.
5. Ford ES, Cowie CC, Li C, et al. Iron-deficiency

anemia, non- iron-deficiency anemia and HbA1c among adults in the US. J Diabetes. 2011; 3:67–73.
6. Lardhi A, Ali RA, Ali R, Mohammed T. Thalassemia minor presenting with vitamin B_{12} deficiency, paraparesis, and microcytosis. J Blood Med. 2018; 9:141-144.
7. Qu Y, Jacober SJ, Zhang Q, et al. Rate of hypoglycemia in insulin-treated patients with type 2 diabetes can be predicted from glycemic variability data. Diabetes Technol Ther 2012; 14:1008–12.
8. Smaldone A, Glycemic control and hemoglobinopathy: when A1C may not be reliable. Diabetes Spectr. 2008; 21:46-9.
9. Coban E, Ozdogan M, Timuragaoglu A. Effect of iron deficiency anemia on the levels of hemoglobin A1c in nondiabetic patients. Acta haematologica. 2004; 112:126-8.
10. Polage C, et al. Effects of beta thalassemia minor on results of six glycated haemoglobin methods. Clin Chim Acta. 2004; 350:123–8.
11. Gram-Hansen P, Eriksen J, Mourits-Andersen T, Olesen L. Glycosylated haemoglobin (HbA1c) in iron- and vitamin B12 deficiency. J Intern Med. 1990; 227:133-6.
12. Battelino T, Danne T, Bergenstal RM, et al. Clinical Targets for Continuous Glucose Monitoring Data Interpretation: Recommendations From the International Consensus on Time in Range. Diabetes Care. 2019; 42:1593-603.

LETTER TO THE EDITOR

Bio-Physico-Metric approach: integrated postural assessment in musculoskeletal dysfunctions

G. Barassi[1,2], E. Di Simone[1], M. Supplizi[1], L. Prosperi[1], C. Marinucci[1], R. Pellegrino[3], P. Galasso[4], S. Guerri[1], M. Della Rovere[1], A. Younes[1], and A. Di Iorio[5]

[1]Center for Physiotherapy, Rehabilitation and Re-education (CeFiRR) Training Center, venue "G. d'Annunzio" University of Chieti-Pescara, Chieti, Italy; [2]Center for Physiotherapy, Rehabilitation and Re-education (CeFiRR) – Gemelli Molise Professionalizing Didactic Center, venue "Sacred Heart Catholic University" of Rome-Campobasso, Italy; [3]Antalgic Mini-Invasive and Rehab-Outpatients Unit, Department of Medicine and Science of Aging, "G. d'Annnunzio" University of Chieti-Pescara, Chieti, Italy; [4]"San Raffaele" University, Rome, Italy; [5]Laboratory of Clinical Epidemiology and Aging, Department of Medicine and Science of Aging, "G. d'Annunzio" University of Chieti-Pescara, Chieti, Italy

Received November 5, 2021 – Accepted February 24, 2022

To the Editor,

Postural deviations can cause alterations in functional activities and pain (1). Based on information from peripheral afferent structures (ears, eyes, muscles, tendons, viscera), the cerebral cortex organizes posture or the execution of movements. Consequently, the dysfunction of one or more of these structures can lead to a postural dysfunction in the form of myofascial adaptations. This situation can remain latent for a long time and predispose to musculoskeletal injuries, in which tissues can undergo an inflammatory process. Inflammation mediators evoke pain through direct activation and sensitization of nociceptors, which consist of unmyelinated C fibres and myelinated Aδ fibres that innervate the skin, muscles, and joints visceral organs (2). During the state of latency of aberrant myofascial adaptations, due to the overlap of "triggering factors", the compensatory capacities of the musculoskeletal system are exceeded and, consequently, alterations are established. The whole process leads to a myofascial dysfunction characterized by pain and limitation of functional activities. In addition, orthopaedic and rheumatological diseases can cause alterations in posture and body balance (3). Altered moods, anxiety and intake of some drugs are also risk factors for posture alterations (4). Therefore, an exhaustive postural evaluation must assess the biomechanical system, the biochemical-metabolic system, the neuro-psychological system and the environmental context. These systems are interconnected, and the deficit of one affects the stability of the whole complex, requiring a multidisciplinary and Bio-Physico-Metric Approach; this is especially true since, to date, there is still little knowledge in the literature of the role that postural analyzes and their interpretations can have in the prevention and evaluation of any musculoskeletal problems caused by postural alterations (5). Therefore, this study aims to provide guidelines for the data interpretation of a validated sequence of postural investigation techniques, based on a questionnaire, called Postural Evaluation Questionnaire (PEQ), and a biomechanics evaluation, called Biomechanical Postural Evaluation (BPE) (6).

Keywords: rehabilitation, posture, postural balance, biometry, musculoskeletal diseases

Corresponding Author:
Dr Giovanni Barassi,
Center for Physiotherapy,
Rehabilitation and Re-education (CeFiRR),
Gemelli Molise - Professionalizing Didactic Center,
Sacred Heart Catholic University of Rome, Campobasso, Italy
e-mail: giovanni.barassi@unicatt.it

0393-974X (2022)
Copyright © by BIOLIFE, s.a.s.
This publication and/or article is for individual use only and may not be further reproduced without written permission from the copyright holder.
Unauthorized reproduction may result in financial and other penalties
DISCLOSURE: ALL AUTHORS REPORT NO CONFLICTS OF INTEREST RELEVANT TO THIS ARTICLE.

MATERIALS AND METHODS

Location and participants selection

This observational study was conducted at the Center for Physiotherapy, Rehabilitation and Reeducation (Ce. Fi.R.R.), located at the University "Gabriele d'Annunzio" of Chieti-Pescara as part of the Centre of Sports Medicine.

A report of a case series was performed in accordance with the Helsinki Declaration and Good Clinical Practice standards. All participants signed the informed consent for the experimental procedure, which complies with the latest revision of the Helsinki Declaration and Good Clinical Practice standards, and with the procedures defined by the ISO 9001-2015 standards for "Research and experimentation", which outline the steps of the study and also protects the privacy of the subjects participating in biomedical research. This study report follows the Joanna Briggs Institute Critical Appraisal Checklist for case series and the Case Report Guideline CARE in all the applied items. The data collection formed part of our clinical routine. Therefore, the normal ethics committee clearance was not required (7).

We observed a study sample of 100 healthy subjects, 82 males and 38 females, aged between 20 and 43 years (with an average age of 23.38 years). The study sample was subjected to the PEQ, the BPE and the Digitized Biometric Evaluation (DBE).

PEQ structure

The PEQ is a set of questions that globally investigate the state of health. The patient compiled it directly before the BPE (Table I).

The PEQ consists of two parts: the first part collects personal, family and employment data, while the second investigates the clinical conditions, the biomechanical and the receptor structures, in particular the structural condition, the osteo-arthro-muscular system, the sensibility, the eye, the inner ear, the stomatognathic system, the internal environment.

The parameters used to investigate the structural condition were height, the correlation between height and shoe number, Body Mass Index, employment, lifestyle, physical activity, weight gain or loss, the presence of fractures, the presence of neck, back and lumbar pain or tension, the presence of reduced sensitivity, associated tingling in the upper or lower limbs, the presence of joint pain in the hip or knee, the presence of muscle strains or other acute events, the presence of cramps and/or sprains, the presence of foot pain and the presence of warts.

The parameters used to investigate the structural condition were eventual vision disturbances, eventual disturbed hearing, ear infections, closed-ear, dizziness or lightheadedness, the presence of migraines, headaches and/or neuralgia, eventual teeth swallowing and/or bruxism, the presence of respiratory problems, possibly associated to smoking, eventual emotional stress and states of anxiety, the presence of sleep disorders, the eventual use of drugs, eventual dextromania and eventual state of pregnancy. The PEQ results in a score. The score is directly proportional to the deviation from the normality of the investigated systems.

BPE structure

The BPE is an analytical manual analysis of the osteo-myofascial system to deepen the postural condition of the subject. The investigation involves two phases. The first consists of evaluating the alignment of the lower limbs and body symmetries, while the second consists of applying pressure stimuli (of about 2 Kg) in specific points and the consequent quantification of the pain evoked by the subject.

The alignment of the lower limbs was assessed with the patient in the supine position before and after the Weber-Barstow Maneuver (WBM). The WBM allows excluding the influence of the pelvis on the alignment of the lower limbs to discriminate a functional heterometry from a structural one. The manoeuvre consists of the synchronous flexion of the knees, the hip flexion and, finally, the return to the supine position. The permanence of heterometry after the manoeuvre suggests the presence of a structural heterometry, that is, of lower limbs of different lengths.

In order to define the intensity of pain evoked by each pressure stimulation, the Numerical Rating Scale (NRS) was administered to the study sample. The NRS allows to evaluate pain from 0 to 10, where 0 corresponds to the absence of pain and 10 to unbearable pain. NRS was administered verbally, asking all patients the same question: "on a scale from 0 to 10, where 0 represents the absence of pain and 10 represents the worst possible pain, what is your pain level"? The data in the literature demonstrate the reliability and validity of the NRS scale

Table I. *Postural Evaluation Questionnaire (PEQ) structure*

Name and surname	
Sex	□ Male □ Female
Date of birth (dd/mm/yyyy)	__/__/____
Country	
Footwear (EUR)	
Height	_____ cm
Profession (for example, professor)	
Physical activity	□ Never □ Sometimes □ Several times a week □ More than 30 minutes a day
Have you gained or decreased weight in the past 24 months?	□ No □ Yes, ____Kg
Have you ever had any fractures? If so, where?	□ No □ Yes, _____
Do you have neck pain or tension? If so, when?	□ No □ Often □ Sometimes □ Upon awakening □ At the end of the day
Do you have back pain or tension? If so, when?	□ No □ Yes, at the dorsal region □ Yes, at the lumbar region □ Yes, at the sacral region □ Often □ Sometimes □ Upon awakening □ At the end of the day □ If I lift weights □ If I stand a long time
Do you have swelling, tingling, reduced sensitivity in your arm? If so, when?	□ No □ Yes, to the right arm □ Yes, to the left arm □ Yes, to both arms □ Often □ Sometimes □ Upon awakening □ At the end of the day
Do you have swelling, tingling, reduced sensitivity in your hand? If so, when?	□ No □ Yes, to the right hand □ Yes, to the left hand □ Yes, to both hands □ Often □ Sometimes □ Upon awakening □ At the end of the day
Do you have hip joint pain? If so, when?	□ No □ Often □ Sometimes □ If I walk a long time
Do you have knee joint pain? If so, when?	□ No □ Often □ When I take the stairs □ If I walk a long time
Do you have swelling, tingling, reduced sensation in the leg? If so, when?	□ No □ Yes, to the right leg □ Yes, to the left leg □ Yes, to both legs □ Often □ Sometimes □ Upon awakening □ At the end of the day
Do you have swelling, tingling, reduced sensation in your foot? If so, when?	□ No □ Yes, to the right foot □ Yes, to the left foot □ Yes, to both feet □ Often □ Sometimes □ Upon awakening □ At the end of the day

Do you have hip joint pain? If so, when?	□ No □ Often □ Sometimes □ If I walk a long time
Do you have knee joint pain? If so, when?	□ No □ Often □ When I take the stairs □ If I walk a long time
Do you have swelling, tingling, reduced sensation in the leg? If so, when?	□ No □ Yes, to the right leg □ Yes, to the left leg □ Yes, to both legs □ Often □ Sometimes □ Upon awakening □ At the end of the day
Do you have swelling, tingling, reduced sensation in your foot? If so, when?	□ No □ Yes, to the right foot □ Yes, to the left foot □ Yes, to both feet □ Often □ Sometimes □ Upon awakening □ At the end of the day
Have you had acute muscle tears or tendinitis in the past 24 months?	□ No □ Yes
Do you suffer from nocturnal cramps? If so, where?	□ No □ Yes, _____ □ Sometimes, _____
Does it take crooked when walking?	□ No □ Often □ Sometimes
Do you have pain in your feet?	□ No □ Often □ Sometimes □ When I walk a long time
Have you had warts on your feet?	□ No □ Yes
Do you often have calluses under your feet?	□ No □ Yes
Do you have vision problems?	□ No □ Yes □ Sometimes □ I use glasses / contact lenses
How long have you not been to the ophthalmologist?	□ 1 month □ Less than 1 year □ Over 1 year □ Over 5 years
Do you have excessive tearing problems?	□ No □ Yes □ In particular atmospheric conditions
Do you have hearing problems? If so, in which ear?	□ No □ Yes, to the right ear □ Yes, to the left ear □ Yes, to both ears □ Constant buzzing
Do you have a closed ear or do you have ear infections? If so, in which ear?	□ No □ Yes, to the right ear □ Yes, to the left ear □ Yes, to both ears □ Sometimes, to the right ear □ Sometimes, to the left ear □ Sometimes, to both ears
Have you ever suffered or do you suffer from dizziness or vertigo?	□ No □ Yes □ Sometimes
Do you have migraine, neuralgia or headache?	□ No □ Yes □ Rarely □ In case of stress □ Often
Do you have toothache or difficulty swallowing?	□ No □ Yes □ Rarely □ Often

Do you have nocturnal bruxism (grinding or rubbing of the teeth)?	□ No □ Yes □ Rarely □ Often
Do you have breathing problems?	□ No □ Yes □ Rarely □ Often
Do you smoke?	□ No □ Yes
Do you have digestive or gastrointestinal disorders?	□ No □ Yes □ Sometimes
Have you been experiencing severe emotional stress in the past 18 months?	□ No □ Yes
Do you suffer from anxiety?	□ No □ Yes □ Sometimes
Do you have sleep disturbances, trouble falling asleep?	□ No □ Yes □ Rarely □ Sometimes
Do you suffer from skin irritation or dermatitis?	□ No □ Yes □ Sometimes
Do you feel tired and unmotivated?	□ No □ Yes □ Sometimes
Take drugs?	□ No □ Yes
In writing is it?	□ Right-handed □ Left-handed
Have you had any pregnancies in the past 18 months?	□ No □ Yes □ Caesarean section
Have you ever worn orthotics?	□ No □ Yes
Have you undergone physiotherapy treatments in the last 24 months?	□ No □ Yes
Have you ever performed gnathological therapy (bite)?	□ No □ Yes

for measuring and monitoring pain intensity. The BPE results in a score given by the average of the single items. The points investigated by the BPE are shown below, divided by body district (Table II).

The Digitized Biometry

DBE is a non-invasive investigation method developed for the quantitative and qualitative evaluation of the equilibrium strategy of a person. It includes the static pressure test, the dynamic pressure test and the stabilometric examination. The study sample was subjected to the static pressure test and the stabilometric examination through the system Ultrasensor 3D Diagnostica 4x1 MT (Sa.Ni Corporate S.r.l., Rome, Italy); the static pressure test analyses the foot pressure points. Each subject was analyzed in orthostatic with the retropodal area of the feet aligned with the frontal plane. The data collected allows one to examine the presence of structural alterations and correlate them to musculoskeletal stress at various levels. In addition, the percentage of load difference was considered, which allows to observe whether the load is homogeneously distributed between the right and left limbs. A difference greater than 3% between the two hemisomes (for example, 47% on the right and 53% on the left or the other way around) is considered non-physiological (8).

The stabilometric examination studies the body's oscillations in orthostatic position in 51.2 seconds. The examination is carried out with open and closed eyes. Temporarily closing the eyes deepens the compensatory capacity of the vestibular and proprioceptive mechanisms. The Romberg Index (RI) was considered. The RI is calculated as the ratio between the surface of the confidence ellipse with eyes closed and the surface of the confidence ellipse with eyes open, all multiplied by 100. It is useful for comparing oscillations with open and closed eyes: values greater than 100 indicate a greater oscillation with

Table II. *Biomechanical Postural Evaluation (BPE) structure*

Foot	I-V Metatarsus	Midfoot	Calcaneus	Achilles Tendon	Anterior Talo-Fibular Ligament	Posterior Talo-Fibular Ligament	Calcaneo-Fibular Ligament	Deltoid Ligament
Limb	Gastrocnemius	Soleus	Peronei longi	Tibialis anterior				
Thigh	Tensor fascia lata	Hamstring	Long adductor					
Pelvis	Ileopsoas	Piriformis						
Rachis	Quadratus lumborum	Erector columnae	Trapezius	Pectoralis minor	SCOM	Masseter		

eyes closed, and vice versa. Values less than 100 could be secondary to visual problems, while values greater than 100 could be secondary to vestibular, somatosensory or CNS disturbances. A reference range is between 65 and 250 (9).

RESULTS

Results of the stabilometric examination

Collected data were analyzed using the Excel software (Microsoft, Redmond, WA, USA).

By correlating the collected RI and PEQ scores, we noticed that:

100% of people who reported a score greater than 20 to the PEQ has a non-physiological RI

100% of people who reported a score less than 11 on the PEQ has a physiological RI

By correlating the RI and the BPE, it can be noted that:

94.6% of people who in the BPE reported a score greater than 6 have a non-physiological RI

93.75% of people who reported a score lower than 4 in the BPE have a physiological RI

DISCUSSION

Diseases affecting the structures which participate strongly in the establishment of posture can cause progressive deterioration of the postural compensation mechanisms of the musculoskeletal system, manifesting an altered efferentiality such as to contribute to the determinism of the "postural disorder" associated with myofascial dysfunction and suppression of the convergence of stimuli at the level of a specific spinal cord metamer and expression of the concept of spinal facilitation (6). Our work has shown that investigating healthy subjects through a clinical postural questionnaire and a manual examination on the precept threshold can be a valid methodology to initiate effective and evidence-based interpretation processes of myofascial postural dysfunction. The DBE played a fundamental role in this study, as it allowed to objectively define the guidelines for a correct interpretation of the scores referred to the PEQ and the BPE. Based on the data obtained, PEQ values greater than 20 and BPE values greater than 6 suggest the presence of postural dysfunction and, therefore, a high degree of myofascial compensation that often may not be perceived by the patient leading to musculoskeletal problems. So, this Bio-Physico-Metric evaluation sequence can be useful both in the preventive and curative fields. Inflammatory mediators such as prostaglandin, proinflammatory cytokines and chemokines induce pain through direct activation of nociceptors (2). Myofascial somatic dysfunction can trigger the mechanisms of neurogenic inflammation due to hyperstimulation (10); therefore, the assessment of the state of health (PEQ) and the threshold of perception of pain (BPE) can also help us to evaluate the presence of major somatic dysfunctions, which can be defined as Key Trigger Points (KTrPts)

(11). The scientific literature suggests that in the soft tissues near the TrPs, neurogenic inflammation, sensitization and dysfunction of the limbic system may play a role in the initiation, amplification and perpetuation of the dysfunction (12). In particular, it has been observed that the local physiological and bioelectrical variations due to the presence of KTrPts are objectively detectable (11). Furthermore, it has been observed that the deactivation of KTrPts allows a rapid and objective improvement of pathologies of the musculoskeletal system, such as Low Back Pain (11). The objective study of posture can become a consolidated way of investigating KTrPts that can be active or latent, and that can be the expression of structural, visceral and emotional dysfunctions. The PEQ allows us to associate the perception threshold (BPE) to the anamnestic data and, together, these data can provide important indications on the identification of the musculoskeletal sites to be treated in physical and rehabilitative medicine.

Conflict of interest

The authors declare that they have no conflicts of interest in relation to this paper.

REFERENCES

1. Rosário JLP, Nakashima IY, Rizopoulos K, Kostopoulos D, Marques AP. Improving posture: comparing Segmental Stretch and muscular Chains Therapy. Clin Chiropractic 2012; 15:121-128.
2. Amaya F, Izumi Y, Matsuda M, Sasaki M. Tissue injury and related mediators of pain exacerbation. Curr Neuropharmacol 2013; 11(6):592-7.
3. Missaoui B, Portero P, Bendaya S, Hanktie O, Thoumie P. Posture and equilibrium in orthopedic and rheumatologic diseases. Clin. Neurophysiol 2008; 38:447-457.
4. Bannwarth B. Drug-Induced Musculoskeletal Disorders. Drug Safety 2007; 30(1):27-46.
5. Sahrmann SA. Does postural assessment contribute to patient care? Journal of Orthopaedic & Sports Physical Therapy 2002; 32(8):376-379.
6. Barassi G, Di Simone E, Galasso P, Cristiani S, Supplizi M, Kontochristos L, Colarusso S, Visciano CP, Marano P, Antonella DI, Giancola O. Posture and Health: Are the Biomechanical Postural Evaluation and the Postural Evaluation Questionnaire Comparable to and Predictive of the Digitized Biometrics Examination?. Int J Environ Res Public Health 2021; 18(7):3507.
7. Winter EM, Maughan RJ. Requirements for ethics approvals. J Sports Sci 2009; 27:985.
8. Wojtków M, Szkoda-Poliszuk K, Szotek S. Influence of body posture on foot load distribution in young school-age children. Acta Bioeng Biomech 2018; 20(2):101-107.
9. Shiffer R, Paolini M. Biomedica posturale e biometria digitalizzata. Edizioni Publiedit s.a.s, Roma, 2015.
10. Duarte FC, West DW, Linde LD, Hassan S, Kumbhare DA. Re-examining myofascial pain syndrome: toward biomarker development and mechanism-based diagnostic criteria. Current rheumatology reports 2021; 23(8):1-10.
11. Barassi G, Pokorski M, Matteo CD, et al. Manual Pressure Release and Low-Grade Electrical Peripheral Receptor Stimulation in Nonspecific Low Back Pain: A Randomized Controlled Trial. Adv Exp Med Biol 2021; 1324:73-81.
12. Shah JP, Thaker N, Heimur J, Aredo JV, Sikdar S, Gerber L. Myofascial Trigger Points Then and Now: A Historical and Scientific Perspective. PM R 2015; 7(7):746-761.

Magnetic resonance high-resolution black blood imaging for the diagnosis of intracranial arterial stenosis

Y.Q. Du[1], L.C. Lei[2], S.C. Wang[1], X.Y. Bian[1], M. Li[1], H. Liu[3] and W. Chen[3]

[1]Department of Physical Examination, Fourth Hospital of Hebei Medical University, Shijiazhuang, China; [2]Department of Radiology, The First Hospital of Hebei Medical University, Shijiazhuang, China; [3]Department of CT, Fourth Hospital of Hebei Medical University, Shijiazhuang, China

To evaluate the diagnostic value of magnetic resonance high-resolution black blood imaging in intracranial arterial stenosis, forty-six patients who underwent intracranial artery examination were selected for MRA, DSA and magnetic resonance high-resolution black blood imaging. The black blood and MRA technology results were compared with the DSA results. The sensitivity, specificity, accuracy, positive predictive value and negative predictive value of MRA were 67.85%, 66.67%, 48.27%, 65.51%, 68.96%, respectively. The high-resolution black blood imaging results were 94.11%, 95.83%, 58.62%, 96.96% and 92%, respectively, and except for accuracy, the difference between MRA and high-resolution black blood imaging was statistically significant (P<0.05). In conclusion, the magnetic resonance high-resolution black-blood technique is highly valued in diagnosing intracranial arterial stenosis.

Intracranial vascular stenosis is the cause of cerebrovascular disease (1). Routine imaging methods, including CTA, MRA and DSA, are lumen imaging methods that can only show the degree of stenosis in the lumen. These techniques cannot show the pathological changes of the vascular wall or show the cause of vascular stenosis. Domestic and foreign studies on the carotid artery are reported more often, and studies of the intracranial artery are reported less often. In this study, magnetic resonance high-resolution black blood imaging was used to analyze the causes of vascular stenosis, which is of great significance in clinical diagnosis.

High-resolution imaging of the arterial wall using 3D-T1 black blood vessel wall imaging isotropic high-definition three-dimensional imaging and volume acquisition, conducive to three-dimensional postprocessing, helps detect intracranial arterial lesions and qualitative arterial blood flow signal suppression helps to identify inflammatory lesions and chronic thrombosis.

MATERIALS AND METHODS

There were forty-six patients with intracranial arterial angiopathy in the fourth hospital of Hebei Medical University, including twenty-six male patients and twenty female patients; all patients were aged 22 to 67 years and underwent a magnetic resonance plain scan, a magnetic resonance high-resolution black-blood technique, DWI, MRA and DSA examination. Signed written informed consents were obtained from the patients

The parameters were as follows:

T1W MRI: TR 150 ms, TE 2.49 ms, and thickness 5.0 mm.

T2WI: TR 7500 ms, TE 81 ms, and thickness 5.0 mm.

DWI: TR 4100 ms, TE 64 ms, and thickness 5.0 mm.

FLAIR: TR 7500 ms and TE 81 ms.

Keywords: Magnetic resonance, black blood technique, intracranial artery stenosis

**Corresponding author:*
Dr Licun Lei,
Department of Radiology,
The First Hospital of Hebei Medical University,
No. 89 Donggang Road, Shijiazhuang 050000, China
e-mail: ceh03z@163.com

0393-974X (2022)
Copyright © by BIOLIFE, s.a.s.
This publication and/or article is for individual use only and may not be further reproduced without written permission from the copyright holder.
Unauthorized reproduction may result in financial and other penalties
DISCLOSURE: ALL AUTHORS REPORT NO CONFLICTS OF INTEREST RELEVANT TO THIS ARTICLE.

MRA: TR 21 ms, TE 3.43 ms, and thickness 0.7 mm.

For the magnetic resonance imaging of high-resolution black artery wall: 3D-T1WI, oblique coronal scanning procedure: TR 600 ms, TE 20 ms, matrix 256×256, thickness 0.9 mm, a total of 60 slices, and scan time of 4 min 28 s.

All images were transmitted to the postprocessing workstation (ADW4.4; GE Health care, Milwaukee) for evaluation and analysis. The interest layer for high-resolution 3 D-T1-MRI axial reconstruction images was independently graded by a radiologist experienced in evaluating high-resolution intracranial artery MRI images according to the Yuan image quality grading criteria (1~5 scores) (2, 3). A score of 1 indicated that the tube wall and boundary could not be identified; a score of 2 indicated that the tube wall was visible, but the boundary could not be seen clearly; a score of 3 indicated that the boundary of the tube wall was blurred but discernible; a score of 4 indicated that the boundary of the tube wall was clear; and a score of 5 indicated that the boundary of the tube wall was particularly sharp.

Statistical Methods

The sensitivity, specificity, accuracy, positive and negative predictive values of MRA and black blood techniques were tested X2 using a software package; $P<0.05$ indicated statistical significance.

RESULTS

A total of 58 vessels were assessed in 46 patients with intracranial arterial disease, including 38 with internal carotid artery stenosis and 20 with vertebral artery stenosis. Also, 38 vessels were part of the internal carotid artery system. Regarding image scores, 36 patients had a total score of 5, 1 patient had a total score of 4, and 1 patient had a total score of 2. A total of 19 patients, 4 patients and 1 patient scored 5 on 20 stenosis vessel images of the vertebral artery system (Table I).

High-resolution black blood imaging images showed that internal carotid artery stenosis showed thickening of the wall. Also, the plaque showed uniform or uneven signals, resulting in eccentric thickening of the lumen (Fig. 1), thickening of the wall in the vertebral basilar artery stenosis vessels, and even or uneven signals of the plaque, resulting in eccentric thickening of the lumen (Fig. 2, 3).

The sensitivity, specificity, accuracy, positive predictive value and negative predictive value were 67.85%, 66.67%, 48.27%, 65.51, 48.27%, 65.51 and 68.96, respectively. Among 58 blood vessels, 55 were correctly diagnosed by the black blood technique. The sensitivity, specificity, accuracy, positive, and negative predictive values were 94.11%, 95.83%, 58.62%, 96.96%, and 92%, respectively. With the exception of accuracy, the specificity, sensitivity, positive predictive value and negative predictive value of the black blood technique were higher than those of the MRA technique, and the difference was statistically significant ($P<0.05$) (Table II).

The results of the MRA/black blood imaging and DSA techniques are compared in Table III.

DISCUSSION

This study found that different plaque components showed different signal intensities, which may be related to the composition of plaques. Some studies

Table 1. *Black blood technique image quality score table*

Score	5	4	3	2	1	Total
Internal carotid artery	36	1	0	1	0	38
vertebral basilar	19	1	0	0	0	20
total	55	2	0	1	0	58

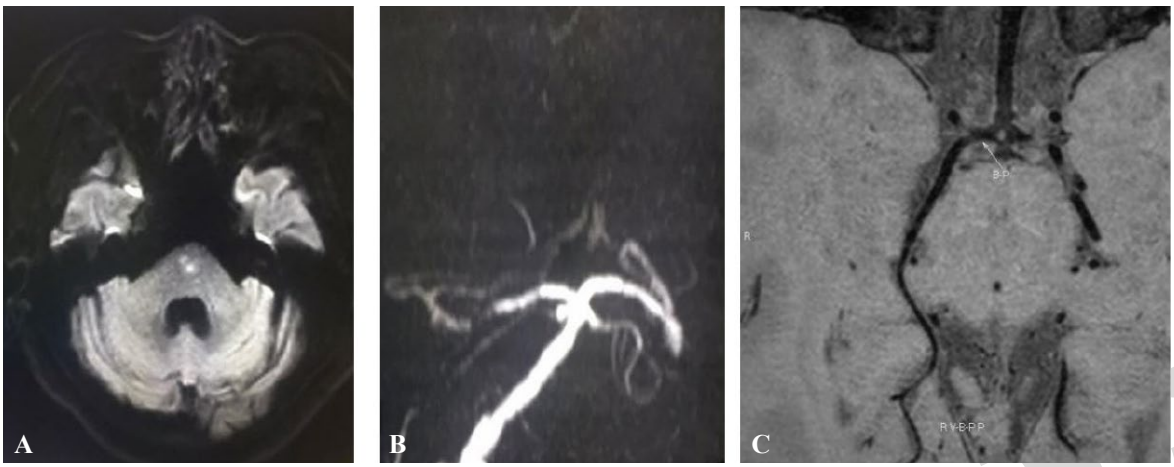


Fig. 1. *A 72-year-old woman with clinical acute cerebrovascular disease.* ***A****) DWI scan shows a slightly higher pontine flake signal.* ***B****) MRA shows right posterior cerebral artery longitudinal segment lumen stenosis.* ***C****) MR high-resolution black blood imaging shows right posterior cerebral artery lumen eccentric stenosis.*



Fig. 2. *A 38-year-old man.* ***A****) Acute cerebral infarction DWI scan shows a punctate high signal in the left parietal lobe.* ***B****) MRA shows left middle cerebral artery horizontal segment localized stenosis, and the distal branch decreased, indicated by the arrow.* ***C****) High-resolution black blood imaging shows left middle cerebral artery horizontal segment concentric stenosis.*

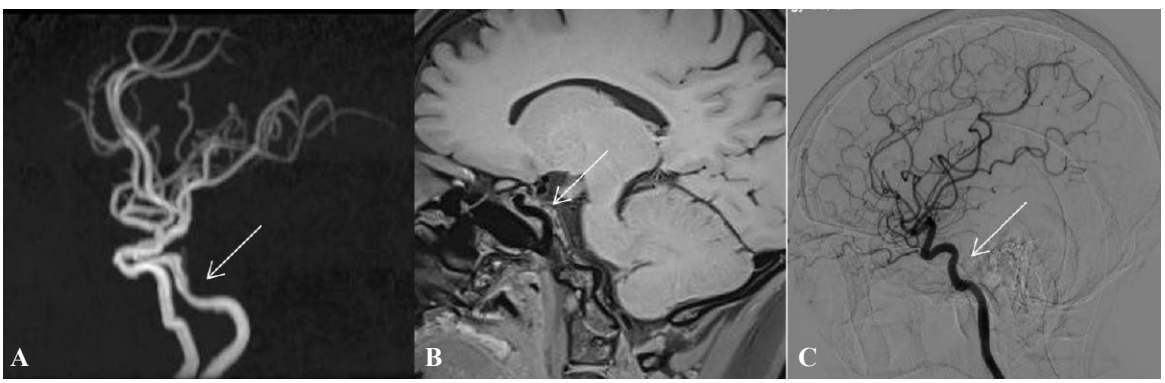


Fig. 3. *Male, 45 years old with clinical TIA onset. A) MRA showed localized stenosis of the right internal carotid artery siphon segment. B) MRA high-resolution black blood imaging was normal and negative. C) DSA confirmed negative findings.*

have shown that there are lipid components or calcification bleeding in plaques. Magnetic resonance high-resolution black blood imaging technology can noninvasively display plaques (4,5). In contrast, conventional imaging examinations, including imaging sequences such as T1 and T2, cannot provide enough details to display the vascular wall, so higher image spatial resolution should be used to display the structure of the vascular wall. Also, the tiny structure of the vascular wall should be revealed by thinning the thickness of the scanned layer.

The high-resolution black blood imaging technique used in this study used 3D T1 imaging sequences, which could better compensate for the cerebrospinal fluid composition. The exclusion of cerebrospinal fluid in the images makes the peripheral blood vessel wall visualization more effective. This study added a shorter TR time of 600 ms to T1WI. To obtain a short scan time (approximately 4 minutes), we reduced the voxel size obtained by using 0.6×0.6×1.0 m3. At the same time, we used parallel processes to image suspicious vessel lesions, which reduced the scan time and helped patients better tolerate the scan and sequence of this study (6).

Intracranial atherosclerosis is a common cause of ischemic stroke worldwide. It is also the most important cause of stroke in Chinese people, accounting for half of the total number of strokes (7). Moreover, patients with intracranial arteriosclerosis have a higher risk of stroke recurrence. MRA and DSA can display intracranial vessels well. However, early manifestations of intracranial atherosclerosis are vascular endothelial cell proliferation, which affects the lumen arrangement. Pathological changes in the vascular wall can only lead to lumen stenosis when the plaque of the vessel progresses to a certain stage; hence, angiographic

Table II. *MRA Comparison of diagnostic parameters of vascular stenosis with black blood imaging*

Methodology	Sensitivity	Specificity	Accuracy	Positive predictive value	Negative predictive value
MRA	67.85	66.67	48.27	65.51	68.96
vascular stenosis with black blood imaging	94.11	95.83	58.62	96.96	92
P	0.016	0.015	0.352	0.002	0.047

Table III. *MRA - comparison of black blood imaging and DSA techniques*

Methodology	Normal group		Narrow group	
	Compliance	Non-compliance	Compliance	Non-compliance
MRA	20	9	19	10
vascular stenosis with black blood imaging	23	2	32	1
Total	43	11	51	11

lumen technology may miss this detail (8,9). Therefore, imaging of intracranial vascular walls has attracted increasing attention in recent years (10).

As the preferred imaging method for intracranial vascular screening, MRA has a high specificity, but there are still some limitations (11). This study shows that the specificity, sensitivity, positive predictive value and negative predictive value of the black-blood technique are all higher than those of the MRA technique, and the difference is statistically significant. Magnetic resonance high-resolution black artery wall imaging technology has the following characteristics: use of three-dimensional high-resolution brain black artery wall imaging, volume acquisition, conducive to three-dimensional postprocessing, providing T1 contrast, helps to detect intracranial lesions and qualitatively, achieves arbitrary program arbitrary angle high-definition three-dimensional reconstruction, and helps to shorten the scanning time of the overall intracranial artery disease detection program (12, 13).

In previous studies, different contrast-weighted sequences were used to obtain and test vessel wall imaging of the carotid artery. These different image contrast weights could be applied to diagnose atherosclerotic plaques (14). Whether this approach also applies to intracranial atherosclerosis is unclear, and intraplaque haemorrhage confirms the use of T1WI and PDWI (15). Due to the lack of pathological control studies, the ability to judge vulnerable plaques will need to be further studied in the future.

ACKNOWLEDGMENTS

This work was supported by the Hebei Provincial Medical Subject Research Fund (No. 20190697).

Conflict of interest

The authors declare that there are no conflicts of interest.

REFERENCES

1. Chinese Stroke Society. Guidelines for Clinical Management of Cerebrovascular Diseases in China. Beijing: People's Health Publishing; 2019:97-100.
2. Yuan C, Mitsumori LM, Ferguson MS, et al. In vivo accuracy of multispectral magnetic resonance imaging for identifying lipid-rich necrotic cores and intraplaque hemorrhage in advanced human carotid plaques. Circulation 2001; 104:2051-2056.
3. Swartz RH, Bhuta SS, Farb RI, et al. Intracranial arterial wall imaging using high-resolution 3-tesla contrast-enhanced MRI. Neurology 2009; 72:627-634.
4. Naghavi M, Libby P, Falk E, et al. From vulnerable plaque to vulnerable patient :a call f or new definition s and risk assessment trategies: Part I. Circulation 2003; 108:1664-1672.
5. Cai JM, Hatsuk ami TS, Ferguson MS, et al. Classification of human carotid atherosclerotic lesions with in vivo multi contrast magnetic resonance imaging. Circulation 2002; 106:1368-1373.
6. Qiao Y, Steinman DA, Qin Q, et al. Intracranial arterial wall imaging using three-dimensional high isotropic resolution black blood MRI at 3.0 Tesla. J Magn Reson Imaging 2011; 34:22–30.
7. Saam T, Hatsukami TS, Takaya N, et al. The vulnerable, or high-risk, atherosclerotic plaque: noninvasive MR imaging for characterization and assessment. Radiology 2007; 244:64–77.
8. Chinese Stroke Society, Neurointervention Branch of Chinese Stroke Society, Interventional Group of Stroke Prevention and Control Committee of Chinese Preventive Medicine Association. Chinese guidelines for endovascular treatment of acute ischemic stroke 2018. Chinese Journal of Stroke 2018; 13:706-728.
9. Yang Y, Xue T, Zhu J, et al. Serum lipoprotein-associated phospho- lipase A2 predicts the formation of carotid artery plaque and its vulnerability in anterior circulation cerebral infarction. Clin Neurol Neurosurg 2017; 160:40-45.
10. Wang R, Dong R. serum inflammatory markers and carotid plaque stability. International Journal of Cerebrovascular Disease 2019; 27:57-62.
11. Takaya N, Yuan C, Chu B, et al. Association between carotid plaque characteristics and subsequent ischemic cerebrovascular events: a prospective assessment with MRI—initial results. Stroke 2006; 37:818–823.
12. Hellings WE, Peeters W, Moll FL, et al. Composition of carotid atherosclerotic plaque is associated with cardiovascular outcome: A prognostic study. Circulation 2010; 121:1941–1950.

PROOF

13. Qiao Y, Etesami M, Astor BC, Zeiler SR, Trout HH 3rd, Wasserman BA. Carotid plaque neovascularization and hemorrhage detected by MR imaging are associated with recent cerebrovascular ischemic events. AJNR Am J Neuroradiol 2012; 33:755–760.
14. Virmani R, Kolodgie FD, Burke AP, et al. Atherosclerotic plaque progression and vulnerability to rupture: angiogenesis as a source of intraplaque hemorrhage. Arter Thromb Vasc Biol 2005; 25:2054–2061.
15. Turan TN, Bonilha L, Morgan PS, et al. Intraplaque hemorrhage in symptomatic intracranial atherosclerotic disease. J Neuroimaging 2011; 21:e159–61.

Correlation between dyslalia and skeletal and dental malocclusions

G. Galbiati[1], L. Giannini[1], E. Del Rosso[1,2], P. Cressoni[1,2], FMR Parisi[1*] and L. Esposito[1,2]

[1]Department of Biomedical, Surgical and Dental Sciences, School of Dentistry, University of Milan, Italy; [2]Fondazione IRCCS Cà Granda, Ospedale Maggiore Policlinico, Milan, Italy

Received November 4, 2021 – Accepted February 10, 2022

To the Editor,

Dyslalia is a speech disorder characterized by the inability to articulate some phonemes properly, and it is one of the disorders that occurs more frequently in children (1, 2); it can only be detected when these disorders persist or occur after the third year of age. These disorders are divided schematically into organic and functional groups, but clinical limits are often rather unclear. Dental origin dyslalia, also called maxillofacial dyslalia, is the most interesting one for orthodontists since they are connected to several masticatory pathologies (3, 4).

The therapy must be addressed to orthodontic treatment and speech therapy treatment to obtain stable results. Furthermore, skeletal and dental malocclusion can determine functional limitations, social well-being and oral symptoms.

It is necessary to investigate genetic factors, relatives and personal medical anamnesis, to search for signs of possible infectious diseases of childhood or any hormonal deficiencies etc. The presence of these maxillo-dental dysmorphisms leads to different medical cases, depending on whether it is an adult or a growing patient (5, 6).

In adults, the loss of many dental elements, their wrong alignment on the arches, bad occlusal relationships due to fractures of the jaw or mono or bilateral temporomandibular joint (T.M.J.) dislocations, have a less impact on the pronunciation of the different phonemes (7). The chewing muscles and others like tongue, lips, cheeks and the shape of dental arches may change the airway and the respiratory breath (8-10).

This work aims to analyze the available literature about the relationship between malocclusions and dyslalia and emphasize the interdisciplinary treatment between them.

MATERIALS AND METHODS

A literature review has been performed through Medline database (PubMed and Cochrane). The various combinations of the chosen keywords have been used as the search strip and they were malocclusion, dyslalia and speech therapy.

The inclusion criteria for the choice of articles were as follow: articles published between 1950 and 2021, only articles referring to "Humans", only systematic revision. The study was conducted according to the Preferred Reporting Items for Systematic Reviews and Meta-Analyses (PRISMA-P) 2015. Grey literature was also reviewed, but none was included. A hand search for relevant studies in selected papers' references was also performed (Fig. 1).

Meta-analysis of data was impossible because of the heterogeneity of study designs and assessed technological tools. However, no other limitations appear to be present

Keywords: skeletal malocclusions, dental, children, dyslalia, speech therapy

**Corresponding author:*
Dr Francesca Maria Rita Parisi
Department of Biomedical, Surgical and Dental Sciences,
School of Dentistry, University of Milan,
Via dell'Unione 8,
20122, Milan, Italy
e-mail: francescamr.parisi@gmail.com

0393-974X (2022)
Copyright © by BIOLIFE, s.a.s.
This publication and/or article is for individual use only and may not be further reproduced without written permission from the copyright holder.
Unauthorized reproduction may result in financial and other penalties
DISCLOSURE: ALL AUTHORS REPORT NO CONFLICTS OF INTEREST RELEVANT TO THIS ARTICLE.

as the present review was conducted according to PRISMA-P guidelines.

All subjects gave informed, signed consent to participate in the study, or informed the family or guardian gave written consent in the case of children or deceased.

RESULTS

Initially 28 articles were found. The primary search retrieved 21 articles, net of elimination of duplicates (n =7). Then 10 articles were deemed irrelevant after screening the abstract, the title or the study design and therefore were excluded. Eleven records were screened from database and other 3 articles were excluded for bias. Finally, 8 studies were read in extenso and were included in the qualitative analysis.

DISCUSSION

The malocclusion with a strong correlation with dyslalia is the open-bite (3). In particular, Harrington and Breinholt correlated incorrect pronunciation of certain consonants, which occurs in open-bite, with protruding anterior teeth, and paid specific attention if incorrect articulation of speech lengthened in time could lead to further negative effects on dental arches and jaw growth. Even Bernstein stressed the relationship between the lips of many patients with open-bite but reported that the severity of the speech defect was not correlated with the level of open-bite or overjet. This author also found that some individuals with open-bites are still able to correctly pronounce the hissing phonemes thanks to compensatory adjustments of the lower lip in relation to the airflow, and in this way it develops the required air turbulence. Some authors have pointed out that the consonants S, Z, F, V are the most frequently altered in the case of open-bite.

Another malocclusion that affects speech is Class III. These patients in fact have a higher prevalence of articulation errors and spectral distortions in consonants relative to controls. It was demonstrated that that severity of malocclusion is quantitatively correlated with the degree of speech distortion for consonants and consequently that there is a relationship between craniofacial structures and speech distortions (11).

Three-dimensional ultrasonographic assessment of the tongue can be considered an objective radiation free diagnostic tool, useful for displaying tongue size, shape and posture and for recording functional tongue movements (12) (Fig. 2).

It cannot be ignored that there is a clear correlation

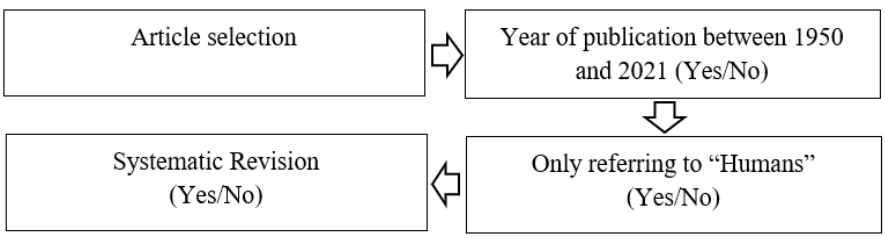


Fig. 1: *Article selection flow chart*



Fig. 2: *Intraoral views of anterior open-bite*

between malocclusions and dyslathic defects. From the study of the literature, a strong correlation between facial dysmorphism and phonetic articulation is pointed out: a neuromuscular dysfunction of stomatognathic system usually allows the beginning of a facial dysmorphism that, therefore, may cause an additional diverting effect on the neuromuscular dysfunction.

From this, it comes out the need for collaboration between speech therapist (specialists in changing muscular movements), and orthodontists (specialists of morphological changes). It becomes fundamental not only to give patients faster and better therapeutic results, but above all in a scientific researching way, to give a more complete pathophysiological explanation.

Author contributions:

All authors actively participated to all phases of the manuscript. All authors have read and agreed to the published version of the manuscript. The authors declare no conflict of interest.

REFERENCES

1. Farronato G, Giannini L, Riva R, Galbiati G, Maspero C. Correlations between malocclusions and dyslalias. Eur J Paediatr Dent 2012; 13(1):13-18.
2. Forsythe R, Murphy CA, Tulip J, Law J. Why Clinicians Choose Their Language Intervention Approach: An International Perspective on Intervention for Children with Developmental Language Disorder. Folia Phoniatr Logop 2021; 73(6): 537-551.
3. Pisani L, Bonaccorso L, Fastuca R, Spena R, Lombardo L, Caprioglio A. Systematic review for orthodontic and orthopedic treatments for anterior open bite in the mixed dentition. Prog Orthod 2016; 17(1): 28.
4. Lanteri V, Farronato M, Ugolini A, et al. Volumetric Changes in the Upper Airways after Rapid and Slow Maxillary Expansion in Growing Patients: A Case-Control Study. Materials (Basel) 2020; 13(10):2239.
5. Contaldo M, Lucchese A, Lajolo C, et al. The Oral Microbiota Changes in Orthodontic Patients and Effects on Oral Health: An Overview. J Clin Med 2021;10(4):780.
6. Blanck-Lubarsch M, Dirksen D, Feldmann R, Sauerland C, Hohoff A. Tooth Malformations, DMFT Index, Speech Impairment and Oral Habits in Patients with Fetal Alcohol Syndrome. Int J Environ Res Public Health 2019; 16(22):4401.
7. Lo Giudice A, Ronsivalle V, Grippaudo C, et al. One Step before 3D Printing-Evaluation of Imaging Software Accuracy for 3-Dimensional Analysis of the Mandible: A Comparative Study Using a Surface-to-Surface Matching Technique. Materials (Basel) 2020;13(12):2798.
8. Di Palma E, Tepedino M, Chimenti C, Tartaglia GM, Sforza C. Longitudinal effects of rapid maxillary expansion on masticatory muscles activity. J Clin Exp Dent 2017; 9(5):e635-40.
9. Farronato G, Giannini L, Galbiati G, Maspero C. Sagittal and vertical effects of rapid maxillary expansion in Class I, II, and III occlusions. Angle Orthod 2011; 81(2):298-303.
10. Gomersall T, Spencer S, Basarir H, et al. Measuring quality of life in children with speech and language difficulties: a systematic review of existing approaches. Int J Lang Commun Disord 2015; 50(4):416-35.
11. Lathrop-Marshall H, Keyser MMB, Jhingree S, et al. Orthognathic speech pathology: impacts of Class III malocclusion on speech. Eur J Orthod 2021, 2021:cjab067.
12. Kravanja SL, Hocevar-Boltezar I, Marolt Music M, et al. Three-dimensional Ultrasound Evaluation of Tongue Posture and Its Impact on Articulation Disorders in Preschool Children with Anterior Open Bite. Radiol Oncol 2018; 52(3):250–256.

DLX6-AS1 increases the malignancy of oral squamous cell carcinoma cells via regulating miR-199a-5p/SOX4 axis

H. Li[1#], H. Huang[1#], Y.S. Li[1], Q. Zhang[1], X.T. Pan[1], H. Yang[1], Y. Zhang[2], F. Huo[2] and J.H. Jiang[3]

[1]Department of Stomatology, The First Affiliated Hospital of Nanchang University, Nanchang, Jiangxi Province, China; [2]Department of Stomatology, Affiliated Hospital of Chengde Medical College, Chengde, Hebei Province, China; [3]Department of Stomatology, Jiangxi Provincial People's Hospital, The First Affiliated Hospital of Nanchang Medical College, Nanchang, Jiangxi Province, China

Received May 18, 2021 – Accepted February 9, 2020

[#]These authors contributed equally

To the Editor,

Oral squamous cell carcinoma (OSCC) incidence increases year by year, especially in less developed countries. Despite the great progress in diagnosis and therapy of OSCC during the last few decades, OSCC patients' 5-year survival rate is still less than 50% (1). In such a context, it is crucial to decipher the molecular mechanisms in OSCC for providing novel insights into the treatment of OSCC.

Identified as a category of non-coding RNAs with a length longer than 200 nucleotides, long non-coding RNAs (lncRNAs) are pivotal in regulating multiple cellular processes, e.g., cell proliferation, migration and apoptosis (2). Many studies illustrate that lncRNAs serve as oncogenic lncRNAs or tumor suppressors and are implicated in OSCC development (3). The gene of lncRNA DLX6 antisense RNA 1 (DLX6-AS1) is located at chromosome 7q21.3. Its transcript acts as an oncogenic lncRNA in many cancers, for instance, laryngeal squamous cell carcinoma (4). Nonetheless, DLX6-AS1 expression characteristics and its biological function in OSCC have not been studied.

In the present work, we report that DLX6-AS1 is up-regulated in OSCC cells and functioning as a competitive endogenous RNA (ceRNA); it facilitates OSCC cell growth, migration and invasion of OSCC cells represses apoptosis through sponging miR-199a-5p and up-regulating SRY-box transcription factor 4 (SOX4).

MATERIALS AND METHODS

Cell culture and transfection

Four human OSCC cell lines (CAL-27, HSU3, SCC-4 and SCC15) were obtained from American Type Culture Collection (ATCC, Manassas, VA, USA), and human normal oral epithelial cell line (NHOK) was obtained from the Cell Bank of the Chinese Academy of Sciences (Shanghai, China). The cells were cultured at 37˚C in 5% CO_2 in Roswell Park Memorial Institute (RPMI)-1640 medium (Sigma-Aldrich, Merck KGaA, Darmstadt, Germany) supplemented with 100 IU/ml penicillin, 100 mg/ml streptomycin and 10% fetal bovine serum (FBS; Sigma-Aldrich). Cell lines SCC-15 and SCC-4 were selected for cell transfection. DLX6-AS1 short-hairpin RNA (sh-DLX6-AS1), shRNA control (sh-NC), miR-199a-5p inhibitors and miR-199a-5p mimics and the corresponding negative controls (miR-NC) were provided by GenePharm (Shanghai, China). SOX4

Keywords: DLX6-AS1; oral squamous cell carcinoma; SOX4; miR-199a-5p

[*]*Corresponding author:*
Dr Jiang Jun-Hong,
Department of Stomatology, Jiangxi Provincial People's Hospital
The First Affiliated Hospital of Nanchang Medical College,
Nanchang, Jiangxi Province, China
e-mail: Jiangjunhong858@163.com

0393-974X (2022)
Copyright © by BIOLIFE, s.a.s.
This publication and/or article is for individual use only and may not be further reproduced without written permission from the copyright holder.
Unauthorized reproduction may result in financial and other penalties
DISCLOSURE: ALL AUTHORS REPORT NO CONFLICTS OF INTEREST RELEVANT TO THIS ARTICLE.

overexpression plasmid pcDNA3.1-SOX4 and empty vector pcDNA3.1 were provided by GeneChem (Shanghai, China). Lipofectamine™ 3000 (Invitrogen, Carlsbad, CA, USA) was adopted for cell transfection according to the manufacturer's protocol.

Quantitative real-time polymerase chain reaction (qRT-PCR)

TRIzol reagent (Invitrogen, Carlsbad, CA, USA) was adopted for RNA extraction from OSCC cells following the manufacturer's protocol. First, the reverse transcription was conducted with a Reverse Transcription Kit (TaKaRa, Dalian, China) to synthesize complementary DNA (cDNA). Then, with cDNA as template and SYBR Premix Ex Taq II (Invitrogen, Carlsbad, CA, USA), on ABI7500 real-time PCR system (Applied Biosystems, Carlsbad, CA, USA), qRT-PCR was performed. GAPDH functioned as the internal reference control for DLX6-AS1 and SOX4, and U6 served as an endogenous control for miR-199a-5p. The relative quantification method ($2^{-\Delta\Delta Ct}$ formula) was utilized to calculate the relative expression levels of the target genes. The primers are as follows: DLX6-AS1: F: 5'-AGTTTCTCTCTAGATTGCCTT-3' and R: 5'-ATTGACATGTTAGTGCCCTT-3'; miR-199a-5p: F: 5'- TCCCAGTGTTCAGACTACC-3' and R: 5'-TTTGGCACTAGCACATT-3'; SOX4: F: 5'-CCAGTTCTTGCACGCTGTTT-3' and R: 5'-TGTTGCAAGGTAGGAAGCCA-3'; U6: F: 5'-CTCGCTTCGGCAGCACA-3' and R: 5'-AACGCTTCACGAATTTGCGT-3'; GAPDH: F: 5'-CCAAAATCAGATGGGGCAATGCTGG-3' and R: 5'-TGATGGCATGGACTGTGGTCATTCA-3'.

Cell proliferation assay

For the MTT assay, SCC-15 and SCC-4 cells were inoculated into 96-well plates (1×10^3 per well). After the cells were cultured for 24 h, 20 μL MTT solution (5 mg / mL) was added into each well, with which the cells were incubated for 4 h; successively, 150 μL of dimethyl sulfoxide (DMSO) was added to each well, and the plate was shaken on a shaker for 10 min to dissolve the formazan crystals. After that, a microplate reader (Bio-Rad, Hercules, CA, USA) was employed to detect the optical density (OD) values of the cells at 490 nm (0 h). Similarly, the OD values were detected at 48 h and 72 h. OSCC cell growth was also measured with EdU Kit (RiboBio, Guangzhou, China). OSCC cells were transferred into a 96-well plate (5×10^3 cells / well) and cultured for 48 h. Subsequently, each well was added with 50 μM of EdU solution, and the cells were incubated for 4 h. Next, the cells were fixed with 4% formaldehyde, and the Apollo Dye Solution and DAPI solution were used to stain the cells. Subsequently, an inverted fluorescence microscope (Nikon Eclipse Ti Microscope, Tokyo, Japan) was employed for observing and photographing the cells. Then the EdU-positive cells were counted.

TUNEL assay

TUNEL assay was performed with a one-step TUNEL apoptosis assay kit (Beyotime, Shanghai, China). First, cells were treated with fluorescein-TUNEL reagent and then stained by DAPI staining solution. Next, apoptotic cells were observed using an inverted microscope (Olympus, Tokyo, Japan).

Transwell assay

OSCC cell migration and invasion were examined by Transwell chambers (Corning, NY, USA) without (for migration assay) and with (for invasion assay) Matrigel (BD, Bedford, MA, USA), respectively. In each well, OSCC cells which were in serum-free RPMI-1640, were inoculated into the upper compartment (5×10^4 OSCC cells / well), and the lower compartment was added with 600 μL of 10% FBS-containing medium. Then the culture was continued, and 48 h later, cells attached to the lower surface of the Transwell membrane were fixed for 30 min with methanol and stained for 20 min with crystal violet solution. Finally, an inverted microscope (Olympus, Tokyo, Japan) was used for counting the stained cells.

Western blotting

Total protein of OSCC samples was extracted by RIPA lysis buffer (Biosharp, Hefei, China). Following the bicinchoninic acid protein assay kit (Biosharp, Hefei, China), sodium dodecyl sulfate-polyacrylamide gel electrophoresis was adopted for separating equal amount of protein samples (20 μg / lane). Then the proteins were transferred onto polyvinylidene fluoride (PVDF) membranes (GE Healthcare Life Sciences, Little Chalfont, UK). Subsequently, membranes were blocked with 5% skim milk (Sigma-Aldrich, Darmstadt, Germany) for 1 h at room temperature. Next, the PVDF membranes were incubated overnight at 4°C with primary antibodies (Abcam, Cambridge, UK) and incubated for 2 h with HRP-

conjugated secondary antibodies (Abcam, Cambridge, UK) at room temperature in sequence. Next, the development of the protein bands was accomplished by the ECL substrate kit (Amersham Biosciences, Little Chalfont, UK).

Dual-luciferase reporter assay and RNA immunoprecipitation (RIP) assay

PCR was used to amplify DLX6-AS1 and SOX4 sequences with the predicted binding site for miR-199a-5p, which were then cloned into pGL3 vectors (Promega, Madison, WI, USA) to construct wild type (WT) luciferase reporter vectors. Subsequently, the binding site-mutated DLX6-AS1 and SOX4 sequences were used to construct mutant type (MUT) luciferase reporter vectors. Next, Lipofectamine™ 3000 (Invitrogen, Carlsbad, CA, USA) was used to transfect the recombinant vectors and miR-199a-5p mimics (or miR-NC) into 293T cells. After 48 h, the dual-luciferase reporter system (Promega, Madison, WI, USA) was employed to determine each group's luciferase activities. The firefly luciferase activity was normalized by Renilla luciferase activity. Following the manufacturer's instruction, a Magna RIP RNA-Binding Protein Immunoprecipitation kit (Millipore, Billerica, MA, USA) was utilized for performing the RIP assay. After OSCC cells were lysed with RIP lysis buffer containing protease inhibitors and RNase inhibitors, the mixtures were incubated at 4 °C with magnetic beads coated with anti-Argonaute 2 (Ago2) antibodies (Millipore, Billerica, MA, USA) for 2 h. Immunoglobin G (IgG) served as the negative control. After that, the immunoprecipitation complex was incubated with proteinase K, and co-immunoprecipitated RNA was extracted with the TRIzol method. Ultimately, qRT-PCR was performed to detect the expression levels of miR-199a-5p and DLX6-AS1 in the immunoprecipitate.

Statistical analysis

The data in this study were processed by GraphPad Prism version 6.0 (GraphPad Software, Inc., San Diego, CA, USA). Mean ± standard deviation (SD) was the expression form of the data. Student's *t*-test or One-Way ANOVA was utilized for evaluating the significance of differences. $P < 0.05$ denoted statistical significance.

RESULTS

In OSCC cell lines, DLX6-AS1 expression was analyzed by qRT-PCR, and it was discovered that in comparison with NHOK cells, DLX6-AS1 expression in OSCC cell lines (HSU3, SCC-4, CAL-27 and SCC-15) was much higher (Fig. 1A). In addition, DLX6-AS1 was the most highly expressed in SCC-15 and SCC-4 cells (Fig. 1A), so these two cell lines were selected for follow-up experiments; in order to investigate the biological functions of DLX6-AS1 in OSCC, three DLX6-AS1 shRNAs (sh-DLX6-AS1#1&#2&#3) were transfected into SCC-15 and SCC-4 cells, and it was revealed that these shRNAs could significantly reduce DLX6-AS1 expression in OSCC cells. Among the three, sh-DLX6-AS1#1 had the highest efficiency, so it was selected for subsequent experiments (Fig. 1B). MTT, EdU and TUNEL assays were utilized to analyse cell proliferation and apoptosis, and it was demonstrated that DLX6-AS1 knockdown notably inhibited OSCC cell proliferation and promoted cell apoptosis compared to the control group (Fig. 1C-F). In addition, the Transwell assay confirmed that transfection of DLX6-AS1 shRNA significantly suppressed SCC-15 and SCC-4 cell migration and invasion abilities (Fig. 1G-H). The results showed that DLX6-AS1 could promote the malignancy of OSCC cells.

Bioinformatics analysis based on the StarBase database (http://starbase.sysu.edu.cn/) suggested that DLX6-AS1 contained a possible binding site of miR-199a-5p (Fig. 2A). Subsequently, qRT-PCR displayed that as against NHOK cells, miR-199a-5p expression in SCC-15 and SCC-4 was much lower (Fig. 2B). Furthermore, dual-luciferase reporter assay indicated that co-transfection of miR-199a-5p mimics and DLX6-AS1-WT could considerably decrease the luciferase activity, while co-transfection of DLX6-AS1-MUT and miR-199a-5p did not influence the luciferase activity (Fig. 2C). Moreover, RIP assay showed that miR-199a-5p and DLX6-AS1 were dramatically enriched in the immunoprecipitate in Ago2 group as against the control group (Fig. 2D). These data suggested that DLX6-AS1 could sponge miR-199a-5p and probably regulate its expression.

Next, rescue experiments were carried out to identify whether DLX6-AS1 played a role in OSCC through a miR-199a-5p-dependent manner. MTT, EdU, and TUNEL assays displayed that miR-199a-5p

inhibitor could partially offset the effect of DLX6-AS1 knockdown on cell proliferation and apoptosis (Fig. 3A-C). Furthermore, Transwell assay showed that co-transfection of miR-199a-5p inhibitors and DLX6-AS1 shRNA could greatly inhibit the impact of DLX6-AS1 knockdown on SCC-15 and SCC-4 cell

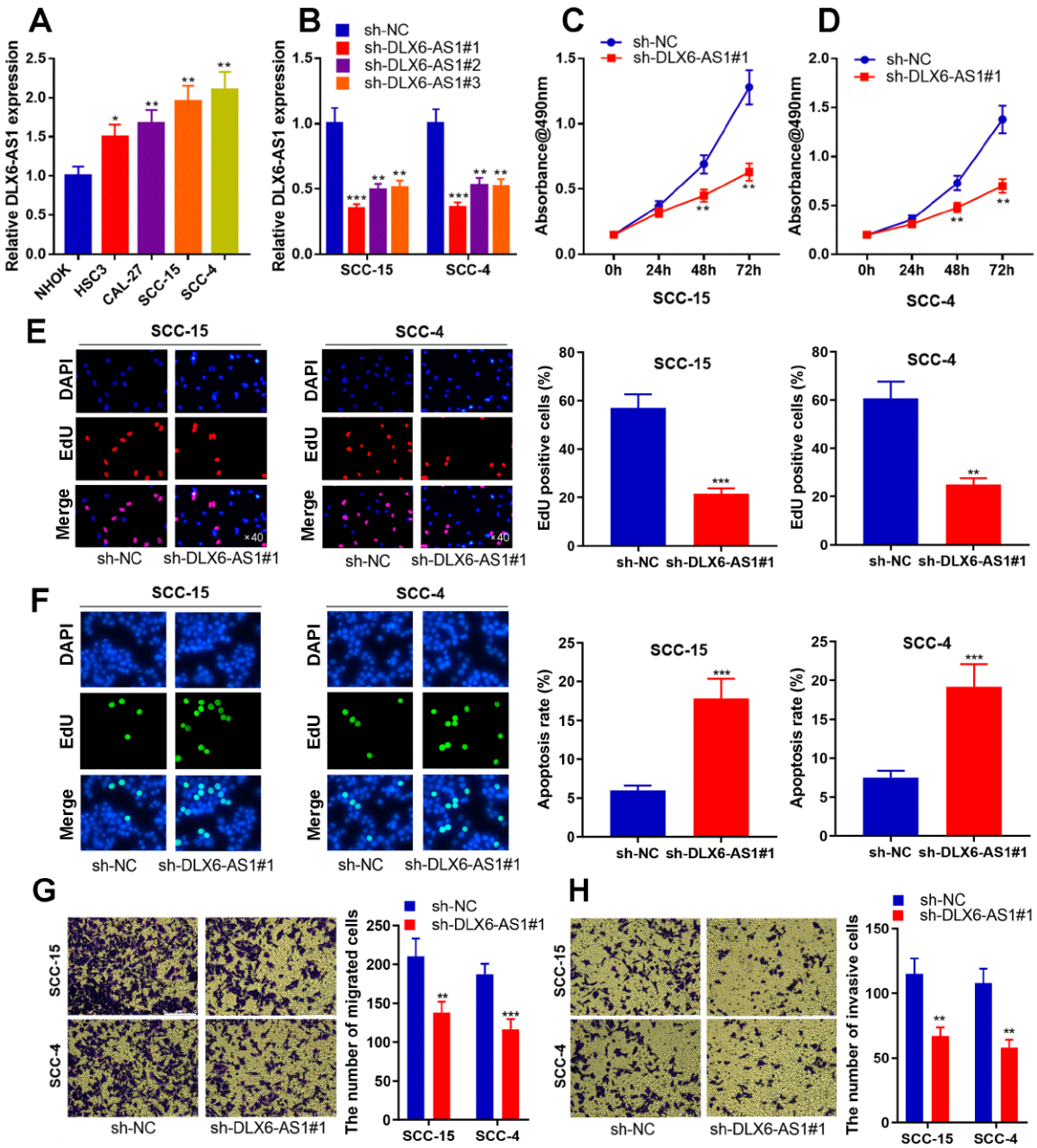


Fig. 1. *DLX6-AS1 is highly expressed in OSCC tissues, and it increases the malignancy of OSCC cells.* ***A****): qRT-PCR was adopted for comparing DLX6-AS1 expression in OSCC cell lines and NHOK cell line;* ***B****): qRT-PCR was utilized for detecting DLX6-AS1 expression after transfection with DLX6-AS1 shRNA into OSCC cells;* ***C-D****): MTT assay was employed for detecting the change in OSCC cell proliferation after transfection with DLX6-AS1 shRNA;* ***E****): EdU assay was conducted for detecting OSCC cell proliferation change after transfection of DLX6-AS1 shRNA;* ***F****): TUNEL assay was conducted for detecting OSCC cell apoptosis change after transfection of DLX6-AS1 shRNA;* ***G-H****): Transwell assay was conducted for examining the change of cell migration and invasion abilities after OSCC cells were transfected with DLX6-AS1 shRNA. *P < 0.05, **P < 0.01, and ***P < 0.001.*

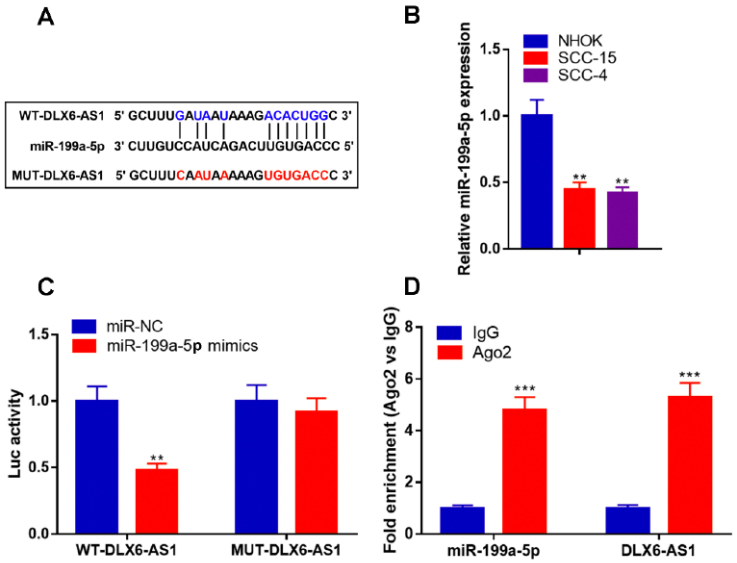


Fig. 2. *miR-199a-5p is a direct target of DLX6-AS1 in OSCC. **A**): StarBase database showed that DLX6-AS1 contained the potential binding site for miR-199a-5p; **B**): qRT-PCR was applied for detecting miR-199a-5p expression in SCC-15 and SCC-4 cells; **C**): Dual-luciferase report assay was conducted for confirming the binding relationship between miR-199a-5p and DLX6-AS1; **D**): RIP assay was utilized for confirming the direct interaction between DLX6-AS1 and miR-199a-5p. **P < 0.01 and ***P < 0.001.*

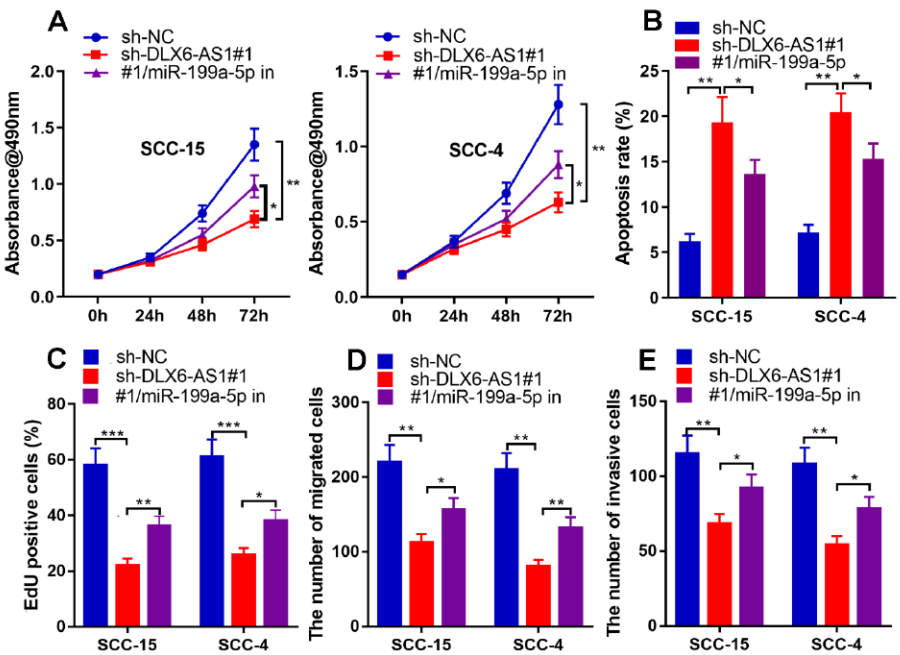


Fig. 3. *miR-199a-5p inhibitor abolishes the impact of DLX6-AS1 knockdown on OSCC cells. **A**): MTT assay was conducted for examining the change in OSCC cell proliferation after co-transfection with miR-199a-5p inhibitor and DLX6-AS1 shRNA into cells; **B**): TUNEL assay was conducted for examining the change in OSCC cell apoptosis after co-transfection with miR-199a-5p inhibitor and DLX6-AS1 shRNA; **C**): EdU assay was conducted for examining the change in OSCC cell proliferation after co-transfection of miR-199a-5p inhibitor and DLX6-AS1 shRNA; **D-E**): Transwell assay was utilized for detecting the change in OSCC cell invasion and migration abilities after co-transfection of miR-199a-5p inhibitor and DLX6-AS1 shRNA. *P < 0.05, **P < 0.01, and ***P < 0.001.*

migration and invasion abilities (Fig. 3D-E). Hence, the findings mentioned above show that DLX6-AS1 can play a role in OSCC progression by repressing miR-199a-5p.

It is reported that miR-199a-5p suppresses the migration and invasion of OSCC cells through inhibiting SOX4 (5). We then explored whether DLX6-AS1/miR-199a-5p axis regulated the expression of

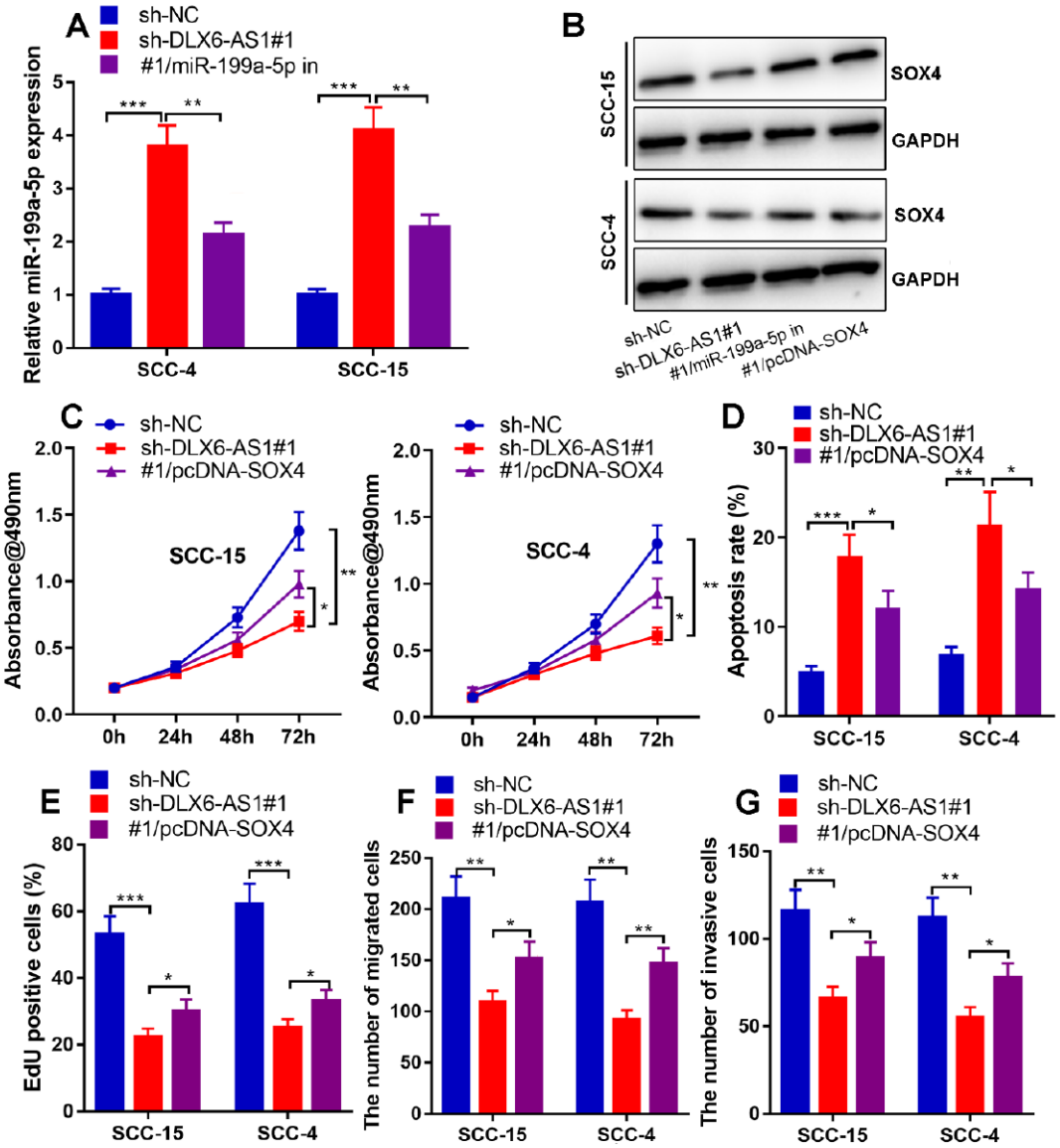


Fig. 4. *DLX6-AS1 plays a part in OSCC via regulating miR-199a-5p/SOX4 axis.* ***A****): qRT-PCR was used to detect the change in miR-199a-5p expression level after co-transfection with miR-199a-5p inhibitor and DLX6-AS1 shRNA into cells;* ***B****): Western blot experiment was conducted for detecting the change of SOX4 expression after co-transfection of DLX6-AS1 shRNA and miR-199a-5p inhibitor or DLX6-AS1 shRNA and SOX4 overexpression plasmid;* ***C****): MTT assay was conducted for examining the change in OSCC cell proliferation after co-transfection with DLX6-AS1 shRNA and SOX4 overexpression plasmid;* ***D****): TUNEL assay was conducted for examining the change in OSCC cell apoptosis after co-transfection with DLX6-AS1 shRNA and SOX4 overexpression plasmid;* ***E****): EdU assay was conducted to examine the change in OSCC cell proliferation after co-transfection of DLX6-AS1 shRNA and SOX4 overexpression plasmid;* ***F-G****): Transwell assay was utilized for detecting the change of OSCC cell migration and invasion abilities after co-transfection of SOX4 overexpression plasmid and DLX6-AS1 shRNA. *P < 0.05, **P < 0.01 and ***P < 0.001.*

SOX4. It was revealed that DLX6-AS1 knockdown could enhance miR-199a-5p expression and reduce SOX4 expression in OSCC cells, while co-transfection of miR-199a-5p inhibitor or SOX4 overexpression plasmid could restore the expression of SOX4 (Fig. 4A-B). Furthermore, MTT, EdU and TUNEL assays implied that co-transfection of SOX4 overexpression plasmid could significantly reverse the inhibiting impact of DLX6-AS1 knockdown on cell proliferation (Fig. 4C-E). After co-transfection with SOX4 overexpression plasmid, the migration and invasion abilities of OSCC cells were also promoted (Fig. 4F-G). These data showed that DLX6-AS1 regulated OSCC progression through miR-199a-5p/SOX4 axis.

DISCUSSION

A previous study showed that DLX6-AS1 expression is high in laryngeal cancer cells and tissues, and its high expression is associated with the poor prognosis of patients, and DLX6-AS1 modulates cancer cell proliferation, mitochondrial calcium uptake and reactive oxygen species production by regulating miR-26a/TRPC3 axis (4, 6). In oesophagal squamous cell carcinoma, DLX6-AS1 can adsorb miR-577 to promote cancer cell proliferation and migration (7). In this research, we demonstrated that DLX6-AS1 expression was elevated in OSCC cell lines for the first time. The *in vitro* functional experiments indicated that DLX6-AS1 silencing could significantly repress OSCC cell proliferation, migration and invasion and promote apoptosis. The data mentioned above suggested that DLX6-AS1 is a tumor promoter in OSCC.

LncRNA can function as ceRNA and negatively regulate miRNA expression and participate in tumor development (8). It is reported that miR-199a-5p expression is reduced in OSCC cell lines and tissues, miR-199a-5p suppresses OSCC progression by inhibiting SOX4 (5). The current study revealed that DLX6-AS1 could adsorb miR-199a-5p as a molecular sponge to modulate SOX4 expression. In addition, miR-199a-5p inhibition or SOX4 overexpression could partially reverse the inhibiting impact of DLX6-AS1 knockdown on OSCC cells. These data suggested that DLX6-AS1, miR-199a-5p and SOX4 formed a ceRNA network to modulate OSCC progression. Collectively, our study suggests that DLX6-AS1 may be a new target of OSCC therapy, which remains to be validated by *in vivo* experimental models in the following studies.

Notes

The authors declare no conflict of interest. The data used to support the findings of this study are available from the corresponding author upon request.

REFERENCES

1. Roi A, Roi CI, Negruțiu ML, Riviș M, Sinescu C, Rusu LC. The Challenges of OSCC Diagnosis: Salivary Cytokines as Potential Biomarkers. J Clin Med 2020; 9(9):2866.
2. Chi Y, Wang D, Wang J, Yu W, Yang J. Long Non-Coding RNA in the Pathogenesis of Cancers. Cells 2019; 8(9):1015.
3. Zhang L, Meng X, Zhu XW, Yang DC, Chen R, Jiang Y, Xu T. Long non-coding RNAs in Oral squamous cell carcinoma: biologic function, mechanisms and clinical implications. Mol Cancer 2019; 18(1):102.
4. Yang Q, Sun J, Ma Y, Zhao C, Song J. LncRNA DLX6-AS1 promotes laryngeal squamous cell carcinoma growth and invasion through regulating miR-376c. Am J Transl Res 2019; 11(11):7009-7017.
5. Wei D, Wang W, Shen B, et al. MicroRNA-199a-5p suppresses migration and invasion in oral squamous cell carcinoma through inhibiting the EMT-related transcription factor SOX4. Int J Mol Med 2019; 44(1):185-195.
6. Liu Y, Liu X, Zhang X, Deng J, Zhang J, Xing H. lncRNA DLX6-AS1 Promotes Proliferation of Laryngeal Cancer Cells by Targeting the miR-26a/TRPC3 Pathway. Cancer Manag Res 2020; 12:2685-2695.
7. Wu SB, Wang HQ. Upregulation of long non-coding RNA DLX6-AS1 promotes cell growth and metastasis in esophageal squamous cell carcinoma via targeting miR-577. Eur Rev Med Pharmacol Sci 2020; 24(14):7557.
8. Tay Y, Rinn J, Pandolfi PP. The multilayered complexity of ceRNA crosstalk and competition. Nature 2014; 505(7483):344-52.

The therapeutic effect of polygonum multiflorum on neurological tissue after spinal cord injury in rats

B. Liu[1], Y-J. Zhao [1], M. Zhang [1], X-Y Gao[1] and P. Hu[1]

Department of Spine Surgery, Affiliated Hospital of Binzhou Medical College, Shandong Province, Binzhou, P.R. China

To the Editor,

The number of spinal cord injury (SCI) patients has increased in recent years, bringing a heavy burden to society. Therefore, it is of great significance to study the treatment of spinal cord injury. After an injury, the body produces a large amount of endogenous harmful reactive oxygen species (ROS), including hydroxyl groups (•OH), superoxide anions (O2-), reactive nitrogen species (RNS), which can attack unsaturated cell membrane fatty acids to form malondialdehyde (MDA). It can then form aldehyde-protein complexes that damage nerve cell proteins, further aggravating the patient's condition. Extensive experiments confirm that ROS is one of the most important mediators after spinal cord injury (1). Polygonum multiflorum (PM) is a traditional Chinese herbal medicine. It is widely used as a tonic and anti-ageing medicine in China. Laboratory research and clinical practice have found that it has a wide range of pharmacological effects, including anti-tumor, anti-inflammatory, treatment of diabetes, hair growth, etc. In addition, recent research reports show that PM can also prevent and treat a variety of neurological diseases, it has neuroprotective effects on nigrostriatal dopaminergic degeneration, and it can also conduct a preventive effect against cognitive deficits induced by amyloid β-peptide 25-35 accumulation in Alzheimer's disease (2). The pharmacological properties of this plant prompted us to hypothesize that PM may have a beneficial effect on SCI. To confirm this hypothesis, we performed preliminary experiments on cellular lipid peroxidation, apoptosis, motor function, spinal cord histology, and Nogo-A protein expression in the spinal cord of rats with spinal cord injury. We assessed whether PME has a therapeutic effect on this disease.

MATERIALS AND METHODS

Chloral hydrate was purchased from Sinopharm Chemical Reagent Co (Shanghai, China). Polygonum multiflorum Thunb was purchased from Binzhou Medical College (Bin Zhou, China). TUNEL anti-apoptosis kit was purchased from Roche. Nogo-A antibody was purchased from Vector Laboratories (Burlingame, CA, USA). Superoxide dismutase kit and malondialdehyde kit were purchased from Jiancheng Bioengineering Institute (Nanjing, China).

Following the method of Kim HN (3), dried roots of polygonum multiflorum (2.5 kg) were extracted 3 times with 6 L of 75% ethanol. The extract was pooled and evaporated under reduced pressure and then lyophilized, yielding PM extract (PME) as a powder.

Sixty-six-week-old male SD rats (weight 225±26g) were purchased from the Orthopaedic Research Institute of Soochow University. They were housed in an animal room maintained constant temperature (23-25°C). Food and water were available. Rats were acclimatized to the laboratory room and handled for 1 week before the start of the experiments, and then randomly divided into 3 groups: sham

Keywords: Polygonum multiflorum extract; spinal cord injury; Superoxide dismutase; Malondialdehyde; apoptosis; Nogo-A protein

Corresponding author:
Dr Peng Hu
Department of Spine Surgery,
Affiliated Hospital of Binzhou Medical College,
No. 661, Huang he 2nd Road,
Shandong Province, Binzhou City, P. R. China.
e-mail: lllbbbsz@bzmc.edu.cn

0393-974X (2022)
Copyright © by BIOLIFE, s.a.s.
This publication and/or article is for individual use only and may not be further reproduced without written permission from the copyright holder.
Unauthorized reproduction may result in financial and other penalties
DISCLOSURE: ALL AUTHORS REPORT NO CONFLICTS OF INTEREST RELEVANT TO THIS ARTICLE.

group, spinal cord injury group (SCI group), and polygonum multiflorum extract group (PME group). The sham group only received a laminectomy at the T9-T11 levels. The other two groups underwent spinal cord injury at the T9-T11 spinal cord segments as follows: The SCI group received only spinal cord injury without any medical treatment. The rats in the PME group were immediately orally administered with polygonum multiflorum extract (2 g/kg) and were fed regularly once a day until the end of the experiment. The incisions of the three groups of animals were disinfected with iodophor daily until the incisions healed. The present study was approved by the Institutional Animal Use and Care Committee of Bin zhou Medical University in Feb 2020.

Spinal cord injury model

All SCI surgeries were performed under aseptic conditions referring to the method of J. WANG (4). In brief, after abdominal disinfection, rats were anesthetized by intraperitoneal injection of 10% chloral hydrate (400mg/kg). The skin on the back was shaved and disinfected, and the dorsal aspect of the spinal column was exposed. Next, a laminectomy was carried out at the T9-T11 levels to expose the spinal segment. The spinal cord was severely compressed for 15 sec, using a pair of forceps. The sham group only received a laminectomy without damaging the spinal cord. After the injury, the rats were placed into a humidity-controlled chamber at 25°C. They were then housed singly with water and food ad libitum. The bladders were emptied manually two times per day.

In the experiment, if the rats have persistent wound infection, eating and drinking disorders, self-harming behaviour, and infectious diseases, we will implement cervical dislocation as a humane endpoint after anesthesia. All experiments were conducted following the guidelines for animal care and use in the field of physiological sciences of the Chinese Physiological Society and were approved by the Institutional Animal Use and Care Committee of Bin Zhou Medical University.

BMS Locomotor analysis

According to the method of Wu B (5), BMS score and BMS subscore tests were used to analyze locomotor behavior at 1, 3, 7, 14, and 28 days by two experienced persons blinded to the treatment. Individual BMS scores from each animal ranged from 0 (no ankle movement) to 9 (entire functional recovery) points and 11 points for the BMS subscore.

Superoxide Dismutase (SOD) and Malondialdehyde (MDA) Detection

Three rats were randomly selected from each group on days 1, 3, 7 and 14 after surgery. Anesthesia was injected with 10% chloral hydrate (400mg/kg) intraperitoneally. We observed the rat's breathing and heartbeat during the experiment to ensure that the depth of anesthesia was safe. After successful anesthesia, the heart was exposed. The blunt needle was inserted into the aorta, and then the right atrial appendage was cut open. After perfusion of 200ml warm saline, 4% paraformaldehyde fixative was injected until the rat's limbs were stiff. The spinal cord was then exposed. We chose 1cm damaged spinal cord and made homogenate. The malondialdehyde content and superoxide dismutase activity were then determined according to the method of Ren (6).

Apoptosis rate and histological analysis

On the 1st, 3rd, 7th, and 14th day after surgery, three different groups of spinal cord tissue were obtained by the above method. The tissue was fixed with 4% paraformaldehyde for 60 minutes, washed twice with PBS, then added with PBS containing 0.1% Triton X-100, and incubated for 2 minutes in an ice bath. After the TUNEL assay solution was prepared, the apoptosis was observed under a fluorescence microscope. Image analysis was performed on the immunohistochemical photographs using Image.Pro Plus 6.0 software calculated the neuronal apoptosis rate according to the following formula:(Number of apoptotic cells/total number of cells under the microscope) × 100%.

After obtaining spinal cord tissue, hematoxylin-eosin staining was performed at 2 and 4 weeks after surgery to observe changes in spinal cord tissue, the sections were made in paraffin.

Immunohistological analysis of Nogo-A protein

The prepared spinal cord tissue sections were washed three times with phosphate buffer at 2 and 4 weeks postoperatively. After treatment with 0.01 mol/L citrate buffer, Nogo-A primary antibody was added and incubated at 37 ° C for 1 h. Then the secondary antibody was added dropwise, incubated at 37 ° C for 30 min, and washed three times with PBS. Immunohistochemical staining sections were then placed under a 400-fold optical microscope after adding the colouration of

diaminobenzidine. Five intact and non-overlapping high-power fields were randomly selected from each specimen, and the average optical density in each field of view was measured. Under the microscope, when the color of the cytoplasm is brown, it means that the Nogo-A protein is positive. The expression of Nogo-A protein was analyzed by Image.Pro Plus 6.0 software.

Statistical analysis

Statistical analysis was performed using SPSS19.0. The results were expressed as mean ± standard deviation (±s). ANOVA analysis or T-test was used. $P < 0.05$ was considered statistically significant.

RESULTS

The general condition of the rats in the three groups was good after the operation; no incision infection occurred, the function of the digestive system was normal, and there were no symptoms of indigestion and diarrhea.

BMS locomotor analysis

The BMS score and BMS subscore were evaluated at 1, 3, 7, 14 and 28 days after SCI. BMS scores and BMS subscores were considerably reduced after spinal cord injury in the SCI group and PME group, except for the Sham group (Fig.1). The BMS score and BMS subscore gradually increased with time in the following days. The BMS score and BMS subscore of the PME group were significantly higher than the spinal cord injury group on days 7, 14 and 28 after injury ($P<0.05$). This indicates that PME can effectively improve the motor function of rats after spinal cord injury.

SOD activity

The results showed that the SOD activity of the SCI group and the PME group was significantly lower than that of the Sham group (Table I , $P<0.05$). Furthermore, compared with the PME group, the SOD activity of the SCI group was significantly reduced at each time point ($P<0.05$), indicating that polygonum multiflorum extract can effectively improve SOD activity.

MDA content

The results showed that MDA level in the SCI

Table I. *SOD activity of three group (x±s, U/mg, n=5).*

	6h	12h	24h	72h
Sham	137.67±11.12#	133.47±10.08#	135.36±10.37#	138.51±12.01#
SCI	55.38±5.31	63.41±6.18	60.37±8.05	65.37±10.65
PME	80.68±10.32*	108.75±11.02*	110.31±12.07*	114.93±10.78*

*# Significant difference compared with the SCI group and PME group(P<0.05). * Significant difference compared with the SCI group (P<0.05).*

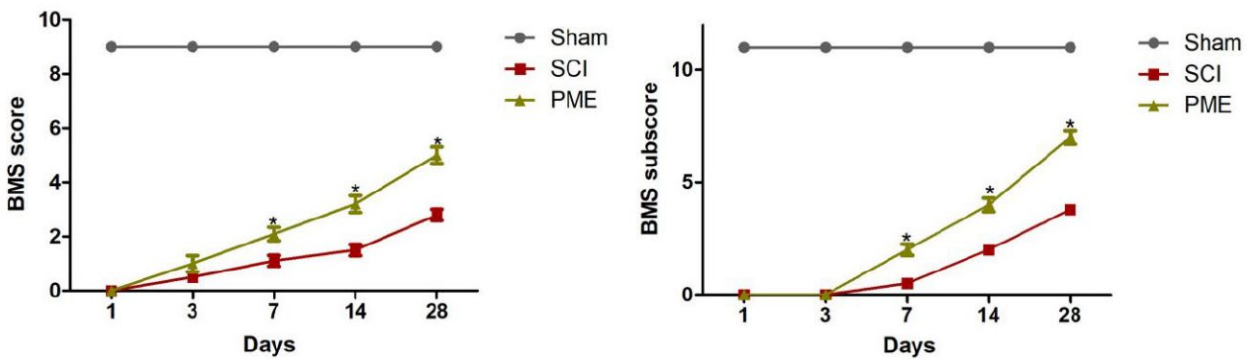


Fig. 1. *The BMS score and BMS subscore of three group at different time. *Significant difference compared with the SCI group (P<0.05)*

group gradually increased and reached the highest at the 24th hour. On the other hand, the MDA level in the PME treatment group was lower than those in the SCI group at each time point (Table II, P<0.05).

Apoptosis rate

The study showed that apoptosis occurred immediately after injury in SCI and PME groups. The apoptosis rate of PME treatment group was significantly lower than that of SCI group from day 1 to day 14. On the third day, the apoptosis rate of the two groups reached the highest, then decreased gradually (Fig. 2).

Histology

There was no abnormality in the spinal cord tissue structure of the Sham group, and the normal nerve cells were observed. The nerve cells in the spinal cord tissue of the SCI group were significantly reduced. On the 4th week, the tissue necrosis was severe in the injured area, and a large amount of scar tissue was formed. The structure was disordered, and the vacuoles were obvious. Also, the cell bodies of the nerve cells shrink and deform, the nerve fibres are arranged in disorder, and more scar tissue is seen. The degree of spinal cord injury in PME treatment was lower than that in SCI group; it had more neuronal cells, smaller vacuoles, and fewer scarring and necrotic cells (Fig. 3).

Immunohistological analysis of Nogo-A protein

After spinal cord injury, the expression of Nogo-A protein-positive cells was significantly increased, and the SCI group and the PME treatment group were higher than the Sham group at different times after operation (p<0.05). However, the Nogo-A protein in the PME group was lower than that in the SCI group at 2 and 4 weeks after the operation (Fig. 4), and the difference was statistically significant (p<0.05).

DISCUSSION

The medicinal uses of polygonum multiflorum have a long history. Compared with other natural extracts, it has been reported to have potent neuroprotective

Table II. *MDA levels of three group (x±s, nmol/mg, n=5).*

	6h	12h	24h	72h
Sham	2.24±1.45#	2.35±0.76#	2.30±0.54#	2.50±0.64#
SCI	8.62±1.27	8.80±1.43	9.20±1.29	5.20±1.24
PME	3.22±0.65*	3.70±1.18*	3.90±1.47*	3.62±1.38*

*# Significant difference compared with the SCI group and PME group(P<0.05). * Significant difference compared with the SCI group (P<0.05).*

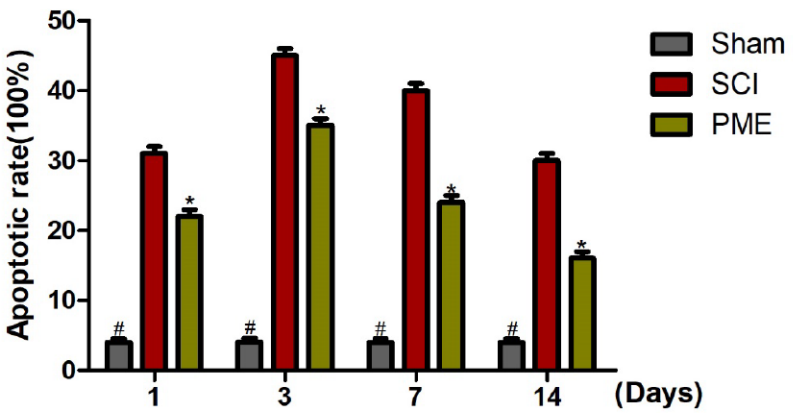


Fig. 2. *Comparison of apoptosis rates in three groups. # Significant difference compared with the SCI group and PME group(P<0.05). * Significant difference compared with the SCI group (P<0.05).*

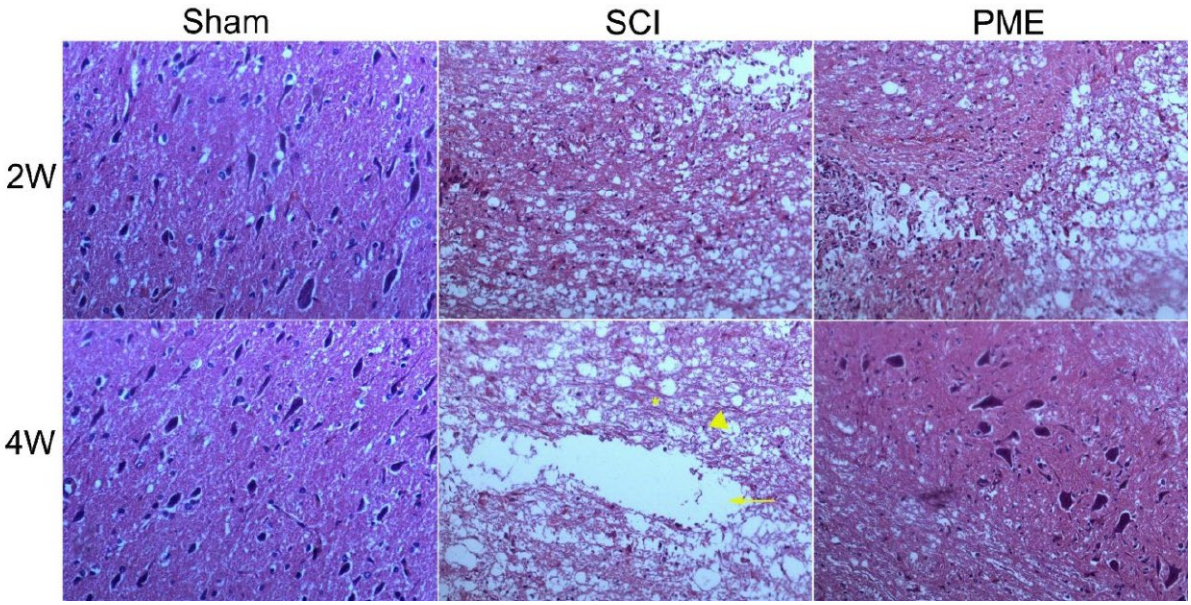


Fig. 3. *Histological changes in different groups at 2 and 4 weeks after surgery (arrow represents vacuoles, triangle represents necrotic cells, and asterisk represents scar tissue)*

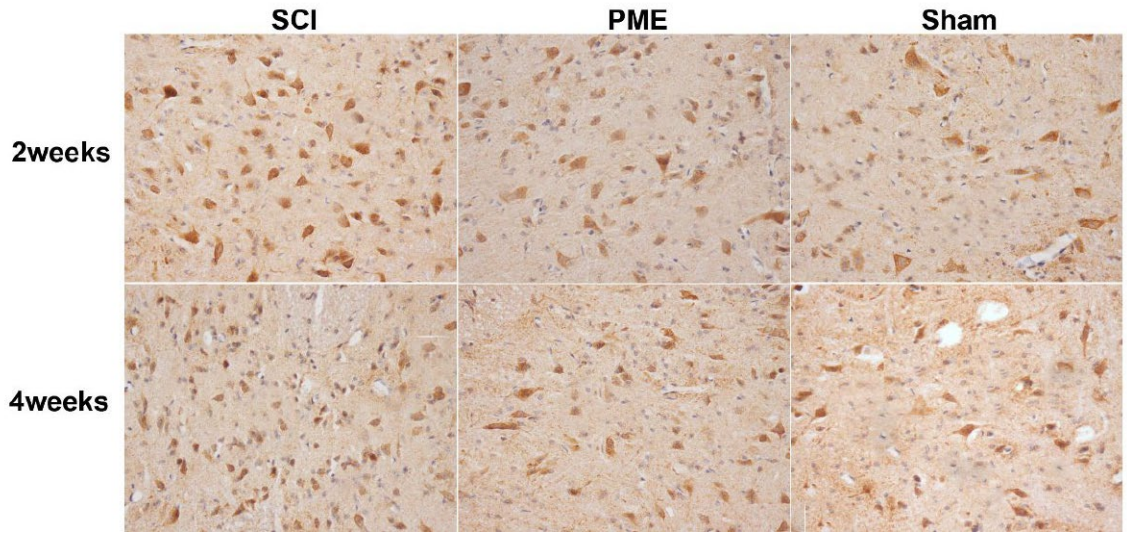


Fig. 4. *Expression of three groups of Nogo-A protein at different times*

effects against neurodegenerative diseases and brain injury, and it also has therapeutic effects on age-related cognitive impairment (7).

Polygonum multiflorum has been reported to have certain hepatotoxicity. Combined with relevant literature and our preliminary experiments, the dose of Polygonum multiflorum in this experiment was within the safe range. The experiment is the first to explore the role of polygonum multiflorum extract in spinal cord injury in rats.

Our results showed that the SOD levels in the PME treatment group were significantly higher than those

in the SCI group, indicating that PME can effectively bind ROS, inhibit lipid peroxidation, and enhance SOD activity. Nogo-A is a protein that inhibits axonal growth in the central nervous system (8).

In this study, we found that Nogo-A expression was significantly decreased in rats after PME treatment. We believe that PME exerts neuroprotective effects mainly through the following mechanism. 1. Polygonum multiflorum extract can improve the biological activity of SOD and reduce the damage of ROS on the nerve cell membrane by reducing lipid peroxidation. 2. It contains many phospholipids, which are the main components of the biofilm. When the cell membrane is destroyed, it can provide the repaired raw materials in time to effectively reduce the damage. 3. When spinal cord injury occurs, it can effectively reduce the apoptosis of nerve cells by inhibiting the expression of Nogo-A protein and then play a therapeutic role.

In conclusion, our data suggest that PME has a therapeutic effect on neurological tissue, which provides a new method for treating spinal cord injury. However, its molecular mechanism of exerting neuroprotective effects needs further study.

Conflict of interest:

We declare that we have no financial and personal relationships with other people or organizations that can inappropriately influence our work.

Financial disclosure:

This research was funded by the Science and Technology Project of the Affiliated Hospital of Binzhou Medical College BY2019KJ32.

REFERENCES

1. Butterfield DA, Reed TT. Lipid peroxidation and tyrosine nitration in traumatic brain injury: Insights into secondary injury from redox proteomics. Proteomics Clin Appl 2016;10:1191-1204.
2. Um MY, Choi WH, Aan JY, et al. Protective effect of Polygonum multiflorum Thunb on amyloid beta-peptide 25-35 induced cognitive deficits in mice. J Ethnopharmacol 2006; 104(1-2):144-148.
3. Kim HN, Kim YR, Jang JY, et al. Neuroprotective effects of Polygonum multiflorum extract against glutamate-induced oxidative toxicity in HT22 hippocampal cells. J Ethnopharmacol 2013; 150(1):108-115.
4. Wang J, Guo G, Wang W, et al. Effect of methylprednisolone and edaravone administration on spinal cord injury. Eur Rev Med Pharmacol Sci 2016; 17: 2766-2772.
5. Wu B, Liang J. Pectolinarigenin promotes functional recovery and inhibits apoptosis in rats following spinal cord injuries. Exp Ther Med 2019; 17:3877-3882.
6. Ren XS, Ding W, Yang XY, et al. Neuroprotective effect of icariin on spinal cord injury in rats. Zhong Guo Gu Shang 2018; 31:1054-1060.
7. Li X, Matsumoto K, Murakami Y, et al. Neuroprotective effects of Polygonum multiflorum on nigrostriatal dopaminergic degeneration induced by paraquat and maneb in mice. Pharmacol Biochem Behav 2005; 82: 345-352.
8. Zhang ZW, Jiang JJ, Luan MC, et al. Nogo-A antibody treatment enhances neuron recovery after sciatic nerve transection in rats. Eur Rev Med Pharmacol Sci 2017; 21:1780-1786.

Overexpression of CCR7 in tolerogenic dendritic cells on T lymphocyte immune function in ankylosing spondylitis

JW. Liu[#], Q. Yan[#], JJ. He, DT. Lin, SL. Zhang, F. Gao, ZH. Chen[*] and H. Lin

Department of Rheumatology and Immunology, Fujian Provincial Hospital Shengli Clinical College of Fujian Medical University, Fuzhou, PR China

[#]These authors contributed equally to this work

To the Editor,

Ankylosing spondylitis (AS) is a chronic and progressive autoimmune disorder causing inflammatory spondylitis, peripheral arthritis, and inflammation of the entheses (1). Although treatments of AS have improved significantly over the last decade, the current treatment options remain suboptimal.

Tolerogenic DCs (tolDCs) are immature or activated dendritic cells (DCs) and have shown promising potentials in the treatment of autoimmune diseases (2). Mature DCs (mDCs) show high expression of MHC-II, CD40, CD80, and CD86 could trigger adaptive immune responses (3). The tolDCs are characterized by the inhibited expression of co-stimulatory molecules and pro-inflammatory cytokines, which results in T cell silence (4). TolDCs could be differentiated *in vitro* through immunosuppressive reagents, cytokines or genetic modifications. Among these induction methods, stimulation of vitamin D3 and Dexamethasone (Dex) for the induction of tolDCs was considered one of the most effective approaches.

C-C chemokine receptor type 7 (CCR7) and its ligands (CCL19 and CCL21) played a key role in the adaptive immune system, including activation and migration of DCs, T cells and B cells (5). ImDCs represent a low expression of CCR7, which causes inhibited imDCs migrations and probably regulates immune tolerance function.

This study generated tolDCs from PBMCs of ankylosing spondylitis and up-regulated CCR7 expression by a recombinant adenovirus vector. The results revealed that overexpression of CCR7 on tolDCs enhanced immune tolerance while keeping relatively high migration capacity, which provided a novel potential strategy for treating ankylosing spondylitis.

MATERIALS AND METHODS

Cells and clinical specimens

According to the institutional Standard Operating Procedures for blood donation, peripheral blood samples from 20 randomized ankylosing spondylitis donors were obtained from the Fujian Provincial Hospital. Informed consent was obtained following the Declaration of Helsinki. Peripheral blood mononuclear cells were isolated by the Ficoll gradient centrifugation method.

Recombinant adenovirus vector for CCR7 overexpression

Ad-CCR7-GFP and CCR7 mock vectors were synthesized and constructed by Shanghai GeneChem, Co.Ltd. The CCR7 gene was subcloned into the adenovirus expression vector (pLKO.1-puro), which encoded the GFP, to generate an overexpression vector carrying CCR7, and

Keywords: CCR7; Tolerogenic dendritic cells; immune tolerance; Ankylosing spondylitis

**Corresponding Author:*
Dr Zhihan Chen
Department of Rheumatology and Immunology,
Fujian Provincial Hospital
Shengli Clinical College of Fujian Medical University,
No.134 East Street, Gulou District,
Fuzhou, 350001, Fujian, PR China.
e-mail: liu202120211008@163.com

0393-974X (2022)
Copyright © by BIOLIFE, s.a.s.
This publication and/or article is for individual use only and may not be further reproduced without written permission from the copyright holder.
Unauthorized reproduction may result in financial and other penalties
DISCLOSURE: ALL AUTHORS REPORT NO CONFLICTS OF INTEREST RELEVANT TO THIS ARTICLE.

before further experiments, tolDCs were infected with Ad-CCR7 or a negative vector at a multiplicity of infection (MOI) of 10 for 48 h.

Generation of PBMCs-derived tolDCs

DC cells were generated from peripheral blood mononuclear cells (PBMCs). Briefly, PBMCs were washed three times in cold fresh PBS containing 0.1 % (w/v) bovine serum albumin (BSA) and 0.45 % sodium citrate. Then PBMCs were seeded in plastic culture flasks for 2 h, and monocytes were isolated by plastic adherence. Monocytes were cultured with RPMI1 1640 medium supplemented with 10% FBS, 100 U/mL penicillin, 100 mg/mL Streptomycin, 20 ng/mL recombinant murine granulocyte-macrophage colony-stimulating factor (GM-CSF) and 10 ng/mL recombinant murine interleukin 4 (IL-4) in a humidified, 5% CO_2-containing atmosphere. After incubation for 7 days, monocytes differentiated to immature DC cells (im-DCs) and then transformed to mature DC cells (mDCs) after incubation with 100 ng/mL of lipopolysaccharide (LPS) on day 6 for 24 h. For the induction of tolDCs, 0.1 nM vitamin D3 was added into the DC cultures and refreshed at day 3.1 μM Dexamethasone (Dex) was added on day 3 and followed by incubation for another 3 days. Then cells were harvested and washed with PBS three times, followed by morphological analysis.

Phenotype analysis of tolDCs

The expression of surface molecules classified the phenotypes of the cells. The following antibodies were used for phenotype analysis: CD40-PE (Elabscience), CD80-FITC (BD Biosciences), CD86-PE (BD Biosciences), MHC-II-FITC (BD Biosciences). Briefly, 2×10^5 cells were harvested and cultured with antibodies on ice for 30 m, followed by washing twice with fresh PBS containing 0.5 % BSA. Then the cells were applied to analysis through a Beckman Coulter NAVIOS flow cytometer (Beckman Coulter Co., Indianapolis, IN, USA).

Mixed leucocytes reactions (MLR) analysis

The allogeneic stimulatory capacities of DCs and tolDCs were examined through a mixed lymphocyte reaction (MLR) employing CCK-8 assay. CD4+ T cells were obtained using an Untouched CD4+ Cell Kit (Miltenyi Biotec GmbH). 1×10^5 DCs or tolDCs were co-cultured with allogeneic T cells (1:5, 1:25, 1:50) in 96-well plates. Cells were incubated for another 3 days in RPMI-1640 medium at 37 ℃ with 5 % CO_2. Then 10 μL CCK-8 solution (Beyotime, China) was added to the culture medium followed by another 2 h incubation at 37°C. The absorbance of each well was detected at the wavelength of 450nm by a microplate reader (Thermo Fisher Scientific, USA).

Transwell assay

Cell migration ability of DCs and tolDCs was determined via transwell chambers of 8 μm pore filters (Corning, USA). Briefly, 1×10^5 of treated cells suspended in 200μL serum-free medium were seeded on the upper transwell chamber. Next, the lower chambers were filled with medium containing 10% FBS and CCL21(20 ng/mL). After incubation for 14 h at 37°C, the cells on the surfaces of lower chambers were fixed with 20% methanol for 10 m and dyed with 1% crystal violet (Beyotime, China). Finally, the migrated cells were photographed and counted under a microscope (Leica, Germany).

Measurement of cytokine levels

The concentration of IL-10, IL-12, IL-1β and TNF-α were determined in the culture supernatants of different groups by ELISA Kit (R&D Systems) in accordance with the manufacturer's protocol.

Real-time quantitative PCR

cDNA was synthesized from total purified RNA from a SuperScript III Reverse Transcriptase (Invitrogen, CA, USA) according to the protocols. Real-time PCR analysis was performed through SYBR-Green real-time PCR mixes (ToyoBo) with the 7900 HT Sequence Detection System (Applied Biosystems). Triplicate data were normalized to the β-actin mRNA levels in the samples. PCR primer pairs were designed and synthesized by Sangon Biotech (Shanghai, China), and the sequences (5'-3') were listed as follows: CCR7 forward: CTCTTCAAGGACCTGGGCTG, CCR7 reverse: AGGCCTGGTTTTCGGAAGAG; β-actin forward: GTGCTATCCCTGTACGCCTC, β-actin reverse: AATGCCAGGGTACATGGTGG.

Western blot

Total protein was extracted using RIPA lysis buffer (Beyotime, China) with a 1% protease inhibitor and phosphatase inhibitor. 35 μg total protein were separated

using SDS-PAGE and transferred onto polyvinylidene difluoride (PVDF) membranes (Millipore). Subsequently, the membranes were blocked in 5% non-fat milk and then incubated at 4°C overnight with primary antibodies including CCR7 (1:1000, Affinity) and β-actin (1:2000, Affinity) after incubation with HRP-labeled secondary antibody (Beyotime, China) for 2 h at room temperature. Afterwards, specific signals were visualized via ECL reagents (Millipore). Bands were quantified through ImageJ and the expression levels normalized against the loading control.

Statistics analysis

Statistical analyses were carried out using GraphPad Prism 7.0 version (GraphPad Software, CA, USA). The data were represented as mean ± standard deviation (SD) in three independent experiments. Statistical significance of different groups was applied via One Way Analysis of Variance (ANOVA). P-value <0.05 was statistically considered significant.

RESULTS

Efficient overexpression of CCR7 gene in tolDCs

In order to investigate the transfection efficiency of the CCR7 overexpression adenovirus vector, the transfected tolDCs were determined under a microscope to examine GFP fluorescence-labelled with Ad-CCR7. As Fig. 1A indicated, most of the tolDCs showed green fluorescence, which unveiled the successful overexpression of CCR7 in tolDCs. Furthermore, the transcription level and protein expression of CCR7 was validated using RT-PCR and western blot analysis, respectively. The results showed

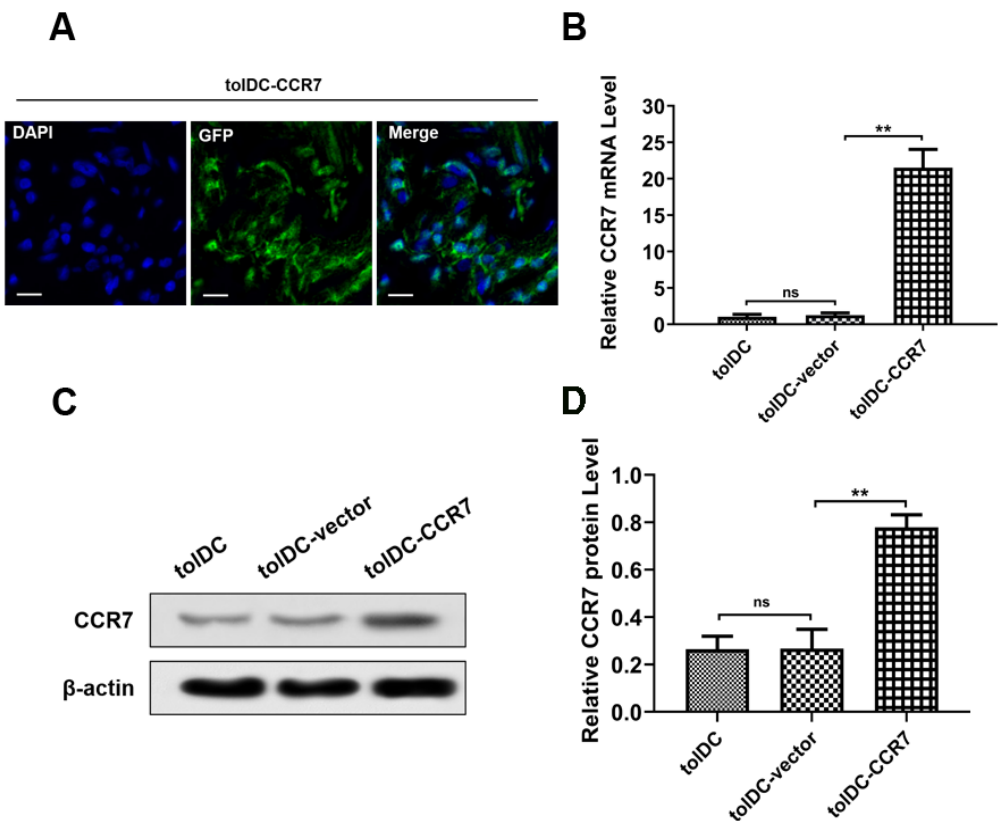


Fig. 1. *Overexpression of CCR7 gene in tolDCs. (A) TolDCs were transfected with Ad-CCR7 for 48 h and measured with GFP fluorescence (labeled Ad-CCR7). Nuclei were stained with DAPI. Scale bar=20 μm. (B) RT-PCR analysis was performed to determine the mRNA level of CCR7 in tolDCs (n=3). (C, D) The CCR7 protein expression was evaluated through western blot assay in tolDCs after transfection with Ad-CCR7 or blank vector, respectively (n=3). β-actin was used as the internal reference. *p<0.05, **p<0.01, ns=non-significant vs. tolDCs group or tolDCs-CCR7 group. CCR7, C-C chemokine receptor type 7; Ad-CCR7, adenovirus expression vector carrying CCR7; tolDCs, tolerogenic DC cells; RT-PCR, reverse transcription polymerase chain reaction.*

that CCR7 was significantly up-regulated both at the transcription (Fig. 1B) and protein level (Fig. 1C-D), indicating successful CCR7 overexpression in tolDCs.

Overexpression of CCR7 exhibited an immature phenotype with low expression of MHC-II and co-stimulatory molecules in tolDCs

Mature DCs express high levels of major histocompatibility complex class II (MHC-II) and co-stimulatory molecules, including CD40, CD80 and CD86, while immature DCs typically exhibit low levels. Thus, we examined the effect of Ad-CCCR7 infection on these cell surface antigens by flow cytometry (Fig. 2A). The results indicated that mDCs exhibited higher expression of CD40, CD80, CD86 and MHC-II compared with imDCs, which were consistent with the results has been reported previously. Moreover, up-regulation of CCR7 in tolDCs remarkably inhibited the levels of CD40, CD80, CD86 and MHC-II compared with cells infected with blank vector (Fig. 2B-E). TolDCs generated by the combination of vitamin D3 and dexamethasone displayed a semi-mature phenotype with characteristic features such as a reduced co-stimulatory capacity. And overexpression of CCR7 in tolDCs further reduced the levels of MHC-II and co-stimulatory molecules, which induced immune tolerance more efficiently.

Overexpression of CCR7 in tolDCs showed low levels of pro-inflammatory cytokines while keeping the high expression of anti-inflammatory cytokine

Except for the levels of co-stimulatory molecules, the expression of pro-inflammatory and anti-inflammatory cytokines secreted from DC cells affect the immunological processes. To determine the immune regulative roles of DCs and tolDCs, the expression of pro-inflammatory cytokines including IL-12, IL-1β and TNF-α were detected using ELISA assay. As shown in Fig 3A-C, the levels of IL-12, IL-1β and TNF-α of imDC cells significantly reduced compared with mDC cells. Moreover, overexpression

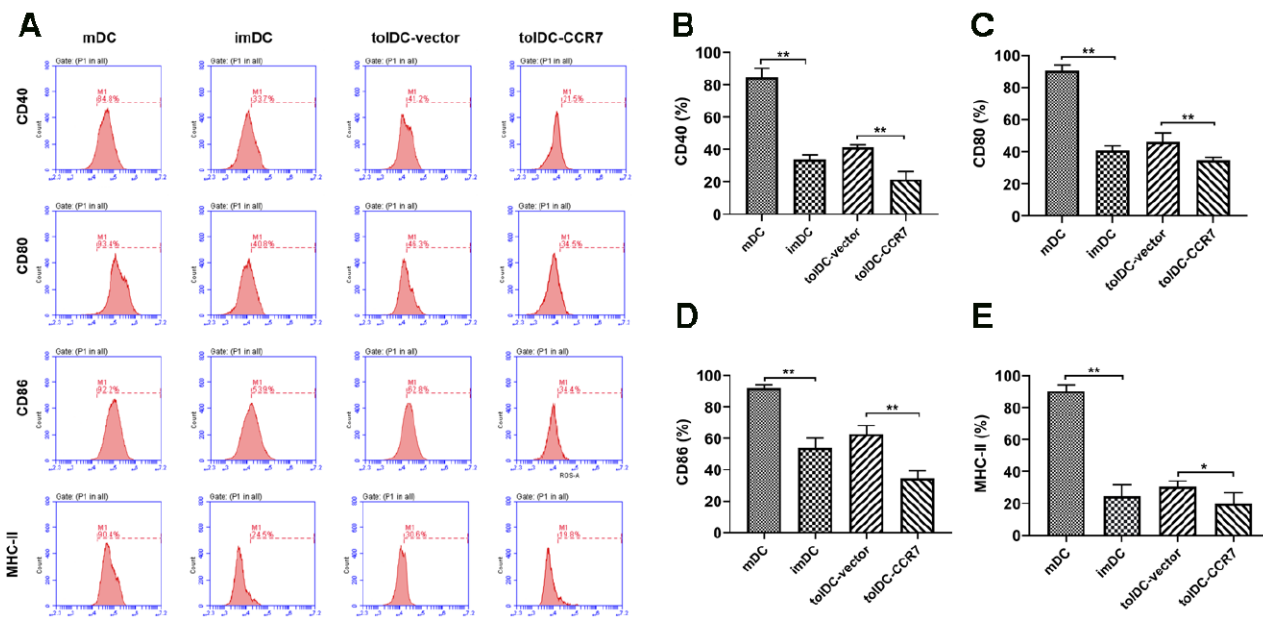


Fig. 2. *Overexpression of CCR7 in tolDCs exhibited an immature phenotype with low expression of MHC-II and co-stimulatory molecules. (A)The expression of CD40, CD80, CD86 and MHC-II on the surface of tolDCs was detected using flow cytometry and the representative histograms are shown for mDCs, imDCs, tolDCs-vector and tolDCs-CCR7 (n=3). Comparisons of the percentages of (B) CD40, C (CD80), D (CD86) and E (MHC-II) on different groups (n=3). * p<0.05, **p<0.01, ns=non-significant. mDCs, mature DC cells. imDCs, immature DC cells; tolDCs, tolerogenic DC cells; MHC-II, major histocompatibility complex (MHC) class II; CCR7, C-C chemokine receptor type 7.*

of CCR7 in tolDCs further suppressed the secretion of pro-inflammatory cytokines compared with the blank vector infection group. In addition, IL-10 is a prominent anti-inflammatory cytokine that could prevent DC cells maturation. As indicated in Fig. 3D, the secretion of IL-10 of imDC cells was dramatically increased compared with mDC cells. Besides, up-regulation of CCR7 also further promoted the level of IL-10 effectively. Taken together, overexpression of the CCCR7 gene in tolDCs effectively inhibited the expression of pro-inflammatory cytokines while accelerating the secretion of anti-inflammatory cytokines.

Up-regulation of CCR7 in tolDCs promoted immune tolerance and maintained enhanced migration ability

The migration ability of tolDCs influenced the capability to reach T cells or lymph nodes, affecting the immune tolerance induction of tolDCs. To further confirm the effect of CCR7 overexpression on the migration capacity of tolDCs, we performed a transwell assay after infection for 48 h in the presence of CCL21 (the ligand of CCR7). The results (Fig. 4A-B) show imDCs showed attenuated migration ability compared with mDCs. Besides, overexpression of CCR7 in tolDCs remarkably increased the migration capacity compared with the control vector infection group. Furthermore, MLR analysis was carried out to assess the regulative role of Ad-CCR7 on the lymphocyte proliferation response. The results revealed that overexpression of CCR7 showed a significant inhibitory effect on lymphocyte proliferation compared with tolDCs infected with blank vector (Fig. 4C). These findings indicated that overexpression of CCR7 in tolDCs exhibited effective immune tolerance while maintaining enhanced migration ability.

DISCUSSION

Ankylosing spondylitis (AS) is a chronic inflammatory arthritis that mainly injures spine joints, resulting in severe, persistent pain (6). Despite the

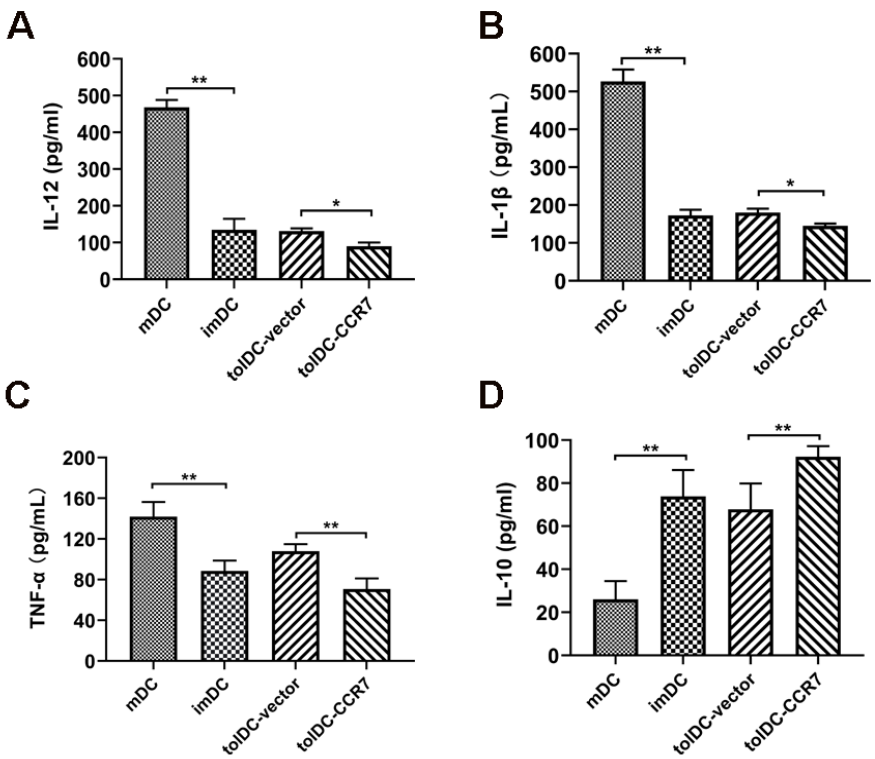


Fig. 3. *Overexpression of CCR7 on tolDCs exhibited low levels of pro-inflammatory cytokine. ELISA assay was assessed to examine the IL-12 (A), IL-1β (B), TNF-α (C) and IL-10 (D) in the culture supernatant of mDCs, imDCs, tolDCs-vector and tolDCs-CCR7. *p<0.05, **p<0.01, ns=non-significant. IL-10, interleukin 10; IL-12, interleukin 12; IL-1β, Interleukin 1 beta; TNF-α, tumor necrosis factor alpha.*

recent advances in treatment, finding an ideal treatment to completely cure this disease is still difficult.

Tolerogenic Dendritic Cells (TolDCs) show promising potentials to transform the host immune response to the tolerance state. The efficiency of tolDCs therapy entails the ability to regulate tolerance and their ability to reach target organs, including lymph nodes (7). Therefore, the migration ability of tolDCs plays a key role in the potential tolDCs applications. C-C chemokine receptor 7 (CCR7) is pivotal in migrating tolDCs to lymph nodes (8). They drive mDCs and T cell subsets to the T cell zone in the lymph nodes and mediate the interaction subsequently (9). The expression of CCR7 is up-regulated in mDCs or after a pro-inflammatory stimulus while down-regulated in imDCs or tolDCs (10). Therefore, the inhibited migration capacity limited tolDCs and found appropriate solutions to promote the migration of tolDCs while maintaining immune tolerance. Hence, overexpression of CCR7 in tolDCs through recombinant gene technology could be considered a promising strategy to promote the limited lymphoid homing ability of tolDCs.

In the present study, we transfected tolDCs with Ad-CCR7 to promote CCR7 expression with an enhanced migration capacity while maintaining a relatively low expression of co-stimulatory molecules. As a result, CCR7-tolDCs exhibited suppressed T cell responses

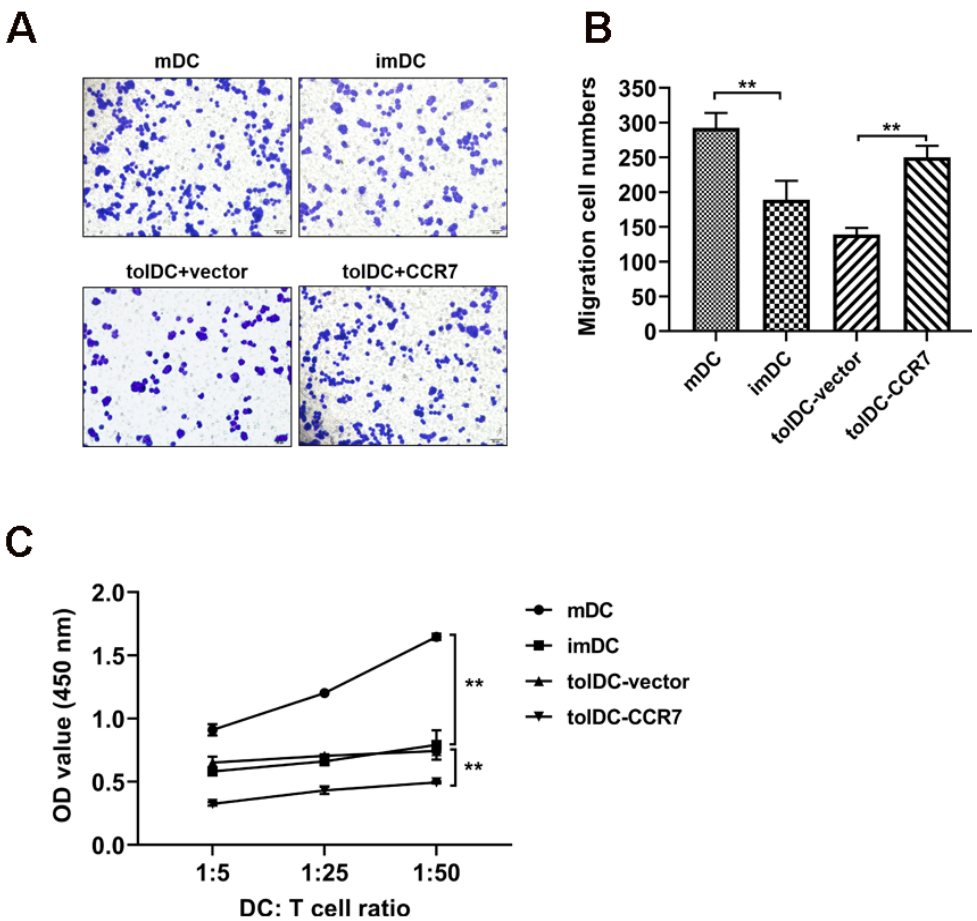


Fig. 4. *Overexpression of CCR7 on regulation of T cells proliferation and tolDCs migration. (A, B) Transwell assay was performed to evaluate that up-regulation of CCR7 on tolDCs enhanced migration ability towards CCR7 ligands CCL21 (n=3). Scale bar=20 μm. (C) MLR analysis was carried out to reveal that the proliferation capacity of T cells co-cultured with tolDCs transfected with ad-CCR7 was lower than that of T cells treated with tolDCs-vector. *p<0.05, **p<0.01, ns=non-significant. CCL21, C-C Motif Chemokine Ligand 21; MLR, mixed lymphocyte reaction.*

increased expression of anti-inflammatory cytokines; altogether, our results could lay the foundation for the further deep study of ankylosing spondylitis and provide a guide for clinical application.

Funding:

The research was supported by the Startup Fund for Scientific Research of Fujian Medical University (No.2017XQ1124).

Competing interests:

The authors declare that they have no competing interests.

REFERENCES

1. Zhu W, He X, Cheng K, et al. Ankylosing spondylitis: etiology, pathogenesis, and treatments. Bone Res 2019; 7:22.
2. Obregon C, Kumar R, Pascual M A, Vassalli G, and Golshayan D. Update on Dendritic Cell-Induced Immunological and Clinical Tolerance. Front Immunol 2017; 8:1514.
3. Gu Y Z, Zhao X,Song X R. Ex vivo pulsed dendritic cell vaccination against cancer. Acta Pharmacol Sin 2020; 41(7):959-69.
4. Švajger U,Rožman P. Induction of Tolerogenic Dendritic Cells by Endogenous Biomolecules: An Update. Front Immunol 2018; 9:2482.
5. Shannon L A, McBurney Tm Fau - Wells M A, Wells Ma Fau - Roth M E, et al. CCR7/CCL19 controls expression of EDG-1 in T cells. J Biol Chem 2012; 287(15):11656-64.
6. Zhai Y, Lin P, Feng Z, et al. TNFAIP3-DEPTOR complex regulates inflammasome secretion through autophagy in ankylosing spondylitis monocytes. Autophagy 2018; 14(9):1629-43.
7. Mosanya CH, Isaacs JD. Tolerizing cellular therapies: what is their promise for autoimmune disease? Ann Rheum Dis 2019; 78(3):297-310.
8. Ding Y, Shimada Y, Maeda M, et al. Association of CC chemokine receptor 7 with lymph node metastasis of esophageal squamous cell carcinoma. Clin Cancer Res 2003; 9(9):3406-12.
9. Förster R, Davalos-Misslitz AC, Rot A. CCR7 and its ligands: balancing immunity and tolerance. Nat Rev Immunol. 2008; 8(5):362-71.
10. Le Nouën C, Hillyer P, Winter CC, et al. Low CCR7-mediated migration of human monocyte-derived dendritic cells in response to human respiratory syncytial virus and human metapneumovirus. PLoS Pathog 2011; 7(6):e1002105.

Circ_0020378 promotes the osteosarcoma malignant progression through miR-1200 / CDH6 axis

XZ. Liu[1*], ZH. Shang[1], YP. Li[1], J. Liang[1], X. Lu[2], Z. Lu[2] and N. Ru[1]

[1]Department of Orthopedics, the People's Hospital of China Three Gorges University, the First People's Hospital of Yichang, Yichang, Hubei, China; [2]Department of Orthopedics, Xiangyang Central Hospital, Xiangyang, Hubei, China

Received September 10, 2021 – Accepted January 18, 2022

To the Editor,

Osteosarcoma (OS) is one of the most common primary bone tumors in children and adolescents (1). The patients with metastatic or recurrent disease suffer poor overall survival rates of less than 20% (2). Thus, searching for diagnostic markers and therapeutic targets for OS is important to improve the prognosis of OS patients.

Circular RNAs (circRNAs) are novel endogenous non-coding RNAs that are abundantly present in the eukaryotic transcriptome (3). CircRNAs play an important role in the regulation of gene expression and various cellular physiological and pathological processes and are also involved in cancer progression (4). In this study, bioinformatics analysis suggested that circ_0020378 was aberrantly highly expressed in OS. However, up to now, nothing has been reported about its function in OS and its mechanism.

MicroRNA-1200 (miR-1200) expression is down-regulated in OS, and miR-1200 overexpression inhibits OS cell proliferation and promotes apoptosis (5). Another study reports that cadherin 6 (CDH6) overexpression promotes OS cell proliferation *in vivo* and *in vitro* (6). In this study, we reported that circ_0020378 was highly expressed in OS tissues, and it could directly target miR-1200 and up-regulate CDH6 to promote the malignant biological behaviours of OS cells.

MATERIALS AND METHODS

Tissue samples

A total of 45 subjects who were diagnosed with OS by the Department of Pathology in our hospital were selected, and the surgically resected tumor tissues and the corresponding paracancerous tissues were collected, and the tissue samples were preserved in liquid nitrogen immediately after surgical resection. All subjects did not receive preoperative radiotherapy or chemotherapy, and informed consent was obtained from the subjects before the study. This study was conducted under the approval and guidance of the Ethics Committee of Xiangyang Central Hospital and the Ethics Committee of The First People's Hospital of Yichang.

Cell culture and transfection

Human osteoblast cell line (hFOB 1.19) and four human OS cell lines (MG-63, Saos-2, U-2OS, and HOS) were procured from American Type Culture Collection (ATCC, Rockville, MD, USA). Subsequently, all cells were cultured in Dulbecco's Modified Eagle's medium (DMEM, Gibco, Gaithersburg, MD, USA) containing 10% fetal bovine serum (FBS, Gibco, Carlsbad, CA, USA), 1% penicillin/streptomycin mixture (Gibco, Carlsbad, CA, USA) at 37 °C with 5% CO_2.

Lipofectamine™ 2000 reagent (Invitrogen; Thermo Fisher Scientific, Inc., Waltham, MA, USA) was utilized to

Key words: osteosarcoma; circ_0020378; miR-1200; CDH6

**Corresponding Author:*
Dr Xinzong Liu,
Department of Orthopedics,
The People's Hospital of China Three Gorges University,
The First People's Hospital of Yichang,
Yichang 443000, Hubei, China
e-mail: 201240604001@ctgu.edu.cn

0393-974X (2022)
Copyright © by BIOLIFE, s.a.s.
This publication and/or article is for individual use only and may not be further reproduced without written permission from the copyright holder.
Unauthorized reproduction may result in financial and other penalties
DISCLOSURE: ALL AUTHORS REPORT NO CONFLICTS OF INTEREST RELEVANT TO THIS ARTICLE.

transfect the small interfering RNA targeting circ_0020378 (si-circ_0020378#1 and si-circ_0020378#2) and its negative control (si-NC), circ_0020378 overexpression plasmid (circ_0020378) and its negative control (NC), the mimic or inhibitor of miR-1200 (miR-1200 or anti-miR-1200) and their negative controls (miR-NC or anti-miR-NC) into OS cells. The transfection efficiency was detected by quantitative Real-Time PCR (qRT-PCR).

qRT-PCR

Total RNA was extracted from tissue samples or cells using TRIzol reagent (Invitrogen; Thermo Fisher Scientific, Inc, Waltham, MA, USA), and a Prime Script TM RT reagent Kit with gDNA Eraser (TaKaRa, Dalian, China) for reverse transcription. qRT-PCR was performed on StepOne Plus real-time PCR system (Applied Biosystems, Foster City, CA, USA) using SYBR Green qPCR Master Mix (Thermo Fisher Scientific, Inc., Waltham, MA, USA). The relative expression levels of the target genes were calculated using the $2^{-\Delta\Delta Ct}$ method with β-actin and U6 as the internal references, and the primer sequences were as follows: circ_0020378 (Forward): 5′ - CGTGGGGCCAACCCA - 3′, circ_0020378 (Reverse): 5′ - GAATGGAAAATGGCG - 3′; miR-1200 (Forward): 5′ - ACACTCCAGCTGGGCTCCTG AGCCATTCTG - 3′, miR-1200 (Reverse): 5′ -CTCAACTGGTGTCGTGGAGTCGGCAATTCAGTTG AGGAGGCTCA- 3′; CDH6 (Forward): 5′ - AAGGAGGTTTACACAGCCACTGT - 3′, CDH6 (Reverse): 5′ - CTTGGTACTGCTCCCTGTTTTCT - 3′; U6 (Forward): 5′ - CTCGCTTCGGCAGCACA- 3′, U6 (Reverse): 5′ - AACGCTTCACGAATTTGCGT- 3′; β-actin (Forward): 5′ - ATCACCATTGGCAATGAGCG- 3′, β-actin (Reverse): 5′ - TTGAAGGTAGTTTCGTGGAT - 3′.

Cell Counting Kit-8 (CCK-8) assay

The transfected OS cells were modulated to a cell density of 2×10^4 cells/mL, and the cell suspension was added into a 96-well plate (100 μL/well), and cultured at 37°C and 5% CO_2. Thereafter, 10 μL of CCK-8 solution (Beyotime Biotechnology, Shanghai, China) was supplemented to each well at 24, 48 and 72 h, respectively, and the absorbance values were measured at 450 nm after 2 h of incubation.

BrdU assay

The transfected OS cells (1×10^5 cells / mL) were inoculated into a 35 mm diameter culture plate (with a coverslip placed inside), cultured for 1 d, then 1.0 mg/mL of BrdU solution (Applied Biosystems, Foster City, CA, USA) was added, and the cells were incubated at 37°C for 4 h, and then the culture solution was discarded. The slips were then rinsed with phosphate buffer saline (PBS) 3 times, and the cells were fixed with methanol for 10 min. After the slide was dried, endogenous oxides were inactivated, the unspecific antigens were blocked with 5% rabbit serum. After DNA was denatured, the cells were rinsed with PBS again, the primary antibody was added, and the cells were incubated at room temperature for 1 h. Next, the cells were incubated with secondary antibodies at room temperature for 1 h. Subsequently, the cells were stained with DAPI staining solution (Beyotime Biotechnology, Shanghai, China). BrdU positive cells in the 3 fields of view were randomly counted under the microscope, and the average value was calculated.

Transwell assay

Cell migration and invasion were measured using Transwell inserts (8 μM pore size, Costar, Cambridge, MA, USA). For each sample, 5×10^4 OS cells in serum-free DMEM were inoculated into the upper chamber. DMEM medium containing 10% FBS was added to the lower chamber. After 24 h of incubation, the cells in the upper chamber were wiped away, and 4% paraformaldehyde was used to fix the cells on the below surface of the filter, and then the cells were stained with 0.1% crystal violet and counted under the microscope. For the invasion assay: the procedures were the same as for the migration assay, but 50 μL of Matrigel was used to coat the filter before the cells were inoculated.

Dual-luciferase reporter gene assay

Wild-type or mutant circ_0020378 or CDH6 3'UTR sequences containing miR-1200 binding sites were inserted into the pmirGLO vector (Promega, Madison, Wisconsin, USA) to construct luciferase reporter vectors (circ_ 0020378-wt, circ_0020378-mut, CDH6-wt, and CDH6-mut). The miR-NC and miR-1200 were co-transfected into the cells using Lipofectamine™ 2000 reagent and incubated for 24 h. Ultimately, the luciferase activity was detected according to the manufacturer's instructions of the Dual-Luciferase Reporter Assay System (Promega, Madison, WI, USA).

Western blot analysis

The transfected OS cells were lysed in RIPA lysis

buffer on ice. Subsequently, the protein concentration was measured by a BCA protein concentration assay kit (Beyotime Biotechnology, Shanghai, China). Subsequently, the proteins were separated by SDS-PAGE, electrotransferred to PVDF membranes and blocked with 5% skim milk. Next, the PVDF membranes were incubated with anti-CDH6 antibody (1:1000, ab133632, Abcam, Shanghai, China) and anti-β-actin antibody (1:3000, ab8227, Shanghai, China) at 4°C overnight, respectively, and then incubated with HRP-labeled secondary antibody (1:5000, ab205718, Shanghai, China) at room temperature for 1 h on a shaker. After the PVDF membranes were washed by tris buffered saline tween (TBST), the ECL kit (Beyotime Biotechnology, Shanghai, China) was used for luminescence development, and the grayscale value of each protein band was analyzed by Image J software.

Statistical analysis

All data in this study were expressed by "mean ± standard deviation" and analyzed statistically by SPSS 22.0 (SPSS Inc., Chicago, IL, USA). The difference between the two groups was analyzed by *t*-test. Pearson correlation test was employed for correlation analysis, and $P<0.05$ signified statistical significance.

RESULTS

Circ_0020378 is abnormally highly expressed in OS

CircRNA expression profiles of OS tissues in GSE140256 were downloaded from the microarray dataset Gene Expression Omnibus (GEO) database. We found that 4 circRNAs were significantly up-regulated, and 6 circRNAs were markedly down-regulated in OS

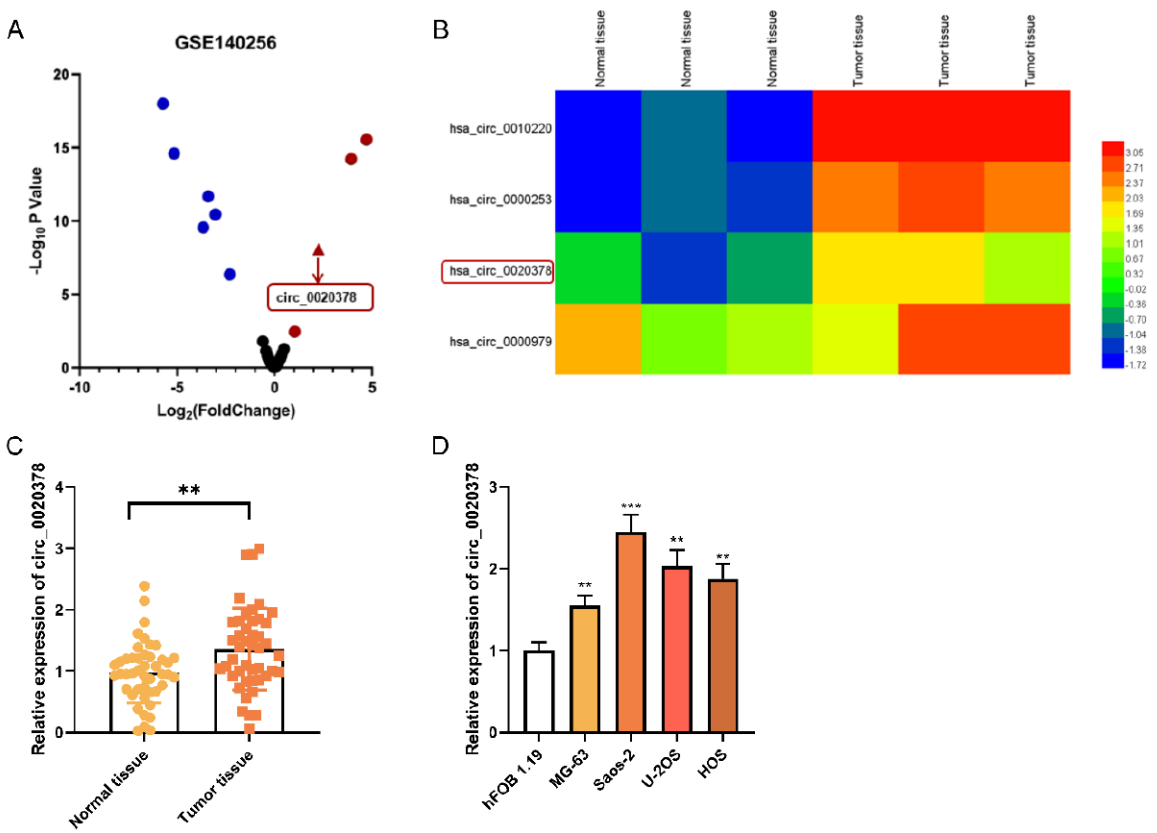


Fig 1. *Circ_0020378 expression is up-regulated in OS tissues and cells. **A**): The gene microarray dataset GSE140256 was downloaded from the GEO database and a volcano plot was utilized to analyze circRNAs with differential expression in OS tissue samples (vs normal tissues); **B**): The heat map showed 4 circRNAs that were significantly up-regulated in OS tissue; **C**): Circ_0020378 expression in 45 cases of OS tissues and their paired paracancerous tissues was detected by qRT-PCR; **D**): qRT-PCR was employed to detect circ_0020378 expression in a human osteoblast cell line (hFOB 1.19) as well as in four human OS cell lines (MG-63, Saos-2, U-2OS, and HOS). *P<0.05, **P<0.01, ***P<0.001.*

tissues (P<0.05, |Log2FC| >1) (Fig 1A). Among the four circRNAs up-regulated, circ_0020378 was found to be significantly up-regulated in OS tissue (Log2FC = 2.257567, P < 0.001, Fig 1B). qRT-PCR was conducted to detect circ_0020378 expression in OS tissues as well as normal tissues, and the data showed that circ_0020378 was significantly highly expressed in OS tissues (Fig 1C). Also, circ_0020378 expression was significantly up-regulated in MG-63, Saos-2, U-2OS, and HOS cells compared to human osteoblast cell line (hFOB 1.19) (Fig 1D). Among the OS cell lines, circ_0020378 expression was relatively low in MG-63 cells and relatively high in Saos-2 cells, so these two cell lines were selected for subsequent experiments.

Effects of Circ_0020378 on proliferation, migration and invasion of OS cells

In order to investigate the biological function of circ_0020378 in OS cells, circ_0020378 overexpression plasmid and its control were transfected into MG-63 cells, and si-circ_0020378#1, si-circ_0020378#2 and its control were transfected into Saos-2 cells. qRT-PCR showed that the transfection was successful (Fig 2A-B). Next, the proliferation of OS cells was analyzed using CCK-8 assay as well as BrdU assay, and the results revealed that circ_0020378 overexpression significantly promoted the proliferation of OS cells, while knockdown of circ_0020378 significantly inhibited the proliferation of OS cells (Fig 2C-D). A

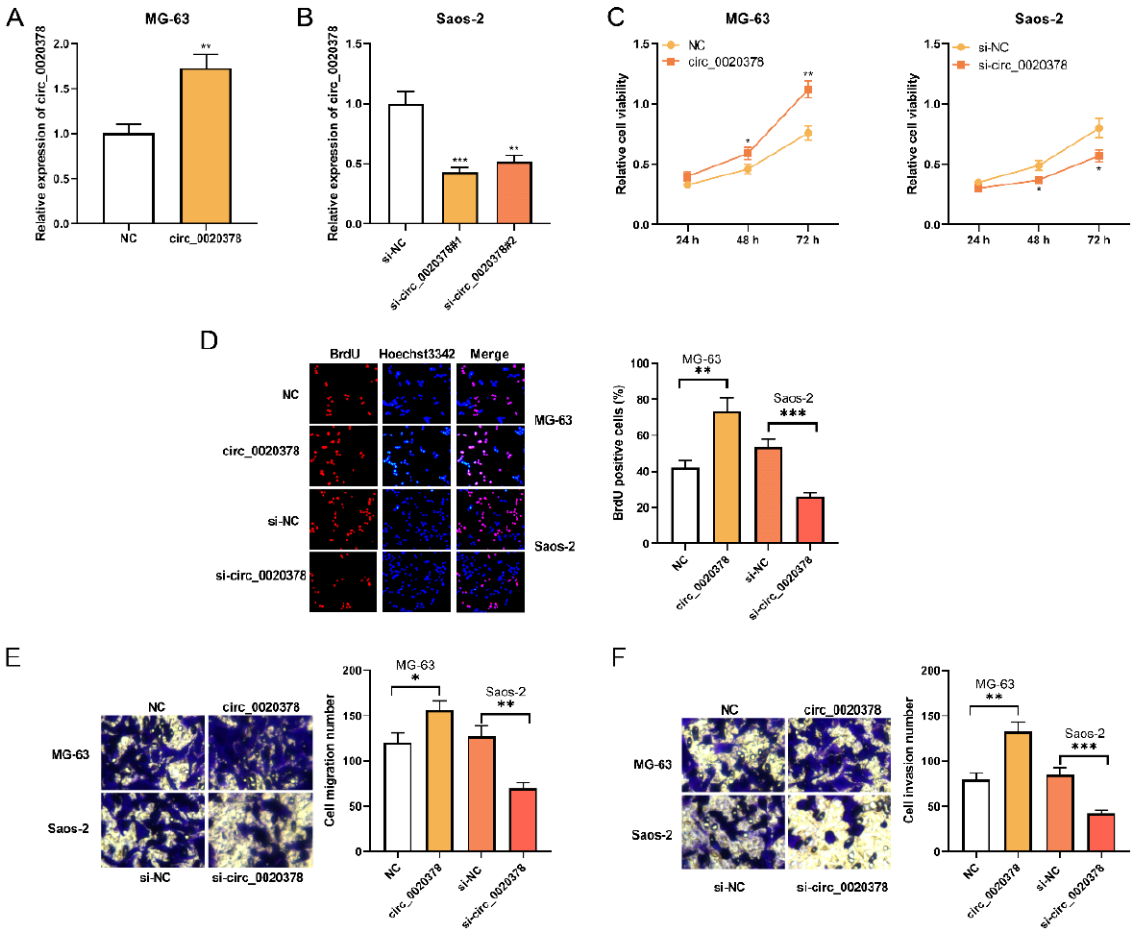


Fig 2. *Role of Circ_0020378 on OS cell proliferation, migration and invasion. **A-B**): qRT-PCR was utilized to detect the transfection efficiency of circ_0020378 overexpression plasmid and circ_0020378 siRNA in MG-63 and Saos-2 cells; **C**): The proliferation of MG-63 and Saos-2 cells was detected by CCK-8 assay after the transfection; **D**): The proliferation of MG-63 and Saos-2 cells was detected by BrdU assay after the transfection; **E-F**): The migration and invasion of MG-63 and Saos-2 cells were evaluated by Transwell assay after the transfection. *P<0.05, **P<0.01, ***P<0.001.*

Transwell experiment was conducted to evaluate the migration and invasion capabilities of OS cells, and the results revealed that circ_0020378 overexpression significantly promoted the migration and invasion of OS cells, while knockdown of circ_0020378 significantly inhibited the migration and invasion of OS cells (Fig 2E-F).

Circ_0020378 specifically and negatively regulates miR-1200 in OS cells

To investigate the targeting regulatory mechanism of circ_0020378, the CircInteractome database (https://circinteractome.nia.nih.gov/) was searched, and it showed a possible binding site between circ_0020378 and miR-1200 (Fig 3A). Moreover, circ_0020378-wt (or circ_0020378-mut) was co-transfected with miR-1200 (or miR-NC) into MG-63 and Saos-2 cells, respectively, and then the luciferase activity in the cells was detected, and the data showed that the luciferase activity was significantly reduced in the cells co-transfected with wild type reporter, while no significant change in luciferase activity was observed in cells co-transfected with mutant type reporter (Fig 3B). qRT-PCR showed that circ_0020378 overexpression significantly inhibited miR-1200 expression in MG-63 cells, while knockdown of circ_0020378 significantly promoted miR-1200 expression in Saos-2 cells (Fig 3C). Through qRT-PCR, we also found that miR-1200 was downregulated in OS tissues, which was negatively correlated with circ_0020378 expression (Fig 3D-E).

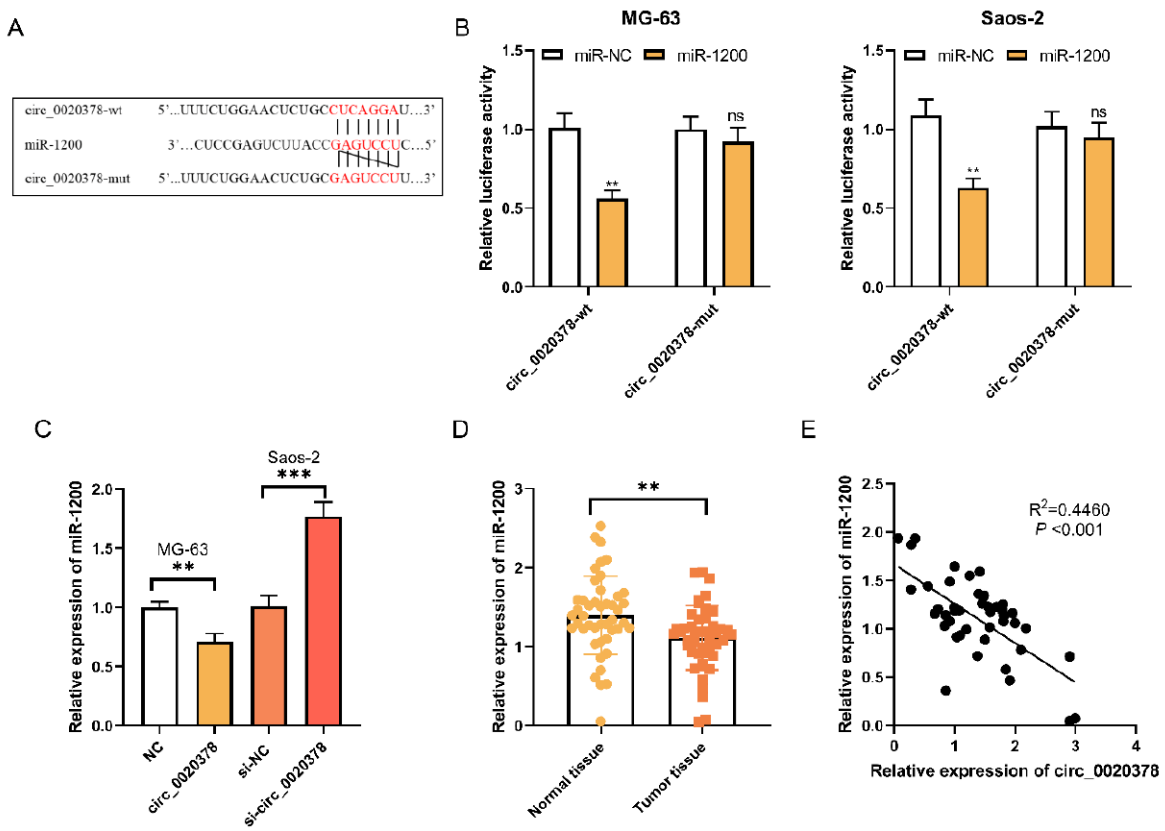


Fig 3. *Circ_0020378 specifically and negatively modulated miR-1200.* ***A****): The binding site between circ_0020378 and miR-1200 was predicted by the CircInteractome database;* ***B****): Dual-luciferase reporter gene assay to verify the binding relationship between circ_0020378 and miR-1200;* ***C****): qRT-PCR was employed to detect miR-1200 expression in OS cells with circ_0020378 overexpression or knockdown;* ***D****): MiR-1200 expression in 45 cases of OS tissues and their paired paracancerous tissues was detected by qRT-PCR;* ***E****): Pearson's correlation coefficient was employed to analyze the correlation between miR-1200 expression and circ_0020378 expression in OS tissues. **P<0.01, ***P<0.001.*

Circ_0020378 targets miR-1200 to regulate CDH6 expression

To explore the downstream mechanism of miR-1200, the downstream targets of miR-1200 were predicted by TargetScan (http://www.targetscan.org/) and miRPathDB (https://mpd.bioinf.uni-sb.de/overview.html), and 4652 candidate target genes of miR-1200 were found (Fig. 4A). Through the KEGG bioinformatics website (http://www.kegg.jp/), the 4652 target genes mentioned above were found to be significantly associated with MAPK and PI3K/Akt pathway (Fig. 4B). One of the potential downstream targets of miR-1200 was CDH6, and the binding sequence was

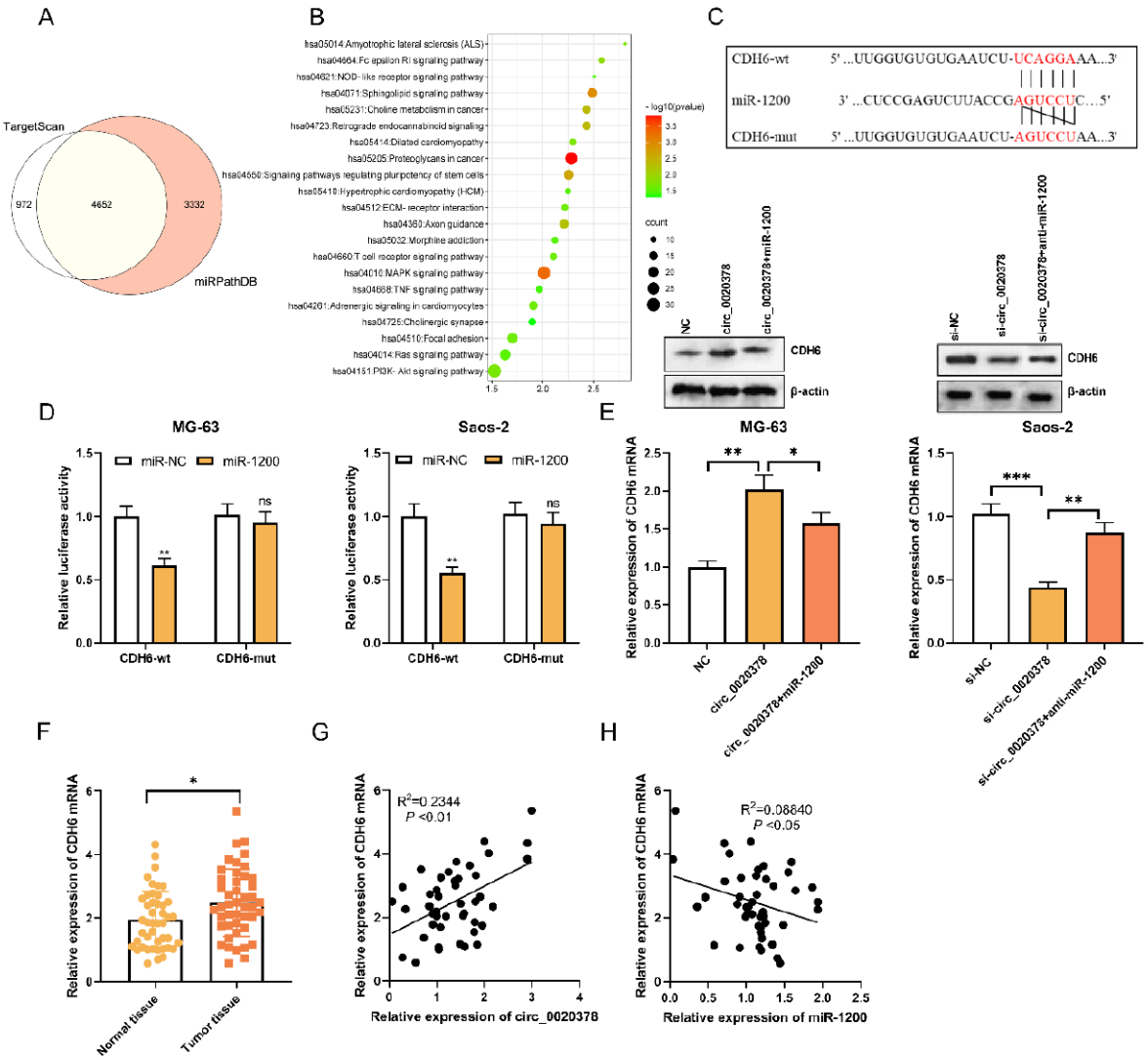


Fig 4. *Circ_0020378 sponges miR-1200 to up-regulate CDH6 expression. **A**): The downstream targets of miR-1200 were predicted through TargetScan and miRPathDB bioinformatics websites; **B**): KEGG analysis was used to analyze the biological function of the target genes of miR-1200; **C**): The binding site between miR-1200 and CDH6 3'UTR was predicted by the TargetScan database; **D**): Dual-luciferase reporter gene assay was employed to verify the binding relationship between miR-1200 and CDH6; **E**): CDH6 expression in MG-63 and Saos-2 cells was detected by qRT-PCR and Western blot; **F**): CDH6 mRNA expression in 45 OS tissues and their paired paracancerous tissues was detected by qRT-PCR; **G**): Pearson's correlation coefficient was employed to analyze the correlation between CDH6 mRNA and circ_0020378; **H**): Pearson's correlation coefficient was utilized to analyze the correlation between CDH6 mRNA and miR-1200. *P<0.05, **P<0.01.*

shown (Fig, 4C). The results of the dual-luciferase reporter gene experiment showed that luciferase activity was significantly reduced in OS cells co-transfected with circ_0020378-wt and miR-1200 mimics, while no significant change in luciferase activity was observed in OS cells co-transfected with circ_0020378-mut and miR-1200 (Fig. 4D). qRT-PCR and Western blot showed that upregulation of circ_0020378 promoted CDH6 expression, while restoration of miR-1200 reversed this effect; knockdown of circ_0020378 inhibited CDH6 expression, while inhibition of miR-1200 reversed this effect (Fig. 4E). Additionally, qRT-PCR revealed that CDH6 mRNA expression was significantly up-regulated in OS tissues, which was positively correlated with circ_0020378 expression and negatively correlated with miR-1200 expression (Fig 4F-H).

DISCUSSION

More and more circRNAs have been unveiled to be involved in regulating the biological behaviours of OS cells. For example, circ_XPR1 promotes the proliferation of OS cells by sponging miR-214-5p to regulate DDX5 expression (7). In this study, circ_0020378 was found to be significantly up-regulated in OS tissues, and it promotes the proliferation, migration and invasion of OS cells. To our best knowledge, this is the first study that investigates the role of circ_0020378 in cancer biology.

MiR-1200 is aberrantly expressed in multiple malignancies (5, 8, 9). Importantly, miR-1200 expression is down-regulated in OS, and miR-1200 overexpression directly targets HOXB2 to regulate PI3K/Akt pathway and Bcl-2 pathway, inhibiting OS progression (5). Consistently, we observed that miR-1200 expression was down-regulated in OS, and it inhibited the malignancy of OS cells. Additionally, it was revealed that miR-1200 could be negatively regulated by circ_0020378, which partly explains the mechanism of miR-1200 dysregulation in OS.

CDH6 is a type 2 cadherin that drives the epithelial-mesenchymal transition during embryonic development (10). CDH6 is considered an oncoprotein, and it regulates several cancer-related pathways such as FAK, AKT and ERK (11, 12). Notably, high CDH6 expression enhances the aggressiveness of OS cells (6). In this work, we found that CDH6 was a downstream target of miR-1200, and circ_0020378 could regulate CDH6 via repressing miR-1200. These data suggest that the competitive endogenous RNA (ceRNA) network of circ_0020378, miR-1200 and CDH6 is involved in OS progression.

Ethics statement

Our study was approved by the Ethics Review Board of Xiangyang Central Hospital.

Data Availability Statement

The data used to support the findings of this study are available from the corresponding author upon request.

REFERENCES

1. Brown HK, Tellez-Gabriel M, Heymann D. Cancer stem cells in osteosarcoma. Cancer Lett 2017; 386:189-195.
2. Harrison DJ, Geller DS, Gill JD, Lewis VO, Gorlick R. Current and future therapeutic approaches for osteosarcoma. Expert Rev Anticancer Ther 2018; 18(1):39-50.
3. Verduci L, Strano S, Yarden Y, Blandino G. The circRNA-microRNA code: emerging implications for cancer diagnosis and treatment. Mol Oncol 2019; 13(4):669-680.
4. Kristensen LS, Hansen TB, Venø MT, Kjems J. Circular RNAs in cancer: opportunities and challenges in the field. Oncogene 2018; 37(5):555-565.
5. Li S, Pei Y, Wang W, Liu F, Zheng K, Zhang X. Circular RNA 0001785 regulates the pathogenesis of osteosarcoma as a ceRNA by sponging miR-1200 to up-regulate HOXB2. Cell Cycle 2019; 18(11):1281-1291.
6. Ji Q, Xu X, Song Q, et al. miR-223-3p Inhibits Human Osteosarcoma Metastasis and Progression by Directly Targeting CDH6. Mol Ther 2018; 26(5):1299-1312.
7. Mao X, Guo S, Gao L, Li G. Circ-XPR1 promotes osteosarcoma proliferation through regulating the miR-214-5p/DDX5 axis. Hum Cell 2021; 34(1):122-131.
8. Zhang Z, Yu X, Zhou B, Zhang J, Chang J. Circular RNA circ_0026359 Enhances Cisplatin Resistance

in Gastric Cancer via Targeting miR-1200/POLD4 Pathway. Biomed Res Int 2020; 2020:5103272.
9. Pan B, Zhao M, Wang N, Xu L, Wu T, Li Z. LncRNA RGMB-AS1 Promotes Glioma Growth and Invasion Through miR-1200/HOXB2 Axis. Onco Targets Ther 2019; 12:10107-10114.
10. Gugnoni M, Sancisi V, Gandolfi G, et al. Cadherin-6 promotes EMT and cancer metastasis by restraining autophagy. Oncogene 2017; 36(5):667-677.
11. Gugnoni M, Manicardi V, Torricelli F, et al. Linc00941 Is a Novel Transforming Growth Factor β Target That Primes Papillary Thyroid Cancer Metastatic Behavior by Regulating the Expression of Cadherin 6. Thyroid 2021; 31(2):247-263.
12. Bartolomé RA, Robles J, Martin-Regalado Á, et al. CDH6-activated αIIbβ3 crosstalks with α2β1 to trigger cellular adhesion and invasion in metastatic ovarian and renal cancers. Mol Oncol 2021; 15(7):1849-1865.

Identification of immune-related genes associated with spared nerve injury neuropathic pain

Y. Lu, W. Chen, Y. Chang and YQ. Chen

Department of Anesthesiology, The First Affiliated Hospital of Wannan Medical College, Wuhu City, Anhui Province, China

Received September 17, 2021 – Accepted January 20, 2022

To the Editor,

Neuropathic pain (NP) represents a complex chronic condition characterized by various sensory, cognitive, and affective symptoms (1). This disease with persistent, unbearable sensations has seriously affected up to 10% of the general population (2). Spared nerve injury (SNI) is an animal model of persistent peripheral neuropathic pain, which may provide an additional resource for unravelling the mechanisms responsible for producing neuropathic pain (3). Nevertheless, present therapies only work for less than 40% of neuropathic pain patients, and treatment outcomes vary from person to person with high instability (4). Hence, identifying the key genes and potential effective therapeutics toward neuropathic pain are urgently needed. Reciprocal interactions between the nervous system and the immune system have been recognized as playing a crucial role in the initiation and maintenance of pain. Several preclinical studies have provided evidence for the involvement of cytokines, predominantly secreted by a variety of immune cells and by glial cells from the nervous system, in neuropathic pain conditions (5). For instance, microglia in the dorsal horn drives neuropathic pain as a kind of immune cell (6). However, the specific immune cell lines and underlying mechanism between gene and immune cell in NP remain excluded. In the present study, we aimed to screen out the immune-related cell that plays an important role in the neuropathic pain procession. The neuropathic pain-related dataset was downloaded from the NCBI public dataset for integrated bioinformatics analyses. This study promoted our understanding of the mechanism or therapy of neuropathic pain.

MATERIALS AND METHODS

Data acquisition

The RNA-Sequencing (RNA-Seq) dataset profile (GSE102721) (3) of neuropathic pain and normal tissues was obtained from the National Center for Biotechnology Information (NCBI) database (http://www.ncbi.nlm.nih.gov/geo). High temporal analysis of global gene expression in spared nerve injury (SNI) correlated with behaviour taken at the same time points. These RNA-seq samples were generated from a total of 12 mice, including the naive group and 1/3/7 days groups (n=3).

Identification of differentially expressed genes (DEGs)

R package DESeq2 was used to identify the DEGs. After integrating the data into an expression matrix and normalizing it, the differential expression genes (DEGs) were screened out with the threshold of adjusted P-value <0.05 and fold change ≥ 1.5.

Analysis of DEGs expression

The software program Short Time-series Expression Miner (STEM) is designed for clustering, comparing,

Key words: neuropathic pain (NP), bioinformatics analysis, immune-related genes, immune cells

*Corresponding author:
Dr Yong-Quan Chen,
No.2 Zheshan West Road,
Jinghu District, Wuhu,
Anhui Province, 241000, China
e-mail: wyfydrchenyongquan@163.com

0393-974X (2022)
Copyright © by BIOLIFE, s.a.s.
This publication and/or article is for individual use only and may not be further reproduced without written permission from the copyright holder.
Unauthorized reproduction may result in financial and other penalties
DISCLOSURE: ALL AUTHORS REPORT NO CONFLICTS OF INTEREST RELEVANT TO THIS ARTICLE.

and imaging gene expression data from short time series microarray trials. In order to search for the differences in gene expression between NP stages, the STEM tool was applied to profile candidate genes simultaneously from normal status to stage IV. Curtly, the union of DEGs from five stages was input and formalized by STEM. The maximum number of model lives was set as 100, and FDR was named as a correction system. The rest parameters remained unchanged. Coloured clusters indicated a statistically significant number of genes assigned.

Function enrichment analysis

The Gene Ontology (GO) annotations and Kyoto Encyclopedia of Genes and Genomes (KEGG) pathway analysis were applied to investigate the roles of all DE-mRNAs. GO annotations, including biological process (BP), cellular component (CC) and molecular function (MF), was performed using the DAVID database (https://david.ncifcrf.gov). KEGG network was constructed by Cytoscape ClueGo. The pathways were significant enrichment with P-value <0.05.

Quantifying tissue-infiltrating immune and stromal cells based on murine Microenvironment Cell Populations counter (mMCP-counter) method

The mMCP-counter analytical tool was developed to analyze the 16 defined cell populations, including the relative

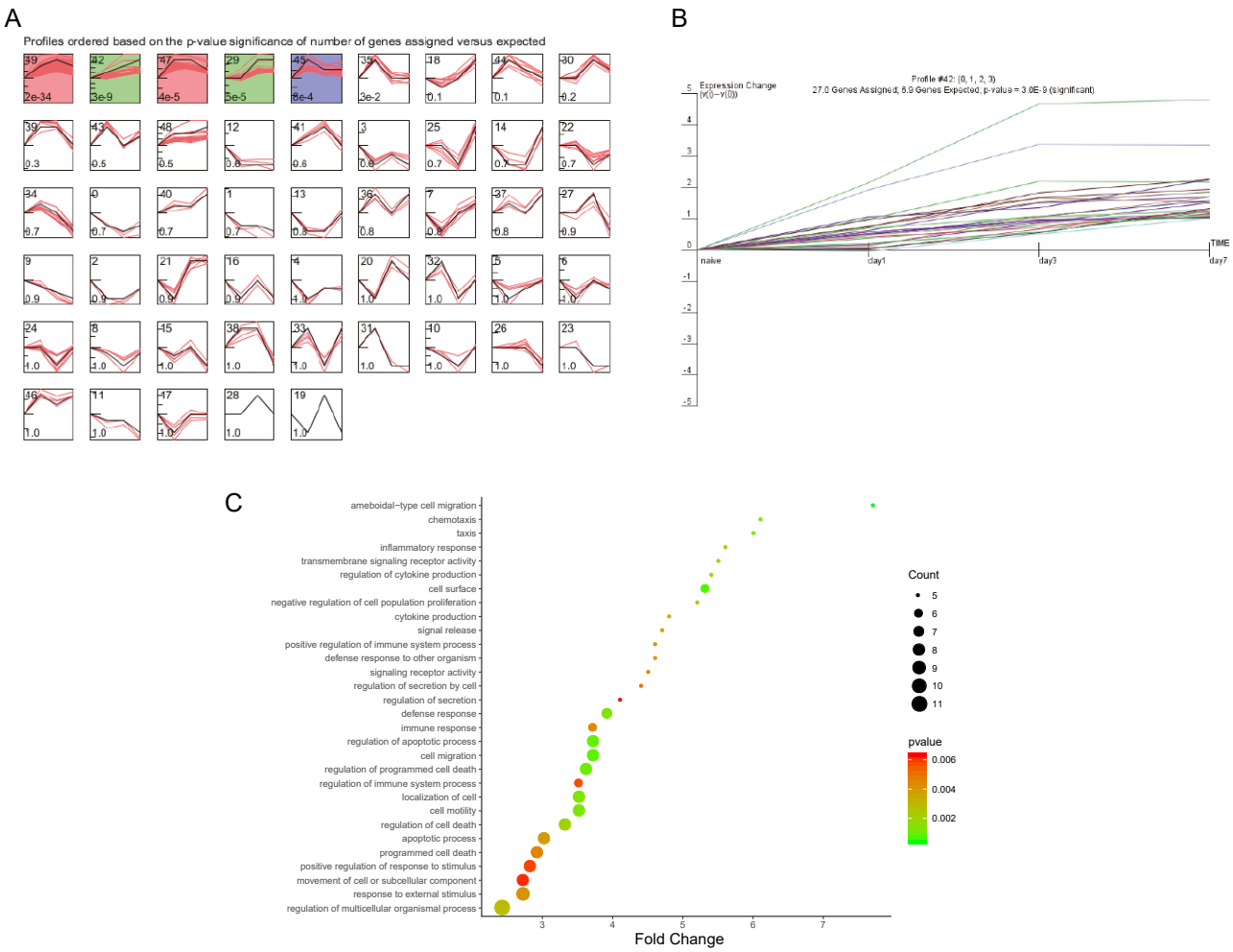


Fig. 1. *The dynamic change trend and enrichment of genes at different time points. **A)** Gene expression patterns from normal tissue to NP stages were clustered, compared, and visualized by the STEM software. Coloured clusters indicated a statistically significant number of genes enriched. The number in the bottom left indicated the number of genes assigned. The number in the top left represented model identifier; **B)** Change trend of module 42 genes; **C)** Biological process for GO enrichment analysis of module 42 genes.*

fractions of 12 immune and 4 stromal murine cell types in each tissue. The mMCP-counter analytical (https://github.com/cit-bioinfo/mMCP-counter) was made based on the release of large datasets of murine sorted immune populations by the Immunological Genome Project (ImmGen). The mMCP-counter values generated were defined as immune cell infiltration fraction per sample. Significant results ($p < 0.05$) were selected for subsequent analysis.

Statistical analysis

We performed correlation analysis using Student's t-test by GraphPad Prism 8; p-value <0.05 was considered statistically

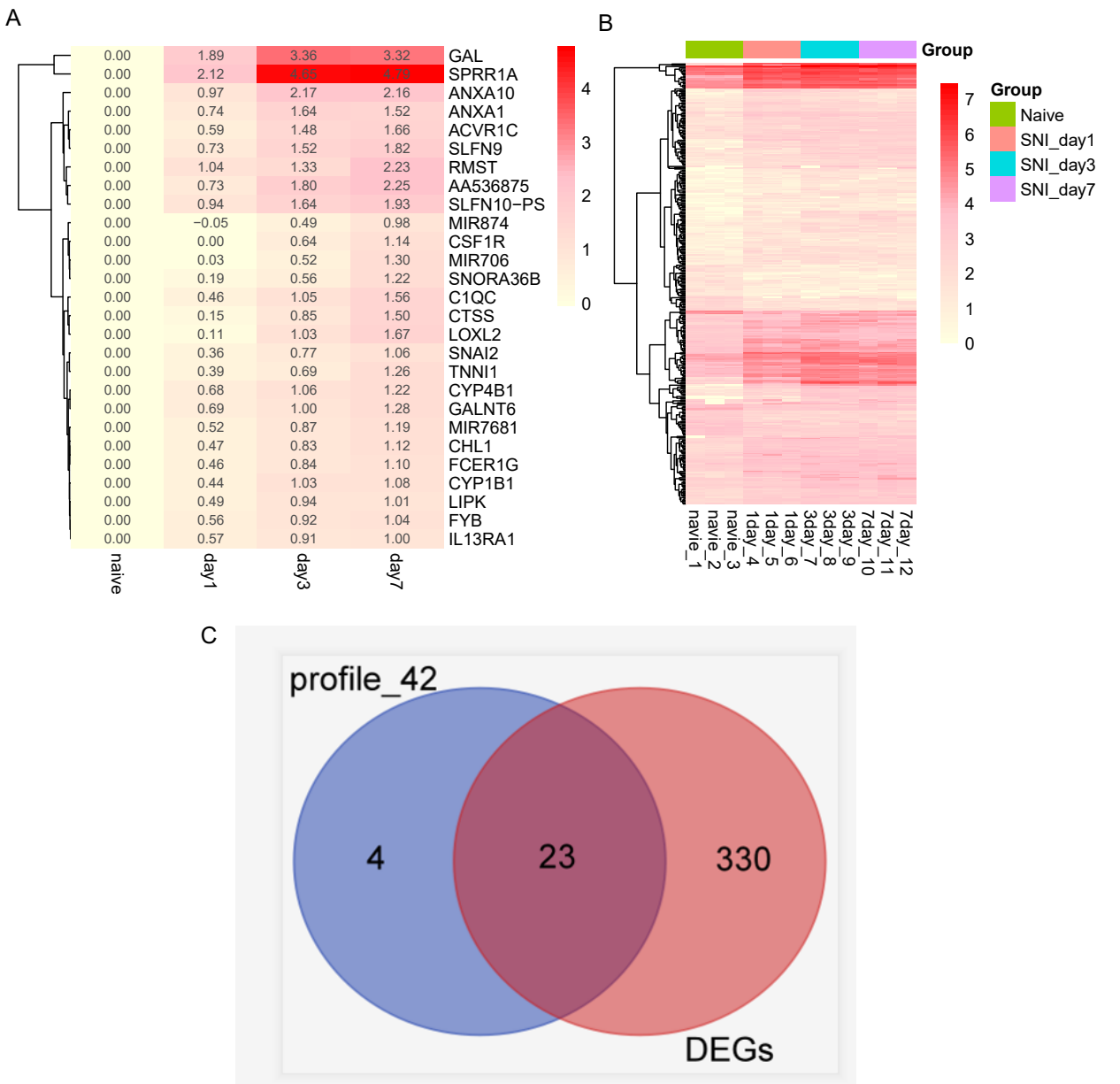


Fig. 2. *Identification of the DEGs in NP.* ***A****) The heat map showing the gene expression of module 42 with a total of 27 genes;* ***B****) The heat map showing the DEGs identified based on the GSE102721 dataset;* ***C****) The Venn diagram showing common immune-related DEGs between module 42 and GSE102721 dataset.*

significant. Data processing and analysis using GraphPad Prism 8 and R software (R software, version 3.5.1).

RESULTS

The dynamic change trend and enrichment of genes at different time points

Researchers performed a series of quality controls to ensure that the chip quality met the study criteria. The data was integrated into an expression matrix and normalized. In order to investigate the differences in gene expression between NP stages, the STEM tool was applied to profile stage course gene expression patterns. A total of 50 expression manners were enriched among assumed expression models (Fig. 1A). Notably, we found some clusters exhibited stage-specific expression trends throughout NP progression. Genes in Model 42 were specifically up-regulated at

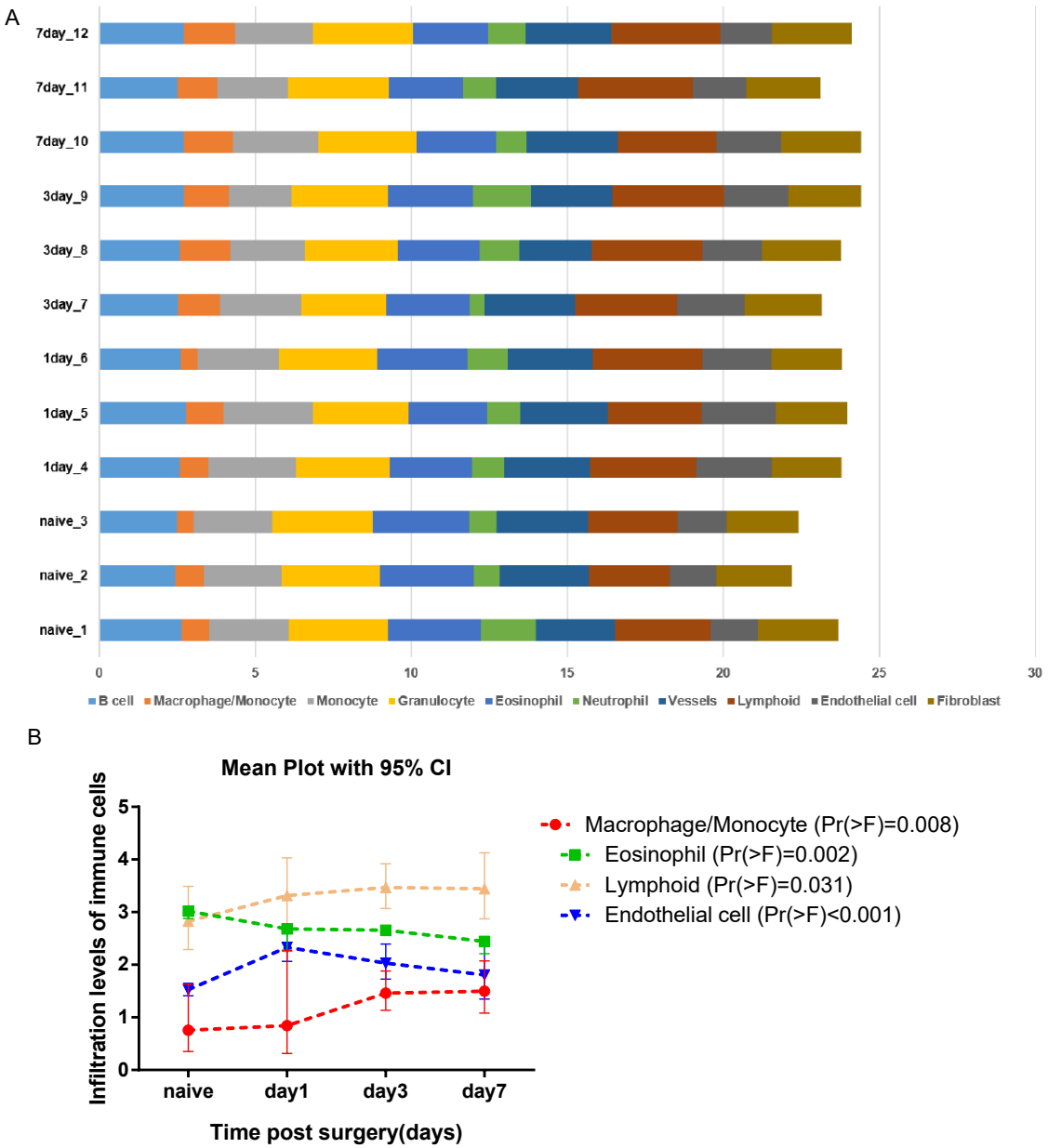


Fig. 3. *The immune infiltration level of mouse model was analyzed by mMCP counter. **A**) The immune cells of 12 samples; **B**) 4 immune cells significantly changed analysis by ANOVA univariate analysis (F test).*

all stages. The changing trend of module 42 genes is shown in Fig. 1B. We performed the GO enrichment analysis and found that the genes in the module were significantly enriched in immune-related biological function. As seen in Fig. 1C, biological process like an inflammatory response, regulation of cytokine production, immune response, positive regulation of immune system process was significantly enriched. Considering the association between NP and immunity, module 42 was selected for the following study.

Identification of immune-related DEGs

In the next step, the DEGs in module 42 were screened out and demonstrated in Fig. 2A. The heat map shows the gene expression of module 42 with a total of 27 genes, including GAL, FYB, FCER1G, Ctss, C1qc, Anxa1, etc. What's more, a total of 353 DEGs in the GSE102721 dataset were also identified (Fig. 2B). To screen out the immune-related DEGs, we carried the Venn analysis, and a total of 23 common DEGs overlapped by the two datasets were identified. Among these 23 common DEGs, 6 DEGs were found to be related to immunity, including GAL, FYB, FCER1G, Ctss, C1qc, and Anxa1 (Fig. 2C). Thus, these six genes were selected for the following study.

The immune cells in neuropathic pain

To analyze the immune landscape of the neuropathic pain microenvironment, the mMCP-counter analytical tool was applied to distinct immune cell subsets between neuropathic pain and the control group. The mMCP-counter is a method based on highly specific transcriptomic markers that allow to accurately quantify 6 immune and 4 stromal murine cell populations using gene expression. The gene matrix was used for predicting the abundance of 10 cell populations in individual tissue samples. The following 10 types of immune cells condition in 12 samples were obtained, including B cells, macrophage/monocyte, monocyte, granulocyte, eosinophil, neutrophil, vessels, lymphoid, endothelial cell and fibroblast. As a result, Fig. 3A showed the effects of different time points on immune cells in neuropathic pain. There are 4 kinds of immune cells that presented significant change (Fig. 3B), including monocytes/macrophages, eosinophil, lymphoid and endothelial cells.

Correlation between the immune cell and immune-related genes

To further investigate the correlation between immune cells and immune-related genes, we

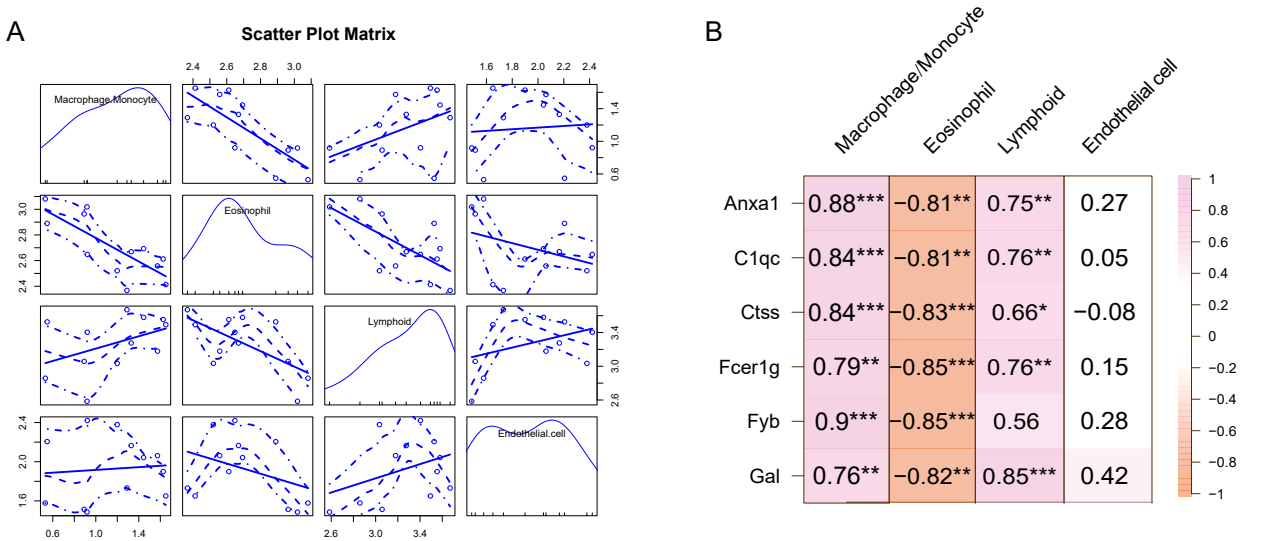


Fig. 4. *Correlation of immune cells and DEGs. **A**) Correlation between four kinds of immune cells, including monocytes/macrophages, eosinophil, lymphoid and endothelial cell; **B**) Correlation between immune-related genes (GAL, FYB, FCER1G, Ctss, C1qc, and Anxa1) and immune cells (including monocytes/macrophages, eosinophil, lymphoid and endothelial cell) by t-test analysis.*

calculated the correlation among the 4 kinds of immune cells (including monocytes/macrophages, eosinophil, lymphoid and endothelial cells) (Fig. 4A). Besides, the t-test analysis was carried out to calculate the correlation of 4 kinds of immune cells and 6 immune-related genes (GAL, FYB, FCER1G, Ctss, C1qc, and Anxa1). As shown in Fig. 4B, the six genes were significantly correlated with monocytes/macrophages, eosinophil, and lymphoid, suggesting that these genes play an important role in immune cell regulation.

DISCUSSION

The consequences of immune-related genes in neuropathic pain, which involve the control of pain, are poorly understood. In this study, we identified 6 immune-related DEGs, including GAL, FYB, FCER1G, Ctss, C1qc, and Anxa1. These genes, which have previously been linked to immune pathways, have few reports in neuropathic pain. Besides, the mMCP-counter was performed, and four types of immune cells that play an important role in the neuropathic pain progression were screened out, including monocytes/macrophages, eosinophil, lymphoid and endothelial cells. Preclinical models of neuropathic pain provide evidence for a critical mechanistic role for immune cells in the chronicity of pain (7). Endothelial cells, monocytes, and macrophages are cell types interacting with sensory neurons (8). Depletion of macrophages reduces axonal degeneration and hyperalgesia following nerve injury (9). Endothelial damage and increased neuronal activity result in recruitment of monocytes/macrophages (peripherally) and activation of microglia (centrally), which release mediators that lead to sensitization of neurons, thereby enabling positive feedback that sustains chronic pain (10). Eosinophilia is frequently associated with peripheral neuropathy, and neuropathic pain is a major presentation (11). For the first time, our result illustrated that the above six genes (GAL, FYB, FCER1G, Ctss, C1qc, and Anxa1) were significantly correlated with monocytes/macrophages, eosinophil, and lymphoid. However, the specific molecular regulation mechanism needs to be embodied in further experiments.

ACKNOWLEDGEMENTS

This work was supported by the Young and middle-aged Scientific Research Fund of Wannan Medical College (No. WK2020F10).

Conflict of interest

The authors declare that they have no competing interests.

REFERENCE

1. Jiang M, Chen X, Zhang L, et al. Electroacupuncture suppresses glucose metabolism and GLUT-3 expression in medial prefrontal cortical in rats with neuropathic pain. Biological research 2021; 54(1):24.
2. Tang S, Jing H, Huang Z, et al. Identification of key candidate genes in neuropathic pain by integrated bioinformatic analysis. J Cell Biochem 2020; 121(2):1635-1648.
3. Cobos E, Nickerson C, Gao F, et al. Mechanistic Differences in Neuropathic Pain Modalities Revealed by Correlating Behavior with Global Expression Profiling. Cell Rep 2018; 22(5):1301-1312.
4. Backonja M-M, Irving G, Argoff C. Rational multidrug therapy in the treatment of neuropathic pain. Curr Pain Headache R 2006; 10(1):34-38.
5. Lacagnina, M., et al., Autoimmune regulation of chronic pain. Pain Rep 2021. 6(1): p. e905.
6. Yang X, Zhu L, Zhao B, et al. Screening and Identification of Key Genes, Pathways, and Drugs Associated with Neuropathic Pain in Dorsal Horn: Evidence from Bioinformatic Analysis. J Pain Res 2021; 14:1813-1826.
7. Malcangio M. Role of the immune system in neuropathic pain. Scand J Pain 2019; 20(1):33-37.
8. Brederson J D, Strakhova M, Mills C, et al. A monoclonal antibody against the receptor for advanced glycation end products attenuates inflammatory and neuropathic pain in the mouse. :Eur J Pain-London 2016; 20(4):607-614.
9. Liu T, van Rooijen N, Tracey D J. Depletion of macrophages reduces axonal degeneration and hyperalgesia following nerve injury. Pain 2000; 86(1-2):25-32.

10. Trevisan G, Benemei S, Materazzi S, et al. TRPA1 mediates trigeminal neuropathic pain in mice downstream of monocytes/macrophages and oxidative stress. Brain: a journal of neurology 2016; 139(Pt 5):1361-1377.
11. Chao C-C, Hsieh S-T, Shun C-T, et al. Skin denervation and cutaneous vasculitis in eosinophilia-associated neuropathy. Arch Neurol 2007; 64(7):959-965.

Efficacy of oral intake of a compound medical device in the treatment of laryngopharyngeal reflux disease: a clinical investigation and nasal cytological correlations

E. Maffezzoni[1], K. Luciano[2], F. Maffezzoni[3], S. Agostini[4] and M. Notargiacomo[2]

[1]Rhinocytoallergology Unit, Istituto Figlie di San Camillo, Cremona, Italy; [2]Otorhinolaryngology Unit, Melzo Hospital, Milan, Italy; [3]Clinical psychology, Poliambulatorio Oberdan, Brescia, Italy; [4]Scientific Direction, Pharma Line, Milan, Italy

To the Editor,

Laryngopharyngeal reflux (LPR) is a condition characterized by gastroduodenal contents rising up the oesophagus, thus coming into contact with the epithelium lining the larynx and hypopharynx (1, 2). Typical manifestations of LPR include raclage, asthma, chronic cough, dysphonia, hypopharyngeal globus sensation and laryngitis (2). In some cases, gastric contents may reach the nasal cavities, inducing or exacerbating rhinitis and sinusitis (2-4). Clinical studies have shown that LPR has a negative effect on nasal resistance and nasal congestion and that treatment of LPR can lead to subjective and objective improvement in nasal complaints (5). The chronic inflammatory process that characterizes LPR leads to an increase in the presence of inflammatory cells, and a progressive remodelling of the nasal mucosa, until the manifestation of goblet cell metaplasia. This situation leads to a progressive impairment of mucociliary clearance, which, in turn, leads to bacterial colonization and the onset of infections, which further support the inflammatory state; this gives rise to a vicious circle with mutual reinforcement of inflammation and metaplasia. Nasal cytology represents a useful, inexpensive and easily applicable diagnostic method that allows, through the quantification of cell populations in the nasal mucosa, to detail the phenotypic characteristics of LPR to better discriminate pathological conditions and assess pathological conditions the effect of the applied therapeutic strategy. A recent study confirmed the relationship between nasal mucosal cytology, chronic rhinosinusitis and gastroesophageal reflux disease by comparing the results of rhinocytogram and pH-impedance testing (4). Suppression of gastric acid production by proton pump inhibitors (PPIs) remains the mainstay of LPR treatment, although the efficacy of PPIs in the treatment of LPR is controversial (6). The objectives of this study are to assess the efficacy of the compound medical device in reducing the signs and symptoms of LPR and in protecting the mucosa of the upper respiratory tract from the potential damage of gastric reflux, also by performing a comparison between the state of the nasal mucosa of healthy subjects and the state of the nasal mucosa of patients suffering from LPR.

MATERIALS AND METHODS

Medical device tested

Leniref® (Lmd; Pharma Line S.r.l. Milan) is a compound medical device (EC certificate no. 471-00-00 DM, obtained on 20 April 2020) based on magnesium alginate, calcium carbonate, potassium bicarbonate, extract of *Opuntia ficus-indica* L. and extract of *Olea europaea* L. The product is indicated for the treatment of gastroesophageal reflux and

Keywords: Laryngopharyngeal reflux, nasal cytology, magnesium alginate, Opuntia ficus-indica extract, Olea europaea extract, medical device

Corresponding author:
Dr. Mario Notargiacomo,
Unità di Otorinolaringoiatria,
Ospedale di Melzo,
Via Volontari del Sangue 5,
20066 Melzo (MI), Italy
e-mail: mario.notargiacomo63@gmail.com

0393-974X (2022)
Copyright © by BIOLIFE, s.a.s.
This publication and/or article is for individual use only and may not be further reproduced without written permission from the copyright holder.
Unauthorized reproduction may result in financial and other penalties
DISCLOSURE: ALL AUTHORS REPORT NO CONFLICTS OF INTEREST RELEVANT TO THIS ARTICLE.

associated symptoms. It is also indicated for the treatment of LPR and its associated symptoms. The product was provided free of charge by Pharma Line (Milan).

Subjects assessed

Sixty-eight subjects were assessed, including 41 patients (23 men, 18 women) with LPR and treated with Lmd, and 27 healthy subjects (12 men, 15 women). The demographic and medical history data of the patients enrolled in the study are shown in Table I.

Adult male and female patients with LPR were included in the study. To be included, patients had to be older than 18 years, having symptoms of LPR for at least 3 months and at least 3 times a week, score on the Reflux Symptom Index (RSI) greater than 13, and at video-laryngoscopy have morphological lesions of the larynx attributable to LPR, as evidenced by a Reflux Finding Score (RFS) greater than 7. Patients who had not undertaken continuous treatment yet for LPR, or those who had already had treatment for LPR, were enrolled. In the latter case, T0 was 15 days after discontinuation of any therapy based on antacids, alginates and related products. Patients already treated chronically with PPIs or H2-receptor antagonists maintained a constant drug dosage throughout the study period.

Subjects with known sensitivity to one or more components of Lmd, malignant or inflammatory diseases of the upper respiratory tract and upper gastrointestinal tract, inhalant or food allergies and pregnant and breastfeeding women were excluded from the study.

Twenty-seven healthy subjects were also enrolled for comparison purposes. These subjects were required to have an RSI score of less than 13 and no morphological lesions of the larynx attributable to LPR at video-laryngoscopy, which was confirmed by an RFS score of less than 7.

Subjects were enlisted with their identification data and signed regular informed consent to both the proposed therapy and the processing of personal data. At the time of enrolment, a medical history form was completed for each patient with the data collected, and a second form was provided to be returned on their next check-up.

Study design

This prospective, multicentre, observational study compares LPR patients treated with the medical device with healthy subjects. The period of patient enrolment and treatment was extended from February to August 2021.

Patients in the Lmd group were screened on three occasions: at the start of Lmd intake (T0), after 30 days of Lmd intake (T1) and after 30 days of stopping Lmd intake (T2). From the time of initiation (T0) and for the following 30 days (T0 to T1), patients took one sachet of Lmd after the two main meals and before going to bed. In addition, healthy subjects were tested on one occasion (T0).

Assessment

At the time of enrolment, subjects underwent an accurate

Table I. *The demographic and medical history data of the patients enrolled in the study and healthy subjects compared. Data are expressed as mean ± SD, unless otherwise stated.*

Variable	Patients treated (n=41)	Healthy subjects (n=27)
Age in years	52.4 ± 13.1	31.6 ± 10.0
Gender, % F (n)	43.9 (18)	56.6 (15)
Height (cm)	169.7 ± 7.6	169.2 ± 7.2
Weight (kg)	68.2 ± 13.2	64.5 ± 10.7
BMI	23.6 ± 3.4	22.4 ± 2.5
Smoking, % yes (n)	31.7 (13)	29.6 (8)
Presence of symptoms since (months)	28.9 ± 46.6	
Days with symptoms per week	5.6 ± 1.8	
PPI intake, % yes (n)	34.1 (14)	

medical history with an assessment of symptoms, allergies, smoking, occupation, familiarity with allergic and non-allergic nasal diseases, operations undertaken and ongoing therapies. Objective examination and rhinocytogram were also conducted. For the latter, all LPR patients were sampled using the scraping technique at T0, T1 and T2, whilst healthy subjects were sampled once (T0). The sample was spread on a slide and stained using the May Grunwald - Giemsa method. The prepared slides were observed at 100, 400, 1000 magnifications, counting the inflammatory cellular elements (neutrophils and lymphocytes), goblet cells and any bacteria present. The outcome of the nasal cytological examination was assessed using the classification shown in Table II (7, 8).

Patients with LPR at T0, T1 and T2 and healthy subjects at T0 only answered the questions on the RSI questionnaire and underwent video-laryngoscopy, whereby the investigating physician completed the RFS index.

Patients were also asked to rate the effectiveness of their treatment using a numerical rating scale (NRS) numbered from 0 (no effectiveness) to 10 (maximum possible effectiveness).

A sample of 23 patients treated with Lmd and 15 healthy subjects was evaluated by using, as a method of symptom detection, the Total Nasal Symptom Score (TNSS), which assigns a 4-point rating (from 0 to 3), depending on the presence and intensity of the symptoms the patient is experiencing, among the following 4 nasal symptoms: nasal obstruction, rhinorrhoea, nasal itching and sneezing. Lastly, reports of any adverse effects attributable to taking Lmd were collected.

Statistical analysis

Descriptive statistics were used to summarise the characteristics of the cohorts in terms of median, mean and standard deviation (SD) or frequencies when appropriate.

The treatment effect was estimated in terms of change in outcome in treated patients between the T1 and T2 visit and the T0 visit and in terms of change in outcome between treated patients at the three visits and healthy subjects. The significance of the differences was determined by applying the non-parametric Mann-Whitney test for paired data of treated patients in the case of the comparison between T2, T1 and T0 and for unpaired data in the case of the comparison of changes between treated patients and healthy subjects. In all the analyses carried out, the results

Table II. *Quantitative classification of nasal cytology results (*average of cells per 10 fields at high magnification - 1000x; from [(8), modified].*

Cellular element	Description	Quantity	Classification
Neutrophils, eosinophils and lymphocytes	None	0*	0
	Sporadic	0.1 – 1.0*	½+
	A few scattered cells, small groups	1.1 – 5.0*	1+
	In discreet numbers, large groups	5.1 – 15*	2+
	Large cellular clusters that do not occupy the entire field	15.1 – 20*	3+
	Large cellular clusters occupying the entire field	> 20*	4+
Goblet cells	None	0	0
	From rare to few cells	1 -24%	1+
	In a significant number	25 - 49%	2+
	In large numbers	50 - 74%	3+
	Lots of cells scattered all over the field	75 – 100%	4+
Bacteria	None	Normal / pathological	0
	Sporadic cell cluster		1+
	In a significant number		2+
	Many easily visible cells		3+
	Bacteria in the entire field		4+

are considered statistically significant for $p < 0.05$.

Statistical analysis was performed using the R software version 3.6.1 for Windows (R Core Team; 2013. A language and environment for statistical computing. R Foundation for Statistical Computing, Vienna, Austria).

RESULTS

On average, patients were evaluated 29.5 ± 2.0 days (T1) after T0 and 28.5 ± 3.8 days (T2) after T1. However, one patient did not complete the study intake cycle and was excluded from the results. Analyses were then conducted using data from the remaining 40 patients.

In patients with LPR, several signs and symptoms can affect the mucous membranes of the upper respiratory tract. In our study, swelling and congestion of the posterior laryngeal mucosa, especially of the posterior thirds of the vocal cords and of the arytenoids, hypertrophic lesions of the posterior laryngeal commissure and a discrete presence of mucus presented most commonly in the enrolled LPR patients. Cytologically, in the nasal mucosa of LPR patients, the characteristic infiltration of neutrophils and lymphocytes caused by exposure to irritants, in the absence of bacteria and spores, already highlighted in previous studies, was observed (4).

RSI, RFS and TNSS

In the treated patients, the RSI, the RFS and the TNSS scores improved significantly at T1 compared with T0 testifying to the improvement in LPR symptoms and signs and nasal symptoms. The RSI and the RFS scores of treated patients worsen at T2, one month after stopping Lmd, compared with T1, but remain significantly lower than at T0 (Table III, Fig. 1A-B). At T0, the RSI and the RFS scores of LPR patients are significantly higher than healthy subjects. Despite the significant improvement in patients treated with Lmd at T1, the difference with healthy subjects remained statistically significant. The median of the TNSS score in the treated patients was the same at T2, one month after stopping Lmd, than at T1 (Table III, Fig. 1C). At T0, the TNSS score in LPR patients is significantly higher than in healthy subjects. Thanks to the significant improvement seen in patients treated with Lmd at T1 and T2, the difference with healthy subjects is statistically less significant.

Rhinocytogram

In treated patients, the presence of lymphocytes is significantly reduced at T1 compared with T0, testifying to the reduction of the inflammatory state. The presence of lymphocytes in treated patients is further reduced at T2, one month after stopping Lmd, compared with T1 (Table IV, Fig. 2A). At T0, the lymphocyte cell count in LPR patients is significantly higher than in healthy subjects. Due to the significant improvement observed in patients treated with Lmd at T1 and T2, the difference with healthy subjects was not statistically significant.

In treated patients, the presence of neutrophils and goblet cells is significantly reduced at T1 compared with T0, indicating a reduction in the inflammatory state. The same cell types in the treated patients were higher at T2, one month after stopping Lmd than at T1, but still significantly better than at T0 (Table IV, Fig. 2B-C). At T0, the neutrophil cell and goblet cell counts in LPR patients are significantly higher than in healthy subjects. Despite the significant improvement in patients treated with Lmd at T1, the differences with healthy subjects remained statistically significant.

Effectiveness of the therapy and adverse effects

After 30 days of therapy (T1), patients treated with Lmd rated the effectiveness of the therapy utilizing an NRS, numbered from 0 to 10. The average rating was 7.13 ± 1.18. One patient treated with Lmd complained of epigastralgia 8 days after starting the product and discontinued treatment.

DISCUSSION

The present clinical study shows a significant improvement in signs, symptoms, and rhino-cytological profile of the nasal mucosa of patients who have LPR and took Lmd for 30 consecutive days. The negative impact of LPR on the respiratory system is mainly caused by inflammation and the accumulation of free radicals in the mucosa, and it is believed that the synergistic action of the ingredients may justify the efficacy of Lmd in treating the signs

Table III. *Medians, 25th and 75th percentiles of the RSI, the RFS and the TNSS scores found in healthy subjects and in patients with LPR at the start of therapy (**T0**), after 30 days of therapy (**T1**) and after 30 days of discontinuation of therapy (**T2**) and statistical significance of comparisons.*

RSI	Healthy subjects (n=27)	Patients treated (n=40)		
		T0	T1	T2
Median [25th – 75th]	2.00 [1.00 – 3.00]	20.00 [17.00 – 23.00]	8.00 [7.00 – 10.00]	10.00 [9.00 – 12.75]
P-value patients treated vs healthy subjects		< 0.0001	< 0.0001	< 0.0001
P-value T1 and T2 vs T0			< 0.0001	< 0.0001
RFS	Healthy subjects (n=27)	Patients treated (n=40)		
		T0	T1	T2
Median [25th – 75th]	0.00 [0.00 – 3.00]	13.00 [12.00 – 14.00]	8.00 [7.00 – 9.00]	9.00 [8.00 – 10.00]
P-value patients treated vs healthy subjects		< 0.0001	< 0.0001	< 0.0001
P-value T1 and T2 vs T0			< 0.0001	< 0.0001
TNSS	Healthy subjects (n=15)	Patients treated (n=22)		
		T0	T1	T2
Median [25th – 75th]	0.00 [0.00 – 2.00]	3.50 [2.00 – 4.25]	2.00 [1.00 – 2.25]	2.00 [1.00 – 3.00]
P-value patients treated vs healthy subjects		0.0002	0.0270	0.0149
P-value T1 and T2 vs T0			< 0.0001	< 0.0001

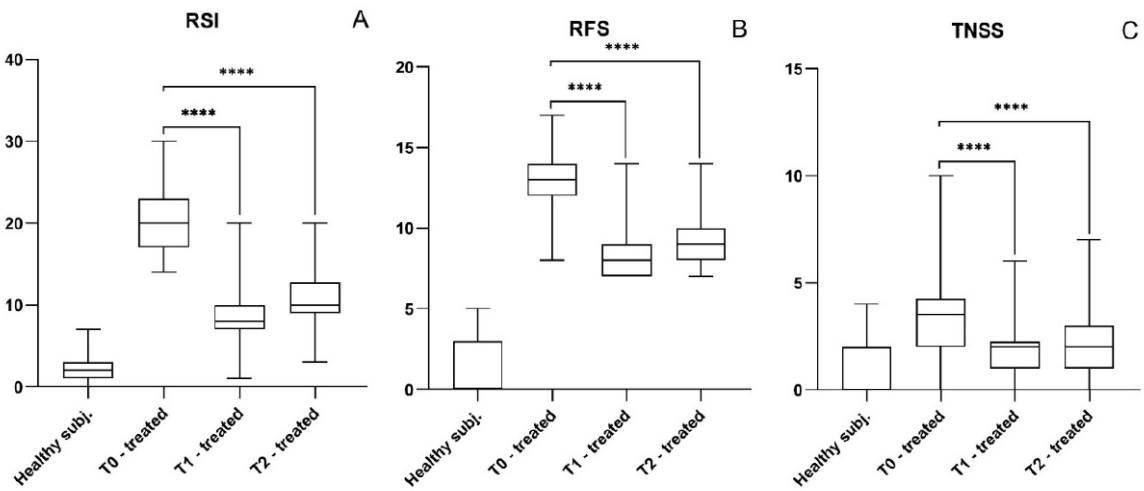


Fig. 1. *Treatment with Lmd for 30 days (**T1**) resulted in a significant reduction in the RSI (**A**), RFS (**B**) and TNSS (**C**) scores which remained significantly lower than the scores at T0 even 30 days after stopping therapy (**T2**) (****p<0.0001).*

and symptoms of LPR. The contact between some ingredients of this formula (alginate, carbonate, and bicarbonate) and the acidic gastric content causes the formation of a 'raft' floating above the gastric content, which impedes its reflux into the oesophagus. In addition, alkalizing substances neutralize the acid pocket formed during a meal. In Lmd, the effects induced by alginate and alkalizing compounds are combined with the therapeutic effects directly induced on the oesophageal and laryngeal mucosa by *O. ficus-indica* cladode extract and *O. europaea* leaf extract. Studies on the therapeutic properties of *O. ficus-indica* have demonstrated an antiulcerogenic activity, which is hypothesized to be determined by the mucilages that form a protective layer on the mucous membranes (9). Studies have shown that aqueous extracts of *O. europaea* can reduce the level of TNF-α in an experimental *in vivo* mouse model and an experimental *in vitro* model on a human lymphocyte cell line. It was also observed that the administration of *O. europaea* extract could prevent the formation of stress-induced gastric lesions in an *in vivo* experimental model. This effect is associated with a decrease in the level of malondialdehyde (an index of lipid peroxidation) and a reduction in the fall in catalase and superoxide dismutase enzyme activity (10). *O. europaea* extract has antioxidant properties, with a protective effect on the mucous membranes. Furthermore, *O. europaea* has been observed to be a stable source of bioactive flavonoids (11). These compounds contribute to the beneficial effects of *O. europaea* extract observed in LPR treatment. Lastly, the protective effect on mucosal cells of the *O. ficus-indica* cladode extract and the *O. europaea* leaf extract has already been shown in vitro in models simulating in vivo conditions (12).

In this study, there was an improvement in all parameters assessed after 30 consecutive days of

Table IV. *Median lymphocyte, neutrophil and goblet cell counts in healthy subjects and LPR patients at the start of therapy (**T0**), after 30 days of therapy (**T1**) and 30 days after discontinuation of therapy (**T2**) and statistical significance of comparisons.*

Cell type	Parameters	Healthy subjects (n=27)	Patients treated (n=40)		
			T0	T1	T2
Lymphocytes	Median [25th – 75th]	0.00 [0.00 – 0.00]	0.50 [0.00 – 2.00]	0.00 [0.00 – 1.00]	0.00 [0.00 – 0.00]
	P-value patients treated vs healthy subjects		0.0029	0.3937	> 0.9999
	P-value T1 and T2 vs T0			< 0.0001	< 0.0001
Neutrophils	Median [25th – 75th]	0.00 [0.00 – 1.00]	2.50 [2.00 – 3.00]	1.00 [0.00 – 1.75]	1.00 [0.00 – 2.00]
	P-value patients treated vs healthy subjects		< 0.0001	0.0164	0.0023
	P-value T1 and T2 vs T0			< 0.0001	< 0.0001
Goblet cells	Median [25th – 75th]	1.00 [1.00 – 1.00]	2.50 [2.00 – 3.00]	1.50 [1.00 – 2.00]	2.00 [1.00 – 2.00]
	P-value patients treated vs healthy subjects		< 0.0001	< 0.0001	< 0.0001
	P-value T1 and T2 vs T0			< 0.0001	< 0.0001

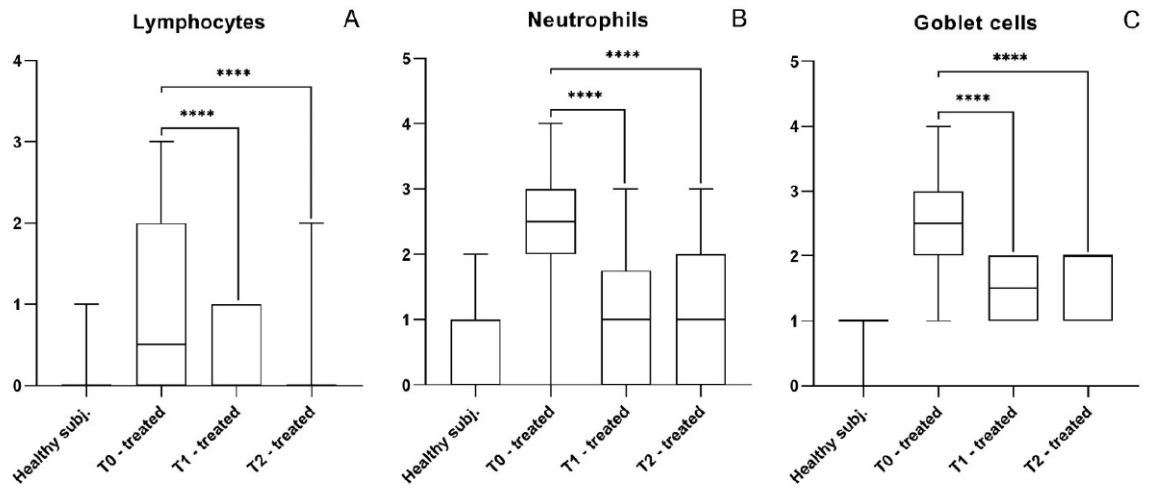


Fig. 2. *Treatment with Lmd for 30 days (**T1**) resulted in a significant reduction, compared with T0, in the number of lymphocytes (**A**) detected, which further reduced 30 days after stopping therapy (**T2**) (******p<0.0001**). At T1 and T2, the number of lymphocytes found in LPR patients was not significantly different from that found in healthy subjects. Treatment with Lmd for 30 days (**T1**) resulted in a significant reduction in the number of neutrophils (**B**) and goblet cells (**C**) detected, which rose slightly 30 days after stopping therapy (**T2**), remaining significantly lower than at T0 (******p<0.0001**).*

taking Lmd by LPR patients. Indeed, the symptoms and signs of LPR, as assessed by the RSI and RFS indices, respectively, improved significantly with treatment.

Cytologically, the element most commonly found in LPR and often associated with nasal symptoms is the neutrophil granulocyte. In addition, there is a percentage increase in goblet cells and an increase in lymphocytes. The rhinocytogram performed at T0 T1 showed that the treatment resulted in a significant reduction in neutrophils, goblet cells and lymphocytes. The reduction of the overexposed elements at the cytological level is accompanied by the already mentioned global improvement of the symptoms, further confirmed by the significant reduction in the TNSS score.

The same parameters, except for the number of lymphocytes, deteriorated slightly in the 30 days following the discontinuation of therapy, showing that in the case of LPR, in order to give stability to the results obtained, it is preferable to continue therapy with the tested medical device for more than one month. Nevertheless, the tolerability of the medical device was good, and the results were considered more than satisfactory by the treated patients.

The results of this clinical study, therefore, demonstrate the efficacy of a medical device composed of magnesium alginate, calcium carbonate, potassium bicarbonate and extracts of O. *ficus-indica* and *O. europaea* in reducing the signs and symptoms commonly associated with LPR and improving the cytological status of the mucous membranes of the upper respiratory tract in patients suffering from this disorder. The study also shows that the medical device used is safe and well-tolerated.

Conflict of interest statement

Enrico Maffezzoni, Federico Maffezzoni, Ketty Luciano and Mario Notargiacomo declare that they have no commercial associations (e.g. consultancies, stock ownership, equity interest, patent/licensing arrangement etc.) that might pose a conflict of interest in connection with the submitted article. Stefano Agostini is an employee of Pharma Line.

Funding

Pharma Line S.r.l sponsors this research. (Milan, Italy). Stefano Agostini is Scientific Director of

Pharma Line. He has disclosed those interests fully to Biolife S.a.s. and has in place an approved plan for managing any potential conflicts arising from this arrangement.

REFERENCES

1. Koufman JA, Aviv JE, Casiano RR, Shaw GY. Laryngopharyngeal reflux: Position statement of the committee on speech, voice, and swallowing disorders of the American Academy of Otolaryngology-Head and Neck Surgery. Otolaryngol Head Neck Surg 2002; 127(1):32-5.
2. Kuo CL. Laryngopharyngeal Reflux: An Update. Arch Otolaryngol Head Neck Surg 2019; 3(1):1.
3. Finocchio E, Locatelli F, Sanna F, et al. Gastritis and gastroesophageal reflux disease are strongly associated with non-allergic nasal disorders. BMC Pulm Med 2021; 21(1):53.
4. Mandolesi D, Schiavon P, Ioannou A, et al. Chronic non-allergic rhinitis with neutrophils is associated with higher acid exposure time: a pH-impedance monitoring study. Dig Liver Dis 2020; 52(4):414–9.
5. Dagli E, Yüksel A, Kaya M, et al. Association of Oral Antireflux Medication with Laryngopharyngeal Reflux and Nasal Resistance. JAMA Otolaryngol Head Neck Surg 2017; 143(5):478-83.
6. Lechien JR, Saussez S, Schindler A, et al. Clinical outcomes of laryngopharyngeal reflux treatment: A systematic review and meta-analysis. Laryngoscope 2019; 129(5):1174-87.
7. Gelardi M, Iannuzzi L, Quaranta N, et al. Nasal cytology: practical aspects and clinical relevance. Clin Exp Allergy 2016; 46(6):785-92.
8. Gelardi M. Atlante di Citologia Nasale. Edi Ermes, Milano, 2012.
9. Galati EM, Mondello MR, Giuffrida D, et al. Chemical characterization and biological effects of Sicilian Opuntia ficus indica (L.) Mill. Fruit juice: antioxidant and antiulcerogenic activity. J Agric Food Chem 2003; 51(17):4903-08.
10. Dekanski D, Janićijević-Hudomal S, Ristić S, et al. Attenuation of cold restraint stress-induced gastric lesions by an olive leaf extract. Gen Physiol Biophys 2009; 28 Spec No:135-42.
11. Goulas V, Papoti VT, Exarchou V, et al. Contribution of flavonoids to the overall radical scavenging activity of olive (Olea europaea L.) leaf polar extracts. J Agric Food Chem 2010; 58(6):3303-08.
12. Rizza L, Frasca G, Nicholls M, et al. Caco-2 cell line as a model to evaluate mucoprotective proprieties. Int J Pharm 2012; 422(1-2):318-22.

High lncRNA DLEU1 predicts poor prognosis and promotes tumor progression by upregulating NUCKS1 through sponging miR-1286 in lung adenocarcinoma

X. Miao[1], LH. Wang[2], JH. Li[3], F. Xue[1] and AP. Dong[1*]

[1]Department of Clinical Laboratory, Weifang People's Hospital, Weifang, Shandong, China;
[2]Department of Prenatal Diagnosis, Weifang People's Hospital, Weifang, Shandong, China;
[3]Department of Clinical Laboratory, Affiliated Hospital of Weifang Medical University, Weifang, Shandong, China.

Received August 26, 2021 – Accepted January 18, 2022

To the Editor,

Lung cancer is one of the commonly occurred malignant tumors with high mortality rate. Non-small cell lung cancer (NSCLC) accounts for 85% of newly diagnosed lung cancers, of which lung adenocarcinoma (LUAD) is the most common histological subtype (1). However, the limited understanding about the pathogenesis of LUAD seriously limits the progress of efficient therapeutic strategies.

Long non-coding RNAs (lncRNAs) have been found to exhibit important regulatory effects on various biological processes (2). In addition, lncRNAs have been identified as competing endogenous RNAs (ceRNAs) of microRNAs (miRNAs), which promoting the understanding about the mechanisms underlying the biological function of lncRNAs (3). LncRNA deleted in lymphocytic leukemia 1 (DLEU1) play important roles in the occurrence and progression of various malignancies (4). It has been proved as an oncogene in the progression of NSCLC (5), but the clinical value and mechanisms of DLEU1 in LUAD remain unknown.

According to The Cancer Genome Atlas (TCGA) database, we found the significantly highly expressed DLEU1 in LUAD tissues, and the relationship between DLEU1 and overall survival of LUAD has also been observed. Thus, this study aimed to verify the prognostic value of DLEU1 in predicting LUAD survival, and to explore the molecular mechanisms underlying the biological function of DLEU1 in LUAD progression.

MATERIALS AND METHODS

Patients and tissue collection

With the approval by the Ethics Committee of Weifang People's Hospital and the written informed consent from patients, lung adenocarcinoma (LUAD) tissues and adjacent normal tissues of 126 patients were dissected as research samples between 2012 and 2016. The patients were in accordance with the following inclusion criteria: (i) tumore tissues were pathologically diagnosed with LUAD; (ii) all patients had not received surgery, radiotherapy or chemotherapy; (iii) had complete clinicopathological information; (iv) none of the patients suffered from autoimmune disease or other malignant tumors. The demographic and clinicopathological characteristics of these patients were recorded and analyzed (Table 1), and the survival information of the patients were followed up through telephone calls.

Key words: Long non-coding RNA; Deleted in lymphocytic leukemia 1; Prognosis; NUCKS1; miR-1286; Lung adenocarcinoma

*Corresponding author
Dr. Aiping Dong,
Department of Clinical Laboratory,
Weifang People's Hospital,
No 151 Guangwen Street, Kuiwen District,
Weifang 261041, Shandong, China.
Tel./fax: 86-0536-8675650
e-mail: dongaiping_wfrm@163.com

0393-974X (2022)
Copyright © by BIOLIFE, s.a.s.
This publication and/or article is for individual use only and may not be further reproduced without written permission from the copyright holder.
Unauthorized reproduction may result in financial and other penalties
DISCLOSURE: ALL AUTHORS REPORT NO CONFLICTS OF INTEREST RELEVANT TO THIS ARTICLE.

Cell culture and transfection.

LUAD cells (A549, NCIH1975, PC-9) and a human normal bronchial epithelial cell line (BEAS-2B) were cultured in Roswell Park Memorial Institute (RPMI) 1640 medium supplemented with 10% FBS, 100 U/ml penicillin, 100 μg/ml streptomycin, and placed in an incubator containing 5% CO_2 at 37˚C.

In the study, cell transfection was used to regulate DLEU1 and miR-1286 *in vitro*. Small interfering (siRNA) for DLEU1 (si-DLEU1), siRNA negative control (si-NC), miR-1286 mimic, miR-1286 inhibitor, mimic NC, inhibitor NC were synthesized by RiboBio (Guangzhou, China). After the cells were inoculated and cultured to 90% confluency, Lipofectamine 3000 (Invitrogen, Carlsbad, CA, USA) was used to transfect the above vectors into A549 and PC-9 cells according to the manufacturer's protocols, and subsequent analysis was performed 48 h later.

RNA extraction and quantitative real-time PCR

Total RNA was extracted using TRIzol reagent (Invitrogen; Thermo Fisher Scientific, Inc.) according to the manufacturer's protocol. cDNA was reversed transcribed from 1 μg RNA by a Reverse Transcription Kit (Takara, Dalian, China). The expression levels of DLEU1, miR-1286 and mRNA of nuclear casein kinase and cyclin-dependent kinase substrate 1 (NUCKS1) were detected by qPCR using SYBR Green Real-time PCR Master Mix kit (Toyobo, Osaka, Japan) on 7900HT fast real-time PCR system (Applied Biosystems, San Francisco, CA, United States). GAPDH and U6 were used as internal controls, and the primers used were all synthesized by GenePharma (Shanghai, China) with the following sequences:

DLEU1	forward	5'-CGTGCATTTAAAACCGCC-3'
	reverse	5'-TGTCTGCATTGTGACT-CAATTC-3'
NU-CKS1	forward	5'-TGCCCAAACCCAGACTA-AAG-3'
	reverse	5'-TGCCCAAACCCAGACTA-AAG-3'
GAP-DH	forward	5'-ATGATGACATCAAGAAGGT-GGTG-3'
	reverse	5'-CCATGAGGTCCACCACCCT-GTTG-3'

The final expression value was calculated using the $2^{-\Delta\Delta Ct}$ method.

Cell proliferation analysis

In this study, CCK-8 was used to analyze the cell proliferation rate. LUAD cells were seeded into 96-well plates at a density of 2×103, and culture in an incubator for 48 h (at 37°C, 5% CO2). A volume of 10 uL CCK-8 reagent (Beyotime Institute of Biotechnology, Inc.) was added into each well, followed by a 2 h-incubation. The proliferation of cells was examined by measuring the absorbance at 450 nm using a microplate reader.

Cell migration and invasion assay

By Transwell chambers (Gibco; Thermo Fisher Scientific, Inc.) with a pore size of 8.0 μm, the migration and invasion of A549 and PC-9 cells were analyzed. For cell migration assay, the chambers were precoated with Matrigel (Gibco; Thermo Fisher Scientific, Inc), while cell invasion assay had no need of Matrigel. Cells were cultured in the upper chambers with serum-free medium, and the bottom chambers contained 500 μL medium containing 10% FBS. After 24 h of incubation at 37 ºC, the cells on the upper layer of the filter were wiped with a cotton swab, and the cells remained on bottom of membranes were stained with 0.1% crystal violet for 10 min at room temperature. The cell was observed under an inverted light microscope (Nikon, Japan), and the migrated or invasive cells in 5 random fields of view were counted.

Bioinformatic analysis

The starBase 3.0 (http://starbase.sysu.edu.cn/index.php) was used to analyze the expression of DLEU1 in 526 LUAD tissues and 59 normal controls, the targeted miRNAs of DLEU1, the targeted mRNAs of miR-1286, and the correlation of DLEU1 and NUCKS1 in 526 LUAD samples. The Gene Expression Profiling Interaction Analysis 2.0 (GEPIA 2.0, http://gepia2.cancer-pku.cn/#index) was used to evaluate the association of DLEU1 with LUAD overall survival based on TCGA database.

Dual-luciferase reporter assay

The fragment of DLEU1, which contained the presumed binding site of miR-1286 (wild type, WT) and mutated binding site (mutant type, MUT), was inserted into the pGL3-basic vector to construct WT-DLEU1 and MUT-DLET1. Similarly, WT-NUCKS1 and MUT-NUCKS1 were also synthesized. The above vectors were co-transfected with miR-1286 mimics, miR-1286 inhibitor, mimics NC or

inhibitor NC into A549 cells following the manufacturer's protocol of Lipofectamine 3000 (Invitrogen, Carlsbad, CA, USA). After 48 h of transfection, the cells were collected, and a dual-luciferase reporter assay system (Promega) was used to detect luciferase activity.

Statistical analysis

In this study, data were expressed as mean ± standard deviation (SD), and SPSS22.0 (IBM Corp.) and GraphPad Prism 7.0 software (GraphPad Software, Inc.) were used for data analysis. Student's t-test was used for the comparisons between two groups, and one-way ANOVA followed by Tukey's post hoc test was used for comparisons between multiple groups. DELU1 expression was divided into low and high expression groups based on the median value. Chi-square test was used to compare categorical variables. The correlation between different variables was analyzed by Pearson correlation analysis. The Kaplan-Meier curve and log-rank test are used to estimate the relationship between DLEU1, miR-1286 and the survival rate of LUAD patients. The prognostic value of DLEU1 was estimated using Cox regression analysis in LUAD patients. All experiments have at least three replicates, and $P < 0.05$ represented statistical significance.

RESULTS

Expression of DLEU1 in LUAD patients

According to the analysis results of DLEU1 in 526 LUAD tissues and 59 normal controls on starBase 3.0, the expression levels of DLEU1 in LUAD tissues were significantly higher than that of normal tissues ($P < 0.001$, Fig. 1A). Consistently, the expression of DLEU1 in tumor tissues collected from 126 LUAD patients was also upregulated compared with normal control tissues ($P < 0.001$, Fig. 1B). In the cell lines analyzed in this study, LUAD cell lines A549, NCIH1975, and PC-9 had significantly elevated

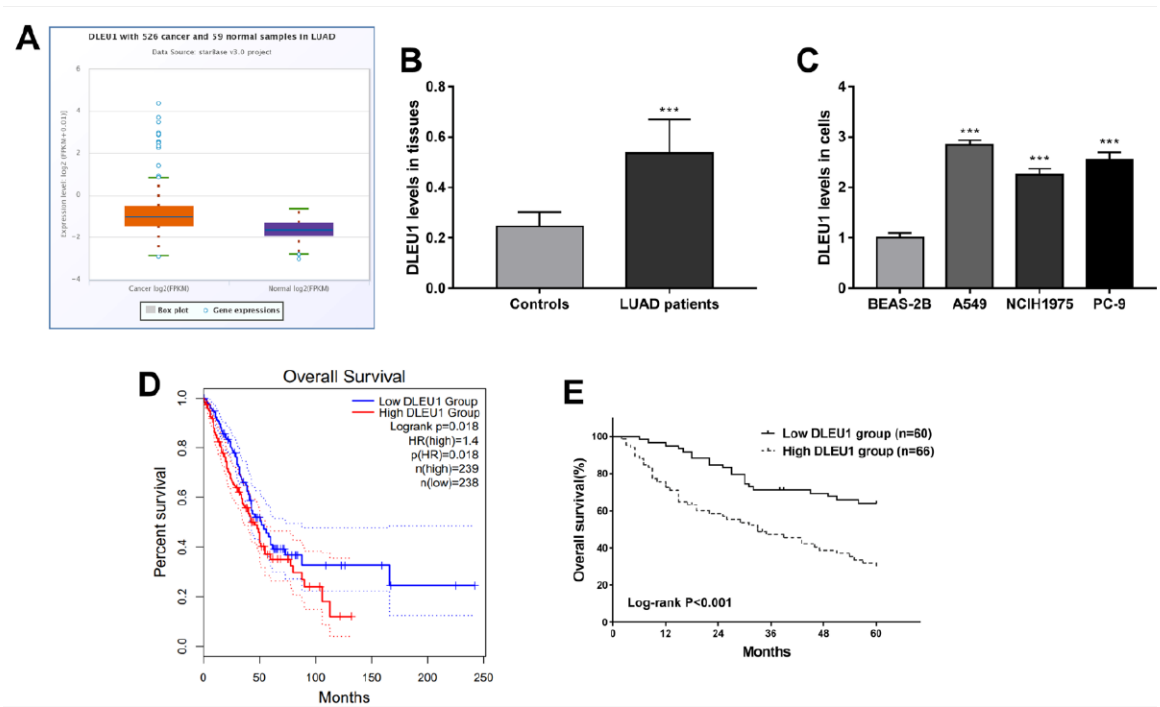


Fig. 1. *Expression and prognostic value of DLUE1 in LUAD. (A) DLEU1 expression was higher in cancer tissues compared with normal control in the data collected from TCGA (P = 9.5e-10). (B) LUAD patients had significant increased DLEU1 expression in tumor tissues than the adjacent normal tissues (***P < 0.001). (C) LUAD cell lines (A549, NCIH1975 and PC-9) had upregulated DLUE1 compared with the normal cell line BEAS-2B (***P < 0.001). (D) Kaplan-Meier survival curves plotted based on DLEU1 data from TCGA database (log-rank P = 0.018). (E) Kaplan-Meier survival curves based on DLEU1 expression of LUAD patients, and high DLUE1 was associated with poor overall survival (log-rank P < 0.001).*

DLEU1 expression compared with the normal cell line BEAS-2B (all $P < 0.001$, Fig. 1C).

Relationship between DLEU1 expression and clinicopathological characteristics in LUAD patients

Table I summarized the clinicopathological characteristics, including age, gender, smoking history, tumor size, lymph node metastasis and TNM stage. According to Chi-square test, the aberrant expression of DLEU1 was significantly related to tumor size, lymph node metastasis and TNM staging (all $P < 0.05$, Table I). No relationship was found between DLEU1 and age, gender or smoking history (all $P > 0.05$).

LUAD patients with high DLEU1 have poor overall survival

By the GEPIA platform, the survival curves based on differentially expressed DLEU1 were plotted in 477 LUAD patients. As shown in Fig. 1D, high DLEU1

Table I. *Relationship between DLEU1 expression and LUAD patients' clinicopathological characteristics*

Features	No. n=126	DLEU1 expression	*P* value	
		Low (n=60)	High (n=66)	
Age (years)				0.917
≤ 60	51	24	27	
> 60	75	36	39	
Gender				0.918
Female	54	26	28	
Male	72	34	38	
Smoking history				0.986
Ever	82	39	43	
Never	44	21	23	
Tumor size (cm)				0.044
≤ 3	68	38	30	
> 3	58	22	36	
Lymph node metastasis				0.016
Negative	72	41	31	
Positive	54	19	35	
TNM stage				0.011
I - II	67	39	28	
III - IV	59	21	38	

was related with poor survival (log-rank $P = 0.018$). The included 126 LUAD patients were followed up to record their survival status, and the Kaplan-Meier survival curves based on DLEU1 showed that patients with high DLEU1 had significantly shorter survival time compared with those with low DLUE1 levels (log-rank $P < 0.001$, Fig. 1E). To confirm the prognostic value of DLUE1 for the prediction of survival, a multivariate Cox regression was performed. The results listed in Table II revealed that advanced TNM stage ($P = 0.008$, HR = 1.993) and high DLEU1 ($P = 0.004$, HR = 2.065) were two independent prognostic factors, which significantly associated with poor prognosis in LUAD.

Effects of DLEU1 on LUAD cell proliferation, migration and invasion

A549 and PC-9 had significantly higher DLEU1 expression, which were used for the subsequent cell experiments. As shown in Fig. 2A and B, DLEU1 expression was successfully inhibited by si-DLEU1 in both A549 and PC-9 cell lines (both $P < 0.001$). By the CCK-8 assay, the proliferation abilities of A549 and PC-9 cells were suppressed by DLEU1 inhibition (all $P < 0.01$, Fig. 2C and D). For cell migration and invasion, the knockdown of DLUE1 in A549 and PC-9 led to markedly decreases in cell numbers that migrated or invaded into the lower chambers of Transwells (all $P < 0.001$, Fig. 2E and F).

miR-1286 is directly inhibited by DLEU1 in LUAD

The fragment of DLEU1 was found to contain a complementary sequence of miR-1286 (Fig. 3A). Thus, the WT-DLEU1 and MUT-DLEU1 were synthesized for an dual-luciferase reporter assay to confirm the interaction between DLEU1 and miR-1266. As shown in Fig. 3B, miR-1286 overexpression inhibited, but miR-1286 reduction promoted the relative luciferase activity in cells transfected with WT-DLEU1 (both $P < 0.05$). However, no changes were observed in luciferase activity in cells with MUT-DLEU1 ($P > 0.05$). In A549 cells with DLUE1 reduction, the expression of miR-1286 was significantly higher compared with the cells transfected with si-NC ($P < 0.001$, Fig. 3C). Furthermore, the expression of miR-1286 in LUAD tissues showed negative expression

Table II. *Multivariate Cox regression analysis for patients*

Variables	Multivariate analysis	
	HR (95% CI)	*P*
Age (>60 years vs. ≤60 years)	1.235 (0.688-1.598)	0.554
Gender (male vs. female)	1.186 (0.694-1.701)	0.367
Tumor size (>3 cm vs. ≤3 cm)	1.308 (0.721-1.970)	0.118
Smoking (ever vs. never)	1.197 (0.658-1.806)	0.284
Lymph node metastasis (positive vs. negative)	1.512 (0.955-2.134)	0.079
TNM stage (III-IV vs. I-II)	1.993 (1.385-2.742)	0.008
DLEU1 (high vs. low)	2.065 (1.536-2.863)	0.004

patterns, which was remarkably decreased in tumor tissues ($P < 0.001$, Fig. 3D) and negatively correlated with DLUE1 levels (r = -0.685, $P < 0.001$, Fig. 3E). According to the median value of miR-1286, LUAD patients were grouped in two groups, and the group with low miR-1286 had significantly poor overall survival (log-rank $P = 0.0003$, Fig. 3F).

DLEU1 regulates LUAD cell biological behaviors by sponging miR-1286

Considering the directly interaction between DLEU1 and miR-1286, the role of miR-1286 playing in the biological function of DLEU1 in LUAD progression was explored. The expression of miR-1286 was inhibited by miR-1286 inhibitor ($P <$

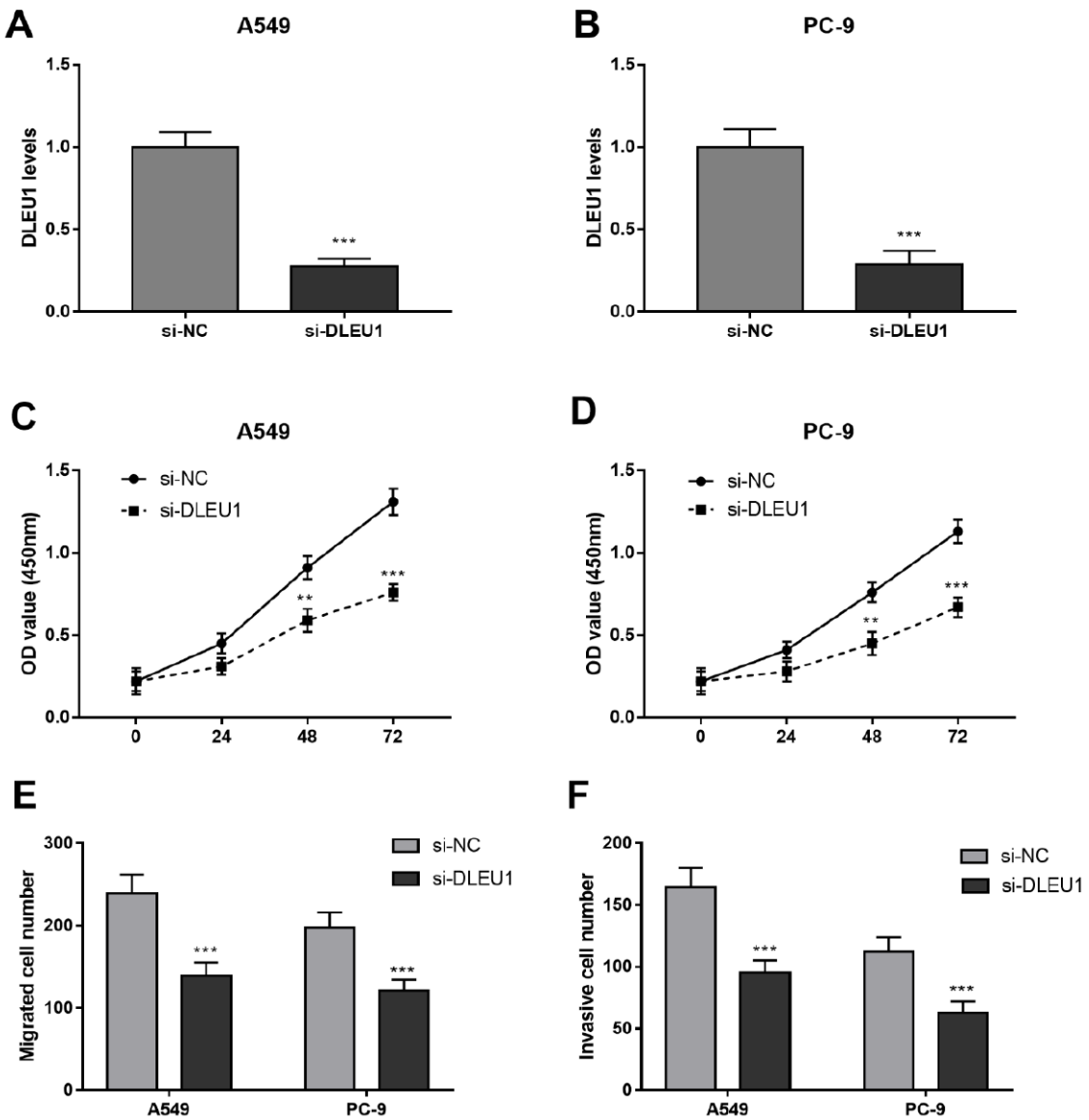


Fig. 2. Silencing of DLEU1 inhibited cell proliferation, migration and invasion of A549 and PC-9 cells. (A and B) DLEU1 expression was significantly reduced by cell transfection with si-DLUE1 (***$P < 0.001$). (C and D) Knockdown of DLEU1 led to inhibited cell proliferation (**$P < 0.01$, ***$P < 0.001$). (E and F) Cell migration and invasion were suppressed by the reduction of DLUE1 (***$P < 0.001$).

0.001), and the miR-1286 inhibitor significantly reduced the enhanced miR-1286 expression caused by DLUE1 knockdown in A549 cells ($P < 0.001$, Fig. 3G). Regarding to cell proliferation, migration and invasion, miR-1286 silencing in A549 promoted these biological processes, and the inhibited cell proliferation, migration and invasion induced by DLUE1 inhibition were reversed by the knockdown of miR-1286 (all $P < 0.05$, Fig. 3H and I).

miR-1286/NUCKS1 axis is negatively regulated by DLEU1 in LUAD

NUCKS1 was predicted as a potential target of miR-1286, which contained a complementary

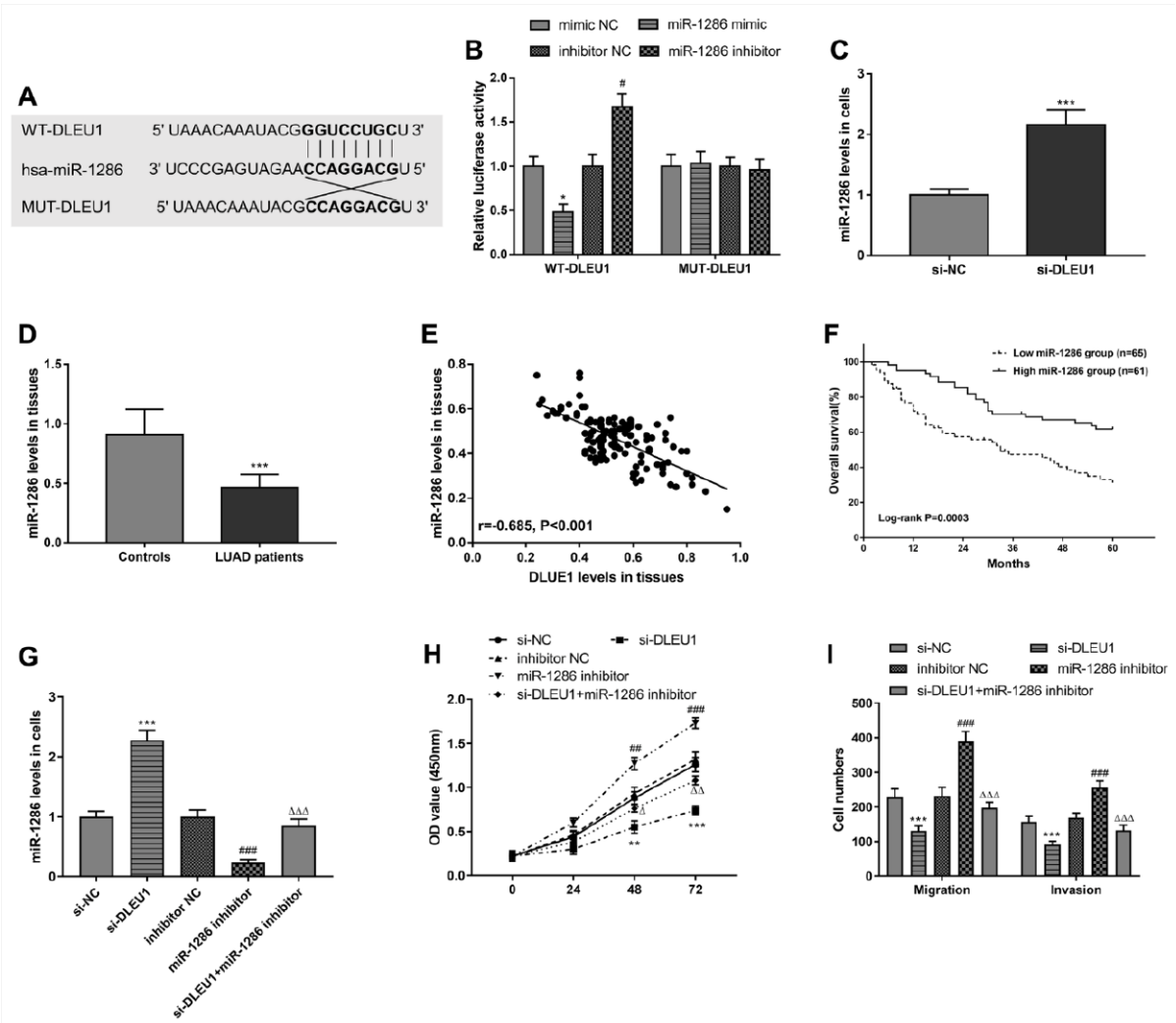


Fig. 3. DLUE1 regulated LUAD progression by sponging miR-1286. (A) The complementary sequence of miR-1286 on the fragment of DLEU1. (B) The relative luciferase activity of WT-DLEU1 group was inhibited by miR-1286 overexpression, but was enhanced by the knockdown of miR-1286 ($^{*}P < 0.05$ *vs.* mimic NC; $^{\#}P < 0.05$ *vs.* inhibitor NC). (C) The expression of miR-1286 was promoted by the silencing of DLUE1 in A549 cells ($^{***}P < 0.001$). (D and E) The decreased expression of miR-1286 in LUAD tissues was negatively correlated with DLUE1 (r = -0.685, $P < 0.001$). (F) LUAD patients with high miR-1286 levels had better survival compared with those with low miR-1286 levels (log-rank $P = 0.0003$). (G) miR-1268 inhibitor significantly inhibited miR-1268 expression in A549 cells, and reversed the effects of si-DLUE1 on miR-1286 expression ($^{***}P < 0.001$ *vs.* si-NC; $^{\#\#\#}P < 0.001$ *vs.* inhibitor NC; $^{\Delta\Delta\Delta}P < 0.001$ *vs.* si-DLEU1). (H and I) The proliferation, migration and invasion of A549 cells were promoted by the knockdown of miR-1286, and the inhibition of these cell behaviors induced by DLUE1 reduction was abolished by miR-1286 inhibition ($^{**}P < 0.01$, $^{***}P < 0.001$ *vs.* si-NC; $^{\#\#}P < 0.01$, $^{\#\#\#}P < 0.001$ *vs.* inhibitor NC; $^{\Delta}P < 0.05$, $^{\Delta\Delta}P < 0.01$, $^{\Delta\Delta\Delta}P < 0.001$ *vs.* si-DLEU1).

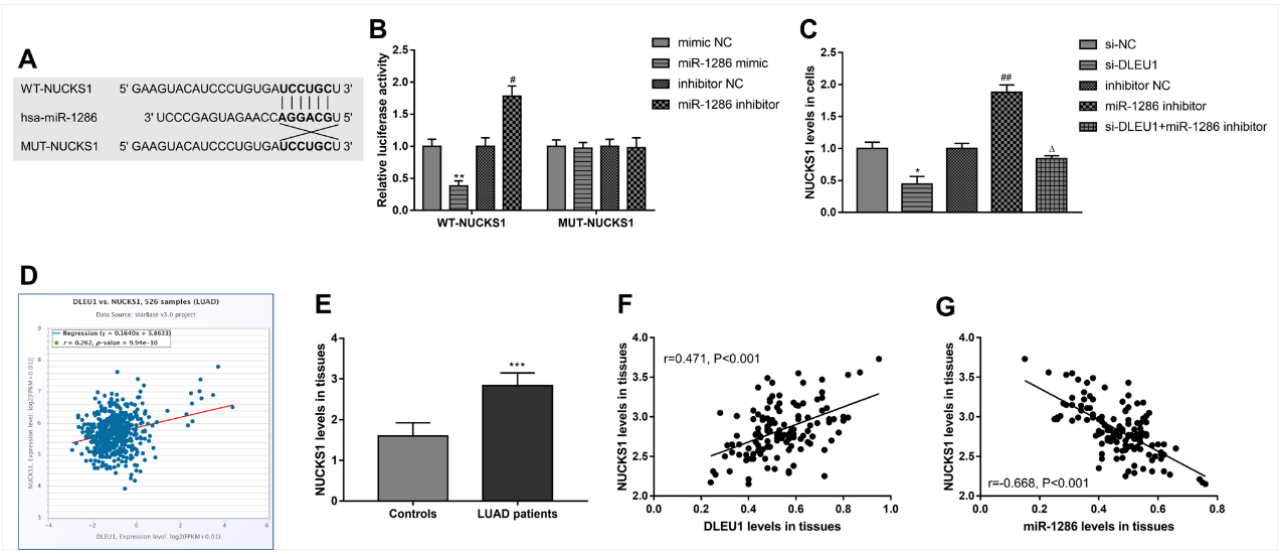


Fig. 4. NUCKS1, as a target of miR-1286, was positively correlated with DLUE1 in LUAD. (A) The complementary sequence of miR-1286 at the 3'-UTR of NUCKS1. (B) The relative luciferase activity of WT-NUCKS1 group was inhibited by miR-1286 overexpression, but was enhanced by the knockdown of miR-1286 (**$P < 0.01$ *vs.* mimic NC; $^{\#}P < 0.05$ *vs.* inhibitor NC). (C) DLUE1 inhibition led to reduced NUCKS1 expression, while miR-1286 inhibition led to enhanced NUCKS1 expression and the abolishment of the effect DLUE1 on NUCKS1 levels (*$P < 0.05$ *vs.* si-NC; $^{\#\#}P < 0.01$, *vs.* inhibitor NC; $^{\Delta}P < 0.05$ *vs.* si-DLEU1). (D) A positive correlation was observed between DLUE1 and NUCKS1 in LUAD based on the data collected from TCGA database (r = 0.262, P = 9.94e-10). (E-G). The elevated NUCKS1 in LUAD tissues was positively correlated with DLUE1 (r = 0.471, $P < 0.001$) but negatively correlated with miR-1286 (r = -0.668, $P < 0.001$).

sequence of miR-1286 at its 3'-UTR (Fig. 4A). The subsequent luciferase reporter assay results indicated that miR-1286 overexpression inhibited, while miR-1286 reduction promoted the relative luciferase activity ($P < 0.05$, Fig. 4B), suggesting the interaction between miR-1286 and NUCKS1. In A549 cells, DLEU1 silencing inhibited NUCKS1 expression, while miR-1286 knockdown promoted NUCKS1 expression, and the inhibition in NUCKS1 by DLUE1 was abolished by miR-1286 silencing (all $P < 0.05$, Fig. 4C). By the bioinformatics analysis for the relationship between DLUE1 and NUCKS1 in LUAD, a positive correlation was observed (r = 0.262, P = 9.94e-10, Fig. 4D). In the included 126 patients of this study, the increased expression of NUCKS1 in tumor tissues was positively correlated with DLEU1, but was negatively correlated with miR-1286 (both $P < 0.001$, Fig. 4E-G).

DISCUSSION

Recently, advances have been achieved in the treatment of lung cancer, but the prognosis remains poor (6). Thus, novel methods to predict patients' survival are necessary. Functional lncRNAs have been reported to be involved in the development and progression of various human diseases, especially in cancers (7).

DLEU1 has been studied in several malignant tumors (8, 9), and identified as an oncogene to facilitate to NSCLC progression (5). Similarity, this study also found that DLEU1 knockdown inhibited LUAD cell proliferation, migration and invasion. In addition, this study firstly found that the elevated DLEU1 expression was related with LUAD tumor size, lymph node metastasis and TNM stage, and predicted poor overall survival of LUAD.

Given the classic ceRNA theory, this study further demonstrated the directly negatively correlation between DLEU1 and miR-1286 in LUAD, and low miR-1286 expression in LUAD patients also served as an independent prognostic factor. miR-1286 has been reported to play a mediator role in the regulatory effects of Sp1/lncRNA TINCR axis on LUAD progression (10). In the present study, we demonstrated that the regulatory function of

DLUE1 in LUAD progression was also mediated by miR-1286.

NUCKS1 has been reported to promote the development of NSCLC, and was associated with LUAD prognosis (11, 12). According to both *in silico* and expression results, we found that NUCKS1 was a target of miR-1286, and positively correlated with DLUE1, indicating that NUCKS1 might be regulated by the DLEU1/miR-1286 axis.

Collectively, this study demonstrated that high DLUE1 expression served as a prognostic biomarker of LUAD, and promoted LUAD proliferation, migration and invasion by upregulating NUCKS1 through sponging miR-1286.

Conflict of interest

The authors declare that they have no conflict of interest.

Funding

This study is funded by 2 Scientific Research Projects of Weifang Health Commission (wfws jk-2019-069 and WFWSJK-2021-066).

REFERENCES

1. Travis WD. Pathology of lung cancer. Clin Chest Med 2002;23:65-81, viii.
2. Amodio N, Raimondi L, Juli G, Stamato MA, Caracciolo D, Tagliaferri P, Tassone P. MALAT1: a druggable long non-coding RNA for targeted anti-cancer approaches. J Hematol Oncol 2018;11:63.
3. Liu T, Yang C, Wang W, Liu C. LncRNA SGMS1-AS1 regulates lung adenocarcinoma cell proliferation, migration, invasion, and EMT progression via miR-106a-5p/MYLI9 axis. Thorac Cancer 2021; 12:2104-12.
4. Gao S, Cai Y, Zhang H, Hu F, Hou L, Xu Q. Long noncoding RNA DLEU1 aggravates pancreatic ductal adenocarcinoma carcinogenesis via the miR-381/CXCR4 axis. J Cell Physiol 2019;234:6746-57.
5. Zhang S, Guan Y, Liu X, Ju M, Zhang Q. Long non-coding RNA DLEU1 exerts an oncogenic function in non-small cell lung cancer. Biomed Pharmacother 2019;109:985-90.
6. Herbst RS, Morgensztern D, Boshoff C. The biology and management of non-small cell lung cancer. Nature 2018;553:446-54.
7. Yu CS, Wang YB, Li Q, Yang EL, Dong BB. Long non-coding RNA OIP5-AS1 serves as a competing endogenous RNA to modulate X-linked inhibitor of apoptosis protein expression via adsorbing miR-429 in papillary thyroid cancer. J Biol Regul Homeost Agents 2021;35:909-20.
8. Zheng C, Liu S, Qin Z, Zhang X, Song Y. LncRNA DLEU1 is overexpressed in premature ovarian failure and sponges miR-146b-5p to increase granulosa cell apoptosis. J Ovarian Res 2021;14:151.
9. Xu D, Yang F, Fan Y, et al. LncRNA DLEU1 Contributes to the Growth and Invasion of Colorectal Cancer via Targeting miR-320b/PRPS1. Front Oncol 2021;11:640276.
10. Gao YW, Ma F, Xie YC, et al. Sp1-induced upregulation of the long noncoding RNA TINCR inhibits cell migration and invasion by regulating miR-107/miR-1286 in lung adenocarcinoma. Am J Transl Res 2019;11:4761-75.
11. Ma H, Xu J, Zhao R, Qi Y, Ji Y, Ma K. Upregulation of NUCKS1 in Lung Adenocarcinoma is Associated with a Poor Prognosis. Cancer Invest 2021;39:435-44.
12. Yu J, Zhang H, Zhao C, Li G, Zhang Y, Sun Y. CircRNA circ_0008037 facilitates tumor growth and the Warburg effect via upregulating NUCKS1 by binding to miR-433-3p in non-small cell lung cancer. Thorac Cancer 2021; Online ahead of print.

A review on dry eyes in polycystic ovary syndrome patients

Y-B. Shang[1] B. Qi[2], J. Wang[2] W-X. Hou[3] and D. Zhou[4*]

[1]Department of Ophthalmology, 1st Clinical Hospital of Jilin Academy of Chinese Medicine, Changchun, China; [2]Ophthalmology Department, The Affiliated Hospital of Changchun University of Chinese Medicine, Changchun, China; [3]College of Acupuncture and Massage, The Changchun University of Traditional Chinese Medicine, Linyi, China; [4]Innovation Practice Center, The Changchun University of Traditional Chinese Medicine, Changchun, China

Received September 8, 2021 – Accepted February 1, 2022

To the Editor,

Tears are produced by the combined actions of lacrimal glands, meibomian glands and goblets cells. Indeed, the tear film is composed of 3 layers, including the mucous layer, the aqueous layer and the lipid layer. The mucous is produced by the goblet cells present in the conjunctiva, and it acts as a lubricant. The thickest part of the tear film is composed of an aqueous layer and is produced by the lacrimal glands. The lipids layer is formed by the secretions of the meibomian glands, and it forms the outermost layer of the tear film. The reduction in tear secretion and the prevalence of dry eye ranges from 5 to 50 % worldwide. The symptoms of dry eyes include stinging, itching and redness. There have been different etiologies for eye dryness, including metabolic syndrome, diabetes mellitus, smoking, menopause, excessive use of computers etc. Female gender, increase in age, Asian race and air pollution are the risk factors in the development of dry eyes. Amongst these, the incidences of dry eyes have been increasingly found in patients with Polycystic ovary syndrome (PCOS).

PCOS is one of the most common endocrine abnormalities in women of reproductive age in which significant alterations in the functions of the body are induced at the hormonal, reproductive, and metabolic levels. It is characterized by an increase in androgen (hyperandrogenism) and prolactin levels in females along with associated problems including hirsutism, acne, irregular periods, obesity etc. There have been clinical studies documenting the presence of dry eyes in PCOS patients (1, 2). However, there is no review describing the clinical studies related to dry eyes and PCOS. Therefore, this present paper reviews the clinical studies that describe the changes in eyes (dryness) in PCOS patients.

Structural and functional changes in the eyes

It has been suggested that there are certain structural changes in the eyes in PCOS patients that may contribute to the inducing dryness in the eyes (1, 2). A prospective, observational study involving recently diagnosed PCOS patients (n=48) and healthy controls (n=33) reported changes in ocular surface disease index (OSDI) score. Moreover, a statistically significant squamous metaplasia was reported in the temporal bulbar conjunctival impression cytology specimens in PCOS patients in comparison to healthy controls. However, no significant difference was reported in tear osmolarity, Schirmer I test, tear-film break-up time (TBUT) and ocular surface fluorescein staining. It suggested that in recently diagnosed PCOS

Key Words: dry eyes, PCOS, androgen, inflammation, Meibomian glands

**Corresponding Author:*
Dr Dan Zhou,
Innovation Practice Center,
The Changchun University of Traditional Chinese Medicine,
No.1035, Boshuo Road,
Jingyue National High-tech Industrial Development Zone,
130000 Changchun, China
e-mail: dan6809_zhou@aliyun.com

0393-974X (2022)
Copyright © by BIOLIFE, s.a.s.
This publication and/or article is for individual use only and may not be further reproduced without written permission from the copyright holder. Unauthorized reproduction may result in financial and other penalties
DISCLOSURE: ALL AUTHORS REPORT NO CONFLICTS OF INTEREST RELEVANT TO THIS ARTICLE.

patients, the changes in the conjunctival morphology is predominantly involved in inducing dryness in the eyes (1). A clinical study compared the ocular changes in 50 right eyes of 50 women with PCOS (group 1) and 50 right eyes of 50 healthy women (group 2). It was reported that the mean central corneal thickness was significantly higher in the PCOS group. However, there was no significant change in the mean intraocular pressures values between these two groups. (p=0.560). Moreover, the serum estradiol and testosterone levels were positively correlated with the mean central corneal thickness. It was also reported that Schirmer's test results and tear film break-up time values were significantly lower in the PCOS group. There was a negative correlation between testosterone levels and Schirmer's test results and tear film break-up time. Accordingly, it was suggested that there are structural changes in the eyes in terms of an increase in central corneal thickness. Moreover, the extent of dryness was significantly greater in PCOS, which was correlated with serum testosterone and estradiol levels (2). There has been another study documenting the significant influence of PCOS on the central corneal thickness, which was much thicker in these patients. The increase in corneal thickness in polycystic ovary syndrome was attributed to a significant increase in the levels of insulin-like growth factor (IGF-1) (3). In a prospective observational case series of studies, it was reported that women with PCOS had greater conjunctival hyperemia, dryness, itching, mucosal discharge, contact lens intolerance than normal women. Moreover, these patients had significantly reduced tear film break-up time along with a significant increase in the goblet cell number (4).

The characteristic of blood flow in the ocular arteries is determined by noting various indices such as peak systolic velocity, diastolic velocity, end-diastolic velocity, mean systolic/diastolic ratio, resistive index and pulsatility index. It has been found there are profound changes in the blood flow in the ophthalmic artery, the central retinal artery and the posterior ciliary artery. It has been reported that there is an increase in peak systolic velocity, diastolic velocity and end-diastolic velocity of these ocular arteries in PCOS patients. Moreover, a decrease in the mean systolic/diastolic ratio, resistive index and pulsatility index has been reported in these arteries in PCOS patients. Overall, the increase in ocular blood flow velocity was positively correlated with serum luteinizing hormone and follicle-stimulating hormone (5).

Changes in the properties of tears

There have been some clinical studies suggesting that the changes in the properties of tears may also contribute to inducing dryness in PCOS patients (6, 7). A clinical study aimed to identify the effects of PCOS on dry eyes involved the enrolment of PCOS (n=35) and healthy controls (n=27) (7). The presence of oligo/anovulation, hyperandrogenism, and >12 ovarian follicles was used for the selection of PCOS patients. The authors employed the combination of three tests, i.e. ocular surface disease index (OSDI), tear break-up time (TBUT), and Schirmer test (to quantify aqueous tear production), to diagnose the presence of dry eyes. The value of TBUT values > 10 seconds is considered normal, while its value <10 seconds is considered pathological. The results showed that there was no significant difference in OSDI and Schirmer tests in PCOS and healthy controls. However, there was a significant decrease in the TBUT in PCOS patients in comparison to healthy. A decrease in TBUT leads to an increase in tear evaporation and dry eye. Moreover, there was a negative correlation between an increase in fasting glucose levels in PCOS patients and a decrease in TBUT, which signifies that an increase in glucose levels may be an important contributing factor in early evaporation of tears and the development of dry eyes. It suggests that the employment of carefully selected sensitive tests may aid in identifying the early stages of dry eyes in PCOS, which may help in preventing long-term ocular complications (7). An earlier clinical study on PCOS (n=25) and healthy individuals (n= 22) also evaluated the influence of PCOS on the changes in the properties of tears. It was reported that the OSDI scores were significantly higher and TBUT was significantly lower in PCOS patients than in healthy controls with no difference in the Schirmer test (6). The results of TBUT in these studies are opposite earlier study (1), which reported no change in TBUT values in PCOS patients. It is difficult to attribute the possible reasons for the contradictory results on the basis of these studies, and hence, more studies are

required to explore the precise changes taking place in TBUT in PCOS patients.

Dysfunction of Meibomian glands

Meibomian glands secrete lipids in tears, which help in providing tear stability and preventing the evaporation of tear film. Indeed, Meibomian Gland Disease (MGD) is characterized by instability of tear film and is the leading cause of dry eye syndrome (8). Yavas et al. conducted a clinical study in PCOS (n=27) and normal individuals (n=22) and proposed the possible role of meibomian glands dysfunction in inducing the state of dryness in PCOS patients. The authors reported the higher frequency of dry eyes along with a shorter tear film break-up time in PCOS, suggesting that meibomian gland function and tear film lipid layer may be affected in these patients (9). A prospective study was conducted to identify the role of Meibomian glands in dry eyes in PCOS patients, and the study included 92 patients of PCOS and 52 healthy controls. The results depicted that the values of TBUT values were significantly lower in PCOS patients, while the Schirmer scores were nearly normal in PCOS and healthy control. An important finding was the presence of a higher rate of MGD (72.82%) in PCOS patients. Due to the presence of normal Schirmer test and the higher frequency of MGD in PCOS patients, it may be suggested that the presence of dry eye symptoms may be due to MGD, and the lacrimal gland function may be normal in PCOS patients. Another important finding of the study was that MGD and tear film instability (reduced value of TBUT) in patients in PCOS was independent of BMI. Accordingly, it may be suggested that dysfunction of Meibomian glands may be an important factor contributing to the development of dry eyes in PCOS (10).

Role of subclinical Inflammation

Subclinical inflammation refers to clinical silent (asymptomatic) or clinically less overt state of inflammation. It may also be called a 'pre-inflammatory state', and its importance in disease initiation has been recognized. It is proposed that the presence of subclinical inflammation may be important in the development of dry eyes. A clinical study in PCOS (n=47) and healthy controls (n=43) identified a significant decline in Schirmer I test scores, and TBUT values were reported. Moreover, there was a significant increase in neutrophil-to-lymphocyte ratio (NLR) in PCOS patients. A negative correlation was reported between NLR and TBUT values in the PCOS group, suggesting that inflammation may be contributing factor in reducing the TBUT values.[16] There has been another study showing the presence of subclinical inflammation along with a decrease in TBUT values in PCOS patients proposing that induction of inflammation in PCOS patients may be important in inducing dryness in the eyes (11).

The clinical studies suggest the correlation between PCOS and dry eyes, which may be due to multiple changes, including structural changes in eyes, alteration in the properties of tears, alterations in Meibomian gland function and presence of subclinical inflammation. The identification of dry eyes in PCOS may help in preventing long term deleterious effects on the eyes. Nevertheless, there is a need to identify the precise mechanisms involved in inducing dryness in the eyes in PCOS patients.

ACKNOWLEDGEMENTS

Subject No. 2021020. Subject Source: Administration of Traditional Chinese Medicine of JiLin Province. Project Name: the technical research of creating a new way of Ren and Du channels acupoint administration to rescue "dry eye in eyedrops".

Declaration of conflict of interest

The authors declare no conflict of interest.

REFERENCES

1. Gonen T, Celik C, Oznur M, et al. Tear osmolarity and ocular surface changes in patient with polycystic ovary syndrome. Curr Eye Res 2013; 38(6):621-625.
2. Karaca Adıyeke S, Karaca I, Yıldırım S, Adıyeke M, Uyar İ, Türe G. Anterior Segment Findings in Women with Polycystic Ovary Syndrome. Turk J Ophthalmol 2017; 47(1):24-27.
3. Kebapcilar AG, Tatar MG, Ipekci SH, et al. Cornea in PCOS patients as a possible target of IGF-1 action and insulin resistance. Arch Gynecol Obstet 2014;

290(6):1255-1263.
4. Bonini S, Mantelli F, Moretti C, Lambiase A, Bonini S, Micera A. Itchy-dry eye associated with polycystic ovary syndrome. Am J Ophthalmol 2007; 143(5):763-771.
5. Örnek N, İnal M, Tulmaç ÖB, Özcan-Dağ Z, Örnek K. Ocular blood flow in polycystic ovary syndrome. J Obstet Gynaecol Res 2015; 41(7):1080-1086.
6. Coksuer H, Ozcura F, Oghan F, Haliloglu B, Karatas S. Effects of hyperandrogenism on tear function and tear drainage in patients with polycystic ovary syndrome. J Reprod Med 2011; 56(1-2):65-70.
7. Yuksel B, Ozturk I, Seven A, et al. Tear function alterations in patients with polycystic ovary syndrome. Eur Rev Med Pharmacol Sci 2015; 19(19):3556-3562.
8. Sambhi R-DS, Sambhi GDS, Mather R, Malvankar-Mehta MS. Intense pulsed light therapy with meibomian gland expression for dry eye disease. Can J Ophthalmol. 2020; 55(3):189-198.
9. Yavas GF, Ozturk F, Kusbeci T, et al. Meibomian gland alterations in polycystic ovary syndrome. Curr Eye Res 2008;33(2):133-138.
10. Baser G, Yildiz N, Calan M. Evaluation of Meibomian Gland Dysfunction in Polycystic Ovary Syndrome and Obesity. Curr Eye Res 2017; 42(5):661-665.
11. Asfuroğlu Y, Kan Ö, Asfuroğlu M, Baser E. Association Between Dry Eye and Polycystic Ovary Syndrome: Subclinical Inflammation May Be Part of the Process. Eye Contact Lens 2021; 47(1):27-31.

A case of combination of multiple interventional therapies: a potential indication of hepatocellular carcinoma treatment

Y. Sun[1], C. Zhang[2], X-Q. Chen[2], X. Wang[2], C. Yuan[2] and X-J. Chen[2*]

[1]Henan University of Chinese Medicine, Zhengzhou, China; [2]Digestive System Department, The First Affiliated Hospital of Henan University of Chinese Medicine, Zhengzhou, China

Received October 26, 2021 – Accepted February 16, 2022

To the Editor,

HCC occurs most often in people with chronic liver diseases, such as cirrhosis caused by hepatitis B or hepatitis C infection, is a primary malignancy of the liver (1). The main treatment for HCC is surgery (2). Recently, some study showed that the efficacy of interventional therapy for HCC is a potential treatment method (3, 4). Herein, we report a case of a 46-year-old man that suffered from HCC and was completely cured by comprehensive interventional therapy with TACE, RFA and iodine-125 seed implantation. These results provide the important reference for treatment option of large primary liver cancer.

Case presentation

A 46-year-old man with chronic hepatitis B but no relevant medical history was admitted to our hospital for acute abdominal pain but no other systemic symptoms on August 2, 2016. Palpation of the right quadrant showed tenderness, but the test of Murphy sign was negative. On the second day after admission, the patient underwent a C.T. scan and found a placeholder measuring 7.04*5.89cm, most of which protruded outside the liver (Fig. 1). Combined with the results of a pathological biopsy, the patient was diagnosed with HCC.

After diagnosis, the patient was treated with TACE using epirubicin and iodized oil. Re-examine the patient's liver function after three days of treatment: T.B. 14umol/L, ALT 133U/L, AST 75U/L, ALB 44.1g/L. According to these results, the patient was performed RFA (Fig. 2). In order to avoid bleeding, we used only one injection, then adjusted the needle in the liver for multi-point ablation and always avoided piercing the liver capsule with the needle tip.

One month later, the patient performed a C.T. scan and found a placeholder measuring 6.7*5.5cm (Fig. 3), which reminded there were still tumor remnants on the liver.

Because most of the tumor protrudes outside the liver capsule, another radiofrequency ablation may affect other organs or cause the tumor to rupture and hemorrhage; we decided to treat conservatively with iodine-125 seed implantation. In addition, there were active tumor cells around the lesion in this patient. Therefore, it was necessary to implant an iodine-125 seed around the lesion, which is difficult to operate. We chose 4 layers for seed implantation, each with a vertical spacing of 1cm. Injected a needle for each layer, then adjusted the frame head to make it fan-shaped, and implant iodine-125 seed to make them distributed in a fan shape with 1cm distance between every two seeds (Fig. 4).

Key words: HCC, TACE, RFA, Iodine-125

**Corresponding author:*
Dr. Xinju Chen
Department of Digestive Diseases,
The First Affiliated Hospital of Henan University of Chinese Medicine,
No. 19, Renmin Road,
Zhengzhou, Henan 450000 P.R. China
e-mail: chenxinju1215@126.com

0393-974X (2022)
Copyright © by BIOLIFE, s.a.s.
This publication and/or article is for individual use only and may not be further reproduced without written permission from the copyright holder.
Unauthorized reproduction may result in financial and other penalties
DISCLOSURE: ALL AUTHORS REPORT NO CONFLICTS OF INTEREST RELEVANT TO THIS ARTICLE.



Fig. 1. *CT-scan showing the size of placeholder on the liver. The lesions are located by the red arrow.*

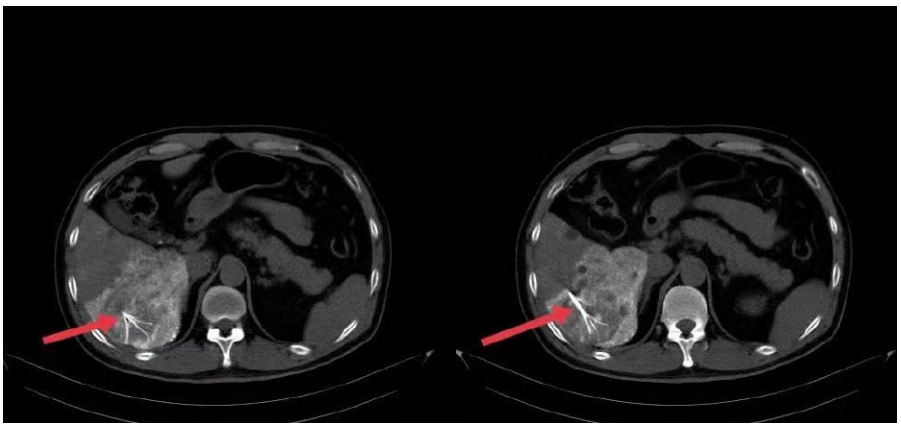


Fig. 2. *RFA with one injection by CT guided, the exact location is indicated by the red arrow.*

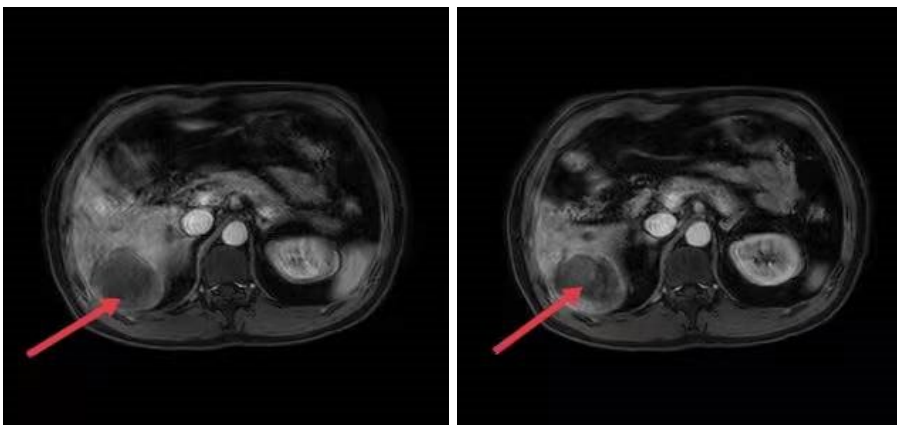


Fig. 3. *MRI showing the size of tumor remnants on the liver, indicated by the red arrow.*

After 2 months of treatment, the C.T. scan showed that the tumour volume was significantly reduced (Fig. 5). Every six months after discharge, re-examinations showed that the lesions were completely necrotic and had no signs of recurrence until the last C.T. scan on November 14, 2020.

DISCUSSION

The main clinical treatment of HCC is surgical resection; however, some types of HCC, like high large primary liver cancer, are not suitable, or the risk of surgery is too high (5, 6), therefore, interventional therapy has become the main treatment for these patients. At present, combination therapy is mainly based on TACE, combined or sequential local treatment (ablation, seed implantation, external radiotherapy), sequential surgical treatment (resection or transplantation), or combined systemic treatment (chemotherapy, molecular targeted therapy, biological Immunotherapy) (7-9). In this case, we used comprehensive interventional therapy with TACE, RFA and iodine-125 seed implantation.

TACE cannot completely necrosis the lesion (10). RFA with small trauma can generate high heat in a very short time, which can cause tumor coagulation and death (11, 12). TACE combined with ablation can eliminate the tumor for large tumours, but it is necessary to ensure sufficient ablation around the lesion. In this case, most of the tumor protruded outside the liver capsule. The thermal expansion caused by high temperature during PFA may lead to tumor rupture. Therefore, we reduced the ablation temperature around the lesion during PFA, leading to active residual lesions. Iodine-125 seed implantation is a method of internal radiotherapy to treat tumors; it

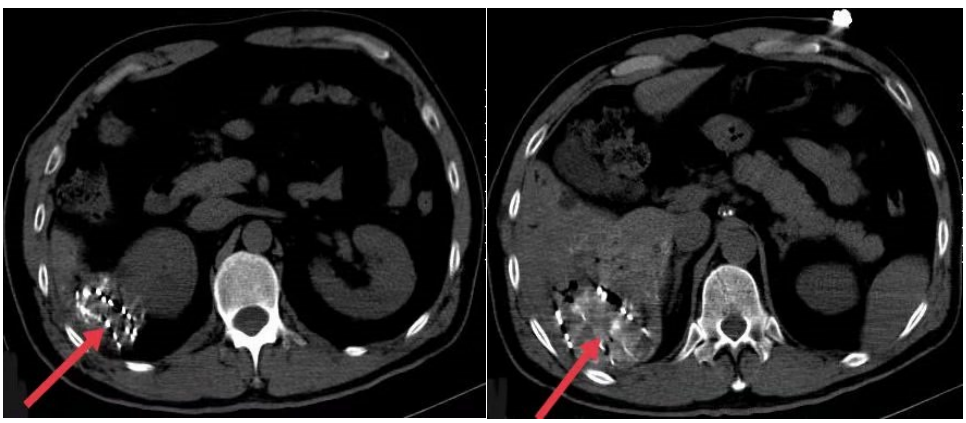


Fig. 4. *Iodine-125 seed implantation around the lesion by CT guided, the exact location is indicated by the red arrow.*

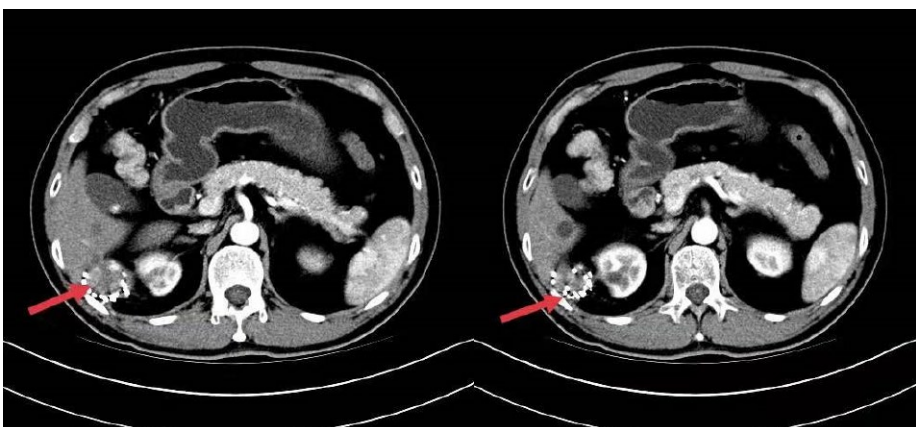


Fig. 5. *CT-scan showing that lesions completely necrotic and no signs of recurrence, indicated by the red arrow.*

targets tumor cells by continuously releasing low-dose gamma rays at close distances but does less damage to other tissues around the tumor. We decided to treat the active tumor cells around the lesion with iodine-125 seed implantation. However, it is very difficult to make the iodine-125 seed evenly distributed around the lesion. We introduced in detail the operation details and matters needing attention. During the execution of the iodine-125 seed implantation operation, we adjusted the frame head to make it fan-shaped and implanted iodine-125 seed to make them around the lesion. After the comprehensive interventional therapy, the patient was completely cured and there have been no signs of recurrence in the last 4 years. This case provided an important reference for large primary liver cancer treatment options.

Two months after radiotherapy, imaging findings showed necrosis of the lesion. The patient was followed up until now. Blood routine examination, liver and kidney function, alpha-fetoprotein, hepatitis B virus and liver imaging examination were repeated every six months. All the indicators were in the normal range, and imaging suggested no new or active lesions. The patient has survived for more than 5 years and is generally in good condition with no obvious adverse reactions.

Collectively, our case provides successful experience and new inspiration for the treatment of HCC. Therefore, comprehensive interventional therapy with TACE, RFA and iodine-125 seed implantation may be a promising therapeutic strategy for large primary liver cancer.

Funding

This study was funded by the National Science and Technology Major Project of the Ministry of Science and Technology of China 2018ZX10303502; the second batch of the discipline construction project of Characteristic backbone disciplines of Henan Province, STG_ZYX01_202101.

Author contributions

Y.S. and XjC carried out the conception and design of the research, XqC participated in the acquisition of data. C.Z. carried out the analysis and interpretation of data. X.W. and C.Y. participated in the study's design and performed the statistical analysis. Y.S. and XjC conceived of the study, participated in its design and coordination, and helped draft the manuscript and revise it for important intellectual content. All authors read and approved the final manuscript. The authors declare that they have no competing interests.

REFERENCES

1. Virzi A, Gonzalez-Motos V, Tripon S, Baumert TF, Lupberger J. Profibrotic Signaling and HCC Risk during Chronic Viral Hepatitis: Biomarker Development. J Clin Med 2021; 10(5):977.
2. Kim TH, Woo S, Han S, Suh CH, Lee DH, Lee JM. Hepatobiliary phase hypointense nodule without arterial phase hyperenhancement: are they at risk of HCC recurrence after ablation or surgery? A systematic review and meta-analysis. Eur Radiol 2020; 30(3):1624-33.
3. Geyer T, Rubenthaler J, Alunni-Fabbroni M, et al. NMR-Based Lipid Metabolite Profiles to Predict Outcomes in Patients Undergoing Interventional Therapy for a Hepatocellular Carcinoma (HCC): A Substudy of the SORAMIC Trial. Cancers (Basel) 2021; 13(11):2787.
4. Iezzi R, Pompili M, Posa A, et al. Interventional oncology treatments for unresectable early stage HCC in patients with a high risk for intraprocedural bleeding: Is a single-step combined therapy safe and feasible? Eur J Radiol 2019; 114:32-37.
5. Leray H, Brouchet L, Tanguy Le Gac Y, et al. Postoperative chest liver herniation after cardiophrenic lymph node resection by a transdiaphragmatic approach following primary cytoreductive surgery for advanced endometrioid ovarian cancer: A case report. Gynecol Oncol Rep 2021; 36:100727.
6. Hu Y, Shen ZH. Practice of precision surgery in primary liver cancer. Hepatobiliary Pancreat Dis Int 2021; 20:108-9.
7. Sun Y, Ji S, Ji H, Liu L, Li C. Clinical efficacy analysis of transcatheter arterial chemoembolization (TACE) combined with radiofrequency ablation (RFA) in primary liver cancer and recurrent liver cancer. J BUON 2019; 24(4):1402-7.
8. Luo Y, Jiang Y. Comparison of Efficiency of TACE

plus HIFU and TACE alone on Patients with Primary Liver Cancer. J Coll Physicians Surg Pak 2019; 29:414-7.

9. Xie L, Qian Z, Xu J. Clinical intervention effect of TACE combined with 3DCRT in patients with primary liver cancer. Am J Transl Res 2021; 13:7960-7.
10. Sun M, Shang P, Bai J, Li S, Li M. High-intensity focused ultrasound ablation combined with transcatheter arterial chemoembolization improves long-term efficacy and prognosis of primary liver cancer. J Clin Lab Anal 2021; 35:e23633.
11. Zimmermann M, Pedersoli F, Schulze-Hagen M, Lurje G, Isfort P, Kuhl C, Bruners P. Salvage RFA in patients with intrahepatic recurrence after major hepatic surgery for colorectal cancer liver metastases: mid-term outcome. Eur Radiol 2020; 30:1221-7.
12. Mariappan P, Weir P, Flanagan R, et al. GPU-based RFA simulation for minimally invasive cancer treatment of liver tumours. Int J Comput Assist Radiol Surg 2017; 12:59-68.

The promotion of the secretion of angiogenesis-related factors in hepatocellular carcinoma cells by macrophage migration inhibitory factor

M. Wei[#], L-X. Lu[#], B. Li[#], C-Y Li, Y. Zheng, J-K. Wang, P. Wang, L-W. Ren, X-H. Yu[*] and J-C. Zhang[*]

Department of Gastroenterology, The 940th Hospital of Joint Service Logistics Support Force of PLA, Lanzhou, China

To the Editor,

Hepatocellular carcinoma (HCC) is one of the most common malignant tumors, and it is the second leading cause of tumor death following gastric cancer (1). In recent years, surgical resection combined with interventional therapy, microwave ablation, and molecular targeting therapy has prolonged the survival of HCC patients to a certain extent, but the 5-year recurrence rate remains as high as 50–70%. The main reason for this is that HCC cells are highly invasive and migratory (2), and the basis of invasion and migration is the formation of tumor neovascularization, which allows tumor cells to be fully supplied with nutrients, after which they undergo uncontrolled growth and migration to surrounding or distant tissues. The formation of tumor neovascularization is related to the high expression of various angiogenic factors in HCC cells. Previous studies revealed that vascular endothelial growth factor (VEGF), interleukin-8 (IL-8), and transforming growth factor-β (TGF-β) could significantly promote tumor angiogenesis. However, the specific regulatory mechanism is very complex. Therefore, an in-depth study of the molecular mechanism of the angiogenesis of HCC cells will help find molecular targets promoting the invasion and migration of HCC, and this will assist in the development of new drugs to improve the cure rate of HCC and reduce the mortality rate.

Macrophage migration inhibitory factor (MIF) is a cytokine mainly secreted by activated T lymphocytes that can inhibit the movement of macrophages/monocytes, playing an important role in the immune and inflammatory responses (3). Furthermore, many studies have revealed that the over-expression of MIF is closely related to tumor cell proliferation, differentiation, invasion, and angiogenesis (4). Therefore, the present study aimed to determine whether MIF could promote the secretion of tumour-related angiogenic factors by SMMC-7721 and HepG2 cells, which is associated with HCC invasion and metastasis.

MATERIALS AND METHODS

Cell lines

SMMC-7721, HepG-2 HCC cells, and normal liver cell line LO2 were provided by the Laboratory of Molecular Biology, Tianjin Cancer Institute, Tianjin Medical University.

Reagents and antibodies

Human recombinant MIF (rMIF) was purchased from Santa Cruz (USA), a VEGF, IL-8, and TGF-β ELISA kit was purchased from R&D Systems Bioengineering Co.

Keywords: macrophage migration inhibitory factor; hepatocellular carcinoma cells; vascular endothelial growth factor; interleukin-8; transforming growth factor-β; angiogenesis

**Corresponding author:*
Dr Xiao-Hui Yu
Department of Gastroenterology,
The 940th Hospital of Joint Service Logistics Support Force of PLA,
No.333 of Nanbinhe Road, Qilihe District,
Lanzhou 730050, China
e-mail: yuxh_abc@163.com

0393-974X (2022)
Copyright © by BIOLIFE, s.a.s.
This publication and/or article is for individual use only and may not be further reproduced without written permission from the copyright holder.
Unauthorized reproduction may result in financial and other penalties
DISCLOSURE: ALL AUTHORS REPORT NO CONFLICTS OF INTEREST RELEVANT TO THIS ARTICLE.

Ltd., and rabbit anti-human MIF monoclonal antibody (MIF mAb) was purchased from Wuhan Boster Biological Technology Ltd.

The culture and passage of HCC cells and normal liver cells

SMMC-7721 and HepG-2 human HCC cell lines were resuscitated and then stored in a culture bottle with DMEM-F12 medium containing 10% fetal bovine serum (FBS) and antibiotics (50 U/ml penicillin and 100 μg/ml streptomycin). LO2 normal human liver cells were resuscitated and then stored in a culture bottle with RPMI-1640 medium containing 10% FBS and antibiotics (50 U/ml penicillin and 100 μg/ml streptomycin). All cells were incubated in 5% CO_2 at 37°C and routinely passaged 2–3 times a week.

The treatment of HCC cells and normal liver cells with different concentrations of rMIF

HCC cells and normal liver cells in the logarithmic growth phase were obtained, and the cell density was adjusted to 5×10^4/mL. They were then inoculated in a 24-well plate with DMEM medium and RPMI-1640 medium containing 10% FBS and cultivated for 24 h, after which they were washed twice with phosphate-buffered saline (PBS). Next, they were cultured in a medium containing different concentrations of rMIF (0-200 ng/ml) for 24 h, and, finally, the culture supernatant of the cells was collected.

The treatment of HCC cells with different concentrations of rMIF

HCC cells were cultured to the logarithmic growth phase, and then the density was adjusted to 5×10^4 cells/ml. The cells were placed in a 48-well plate in line with the 1.2 ml/well specification, then cultured for 24 h. Different concentrations (0, 10, 50, and 250 μg/ml) of MIF mAb and 25 ng/ml of suramin were added to the HCC cells. Each group had five duplicated wells cultured in an incubator in 5% CO2 for 24 h, any changes in the cell morphology were observed under an inverted microscope.

The detection of the levels of VEGF, IL-8, and TGF-β in HCC cell culture supernatant with enzyme-linked immunosorbent assay

The levels of IL-8 and VEGF in the supernatant of the LO2, SMMC-7721 and HepG-2 cells, cultured with different concentrations of rMIF, were detected throught the enzyme-linked immunosorbent assay (ELISA) kit. At the same time, HCC cells were cultured with different concentrations of MIF mAb for 24 h, and the levels of VEGF and TGF-β in the cell culture supernatant were detected through the instructions of the kit.

Statistical analysis

All data were expressed as mean ± standard deviation (x ± SD) and statistically analyzed using statistical software SPSS 20.0. Data were compared among groups using univariate analysis of variance. The experiment was repeated three times. A p-value<0.05 was considered statistically significant.

RESULTS

rMIF promotion of the expression of VEGF and IL-8 in hepatoma cells

Different concentrations (0, 10, 100, and 200 ng/ml) of rMIF were added to the SMMC-7721 and HepG2 cells and left for 24 h. The results showed that as the concentration of rMIF increased, the number of SMMC-7721 and HepG2 cells also increased significantly in each high-power field; the most significant increase is seen in the cells cultured with a concentration of rMIF of 200 ng/ml (Fig. 1A-D). In addition, the culture supernatants of the cells in the control and experimental groups were collected after being treated with rMIF for 24 h, and ELISA detected the levels of VEGF and IL-8. The results revealed that, compared with the control group, with the increase of rMIF concentration, the levels of VEGF and IL-8 in the HepG2 cells also increased in a concentration-dependent manner ($p<0.05$); however, in the SMMC-7721 HCC cells, after treatment with different concentrations of rMIF, the level of VEGF in cell supernatant increased in a concentration-dependent manner ($p<0.05$), but the increase of IL-8 was not significant ($p > 0.05$) (Fig. 1E–F).

The inhibition of the expressions of VEGF and TGF-β in HCC cells by MIF mAb

Different concentrations (0, 10, 50, and 250 μg/ml) of MIF mAb and 25 ng/ml of suramin were used

to culture SMMC-7721 and HepG2 cells for 24 h after which the cell morphology was observed under the inverted microscope (Fig. 2A-F). Among all the cells, in those treated with 0 μg/ml of MIF mAb, that is, in the blank control group, the growth of the HCC cells was good, and the cells were spindle-shaped; compared with the blank control group, in the experimental group and the positive control group, the growth of the HCC cells was slow, the number of tumor cells decreased significantly, the cells were spherical or ovoid, and the nuclei were dense. The culture supernatant of the HCC cells was collected again, and the levels of VEGF and TGF-β were detected by ELISA (Fig. 2G-J). The results showed that levels of VEGF and TGF-β in different concentrations in the MIF mAb group fell ($p<0.05$), compared to the blank control group; the expression was lower at a concentration of 250 μg/ml ($p<0.001$), but there was no significant difference between the blank control group and the positive control group ($p > 0.05$), suggesting that MIF mAb can inhibit the expression of VEGF and TGF-β in SMMC-7721 and HepG2 cells.

DISCUSSION

When the liver cells become cancerous, the formation of tumorous neogenetic blood vessels is an important hemodynamic basis for tumor invasion and metastasis, which is because HCC cells can secrete tumour-related angiogenic factors, such as TGF-β, VEGF, and IL-8. It is also an important reason for the poor prognosis of HCC after intervention using currently available means (5, 6). One study reports that the abnormal secretion of tumour-related angiogenic factors may be regulated by some related proteins expressed by HCC cells, and MIF is one of them (7).

As one of the earliest discovered cytokines, MIF is overexpressed in many cancers and is closely related to invasion, metastasis, and poor prognosis. In our previous studies, the positive expression rate of MIF and MIF mRNA in HCC tissues was 70.00% (8), which was significantly higher than that in normal liver tissues ($p<0.05$). In another study, It was reported that MIF could promote the angiogenesis of lymphoma by stimulating the proliferation of vascular endothelial cells *in vitro* (9), and could induce angiogenesis directly

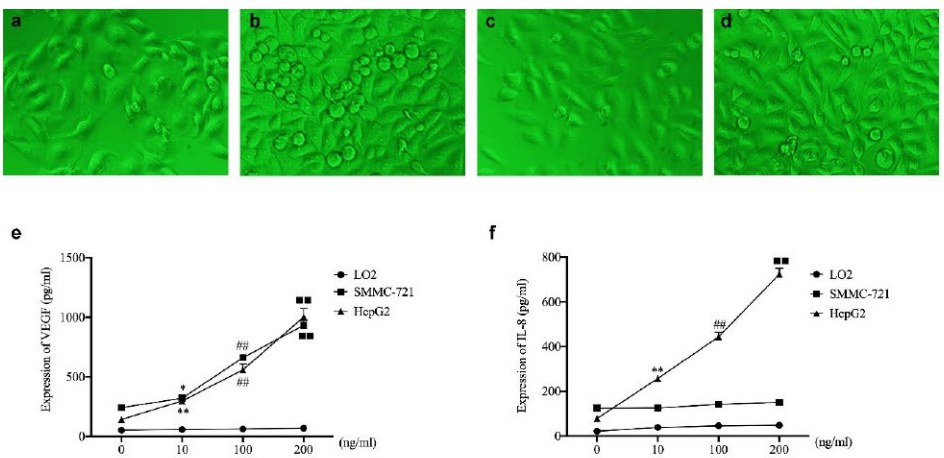


Fig. 1: *Secretion of VEGF and IL-8 from SMMC-7721 and HepG2 HCC cells inducing by rMIF. Figures (a) and (c) show the growth of SMMC-7721 and HepG2 HCC cells after treated with 0 ng/ml of rMIF for 24 h; figures (b) and (d) show the growth of SMMC-7721 and HepG2 HCC cells after treated with 200 ng/ml of rMIF for 24 h; and figures (e-f) show the secretion of VEGF and IL-8 in the supernatant of LO2 normal liver cells, SMMC-7721 and HepG2 HCC cells treated with different concentrations of rMIF for 24 h. Notes: Compared with the 0 ng/ml group: $^{*}P<0.05$, $^{**}P<0.01$; compared with the 10 ng/ml group: $^{\#}P<0.05$, $^{\#\#}P<0.01$; and compared with the 100 ng/ml group: $^{\blacksquare}P<0.05$, $^{\blacksquare\blacksquare}P<0.01$.*

or indirectly by stimulating IL-8, VEGF, monocyte chemotactic protein-1, angiogenic CXC chemokines, and other angiogenic factors in order to promote the invasion and metastasis of colorectal cancer, endometrial cancer, and non-small cell lung cancer (10, 11). However, there are few studies on whether MIF can promote the invasion and metastasis of HCC by regulating the abnormal expression of tumour-related angiogenic factors. In this study, different concentrations of rMIF were used to stimulate HCC cells (SMMC-7721 and HepG2) and normal liver cells (LO2) for 24 h, then the levels of VEGF and IL-8 in the supernatant of three kinds of cells were detected by ELISA. The results revealed that rMIF could stimulate the abnormal expression of VEGF and IL-8 in HepG2 cells in a concentration-dependent manner and could also promote the abnormal expression of VEGF in SMMC-7721 cells, but the expression of

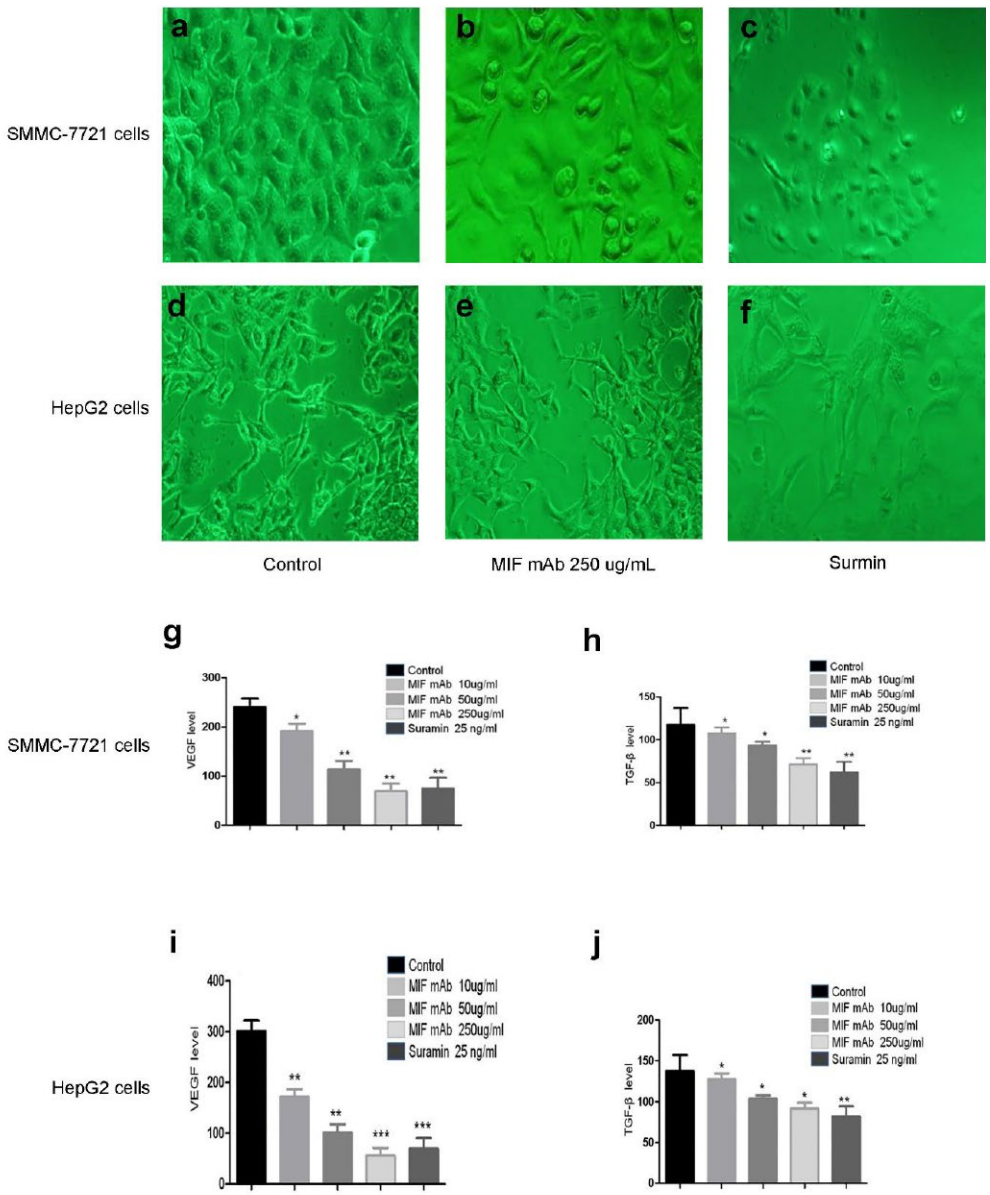


Fig. 2: *MIF mAb can inhibit the growth of HCC cells and reduce the expression of VEGF and TGF-β in HCC cells. Figures (a-f) show the growth of SMMC-7721 and HepG2 cells after treated with 0 μg/ml and 250 μg/ml of MIF mAb and surmin respectively for 24 h; figures (g-j) show the expressions of VEGF and TGF-β in the supernatants of SMMC-7721 and HepG2 HCC cells after treated with (0 μg/ml, 10 μg/ml, 50 μg/ml and 250 μg/ml) of MIF mAb and 25 ng/ml of surmin for 24 h. Notes: Compared with the blank control group, that is, the 0 μg/ml group: $^{*}P<0.05$, $^{**}P<0.01$, $^{***}P<0.001$.*

IL-8 was not significant. A preliminary analysis put this down to the non-expression or low expression of IL-8 receptors in SMMC-7721 cells. Therefore, MIF mAb was further used to treat HepG2 and SMMC-7721 cells, and the results revealed that the expressions of VEGF and TGF were down-regulated, suggesting that as a proinflammatory cytokine, MIF can promote the abnormal expression of VEGF, IL-8, and TGF-β in HCC cells and can promote the invasion and migration of HCC cells. Ren et al. (12) found that MIF could stimulate Hep3B, PLC, and Huh 7 HCC cells to secrete IL-8 and VEGF, which is consistent with the results of this study. These results suggest that MIF may promote HCC invasion and metastasis by inducing tumor cells to express angiogenic factors.

Based on the reviewed literature and the findings of this study, the investigators believe that MIF can participate in HCC invasion and metastasis by inducing HCC cells to secrete VEGF, IL-8, and TGF-β. However, the specific mechanism concerning how MIF promotes the secretion of tumour-related angiogenic factors is still worthy of further study.

Acknowledgements

We are particularly grateful to all the people who have given us help with our article.

Competing interests

No conflict of interest.

Funding

Key R & D Program of Gansu Province (Project Number: 20YF8FA099).

REFERENCES

1. Ferlay J, Colombet M, Soerjomataram I, et al. Estimating the global cancer incidence and mortality in 2018: GLOBOCAN sources and methods. Int J Cancer 2019; 144(8):1941-53.
2. Sarveazad A, Agah S, Babahajian A, Amini N, Bahardoust M. Predictors of 5 year survival rate in hepatocellular carcinoma patients. J Res Med Sci 2019; 24:86.
3. Zhao R, Yao WJ. [The functions and clinical studies of macrophage migration inhibitory factor]. [Article in Chinese] Sheng Li Ke Xue Jin Zhan 2014; 45(2): 93-9.
4. Koh HM, Kim DC. Prognostic significance of macrophage migration inhibitory factor expression in cancer patients: A systematic review and meta-analysis. Medicine (Baltimore) 2020; 99(32):e21575.
5. Wang T, Zhang Q, Wang N, Liu Z, Zhang B, Zhao Y. Research Progresses of Targeted Therapy and Immunotherapy for Hepatocellular Carcinoma. Curr Med Chem 2021; 28(16):3107-46.
6. Elewa MA, Al-Gayyar MM, Schaalan MF, Abd El Galil KH, Ebrahim MA, El-Shishtawy MM. Hepatoprotective and anti-tumor effects of targeting MMP-9 in hepatocellular carcinoma and its relation to vascular invasion markers. Clin Exp Metastasis 2015; 32(5):479-93.
7. Ren Y, Tsui HT, Poon RT, et al. Macrophage migration inhibitory factor: roles in regulating tumor cell migration and expression of angiogenic factors in hepatocellular carcinoma. Int J Cancer 2003; 107(1):22-9.
8. Yu XH, Liu C, Wu XZ, et al. Expression of macrophage migration inhibitory factor in liver disease associated with hepatitis B virus infection.] [Article in Chinese] Zhonghua Gan Zang Bing Za Zhi 2007; 15(1):60-1.
9. Chesney J, Metz C, Bacher M, Peng T, Meinhardt A, Bucala R. An essential role for macrophage migration inhibitory factor (MIF) in angiogenesis and the growth of a murine lymphoma. Mol Med 1999; 5(3):181-91.
10. Veillat V, Carli C, Metz CN, Al-Abed Y, Naccache PH, Akoum A. Macrophage migration inhibitory factor elicits an angiogenic phenotype in human ectopic endometrial cells and triggers the production of major angiogenic factors via CD44, CD74, and MAPK signaling pathways. J Clin Endocrinol Metab 2010; 95(12):E403-12.
11. White ES, Flaherty KR, Carskadon S, et al. Macrophage migration inhibitory factor and CXC chemokine expression in non-small cell lung cancer: role in angiogenesis and prognosis. Clin Cancer Res 2003; 9(2):853-60.
12. Enomoto H, Nakamura H, Liu W, Nishiguchi S. Hepatoma-Derived Growth Factor: Its Possible Involvement in the Progression of Hepatocellular Carcinoma. Int J Mol Sci 2015; 16(6):14086-97.

Protective effect and mechanism of Baicalin on H9c2 cardiomyocyte inflammation induced by lipopolysaccharide by regulating the miR-181a-5p/HMGB1 axis

G-Q. Yan[1#], M-N. Dong[2#], C-H. Zhang[2#] and M-W. Liu[2*]

[1]Department of Science and Education, The First Affiliated Hospital of Kunming Medical University, Wuhua District, Kunming, China; [2]Department of Emergency Medicine, the First Affiliated Hospital of Kunming Medical University, Wuhua District, Kunming, China

Received August 25, 2021 – Accepted December 17, 2021

[#]These Authors contributed equally to this work

To the Editor,

When the body produces sepsis, it can overproduce inflammatory factors, including TNF-α, IL-1β, and IL-6. These inflammatory factors damage the heart by activating sphingomyelinase, inhibiting calcium transport resulted in intracellular diastolic Ca^{2+} overload (1) and stimulating tissue nitric oxide production (1). They also degrade the primary myocardial contractile proteins by stimulating myocardial hydrolase, affecting cardiac contractility (2). However, its mechanism is unclear.

Overexpressed microRNA-181a (miR-181a) can downregulate the toll-like receptor (TLR)/nuclear factor (NF)-κB pathway by binding to cryptochrome-1, reducing glomerular sclerosis and tubular epithelial damage in rats with chronic kidney disease (3). miR-181a can inhibit the inflammatory response induced by LPS by inhibiting the generation of reactive oxygen species and the activity of the TLR4-NF-κB pathway (3). The high mobility group box 1 protein (HMGB1)/TLR4/NF-κB signaling pathway is an important inflammation-related signal transduction pathway. Some studies have shown that inhibiting the expression levels of genes, such as HMGB1, TLR4, NF-κB, and other cytokines, can reduce damage to vital organs during sepsis (4). Baicalin exhibits anti-inflammatory, antioxidant, free radical scavenging, antitumor, and antibacterial (5, 6). Studies have reported that Baicalin can protect the body from septic injury by inhibiting inflammatory response and oxidative stress or by reducing apoptosis (7); however, research on the role of Baicalin in myocardial injury during sepsis is less.

In the current experiment, we predicted that HMGB1 may be the regulatory target of miR-181a-5p by using TargetScan. Therefore, we speculated that the inhibition of Baicalin can increase the expression of miR-181a-5p, inhibit the activity of the HMGB1/TLR4/NF-κB pathway, reduce LPS-induced H9c2 cardiomyocyte inflammation and apoptosis, and improve endotoxin-induced myocardial injury.

MATERIALS AND METHODS

Drug, culture and grouping of H9c2 cardiomyocytes

Baicalin (10 mM × 1 mL in DMSO, purity: 98.01%) was purchased from (Sigma-Aldrich, Germany).

H9c2 cardiomyocytes were obtained from the cell

Key words: Baicalin; lipopolysaccharide; cardiomyocytes; NF-κB; HMGB1; sepsis

Corresponding Author:
Dr. Ming-wei Liu
Department of Emergency Medicine,
The First Affiliated Hospital of Kunming Medical University,
245 Xichang Road,
Wuhua District, Kunming, 650032, China
e-mail: lmw2004210@163.com; liumingwei.92233@ydyy.net.cn

0393-974X (2022)
Copyright © by BIOLIFE, s.a.s.
This publication and/or article is for individual use only and may not be further reproduced without written permission from the copyright holder.
Unauthorized reproduction may result in financial and other penalties
DISCLOSURE: ALL AUTHORS REPORT NO CONFLICTS OF INTEREST RELEVANT TO THIS ARTICLE.

bank of the Institute of Biochemistry and Cell Biology (Shanghai, China), and cultured in RPMI 1640 medium (Gibco, USA) containing 10% fetal bovine serum. When growth and confluence reached 70%, cardiomyocytes were seeded into a petri dish at a density of 1×10^4/mL per well plate and cultivated at 37°C in a 5% CO_2 incubator. The cardiomyocytes were digested with 0.25% trypsin and cultured for 7 days at a passage of 1:2. Then, the cells were inoculated in a 25 cm^2 culture flask at a density of 1×10^5 cells/mL. When confluence reached approximately 60%, the cells were synchronized to grow for 24 h and then grouped. To observe the effect of LPS on the viability and survival rate of H9c2 cardiomyocytes, we added different concentrations of LPS (0.5, 1.0, 1.5, and 2.0 mg/L) and cultured the cells for 24 h. To observe the effect of Baicalin on H9c2 cardiomyocyte damage induced by endotoxin, according to the previously described (8), the cells were divided into the normal control group, LPS induction group, LPS + low dose (25 μmol/L) baicalin group, LPS + medium dose (50 μmol/L) baicalin group, and LPS + high-dose (75 μmol/L) baicalin group. We first added different concentrations of Baicalin (25–75 μM) and incubated the cells for 2 h. Then, we added LPS (1.0 μM) solution after 2 h, incubated the cells for 24 h, and measured various indicators.

Cholecystokinin (CCK)-8 measurement of H9c2 cardiomyocyte vitality

The proliferation activity of H9c2 cells in different treatment groups was measured with a CCK-8 kit (cck-8, Seven Seas). H9c2 cells were inoculated into a 96-well plate until the cells were 70% confluent. The serum-free medium was replaced. After treatment under different conditions, 10 μL of CCK-8 solution was added to each well and the cells were incubated for 2–4 h in the dark. Then, a microplate reader was used to measure the absorbance value (A450 nm) at a wavelength of 450 nm.

Transfection of H9c2 cardiomyocytes

An appropriate amount of H9c2 cardiomyocytes in the logarithmic growth phase were seeded into a six-well plate. Once the cells adhered to the wall overnight and grew up to 60%, miR-181a-5p mimic, miR-181a-5p inhibitor, mimic control, and inhibitor control were transfected into H9c2 cardiomyocytes by following the operating instructions of Lipofectamine 2000 transfection reagent. The transfection concentration was 50 nmol/L. After 6 h of transfection, the medium was replaced with a fresh one, and culture was continued up to 24 h. The cells were collected for reverse transcription polymerase chain reaction (RT-PCR) and Western blot analysis.

Determining the growth rate of H9c2 cardiomyocytes

The liquid in each well of the 96-well plate was aspirated and discarded. Then, 270 μL of Dulbecco's modified Eagle's medium was added, followed by 30 μL of 5 g/L MTT working solution. The mixture was combined well and then incubated at 37 °C for 4 h. The culture medium in the well was discarded and 270 μL of dimethyl sulfoxide was added to each well. The mixture was shaken for 10 minutes to dissolve the components completely. The optical density (OD) value of each well was measured using a microplate reader with a wavelength of 490 nm. The OD value of the normal group was used as the control. The cell survival rate of each well was calculated as follows: (%) = OD value of each well/average OD value of the normal group × 100 (5).

Prediction of target genes

Using target gene prediction software, miRBase (http://www.mirbase.org/), TargetScan (http://www.targetscan.org/), and PicTar (http://pictar.m dc-berlin.de/), the target gene of miR-181a-5p was predicted to be peroxisome proliferator-activated receptor-α. The wild-type (wt)-HMGB1 and mutant (mut)-HMGB1 luciferase gene vectors were constructed using conventional methods, and the two plasmids were combined with miR-181a-5p mimic, miR-181a-5p inhibitor, mimic control, and inhibitor control. The controls were mixed and co-transfected into H9c2 cardiomyocytes and counted as Wt+miR-181a-5p mimic, Mut+miR-181a-5p, Wt+negative control, and Mut+negative control. After culturing at 37°C in a 5% CO_2 incubator for 48 h, a dual luciferase reporter gene kit was used to detect dual luciferase activity. Simultaneously, RT-PCR and Western blotting were performed to detect the level of HMGB1 in H9c2 cardiomyocytes overexpressing miR-181a-5p.

Quantitative real-time PCR

H9c2 cells were collected from each treatment group. Cellular RNA was extracted using a total RNA extraction kit (Takara, Shiga, Japan) and reverse-transcribed into complementary DNA in accordance with the PrimeScript TM RT reagent kit (Thermo Scientific, USA). Quantitative

real-time PCR was performed to detect the expression of HMGB1mRNA and miR-181a-5p in cells. The primer sequence was as follows:

miR-181a-5p:	F-5'-TGAGGGCTAGAGACAAG-CAG-3'
	R-5'-TGGTGTCGTGGAGTCG-3'
U6:	F-5'-GTCAAGTGCACACGCGT-GAC-3'
	R-5'-ACCTGTATTCTCGTGCTCAT-3'
HMGB1mRNA:	F-5'- GCAGCAGTGTTGTTCCA-CAT-3'
	R-5'-CGGCCTTCTTCTTGTTCT-GT-3';
β-actin:	F-5'-ATGGAGGGGAATACAGC-CC-3',
	R-5'-TTTCTTTGCAGCTCCTTC-GTT-3'.

The reaction system was as follows: SYBR Premix Ex TaqTMII (10 μL), PCR primers (2 μL), DNA template (2 μL), diethyl pyrocarbonate-treated water (6 μL), and total reaction system (20 μL). Three parallel multiple wells were set for each sample, and the reaction system was placed on the PCR machine to complete the reaction. To detect the level of miR-181a-5p, we used TaqMan™ MicroRNA Assay kit (Applied Biosystems, Foster City, CA, USA) to measure the expression level of miR-9-5p by using the $2^{-\Delta\Delta Ct}$ method. The reaction conditions were as follows: 95 °C pre-denaturation for 30 s, 95 °C reaction for 5 s, and 60 °C annealing for 30 s (40 cycles). U6 was used as the internal reference of miR-181a-5p. β-actin was used as an internal reference for HMGB1 gene expression. After the reaction was completed, the cycle threshold of each gene was calculated and compared with the internal reference gene U6 to determine the expression level.

Western blot analysis

H9c2 cells were collected from each treatment group. Cell lysis buffer, protease inhibitors, and phosphatase inhibitors were mixed at a ratio of 8:1:1 to prepare the cell lysis buffer, and 150 μL of radioimmunoprecipitation assay cell lysis buffer was added to each well. The cells were placed on an ice bath to lyse for 30 min, and then the total protein of each group of cells was extracted. The cells were centrifuged for 15 min at 4 °C, and protein purity was detected using a bicinchoninic acid protein quantification kit. The 50 μg protein extract was separated via 10% sodium dodecyl sulfate-polyacrylamide gel electrophoresis, and 5% skim milk was added to incubate and block for 1.5 h. The corresponding NF-κB65, TLR4, HMGB1, β-actin, and p-IκB-α primary antibodies (1:1000, Cell Signaling Technology, Danvers, MA, USA) were added at 4 □ overnight. The membrane was washed three times with TBST on the following day, and then horseradish peroxidase-labeled goat anti-rabbit immunoglobulin G (1:500, BD Biosciences, San Jose, CA, USA) was added (diluted by volume 1:3000) and reacted at room temperature for 1 h. Then, the membrane was washed three times with TBST for 10 min each time, and an electrochemiluminescence solution was added to develop color. The LiCor Odyssey imaging system™ was used to analyze the band gray value, and β-actin was used as an internal reference.

Enzyme-linked immunosorbent assay (ELISA)

H9c2 cells in the logarithmic growth phase were digested, resuspended, and seeded into six plates. The old medium was aspirated after the cells adhered. The cells in each treatment group were cultured for 24 h, and then, the cells and cell supernatant were collected. The cell supernatant was used to detect the levels of inflammatory factors, namely, interleukin (IL)-6, IL-1β, and tumor necrosis factor (TNF)-α, with an ELISA kit (IBL, Germany). The operation steps were performed in strict compliance with the instructions.

Statistical analysis

We used GraphPad Prism 6 for statistical analysis. The experimental data were expressed as mean ± standard deviation (SD), and under the condition of homogeneity of variance, one-way ANOVA analysis was used to analyze the intergroup comparison. $P<0.05$ indicated that the difference was statistically significant.

RESULTS

Baicalin increased survival rate in LPS-induced H9c2 cells

H9c2 cells were incubated with LPS (1.0 μM) and various concentrations of Baicalin (25, 50, and 75 μM) for 24 h. The survival rate was measured via MTT assay. As shown in Table I, Baicalin increased cell survival rate in LPS-induced H9c2 cells.

Baicalin decreased H9c2 cell inflammation in LPS-induced H9c2 cells

H9c2 cells were incubated with LPS (1.0 μM) and various concentrations of Baicalin (25, 50, and 75 μM) for 24 h. IL-6, IL-1β, and TNF-α in H9c2 cells were measured using ELISA. As shown in Table I, Baicalin decreased IL-6, IL-1β, and TNF-α in LPS-induced H9c2 cells.

Baicalin decreased the activity of the HMGB1/TLR4/ NF-κB signaling pathway and upregulated miR-181a-5p expression in LPS-induced H9c2 cells

H9c2 cells were incubated with LPS (1.0 μM) and various concentrations of Baicalin (25, 50, and 75 μM) for 24 h. HMGB1, TLR4, NF-κB65, and p-IκB-α protein expression levels were measured via Western blotting. The expression of miR-181a-5p was measured through RT-PCR. As shown in Fig. 1, Baicalin diminished the increase in HMGB1, NF-κB65, TLR4, and p-IκB-α protein expression in LPS-induced H9c2 cells.

HMGB1 is a regulatory target of miR-181a-5p

To determine how miR-181a-5p mediated in LPS-induced H9c2 cell inflammation, we used a well-known database to predict the probable targets of miR-181a-5p. Consequently, we determined that HMGB1 is an important regulator of LPS- induced H9c2 cell inflammation. Our analysis indicated that HMGB1 messenger RNA and protein levels were dramatically decreased after miR-181a-5p overexpression (Figs. 2-a–2-b, 2-d). To validate the interaction between miR-181a-5p and HMGB1, we constructed wild-type and mutant HMGB1 for a dual luciferase reporter assay (Fig. 2-c). As hypothesized, miR-181a-5p became bound to wild-type HMGB1 rather than to the mutants (Fig. 2-d).

Effect of Baicalin plus miR-181a-5p mimic on the activity of the HMGB1/TLR4/ NF-κB signaling pathway in LPS-induced H9c2 cells

H9c2 cells were transfected with miR-181a-5p mimic in the presence of 1 mg/l LPS and Baicalin (50 μM) for 24 h. HMGB1, TLR4, NF-κB65, and p-IκB-α protein expression levels were measured via Western blotting. As shown in Fig. 3, miR-181a-5p mimic diminished the increase in HMGB1, NF-κB65, TLR4, and p-IκB-α protein expression. In addition, Baicalin plus miR-181a-5p mimic further diminished the increase in HMGB1, NF-κB65, TLR4, and p-IκB-α protein expression in LPS-induced H9c2 cells (Fig. 3).

Effects of Baicalin plus miR-181a-5p mimic on LPS-induced H9c2 cell inflammation and survival rate

H9c2 cells were transfected with miR-181a-5p

Table I. *Effects of Baicalin on H9c2 cell survival rate and inflammation in LPS-induced H9c2 cells. H9c2 cells were incubated with LPS (1.0 mg/L) and various concentrations of Baicalin (25, 50, and 75 μM) for 24 h. The survival rate of H9c2 cells were measured via MTT assay. IL-6, IL-1β, and TNF-α in H9c2 cells were measured using ELISA. Data from three independent experiments are presented as mean ± SD. *P<0.05 vs. the control group. #P<0.05 vs. the baicalin (25 μM) group.*

Group	IL-6 (pg/mL)	IL-1β (pg/mL)	TNF-α (pg/mL)	Survival
Control	51.23±19.37	27.95±7.68	86.33±31.85	0.84±0.32
LPS	75.67±28.49*	63.85±28.53*	142.93±43.26*	0.43±0.15*
LPS+ baicalin (25μM)	69.72±21.68	57.48±23.39	136.48±40.98	0.54±0.19#
LPS+ baicalin (50μM)	61.58±18.29#	42.93±16.74#	103.71±32.52#	0.62±0.23#
LPS+ baicalin (75μM)	56.75±16.92#	36.58±12.42#	94.81±27.84#	0.71±0.28#

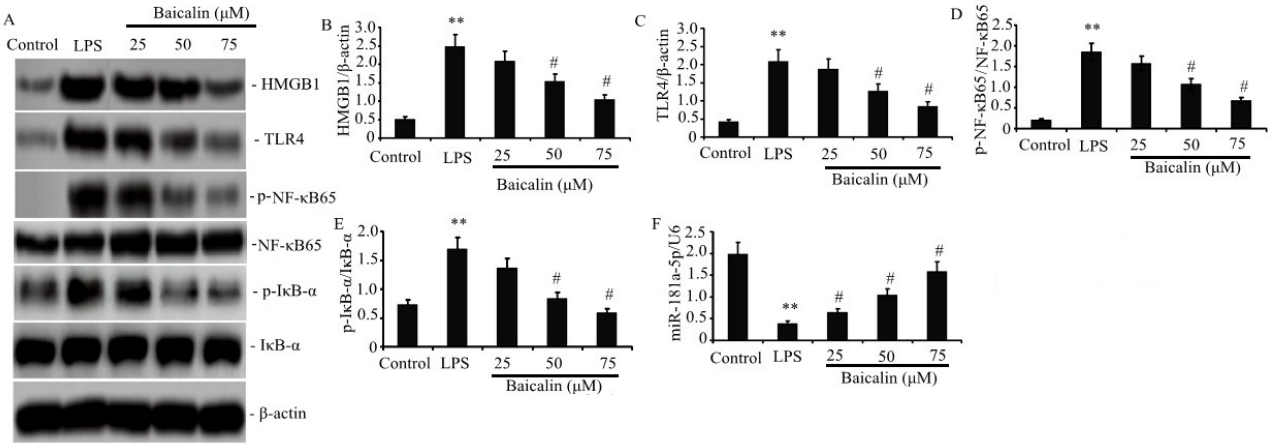


Fig. 1. *Effect of Baicalin on miR-181a-5p expression and the activity of the HMGB1/TLR4/NF-κB signaling pathway in LPS-induced H9c2 cells. H9c2 cells were incubated with LPS (1.0 mg/L) and various concentrations of Baicalin (25, 50, and 75 μM) for 24 h. HMGB1, TLR4, NF-κB65, and p-IκB-α protein expression levels were measured via Western blotting. The expression of miR-181a-5p was measured via RT-PCR. Data from three independent experiments are presented as mean ± SD. *P<0.05 vs. the control group. #P<0.05 vs. the baicalin (25 μM) group. A: Representative bands of protein expression of HMGB1, TLR4,p-NF-κB65, and p-IκB-α in different treatment groups. B-E: Statistical analysis of protein expression of HMGB1, TLR4,p-NF-κB65, and p-IκB-α in different treatment groups. F: Statistical analysis of protein expression of miR-181a-5p expression in different treatment groups.*

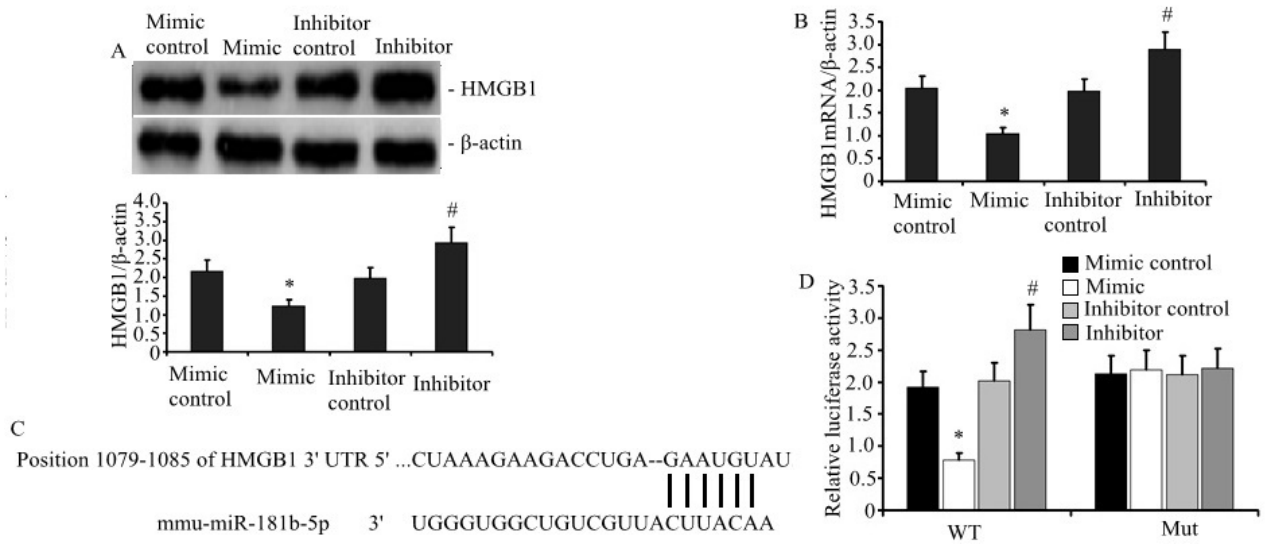


Fig. 2. *HMGB1 is a downstream target of miR-181a-5p. a–b: HMGB1 was decreased in LPS-induced H9c2 cells with miR-181a-5p overexpression relative to the empty vector control (P<0.05). HMGB1 was significantly increased in cells with miR-181a-5p downregulation. c–d: Decreased mRNA levels of HMGB1 in LPS-induced H9c2 cells after miR-181a-5p overexpression (P<0.05). Levels were enhanced after miR-181a-5p upregulation (P<0.05). e: miR-181a-5p was bound to the 3'-untranslated regions (UTRs) of HMGB1. Binding was interrupted in mutant HMGB1. f: Dual luciferase reporter assay indicated that miR-181a-5p mimic was bound to the 3'-UTRs of wild-type HMGB1 rather than to HMGB1 mutants (P<0.05).*

mimic in the presence of 1 mg/l LPS and Baicalin (50 μM) for 24 h. H9c2 cell survival rate was measured via MTT assay. IL-6, IL-1β, and TNF-α in H9c2 cells were measured using ELISA. As indicated in Table I, miR-181a-5p mimic decreased the levels of IL-6, IL-1β, and TNF-α in H9c2 cells and increased the survival rate of LPS-induced H9c2 cells. Meanwhile, Baicalin plus miR-181a-5p mimic further decreased the levels of IL-6, IL-1β, and TNF-α in H9c2 cells and increased the survival rate of LPS-induced H9c2 cells.

Effect of Baicalin plus miR-181a-5p mimic on LPS-induced H9c2 cell apoptosis

H9c2 cells were transfected with miR-181a-5p mimic in the presence of 1 mg/l LPS and Baicalin (50 μM) for 24 h. Apoptosis in H9c2 cells were measured via flow cytometry. As presented in Table II, miR-181a-5p mimic decreased LPS-induced H9c2 cell apoptosis, while Baicalin plus miR-181a-5p mimic further decreased LPS-induced H9c2 cell apoptosis.

DISCUSSION

HMGB1 is a highly conserved nucleoprotein. After being stimulated by LPS, TNF-α, or IL-1, it is released by monocytes, macrophages, and other immune cells. HMGB1 can also be passively released by damaged and necrotic tissue cells to promote multiplication further. TLR4 is an essential receptor for HMGB1 to induce inflammation. HMGB1 can activate TLR2 and TLR4 to target NF-κB and initiate downstream inflammation. Studies have found that MiR-181a-5p mimic blocks NF-κB activation and vascular inflammation by targeting TAB2, delaying the progression of atherosclerosis (9). miR-181a/b-5p improves the inflammatory response of rats with monocrotaline-induced pulmonary hypertension by targeting endoglycans (10). The study confirms that HMGB1 is the regulatory target of miR-181a-5p. Increasing the expression of miR-181a-5p can inhibit the activity of the HMGB1/TLR4/NF-κB signaling pathway and improve endotoxin-induced acute myocardial injury.

Studies have reported that Baicalin exhibits a

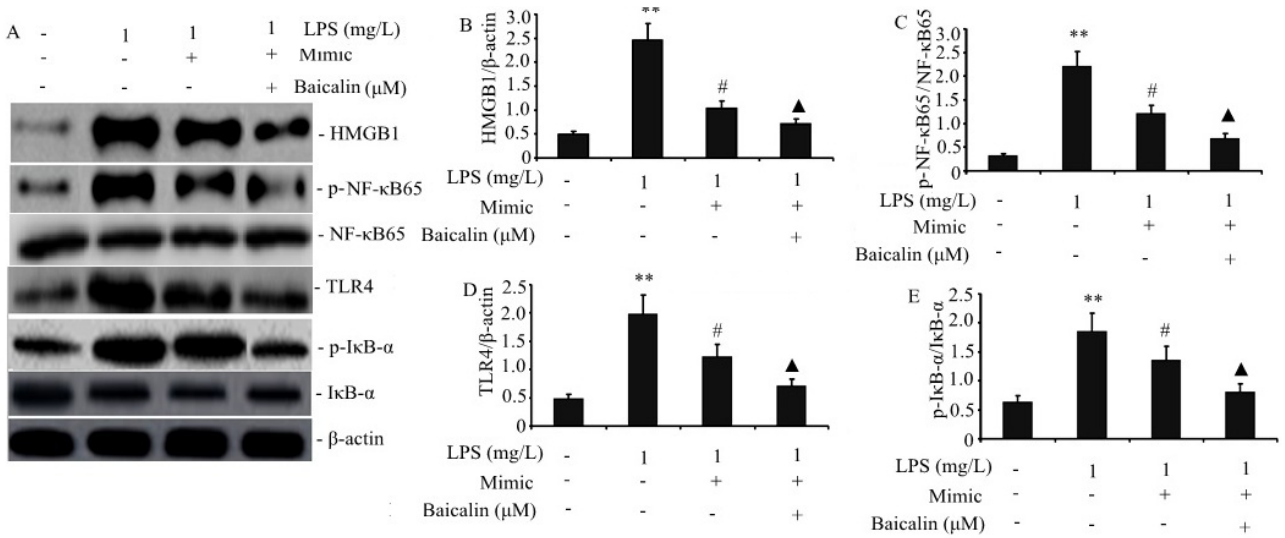


Fig. 3. *Effect of Baicalin plus miR-181a-5p mimic on the activity of the HMGB1/TLR4/NF-κB signaling pathway in LPS-induced H9c2 cells. H9c2 cells were transfected with miR-181a-5p mimic in the presence of 1 mg/l LPS and Baicalin (50 μM) for 24 h. HMGB1, TLR4, NF-κB65, and p-IκB-α protein expression levels were measured via Western blotting. Data from three independent experiments are presented as mean ± SD. *P<0.05 vs. the control group. #P<0.05 vs. the only LPS group. ▲P<0.05 vs. the mimic group. A: Representative bands of protein expression of HMGB1, TLR4,p-NF-κB65, and p-IκB-α in different treatment groups. B-E: statistical analysis of protein expression of HMGB1, TLR4,p-NF-κB65, and p-IκB-α in different treatment groups.*

Table II. *Effects of Baicalin plus miR-181a-5p mimic on the inflammation and survival rate of LPS-induced H9c2 cells. H9c2 cells were transfected with miR-181a-5p mimic in the presence of 1 mg/l LPS and Baicalin (50 μM) for 24 h. The survival rate of H9c2 cells was measured via MTT assay. IL-6, IL-1β, and TNF-α in H9c2 cells were measured using ELISA. Apoptosis in H9c2 cells were measured through flow cytometry. Data from three independent experiments are presented as mean ± SD.*

Group	IL-6 (pg/mL)	IL-1β (pg/mL)	TNF-α (pg/mL)	Survival	Apoptosis(%)
Control	49.35±15.74	26.58±7.62	85.81±29.59	0.82±0.29	8.94±2.48
LPS	76.58±21.93*	67.54±19.16*	139.87±41.85*	0.41±0.15*	29.72±6.53*
LPS+ mimic	63.72±17.63#	48.36±17.28#	109.53±36.27#	0.64±0.19#	19.85±5.02#
LPS+ baicalin+ mimic	56.48±14.94▲	37.93±14.37▲	96.48±25.81▲	0.76±0.24▲	11.67±3.86▲

**P<0.05 vs. the control group. #P<0.05 vs. the only LPS group. ▲P<0.05 vs. the mimic group.*

protective effect on reperfusion cardiomyocyte injury (11,12). Recent studies have also found that Baicalin can reduce oxidative stress and inflammation by inhibiting the activation of the NLRP3, NF-κB and p38 mitogen-activated protein kinase pathways, reducing atherosclerosis (5,12). In the current study, Baicalin increased the expression of miR-181a-5p, inhibited the activity of the HMGB1/TLR4/NF-κB signaling pathway, and improved endotoxin-induced acute myocardial injury.

Therefore, Baicalin can improve acute myocardial injury induced by LPS. The mechanism behind such improvement is that Baicalin increases the expression of miR-181a-5p and targets the inhibition of the activity of the HMGB1/TLR4/NF-κB signaling pathway.

ACKNOWLEDGEMENTS

The authors thank language editing company "enpaper" for editing the language of the paper.

Declaration of conflicting interests

The author(s) declared no potential conflicts of interest with respect to the research, authorship, and/or publication of this article.

REFERENCES

1. Lv X, Wang H. Pathophysiology of sepsis-induced myocardial dysfunction. Mil Med Res 2016; 3:30.
2. Joseph LC, Kokkinaki D, Valenti MC, et al. Inhibition of NADPH oxidase 2 (NOX2) prevents sepsis-induced cardiomyopathy by improving calcium handling and mitochondrial function. JCI Insight 2017; 2(17):e94248.
3. Liu L, Pang XL, Shang WJ, Xie HC, Wang JX, Feng GW. Over-expressed microRNA-181a Reduces Glomerular Sclerosis and Renal Tubular Epithelial Injury in Rats with Chronic Kidney Disease via Down-Regulation of the TLR/NF-κB Pathway by Binding to CRY1. Mol Med 2018; 24(1):49.
4. Wang Z, Chen W, Li Y, Zhang S, Lou H, Lu X, Fan X. Reduning injection and its effective constituent luteoloside protect against sepsis partly via inhibition of HMGB1/TLR4/NF-kappaB/MAPKs signaling pathways. J Ethnopharmacol 2021; 270:113783.
5. Fu YJ, Xu B, Huang SW, et al. Baicalin prevents LPS-induced activation of TLR4/NF-kappaB p65 pathway and inflammation in mice via inhibiting the expression of CD14. Acta Pharmacol Sin. 2021; 42(1):88-96.
6. Huang T, Liu Y, Zhang C. Pharmacokinetics and Bioavailability Enhancement of Baicalin: A Review. Eur J Drug Metab Pharmacokinet 2019; 44(2):159-168

7. Ishfaq M, Zhang W, Liu Y, et al. Baicalin attenuated Mycoplasma gallisepticum-induced immune impairment in chicken bursa of fabricius through modulation of autophagy and inhibited inflammation and apoptosis. J Sci Food Agric 2021; 101(3):880-890
8. Sun Y, Liu MW, Zhao YH, Lu YX, Wang YA, Tong CW. Baicalin attenuates lipopolysaccharide-induced renal tubular epithelial cell injury by inhibiting the TXNIP/NLRP3 signalling pathway via increasing miR-223-3p expression. J Biol Regul Homeost Agents 2020; 34(1):69-82.
9. Su Y, Yuan J, Zhang F, et al. MicroRNA-181a-5p and microRNA-181a-3p cooperatively restrict vascular inflammation and atherosclerosis. Cell Death Dis 2019; 10(5):365.
10. Zhao H, Guo Y, Sun Y, Zhang N, Wang X. miR-181a/b-5p ameliorates inflammatory response in monocrotaline-induced pulmonary arterial hypertension by targeting endocan. J Cell Physiol 2020; 235(5):4422-4433.
11. Liu X, Zhang S, Xu C, et al The protective of Baicalin on myocardial ischemia-reperfusion injury. Curr Pharm Biotechnol 2020;21(13):1386-1393
12. Chen Z, Pan X, Sheng Z, Yan G, Chen L, Ma G. Baicalin suppresses the proliferation and migration of Ox-LDL-VSMCs in atherosclerosis through upregulating miR-126-5p. Biol Pharm Bull 2019;42(9):1517-1523.